Blundell, Rebecca K. (2016) XPS of Quaternary Ammonium and Phosphonium Ionic Liquids. PhD thesis, University of Nottingham.

XPS of Quaternary Ammonium and Phosphonium Ionic Liquids

Rebecca K. Blundell, MSci (Hons)

Thesis submitted to the University of Nottingham
for the degree of Doctor of Philosophy

July 2016

Abstract

X-ray Photoelectron Spectroscopy (XPS) has been used to probe the influence of cation structure on fundamental interactions within Ionic Liquid (IL) systems. A series of tetraalkylammonium-based ILs and their phosphonium analogues have been investigated. A robust C 1s peak fitting model has been developed and described for the tetraalkylphosphonium and tetraalkylammonium families of ionic liquid, with comparisons made between the two series. Cation-anion interactions have been investigated to determine the impact of changing the cationic core from nitrogen to phosphorus on the electronic environment of the anion. Comparisons between long and short chain cationic systems, and the effect of cation conformational restriction, are also described.

Additionally, a high-energy Ag Lα’ X-ray source has been utilised to probe the structure of the IL/vacuum interface using Energy-resolved XPS (ERXPS) for tetraalkylammonium- and tetraalkylphosphonium-based ILs, with comparison made to data obtained with Angle-resolved XPS (ARXPS) experiments using a standard Al Kα X-ray source. The capability of the Ag Lα’ source for IL analysis is confirmed, alongside the characterisation of previously undetected high energy core level photoelectron emissions.

The effect of cation functionalisation is also studied by XPS, with a view to establish fine-tuning of charge transfer from anion to cation using electron-withdrawing substituents embedded within the alkyl side chain of the cation. Binding energy analysis indicated cation functionalisation had minimal influence on the electronic environment of the ionic head groups with respect to the non-functionalised analogues. The performance of ILs, with respect to cation functionalisation, as solvents in the Suzuki reaction is also reported in this *Thesis*, whereby evidence is provided for changing the nature of catalysis *via* cation functionalisation.

Acknowledgements

I must express particular thanks to my supervisor, Prof. Peter Licence. His constant enthusiasm and guidance has been invaluable for the duration of my PhD, and in the assembly of this *Thesis*, and I am extremely grateful.

I am indebted to Dr. Emily Smith for XPS instrument and data analysis training, alongside providing thought-provoking discussions throughout my studies. Additionally, I extend my gratitude to Dr. Michael Fay, Dr. Thomas Chamberlain and Prof. Jairton Dupont for their help with TEM analysis and discussions on palladium nanoparticles. I gratefully acknowledge Sarah Coultas of Kratos Ltd for their XPS facilities; Cytec Ind. Inc. for the kind donation of several phosphonium precursors; the Nottingham Nanoscale and Microscale Research Centre (NMRC); and the University of Nottingham for funding.

I also thank Rachel Gover for her limitless patience and for helping with this work in ways too numerous to cite. I must also thank Astrid Delorme for her valuable contribution and hard-work towards the depth profiling studies; it was a great pleasure to mentor Astrid throughout her MSci project.

I must also thank all the past and present members of the Licence group who I've had the pleasure of working alongside: Alasdair, Emma, Dan, Coby, Zoë, Ana, Luiz, Bogdan, Ejike, Amalina, Ste, Rossella and Laís. It is to the credit of this group that I have had such an enjoyable time during my PhD, and I feel fortunate to have met you all.

Lastly, I extend thanks to Tom, my friends, and my family; in particular, my parents, Rosemary and John, for their continuous love and support which has always provided a source of encouragement and for which I will always be grateful.

Abbreviations & Acronyms

ARXPS	Angle-resolved X-ray photoelectron spectroscopy
a.u.	Arbitrary units
BASIL™	Biphasic Acid Scavenging utilising Ionic Liquids
BE	Binding energy
BNC	Bayonet Neill-Concelman
$C_{aliphatic}$	Aliphatic carbon component
CHA	Concentric hemispherical analyser
C_{hetero}	Heteroatom carbon component
C_{inter}	Intermediate carbon component
$[C_nC_1Im]^+$	1-alkyl-3-methylimidazolium
DLD	Delay line detector
e_A^-	Auger electron
E_C	Coulomb potential
e_P^-	Photoelectron
ERXPS	Energy-resolved X-ray photoelectron spectroscopy
ESI-MS	Electrospray Ionisation Mass Spectrometry
eV	Electronvolt
FAT	Fixed analyser transmission
FWHM	Full width half maximum
h	Planck’s constant

HMQC	Heteronuclear Multiple Quantum Correlation
HREELS	High-resolution electron energy loss spectroscopy
IC	Ion chromatography
ID	Information depth
IL	Ionic liquid
IR	Infrared
J	Coupling constant
j	Total angular momentum quantum number
KE	Kinetic energy
l	Orbital angular momentum quantum number
LEIS	Low-energy ion scattering
M	Madelung constant
MD	Molecular dynamics
MIES	Metastable impact electron spectroscopy
n	Number of carbons in alkyl chain
$\mathrm{N_{anion}}$	Anionic nitrogen component
$\mathrm{N_{cation}}$	Cationic nitrogen component
NICISS	Neutral impact collision ion scattering spectroscopy
NMR	Nuclear magnetic resonance
p	Pressure
p_v	Vapour pressure

Pd-NPs	Palladium nanoparticles
pKa_H	Acid dissociation constant of conjugate acid (logarithmic scale)
ppm	Parts per million
RBS	Rutherford back scattering
RSF	Relative sensitivity factor
RTIL	Room temperature ionic liquid
SE	Surface enrichment factor
SFG	Sum frequency generation
SILP	Supported ionic liquid phase
S_N2	Substitution nucleophilic (bi-molecular)
t	Time
T	Temperature
TEM	Transmission electron microscopy
T_m	Melting temperature
TOF	Turn over frequency
Tppts	tris(3-sodium sulfonatophenyl)phosphine
TSIL	Task specific ionic liquid
UHV	Ultra-high vacuum
UPS	Ultraviolet photoelectron spectroscopy
VOC	Volatile organic compound

VT-ARXPS	Variable temperature X-ray photoelectron spectroscopy
XAS	X-ray absorption spectroscopy
XPS	X-ray photoelectron spectroscopy
β	Kamlet-Taft hydrogen bond acceptor ability
δ	Chemical shift
ΔBE	Difference in binding energy
$\Delta_{Vap}H$	Enthalpy of vaporisation
$\Delta_{Vap}H_{298}$	Standard enthalpy of vaporisation
ε_0	Vacuum permittivity
λ_{AL}	Attenuation length
λ_{IMFP}	Inelastic mean free path
ν	Frequency
ϕ	Workfunction

Table of Contents

1. Introduction

1.1 Ionic Liquids: A Background

The generally accepted definition of an ionic liquid (IL) is a compound solely composed of ions with a melting point (T_m) below 373 K (100 °C). Although this temperature is purely arbitrary in nature, *i.e.* based on the boiling point of water, it provides a means to distinguish ionic liquids, albeit somewhat loosely, from traditional, high temperature molten salts. However, it should be noted that the alternative term "*room-temperature ionic liquid*" (RTIL) is frequently applied to ILs where $T_m < 298$ K.

It is widely acknowledged that the field of ionic liquid research began in 1914 when Paul Walden observed the salt ethylammonium nitrate, $[EtNH_3][NO_3]$, to be liquid at ambient temperature.[1] However, it was not until the late 20th Century that IL research began to attract significant attention from the scientific community.[2] Investigations conducted by the United States Air Force and Colorado State University into the fundamental properties of chloroaluminate-based ionic liquids formed the initial drive in this new era of ionic liquid research, mainly for their application as a low temperature alternative to the LiCl/KCl molten salt electrolyte used in thermal batteries.[3, 4] These early ionic liquids, however, suffered from a clear limitation of being air and water sensitive, thus prompting the development of "second-generation ILs" containing anions stable to moisture.[5, 6]

During the late 1990s the IL field experienced a surge of interest, due in part to the green chemistry movement.[1, 7] This is typically focused on their use as potentially "green" alternatives to traditional solvents, most of which are volatile organic compounds (VOCs), which are recognised as a source of significant levels of environmental pollution impacting land-based, aquatic and atmospheric ecosystems.[8] Alongside their outstanding solvation ability, a key property of ILs which contributes to this claim is their almost negligible vapour pressure. Consequently, ILs present a reduced exposure risk than VOCs, and do not have damaging atmospheric photochemistry.[9] In recent years, however, there have been significant toxicological and environmental concerns associated with ILs.[10-13] Despite this, the broad utility of these compounds is indisputable due chiefly to the sheer number of potential ILs, to an extent such that ILs are often referred to as "*designer solvents*". Consequently, the field has rapidly expanded from its electrochemical roots with ILs being investigated for application in areas as diverse as hypergolic rocket fuels,[14, 15] pharmaceuticals,[16, 17] biomedical sensors,[18] and fragrance delivery systems.[19] In addition, the first naturally occurring IL has recently been discovered, thus highlighting the possibility that ILs may exist in nature to play specific biological roles.[20]

Whilst the field continues to have widespread interest, growth and success, it has been expressed that ILs currently suffer from clear and significant disadvantages that stand in the way of commercial applications.[9] Subsequently, although there have been many notable successes in the use of ILs in industry, for example the BASIL™ (Biphasic Acid Scavenging utilising Ionic Liquids) process,[21] it has been stated that ILs are typically limited to niche, small-scale applications at present.[22, 23] This can be attributed, in part, to the sheer number and diversity of ILs, and the consequent lack of understanding on how structural changes to an IL can influence its physicochemical properties and hence function.[23] As such, it has become increasingly important to understand ILs at a molecular level through fundamental investigations into their physicochemical and structural properties,[23-25] and with this knowledge it is irrefutable that the utilisation of ILs in new and existing commercial applications will continue to increase.

1.2 Properties of Ionic Liquids

1.2.1 Chemical Structure

An expansive range of cations and anions can be used to form ionic liquids with the most common ions presented in Figure 1.1. Typically these consist of bulky, aprotic, asymmetric organic cations coupled with polyatomic anions. The ubiquitous 1-methyl-3-alkylimidazolium cation, $[C_nC_1Im]^+$, has remained ever popular since the pioneering work of Wilkes *et al.*[4, 5] and ILs based on this cation are undeniably the most extensively investigated.[1] In particular, tetraalkylammonium- and tetraalkylphosphonium-based ILs have often been overlooked in favour of their imidazolium relatives.[26, 27] In recent years, however, they have become the subject of increasing interest as understanding the influence of chemical structure on IL properties, and function, becomes progressively important to establish methodologies to predict IL properties.[23-25, 28]

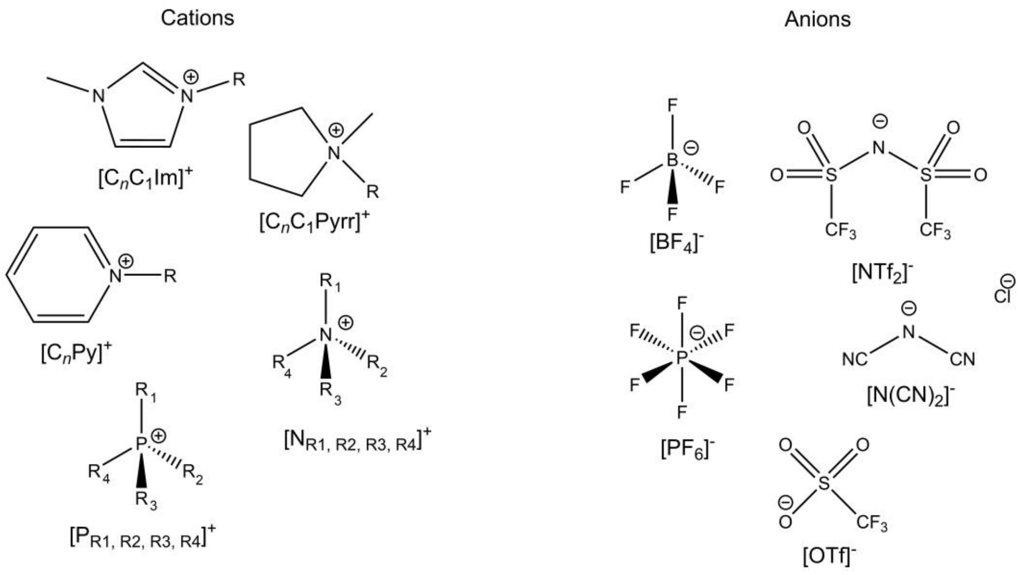

Figure 1.1. Common cations and anions used to form ionic liquids.

It is clear that modern applications of ILs have evolved far beyond their origins as solvents, and they are no longer solely limited to being a reaction medium. This is attributed to another important class of ionic liquids known as "*task specific ILs"* (TSILs). This term is traditionally used in reference to ILs with additional functionality chemically incorporated into the cation or anion to impart a particular type of reactivity or property.[29-31] Furthermore, the task-specific/functionality of these ILs can be utilised to form various IL-based functional materials *via* physical incorporation of ILs with traditional materials;[32] for example, IL/carbon nanomaterial hybrids,[33] IL composite/hybrid luminescent materials,[34, 35] and ionic liquid gels.[36-38]

Due to the vast number and structural diversity of ILs, a multitude of interesting and unusual properties, that can be seemingly unsystematic in nature,[39] are exhibited by this class of materials in comparison to molecular liquids. As such in this section some of the more general trends in physicochemical properties of ILs are discussed with focus on properties which are particularly relevant in this work.

1.2.2 Melting Point

The dominant force in ionic liquids is Coulombic interaction between ions as represented by Equation 1.1, where M = Madelung constant, Z^+ and Z^- = respective charges of ions, ε_o = vacuum permittivity and r = distance between ions.[1]

$$E_c = MZ^+Z^-/4\pi\varepsilon_o r \qquad \textbf{1.1}$$

Subsequently, the difference in melting point between a classical salt, such as sodium chloride, and that of an ionic liquid can be explained in part by consideration of the Kapustinskii and Born-Landé equations which are used to define the overall lattice energy for ionic solids. By consideration of these relationships it is seen that lattice energy is largest for: (1) highly charged ions, (2) small inter-ion separation and (3) high packing efficiency of ions; thus, when considering ionic liquids these effects must be reduced in order to decrease lattice energy, and hence reduce melting temperature. Ionic liquids, therefore, typically consist of bulky, unsymmetrical ions to prevent the formation of an ordered, regular crystalline lattice and increase inter-ion separation. Choosing structures that allow for delocalisation of charge also contributes to a reduction in lattice energy.

It is important to note that other contributions also affect IL melting point including π-π stacking, hydrogen-bonding and van der Waals interactions.[1] This is exemplified by lengthening the alkyl chain in $[C_nC_1Im]^+$ ionic liquids, where an initial increase in chain length is associated with a reduction in melting point; however, generally at chain lengths where $n > 7$, salts with higher melting points result, as a consequence of increasing van der Waals interactions, see Figure 1.2.

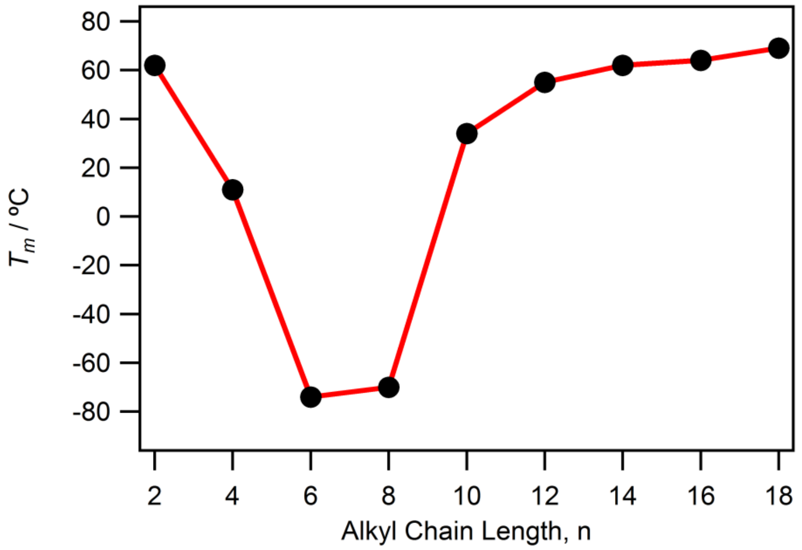

Figure 1.2. Melting points for ionic liquids of the type [C_nC_1Im][PF_6] as a function of chain length (*n*).[40]

Interestingly, Davis *et al.* have recently shown a way to synthesise low melting salts that contain a long, linear hydrocarbon chain (n > 16) through the incorporation of a *cis* double bond "kink".[41] This is believed to result from a reduction in packing efficiency of the hydrophobic component in a fashion similar to homeoviscous adaption in cell membranes.[41, 42]

1.2.3 Volatility

Ionic liquids were initially considered to be non-volatile until a revolutionary paper by Earle *et al.* described the distillation, without decomposition, of several aprotic ILs at elevated temperatures ($T > 473$ K) and reduced pressures ($p < 10^{-2}$ mbar).[43] This subsequently encouraged considerable interest in the nature of the IL vapour phase and the measurement of liquid-vapour equilibrium data, namely vapour pressure (p_v) and the enthalpy of vaporisation ($\Delta_{vap}H$) and as such a wide range of ILs have been vaporised, and distilled, since.[44-49] It has been concluded from a number of these studies that the vapour phase of ILs (that vaporise without decomposition) is composed of neutral ion pairs.[44, 49-52] This finding is imperative for the determination of $\Delta_{vap}H$ data by experimental or theoretical techniques that rely intrinsically on the nature of the vapour species.[53]

The accurate determination of vapour pressure, p_v, still remains a particular challenge for many families of ILs as the onset of decomposition ensues at temperatures too low for significant vaporisation to occur.[53] Additionally, the low vapour pressure of ILs also hampers reliable quantification of data. Despite this for a select few ILs vapour pressure measurements have been estimated at values ~10^{-11} mbar at room temperature.[54-56] Consequently, ionic liquids can be analysed using ultra-high vacuum (UHV) ($\leq 10^{-9}$ mbar) techniques at room temperature, and even modestly elevated temperatures, without contributing to an increase in the measured base pressure of the instrument.[57] This inherent property of ILs enables their analysis by X-ray Photoelectron Spectroscopy (XPS), which forms the foundation of this work.

1.2.4 Conductivity

The conductivity of a material is a measure of the mobility and availability of its charge carriers. As ionic liquids are composed entirely of ions they exhibit good conductivities comparable to non-aqueous/electrolyte systems, and depending on IL structure cover a broad range of conductivities (~ 0.1 – 20 mS/cm).[58] In comparison to concentrated aqueous electrolytes, however, their conductivities are significantly lower, for example the conductivity of an aqueous KOH solution (29.4 wt. %) used in alkaline batteries is ~ 540 mS/cm.[58]

It is perhaps surprising that ILs exhibit such low conductivities however this can be partly explained by consideration of the relatively high viscosity of ILs and the inverse relationship between viscosity and conductivity.[58] Additionally, reduction in the number of available charge carriers due to ion-pairing and/or aggregation, and reduction in ion mobility due to the large size of the ions can also contribute to a lower than expected conductivity.[1]

The conductivity of ILs and its relevance to surface charging during XPS measurements is a significant feature of these materials and is discussed further in *Chapter 2 Section 2.1.3*.

1.2.5 Structural Organisation

Molecular dynamics (MD) simulation studies conducted by Canongia Lopes *et al.* in 2006 described the nanostructural organisation of ILs into polar domains, composed of cations and anions, and non-polar domains, where aggregation of alkyl chains occurs.[59] Since these initial investigations there has been overwhelming theoretical and experimental evidence, including X-ray scattering,[60] neutron diffraction,[61] X-ray diffraction,[62] and optical Kerr effect studies,[63] which indicate IL structure in the liquid phase to be highly ordered into nanosegregated domains.[23]

Many of these structural investigations are based on a homologous series of ILs of the type [C_nC_1Im][X] and it has been shown that formation of nanosegregated domains becomes more apparent with increasing alkyl chain length. Subsequently, many trends in IL behaviour such as melting point, viscosity and conductivity can be attributed to the magnitude of nanosegregation. Additionally, MD simulations on other cationic families have indicated that cation structure has a strong influence on the morphology of the domains and/or the degree of nanosegregation. For example, the polar domains for ILs with tetraalkylammonium or tetraalkylphosphonium cations appear to consist of filament networks in comparison to globular structures exhibited by imidazolium cations.[64, 65] Furthermore, suppression in formation of nanostructured domains has been shown for polyether functionalised cations;[66] whereas, for perfluorinated cations the formation of three domains is suggested – polar, non-polar and fluorous.[67]

In addition to bulk nanostructure it is important to consider IL structure in the interfacial region, *i.e.* IL/solid, IL/liquid or IL/gas (vacuum). Ions at the IL surface experience a non-isotropic environment; consequently, the structure of this region is often very different from that of the bulk. [68] This arises as surface molecules will be arranged to expose atomic groups with weaker interactions to the outer most layer in order to minimise free energy of the surface.[69] Using the IL/vacuum interface as an example, for most IL systems collective van der Waals interactions of the alkyl chains are weaker than the electrostatic interaction between ions, as a result there is increased aggregation of alkyl chains at the outer surface where they project towards the vacuum phase.[69-76]

Many successful applications of ionic liquids are dependent on the structural organisation of the IL interfacial regions, therefore it is critical to understand surface structure at a molecular level and the properties this can impart. For example, an understanding of the IL/solid interface is important for electrochemistry,[77] and tribological processes.[78] The IL/liquid interface also plays a vital role in processes such as separation and extraction of materials.[79, 80] The focus of this *Thesis* however is on the IL/vacuum interface, which is discussed further in *Section 1.3* with respect to XPS.

1.2.6 Solvation Properties

In comparison to molecular solvents, which are typically classified as polar or non-polar, and generally follow the adage "*like dissolves like*", ILs can dissolve both polar and non-polar compounds. The currently accepted definition of polarity is that it is a sum of all possible intermolecular interactions between the solvent and solute (excluding interactions leading to definite chemical changes) including Coulombic interactions, dipole interactions and H-bonding.[9] Consequently, as ILs can provide a diverse range of potential solute-solvent interaction types they can dissolve a wide range of materials of varying polarity, including cellulose,[81] metal oxides,[82] transition metal complexes,[1] enzymes,[83] and polymers.[84] In addition, the nanosegregation of polar and non-polar domains within ILs can result in preferential dissolution of solutes within these domains depending on their polarity, *i.e.* polar substrates reside within the polar domains, whereas non-polar substrates reside within non-polar domains.[23, 85, 86] It is important to note that the solvation ability will vary between different ILs for a given solute, and as such a solute freely soluble in one IL may be insoluble in another. This highlights the importance of understanding ILs and their properties to enable predictive design and subsequent application.[87]

The combined properties of low volatility, tunability and outstanding solvation ability define ILs as attractive alternatives to typical solvents and they have found use in many applications.[1, 9] In particular, the ability of hydrophobic ILs to participate in biphasic reactions has great potential for combining the advantages of homogeneous and heterogeneous catalysis and providing an efficient method for catalyst recovery and recycling alongside product extraction.[1, 88, 89] Also, depending on the coordinative properties of the anion and the degree of cation reactivity, ILs are not solely limited to providing an "innocent" solvent medium. In many instances ILs can also act as ligand, co-catalyst or even a catalyst. For example, palladium catalysed cross-couplings have shown enhanced rates when conducted in an imidazolium-based IL solvent, which is attributed to formation of a palladium-imidazolylidene complex.[90-94] Therefore, it is critical to fully understand on a molecular level how an IL interacts and participates within catalytic reactions in order to develop fully tuneable systems.

1.2.7 ILs Investigated in this *Thesis*

Considering the broad range of potential cations and anions proposed to form ionic liquids it is surprising that the field remains dominated by the 1,3-dialkylimidazolium cation and derivatives thereof. The work in this *Thesis* addresses this and aims to understand if cations of different structures, with focus on tetraalkylammonium and tetraalkylphosphonium cations, follow the same trends in their electronic environment and structural organisation as their imidazolium relatives. As such, a range of tetraalkylammonium and tetraalkylphosphonium ILs with cations of varying size and symmetry have been synthesised and investigated. A list of the cations and anions studied, alongside their nomenclature, are presented in Table 1.1 and Table 1.2.

Table 1.1. Cations studied in this *Thesis*.

Cation	Name
$[N_{6,6,6,14}]^+$	Trihexyl(tetradecyl)ammonium
$[N_{8,8,8,8}]^+$	Tetraoctylammonium
$[N_{4,4,4,4}]^+$	Tetrabutylammonium
$[N_{4,4,4,1}]^+$	Tributyl(methyl)ammonium
$[P_{6,6,6,14}]^+$	Trihexyl(tetradecyl)phosphonium
$[P_{8,8,8,8}]^+$	Tetraoctylphosphonium
$[P_{4,4,4,4}]^+$	Tetrabutylphosphonium
$[P_{4,4,4,1}]^+$	Tributyl(methyl)phosphonium
$[C_8C_1Pyrr]^+$	1-methyl-1-octylpyrrolidinium
$[Et(PEG)_2MPyrr]^+$	1-methyl-1-(2-(2-ethoxyethoxy)ethyl)pyrrolidinium
$[C_8C_1Im]^+$	1-methyl-3-octylimidazolium
$[Et(PEG)_2MIm]^+$	1-methyl-3-(2-(2-ethoxyethoxy)ethyl)imidazolium
$[(F_{13}H_4C_8)C_1Im]^+$	1-methyl-3-(1*H*,1*H*,2*H*,2*H*-perfluorooctyl)imidazolium
$[N_{2,2,2,8}]^+$	Triethyl(octyl)ammonium
$[N_{2,2,2,(Et(PEG)2)}]^+$	Triethyl(2-(2-ethoxyethoxy)ethyl)ammonium

Table 1.2. Anions studied in this *Thesis*.

Anion	Name
Cl^-	Chloride
$[BF_4]^-$	Tetrafluoroborate
$[PF_6]^-$	Hexafluorophosphate
$[OTf]^-$	Trifluoromethanesulfonate
$[NTf_2]^-$	Bis(trifluoromethanesulfonyl)imide

1.3 Probing the IL/Vacuum Interface using UHV Techniques

Many successful applications of ionic liquids, especially those that involve gas adsorption/desorption, depend on the interaction of the IL/gas(vacuum) interface with different species. Consequently, the chemical nature of the IL/vacuum interface plays a crucial role in such applications, including but not limited to, supported ionic liquid phase (SILP) catalysis,[95-97] gas capture/separation,[98-100] and imaging.[101] Therefore, it is vital to study and understand the structure of the interfacial regions and relate this to application-based results such that appropriate systems can be predicted and developed to maximise performance.

Previously, before the UHV stability of ionic liquids was established, surface sensitive investigations were carried out using non-UHV techniques such as sum frequency generation spectroscopy (SFG),[76, 102-104] X-ray and neutron reflectivity,[104-106] surface tension measurements,[76, 107, 108] and MD simulations.[70, 109, 110] These early investigations provided considerable insight into the structure of IL surfaces and although there are still discrepancies in ion orientation, there is general agreement that both cations and anions are present at the surface, with projection of aliphatic chains towards the vacuum for ILs of the type [C_nC_1Im][X].

Conventionally, due to the high vapour pressure of typical liquids and their subsequent rapid rate of evaporation, surface sensitive UHV-based techniques were limited to the analysis of compounds in the solid state. However, in 2005 – 2006 it was recognised that ILs possessed almost negligible vapour pressures (~10^{-11} mbar), thus permitting UHV-based investigations without modification to the experimental set-up, and without risk of significant sample loss and/or contamination of the analytical chamber.[80, 111] Additionally, the UHV environment provides a greater degree of accuracy through removal of volatile impurities, and reduced collisions with gas phase contaminants, which may hamper or influence measurements.[28] Consequently, during the last decade a new field of "Ionic Liquid Surface Science" has emerged in which a multitude of UHV-based techniques have been utilised to probe the nature of the surface (and bulk) structure including, but not limited to, X-ray photoelectron spectroscopy (XPS),[68, 73, 74, 112-125] ultraviolet photoelectron spectroscopy (UPS),[113, 114, 126-128] metastable impact electron spectroscopy (MIES),[113, 114] X-ray absorption spectroscopy (XAS),[128] low energy ion scattering (LEIS),[112, 129, 130] and high-resolution electron energy loss spectroscopy (HREELS).[114]

Of these techniques XPS has been described as *"the most common and most powerful tool to analyse the chemical composition of the near-surface region of condensed matter"*;[57] additionally, as core level binding energies are sensitive to small changes in electronic environment, much like the chemical shift in NMR spectroscopy, the chemical state of atoms can be probed. Many significant contributions have been provided by XPS in the field of "IL surface science", with particular focus on the areas: (i) impurity detection, (ii) surface enrichment/depletion of additives, and (iii) surface composition of pure ILs.

1.3.1 Impurity Detection

Confirmation of surface purity is a vital aspect of surface science; the presence of even trace amounts of surface contaminants can cause significant deviations in measurements, especially as many common contaminants are composed of carbon, hydrogen, oxygen and nitrogen, which are also common to most ILs. Furthermore, surface contaminants can cause deleterious effects to the IL surface chemistry, and thereby hinder surface-based applications as a result.

XPS has proved to be a powerful tool with which to detect contaminants in the near-surface region of ILs. The first reported XPS study on the commercially obtained 1-ethyl-3-methylimidazolium ethylsulfate, $[C_2C_1Im][EtOSO_3]$, detected trace amounts of silicon, which were initially attributed to the silicone septum on the bottle used to store $[C_2C_1Im][EtOSO_3]$.[115] A follow-up study by Gottfried *et al*.[131] using angle-resolved XPS (ARXPS) indicated the silicon contamination to be enriched at the uppermost layers, and was also associated with additional carbon and oxygen impurities – the constituents of silicones. Doping a clean sample of $[C_2C_1Im][EtOSO_3]$ with high-vacuum silicone grease produced spectra with identical contaminants, suggesting a conceivable origin of the silicone impurity.[131] It is important to note here that the contamination was shown to be highly surface active as it was undetectable by bulk analytical methods.[57, 131]

Similarly, using ARXPS Kolbeck *et al.*[132] observed a surface active contaminant that only contained the same elements as the IL, namely oxygen and carbon. This highlights the high sensitivity of XPS to detect trace levels of impurities, as many surface techniques are incapable of distinguishing spectral features of ILs and those of contaminants.[28]

It has also been shown that surface active contaminants can be routinely removed *in situ* by Ar ion sputtering.[132, 133] This technique involves bombarding the surface with a beam of energetic Ar^+ ions which removes the top few layers of atoms, thus exposing a clean surface below. Impurities removed from the surface have been seen to recover over time, demonstrating slow segregation of the impurities from the bulk to the surface.[125, 132]

Surface purity is integral to many IL applications; consequently, the element specific and surface sensitive nature of XPS provides an excellent means to assess the surface purity of ILs and make valid, reliable deductions on IL surface chemistry.

1.3.2 Surface Enrichment/Depletion of Additives

The surface enrichment of a species present at low concentration in the bulk can also be a significant advantage. This is particularly relevant in the case of SILP catalysis; in this example, thin films of ionic liquid are layered on a high surface area support. The IL layers serve as a homogeneous phase, in which a catalytically active transition metal complex is dissolved. For reaction to occur, gas phase reactants adsorb onto the IL surface, diffuse to meet the catalyst, react, then diffuse back to the surface and desorb. Consequently, the ability to tune the IL phase such that it maximises the surface concentration of the catalyst, and increases its accessibility to the reactant, is extremely advantageous.[97]

ARXPS studies by Maier *et al.*[117] have shown that XPS is an excellent technique with which to study surface enrichment of transition metal complexes in ILs. Initial investigations for a mixture of $[Pt(NH_3)_4]Cl_2$ in $[C_2C_1Im][EtOSO_3]$ indicated that the metal complex, $[Pt(NH_3)_4]^{2+}$, was highly enriched in the top surface layers of the sample, with a depletion of chloride counter ion.[117] A further study expanding on these findings has recently been described by Kolbeck *et al.*[134] in which, a range of Pt(II) and Pt(IV) complexes dissolved in different ILs were investigated. A surface enrichment dependency of a $[PtCl_6]^{2-}$ complex with IL cation was observed, whereby depletion effects occurred for imidazolium cations in comparison to enrichment with pyrrolidinium cations.

XPS has also provided direct insight into the mechanisms and processes of industrially relevant catalytic reactions. This is particularly exemplified by the work of Kolbeck *et al.*,[135] in which ARXPS was used to determine the influence of the tris(3-sodium sulfonatophenyl)phosphine (tppts) ligand on Rh-catalyst concentration at the IL surface –which is of significant interest in the application of hydroformylation catalysis.[135] Here three different systems were investigated: (1) [Rh(acac)(CO)$_2$] in [C_2C_1Im][EtOSO$_3$], (2) tppts in [C_2C_1Im][EtOSO$_3$] and (3) [Rh(acac)(CO)$_2$] and tppts in [C_2C_1Im][EtOSO$_3$].

In the first system, XPS indicated that an absence of ligand was associated with a depletion of Rh-catalyst at the surface. The second system consisting of solely of ligand and IL highlighted the high surface activity of the tppts ligand. However, it is the third system which is of most interest, when both Rh-catalyst and ligand are dissolved in [C_2C_1Im][EtOSO$_3$] the surface is enriched with Rh-catalyst, thus providing spectroscopic evidence that the nature of the applied ligand influences the preferred position of the catalyst complex in either the bulk or at the interface.

1.3.3. Bulk *versus* Surface Composition in Pure ILs

In order to understand the surface chemistry of ionic liquids it is paramount to understand the structure of the IL/vacuum interface. Considering the sheer number of possible ILs and the resultant costliness of a brute force approach, *i.e.* investigating each IL individually with all possible surface sensitive techniques, a more pressing challenge is the development of design rules such that the surface structure of any given IL can be predicted.

The surface structure of imidazolium-based ILs has been well characterised by many different techniques, to the extent that preliminary design rules have been postulated. XPS has played an influential role in this development through its ability to provide excellent data on atom location (*i.e.* enrichment/depletion effects). A summary of these findings is discussed in this section.

The first reported use of ARXPS to analyse the IL/vacuum interface was in 2006 by Maier *et al.* where it was shown for [C_2C_1Im][EtOSO$_3$] that spectra taken at emission angles 0° and 70° (probe depths are 7-9 nm and 2-3 nm respectively) were virtually identical, indicating a homogeneous distribution of ions in the near-surface region.[117] A subsequent investigation by Lockett *et al.* on ILs of the type [C_nC_1Im][BF$_4$] (where n = 4,6,8) using higher emission angles (θ = 0° – 84°), and hence greater surface sensitivity, indicated an increasing amount of aliphatic carbon with emission angle.[119] Further studies elucidated that this effect was enhanced with increasing alkyl chain length and decreasing anion size, thereby providing evidence that the alkyl chains project towards the vacuum phase for ILs [C_nC_1Im][X] (where $n \geq 4$).[72-74, 120, 136] As such a model of the IL surface is proposed consisting of a hydrophobic overlayer of alkyl chains with an ionic sublayer of charged head groups. This is consistent with findings from other techniques including SFG,[76, 103, 104, 128] neutral impact-collision ion scattering spectroscopy (NICISS),[137, 138] Rutherford back scattering (RBS),[139, 140] and MD simulations.[69-71, 109, 110]

There are considerably fewer surface investigations on non-imidazolium ionic liquids, which give rise to the questions: how does cation structure influence surface structure? Are the proposed design rules for imidazolium ILs applicable to other varieties of cations? Preliminary investigations on pyrrolidinium-based ILs indicate that this particular cation variety does indeed follow the same trends to their imidazolium analogues.[72, 75, 123, 141] Considering the structural similarities of pyridinium ILs, *i.e.* a polar heterocyclic ring with a long non-polar alkyl chain, it is likely these will also show similar surface behaviour.[28] However, this cannot be expected to be the case for tetraalkylammonium and tetraalkylphosphonium cations, in which the highly polar central atom is shielded by four conformationally flexible alkyl chains. It is, therefore, important to determine trends in surface structure for common acyclic ILs to answer how cation structure may influence surface structure.

1.4 Summary: Aims and Objectives

To fully understand the structure-property relationships of ionic liquids it is necessary to characterise neat ILs at a molecular level. Over the past ten years XPS has established itself as a robust technique to characterise ionic liquid-based systems. Binding energies obtained from XPS have provided extensive information on the effect of structural changes to local electronic environment and also cation-anion interactions. Additionally, the surface sensitive nature of XPS enables depth-profiling experiments to determine the nature of the IL/vacuum interface.

However, the majority of these studies have been focused on non-functionalised, heterocyclic cations with particular emphasis on the imidazolium variety. The work in this *Thesis* addresses this gap in knowledge through XPS investigations into tetraalkylammonium and tetraalkylphosphonium cations, and also the influence of cation functionalisation. A summary of the principles behind XPS are described in *Chapter 2*.

In *Chapter 3* the use of XPS to gather binding energy information for tetraalkylammonium and tetraalkylphosphonium ILs is described; the main theme for *Chapter 3* is the influence of cation structure on cation-anion interactions with three main questions: (i) Are the trends in anionic influence exhibited for imidazolium ILs also applicable to these classes of IL? (ii) How does size and polarity of the cationic heteroatom influence cation-anion interactions, *i.e.* ammonium *versus* phosphonium? (iii) How does conformational flexibility of the cation alkyl chains influence cation-anion interactions?

Chapter 4 describes the use of XPS to characterise the surface structure for tetraalkylammonium and tetraalkylphosphonium ILs. The primary focus here is to determine if acyclic tetraalkylammonium and tetraalkylphosphonium ILs exhibit different surface preferences to the cyclic imidazolium and pyrrolidinium families of ILs. To investigate this, two depth profiling techniques are used: angle-resolved XPS (ARXPS) and energy-resolved XPS (ERXPS). ARXPS studies have been extensively used to investigate ILs as discussed in *Section 1.3.3*. Considerably fewer ERXPS studies on ILs exist as they typically require high-energy synchrotron X-ray sources; however, in *Chapter 4* the first use of a high-energy, commercially available Ag Lα’ X-ray source to conduct ERXPS investigations on ILs is described.

Lastly, *Chapter 5* investigates if an extra degree of tunability can be achieved through the cation by functionalisation of the cation alkyl side chain, and the effect this imparts on cation-anion interactions. The application of cation functionalisation and its influence on catalytic performance in the Suzuki cross-coupling reaction is also studied.

1.5 References

1. P. Wasserscheid and T. Welton, *Ionic Liquids in Synthesis*, Wiley-VCH, Weinham, 2nd edn., 2008.

2. N. V. Plechkova and K. R. Seddon, *Chem. Soc. Rev.*, 2008, **37**, 123-150.

3. R. J. Gale, B. Gilbert and R. A. Osteryoung, *Inorg. Chem.*, 1978, **17**, 2728-2729.

4. J. S. Wilkes, J. A. Levisky, R. A. Wilson and C. L. Hussey, *Inorg. Chem.*, 1982, **21**, 1263-1264.

5. J. S. Wilkes and M. J. Zaworotko, *J. Chem. Soc., Chem. Commun.*, 1992, 965-967.

6. P. Bônhote, A. P. Dias, N. Papageorgiou, K. Kalyanasundaram and M. Grätzel, *Inorg. Chem.*, 1996, **35**, 1168-1178.

7. P. T. Anastas and J. C. Warner, *Green Chemistry: Theory and Practice*, Oxford University Press, New York, 2000.

8. R. D. Rogers and K. R. Seddon, *Science*, 2003, **302**, 792-793.

9. J. P. Hallett and T. Welton, *Chem. Rev.*, 2011, **111**, 3508-3576.

10. D. Coleman and N. Gathergood, *Chem. Soc. Rev.*, 2010, **39**, 600-637.

11. M. Deetlefs and K. R. Seddon, *Green Chem.*, 2010, **12**, 17-30.

12. R. P. Swatloski, J. D. Holbrey and R. D. Rogers, *Green Chem.*, 2003, **5**, 361-363.

13. M. Petkovic, K. R. Seddon, L. P. N. Rebelo and C. S. Pereira, *Chem. Soc. Rev.*, 2011, **40**, 1383-1403.

14. S. Schneider, T. Hawkins, M. Rosander, G. Vaghjiani, S. Chambreau and G. Drake, *Energy Fuels*, 2008, **22**, 2871-2872.

15. T. Liu, X. Qi, S. Huang, L. Jiang, J. Li, C. Tang and Q. Zhang, *Chem. Commun.*, 2016, **52**, 2031-2034.

16. J. L. Shamshina, S. P. Kelley, G. Gurau and R. D. Rogers, *Nature*, 2015, **528**, 188-189.

17. W. L. Hough, M. Smiglak, H. Rodriguez, R. P. Swatloski, S. K. Spear, D. T. Daly, J. Pernak, J. E. Grisel, R. D. Carliss, M. D. Soutullo, J. H. Davis and R. D. Rogers, *New J. Chem.*, 2007, **31**, 1429-1436.

18. Y. Wang, S. Gong, S. Jia Wang, G. P. Simon and W. Cheng, *Mater. Horiz.*, 2016, DOI: 10.1039/C5MH00284B.

19. H. Q. N. Gunaratne, P. Nockemann and K. R. Seddon, *Chem. Commun.*, 2015, **51**, 4455-4457.

20. L. Chen, G. E. Mullen, M. Le Roch, C. G. Cassity, N. Gouault, H. Y. Fadamiro, R. E. Barletta, R. A. O. Brien, R. E. Sykora, A. C. Stenson, K. N. West, H. E. Horne, J. M. Hendrich, K. R. Xiang and J. H. Davis, *Angew. Chem. Int. Ed.*, 2014, **53**, 11762-11765.

21. M. Freemantle, *Chem. Eng. News*, 2003, **81**, 9-9.

22. L. Chen, M. Sharifzadeh, N. Mac Dowell, T. Welton, N. Shah and J. P. Hallett, *Green Chem.*, 2014, **16**, 3098-3106.

23. R. Hayes, G. G. Warr and R. Atkin, *Chem. Rev.*, 2015, **115**, 6357-6426.

24. H. Weingärtner, *Angew. Chem. Int. Ed.*, 2008, **47**, 654-670.

25. E. W. Castner, C. J. Margulis, M. Maroncelli and J. F. Wishart, in *Ann. Rev. Phys. Chem.*, eds. S. R. Leone, P. S. Cremer, J. T. Groves and M. A. Johnson, Annual Reviews, Palo Alto, 2011, vol. 62, pp. 85-105.

26. K. J. Fraser and D. R. MacFarlane, *Aust. J. Chem.*, 2009, **62**, 309-321.

27. R. E. Del Sesto, C. Corley, A. Robertson and J. S. Wilkes, *J. Organomet. Chem.*, 2005, **690**, 2536-2542.

28. K. R. J. Lovelock, *Phys. Chem. Chem. Phys.*, 2012, **14**, 5071-5089.

29. A. E. Visser, R. P. Swatloski, W. M. Reichert, R. Mayton, S. Sheff, A. Wierzbicki, J. H. Davis and R. D. Rogers, *Chem. Commun.*, 2001, 135-136.

30. S. G. Lee, *Chem. Commun.*, 2006, 1049-1063.

31. R. Giernoth, *Angew. Chem. Int. Ed.*, 2010, **49**, 2834-2839.

32. S. Zhang, Q. Zhang, Y. Zhang, Z. Chen, M. Watanabe and Y. Deng, *Prog. Mater. Sci.*, 2016, **77**, 80 - 124.

33. M. Tunckol, J. Durand and P. Serp, *Carbon*, 2012, **50**, 4303-4334.

34. A. V. Mudring, A. Babai, S. Arenz, R. Giernoth, K. Binnemans, K. Driesen and P. Nockemann, *J. Alloys Compd.*, 2006, **418**, 204-208.

35. S. Arenz, A. Babai, K. Binnemans, K. Driesen, R. Giernoth, A. V. Mudring and P. Nockemann, *Chem. Phys. Lett.*, 2005, **402**, 75-79.

36. P. C. Marr and A. C. Marr, *Green Chem.*, 2016, **18**, 105-128.

37. D. M. Li, F. Shi, S. Guo and Y. Q. Deng, *Tetrahedron Lett.*, 2004, **45**, 265-268.

38. Y. M. Wang, V. Ulrich, G. F. Donnelly, F. Lorenzini, A. C. Marr and P. C. Marr, *ACS Sustain. Chem. Eng.*, 2015, **3**, 792-796.

39. D. R. MacFarlane and K. R. Seddon, *Aust. J. Chem.*, 2007, **60**, 3-5.

40. I. Lopez-Martin, E. Burello, P. N. Davey, K. R. Seddon and G. Rothenberg, *ChemPhysChem*, 2007, **8**, 690-695.

41. S. M. Murray, R. A. O'Brien, K. M. Mattson, C. Ceccarelli, R. E. Sykora, K. N. West and J. H. Davis, *Angew. Chem. Int. Ed.*, 2010, **49**, 2755-2758.

42. M. Sinensky, *Proc. Nat. Acad. Sci. USA*, 1974, **71**, 522-525.

43. M. J. Earle, J. Esperanca, M. A. Gilea, J. N. Canongia Lopes, L. P. N. Rebelo, J. W. Magee, K. R. Seddon and J. A. Widegren, *Nature*, 2006, **439**, 831-834.

44. J. P. Armstrong, C. Hurst, R. G. Jones, P. Licence, K. R. J. Lovelock, C. J. Satterley and I. J. Villar-Garcia, *Phys. Chem. Chem. Phys.*, 2007, **9**, 982-990.

45. V. N. Emel'yanenko, S. P. Verevkin, A. Heintz, J. A. Corfield, A. Deyko, K. R. J. Lovelock, P. Licence and R. G. Jones, *J. Phys. Chem. B*, 2008, **112**, 11734-11742.

46. K. R. J. Lovelock, A. Deyko, J. A. Corfield, P. N. Gooden, P. Licence and R. G. Jones, *ChemPhysChem*, 2009, **10**, 337-340.

47. L. Santos, J. N. Canongia Lopes, J. A. P. Coutinho, J. Esperanca, L. R. Gomes, I. M. Marrucho and L. P. N. Rebelo, *J. Am. Chem. Soc.*, 2007, **129**, 284-285.

48. A. W. Taylor, K. R. J. Lovelock, A. Deyko, P. Licence and R. G. Jones, *Phys. Chem. Chem. Phys.*, 2010, **12**, 1772-1783.

49. J. P. Leal, J. Esperanca, M. E. M. da Piedade, J. N. Canongia Lopes, L. P. N. Rebelo and K. R. Seddon, *J. Phys. Chem. A*, 2007, **111**, 6176-6182.

50. D. Strasser, F. Goulay, M. S. Kelkar, E. J. Maginn and S. R. Leone, *J. Phys. Chem. A*, 2007, **111**, 3191-3195.

51. J. H. Gross, *J. Am. Soc. Mass Spectrom.*, 2008, **19**, 1347-1352.

52. J. P. Leal, M. E. M. da Piedade, J. N. Canongia Lopes, A. A. Tomaszowska, J. Esperanca, L. P. N. Rebelo and K. R. Seddon, *J. Phys. Chem. B*, 2009, **113**, 3491-3498.

53. J. Esperanca, J. N. Canongia Lopes, M. Tariq, L. Santos, J. W. Magee and L. P. N. Rebelo, *J. Chem. Eng. Data*, 2010, **55**, 3-12.

54. A. Seeberger, A. K. Andresen and A. Jess, *Phys. Chem. Chem. Phys.*, 2009, **11**, 9375-9381.

55. G. J. Kabo, A. V. Blokhin, Y. U. Paulechka, A. G. Kabo, M. P. Shymanovich and J. W. Magee, *J. Chem. Eng. Data*, 2004, **49**, 453-461.

56. M. Ahrenberg, M. Brinckmann, J. W. P. Schmelzer, M. Beck, C. Schmidt, O. Kessler, U. Kragl, S. P. Verevkin and C. Schick, *Phys. Chem. Chem. Phys.*, 2014, **16**, 2971-2980.

57. H.-P. Steinrück, *Surf. Sci.*, 2010, **604**, 481-484.

58. P. Hapiot and C. Lagrost, *Chem. Rev.*, 2008, **108**, 2238-2264.

59. J. N. Canongia Lopes and A. A. H. Padua, *J. Phys. Chem. B*, 2006, **110**, 3330-3335.

60. D. Xiao, L. G. Hines, S. F. Li, R. A. Bartsch, E. L. Quitevis, O. Russina and A. Triolo, *J. Phys. Chem. B*, 2009, **113**, 6426-6433.

61. R. Atkin and G. G. Warr, *J. Phys. Chem. B*, 2008, **112**, 4164-4166.

62. A. Triolo, O. Russina, H. J. Bleif and E. Di Cola, *J. Phys. Chem. B*, 2007, **111**, 4641-4644.

63. D. Xiao, L. G. Hines, R. A. Bartsch and E. L. Quitevis, *J. Phys. Chem. B*, 2009, **113**, 4544-4548.

64. K. Shimizu, A. A. H. Padua and J. N. Canongia Lopes, *J. Phys. Chem. B*, 2010, **114**, 15635-15641.

65. K. Shimizu, M. F. C. Gomes, A. A. H. Padua, L. P. N. Rebelo and J. N. Canongia Lopes, *J. Mol. Struc. (THEOCHEM)*, 2010, **946**, 70-76.

66. K. Shimizu, C. E. S. Bernardes, A. Triolo and J. N. Canongia Lopes, *Phys. Chem. Chem. Phys.*, 2013, **15**, 16256-16262.

67. A. B. Pereiro, M. J. Pastoriza-Gallego, K. Shimizu, I. M. Marrucho, J. N. Canongia Lopes, M. M. Pineiro and L. P. N. Rebelo, *J. Phys. Chem. B*, 2013, **117**, 10826-10833.

68. H.-P. Steinrück, *Phys. Chem. Chem. Phys.*, 2012, **14**, 5010-5029.

69. Y. Wang, W. Jiang, T. Yan and G. A. Voth, *Acc. Chem. Res.*, 2007, **40**, 1193-1199.

70. R. M. Lynden-Bell and M. Del Popolo, *Phys. Chem. Chem. Phys.*, 2006, **8**, 949-954.

71. B. L. Bhargava and S. Balasubramanian, *J. Am. Chem. Soc.*, 2006, **128**, 10073-10078.

72. V. Lockett, R. Sedev, S. Harmer, J. Ralston, M. Horne and T. Rodopoulos, *Phys. Chem. Chem. Phys.*, 2010, **12**, 13816-13827.

73. K. R. J. Lovelock, C. Kolbeck, T. Cremer, N. Paape, P. S. Schulz, P. Wasserscheid, F. Maier and H.-P. Steinrück, *J. Phys. Chem. B*, 2009, **113**, 2854-2864.

74. F. Maier, T. Cremer, C. Kolbeck, K. R. J. Lovelock, N. Paape, P. S. Schulz, P. Wasserscheid and H.-P. Steinrück, *Phys. Chem. Chem. Phys.*, 2010, **12**, 1905-1915.

75. C. Aliaga, G. A. Baker and S. Baldelli, *J. Phys. Chem. B*, 2008, **112**, 1676-1684.

76. C. S. Santos and S. Baldelli, *J. Phys. Chem. B*, 2009, **113**, 923-933.

77. M. C. Buzzeo, R. G. Evans and R. G. Compton, *ChemPhysChem*, 2004, **5**, 1106-1120.

78. Q. M. Lu, H. Z. Wang, C. F. Ye, W. M. Liu and Q. J. Xue, *Trib. Int.*, 2004, **37**, 547-552.

79. T. Iwahashi, T. Ishiyama, Y. Sakai, A. Morita, D. Kim and Y. Ouchi, *Phys. Chem. Chem. Phys.*, 2015, **17**, 24587-24597.

80. C. Aliaga, C. S. Santos and S. Baldelli, *Phys. Chem. Chem. Phys.*, 2007, **9**, 3683-3700.

81. R. P. Swatloski, S. K. Spear, J. D. Holbrey and R. D. Rogers, *J. Am. Chem. Soc.*, 2002, **124**, 4974-4975.

82. P. Nockemann, B. Thijs, S. Pittois, J. Thoen, C. Glorieux, K. Van Hecke, L. Van Meervelt, B. Kirchner and K. Binnemans, *J. Phys. Chem. B*, 2006, **110**, 20978-20992.

83. R. M. Lau, M. J. Sorgedrager, G. Carrea, F. van Rantwijk, F. Secundo and R. A. Sheldon, *Green Chem.*, 2004, **6**, 483-487.

84. P. Kubisa, *Prog. Polym. Sci.*, 2009, **34**, 1333-1347.

85. U. Schroder, J. D. Wadhawan, R. G. Compton, F. Marken, P. A. Z. Suarez, C. S. Consorti, R. F. de Souza and J. Dupont, *New J. Chem.*, 2000, **24**, 1009-1015.

86. J. L. Anderson and D. W. Armstrong, *Anal. Chem.*, 2003, **75**, 4851-4858.

87. C. Chiappe, *Monatsh. Chem.*, 2007, **138**, 1035-1043.

88. Y. Chauvin, L. Mussmann and H. Olivier, *Angew. Chem. Int. Ed.*, 1995, **34**, 2698-2700.

89. P. A. Z. Suarez, J. E. L. Dullius, S. Einloft, R. F. DeSouza and J. Dupont, *Polyhedron*, 1996, **15**, 1217-1219.

90. A. J. Carmichael, M. J. Earle, J. D. Holbrey, P. B. McCormac and K. R. Seddon, *Org. Lett.*, 1999, **1**, 997-1000.

91. W. P. Chen, L. J. Xu, C. Chatterton and J. L. Xiao, *Chem. Commun.*, 1999, 1247-1248.

92. F. McLachlan, C. J. Mathews, P. J. Smith and T. Welton, *Organometallics*, 2003, **22**, 5350-5357.

93. L. J. Xu, W. P. Chen and J. L. Xiao, *Organometallics*, 2000, **19**, 1123-1127.

94. N. D. Clement, K. J. Cavell, C. Jones and C. J. Elsevier, *Angew. Chem. Int. Ed.*, 2004, **43**, 1277-1279.

95. A. Riisager, R. Fehrmann, M. Haumann and P. Wasserscheid, *Eur. J. Inorg. Chem.*, 2006, 695-706.

96. A. Riisager, R. Fehrmann, M. Haumann and P. Wasserscheid, *Top. Catal.*, 2006, **40**, 91-102.

97. H.-P. Steinrück, J. Libuda, P. Wasserscheid, T. Cremer, C. Kolbeck, M. Laurin, F. Maier, M. Sobota, P. S. Schulz and M. Stark, *Adv. Mater.*, 2011, **23**, 2571-2587.

98. K. R. J. Lovelock, E. F. Smith, A. Deyko, I. J. Villar-Garcia, P. Licence and R. G. Jones, *Chem. Commun.*, 2007, 4866-4868.

99. A. Deyko and R. G. Jones, *Faraday Discuss.*, 2012, **154**, 265-288.

100. I. Niedermaier, M. Bahlmann, C. Papp, C. Kolbeck, W. Wei, S. K. Calderon, M. Grabau, P. S. Schulz, P. Wasserscheid, H.-P. Steinrück and F. Maier, *J. Am. Chem. Soc.*, 2014, **136**, 436-441.

101. F. J. M. Rutten, H. Tadesse and P. Licence, *Angew. Chem. Int. Ed.*, 2007, **46**, 4163-4165.

102. S. Rivera-Rubero and S. Baldelli, *J. Phys. Chem. B*, 2006, **110**, 4756-4765.

103. T. Iimori, T. Iwahashi, K. Kanai, K. Seki, J. H. Sung, D. Kim, H. O. Hamaguchi and Y. Ouchi, *J. Phys. Chem. B*, 2007, **111**, 4860-4866.

104. Y. Jeon, J. Sung, W. Bu, D. Vaknin, Y. Ouchi and D. Kim, *J. Phys. Chem. C*, 2008, **112**, 19649-19654.

105. J. Bowers, M. C. Vergara-Gutierrez and J. R. P. Webster, *Langmuir*, 2004, **20**, 309-312.

106. E. Sloutskin, E. Solutskin, B. M. Ocko, L. Tamam, L. Taman, I. Kuzmenko, T. Gog and M. Deutsch, *J. Am. Chem. Soc.*, 2005, **127**, 7796-7804.

107. V. Halka, R. Tsekov and W. Freyland, *Phys. Chem. Chem. Phys.*, 2005, **7**, 2038-2043.

108. M. G. Freire, P. J. Carvalho, A. M. Fernandes, I. M. Marrucho, A. J. Queimada and J. A. P. Coutinho, *J. Colloid Interface Sci.*, 2007, **314**, 621-630.

109. W. Jiang, Y. T. Wang, T. Y. Yan and G. A. Voth, *J. Phys. Chem. C*, 2008, **112**, 1132-1139.

110. A. S. Pensado, P. Malfreyt and A. A. H. Padua, *J. Phys. Chem. B*, 2009, **113**, 14708-14718.

111. K. R. Seddon and N. V. Plechkova, *Ionic Liquids unCOILed: Critical Expert Overviews*, John Wiley & Sons, New Jersey, 2012.

112. S. Caporali, U. Bardi and A. Lavacchi, *J. Electron Spectrosc. Relat. Phenom.*, 2006, **151**, 4-8.

113. O. Höfft, S. Bahr, M. Himmerlich, S. Krischok, J. A. Schaefer and V. Kempter, *Langmuir*, 2006, **22**, 7120-7123.

114. S. Krischok, M. Eremtchenko, M. Himmerlich, P. Lorenz, J. Uhlig, A. Neumann, R. Ottking, W. J. D. Beenken, O. Höfft, S. Bahr, V. Kempter and J. A. Schaefer, *J. Phys. Chem. B*, 2007, **111**, 4801-4806.

115. E. F. Smith, I. J. Villar Garcia, D. Briggs and P. Licence, *Chem. Commun.*, 2005, 5633-5635.

116. E. F. Smith, F. J. M. Rutten, I. J. Villar-Garcia, D. Briggs and P. Licence, *Langmuir*, 2006, **22**, 9386-9392.

117. F. Maier, J. M. Gottfried, J. Rossa, D. Gerhard, P. S. Schulz, W. Schwieger, P. Wasserscheid and H.-P. Steinrück, *Angew. Chem. Int. Ed.*, 2006, **45**, 7778-7780.

118. D. S. Silvester, T. L. Broder, L. Aldous, C. Hardacre, A. Crossley and R. G. Compton, *Analyst*, 2007, **132**, 196-198.

119. V. Lockett, R. Sedev, C. Bassell and J. Ralston, *Phys. Chem. Chem. Phys.*, 2008, **10**, 1330-1335.

120. C. Kolbeck, T. Cremer, K. R. J. Lovelock, N. Paape, P. S. Schulz, P. Wasserscheid, F. Maier and H.-P. Steinrück, *J. Phys. Chem. B*, 2009, **113**, 8682-8688.

121. T. Cremer, C. Kolbeck, K. R. J. Lovelock, N. Paape, R. Wölfe, P. S. Schulz, P. Wasserscheid, H. Weber, J. Thar, B. Kirchner, F. Maier and H.-P. Steinrück, *Chem. Eur. J.*, 2010, **16**, 9018-9033.

122. I. J. Villar-Garcia, E. F. Smith, A. W. Taylor, F. L. Qiu, K. R. J. Lovelock, R. G. Jones and P. Licence, *Phys. Chem. Chem. Phys.*, 2011, **13**, 2797-2808.

123. S. Men, B. B. Hurisso, K. R. J. Lovelock and P. Licence, *Phys. Chem. Chem. Phys.*, 2012, **14**, 5229-5238.

124. S. Men, D. S. Mitchell, K. R. J. Lovelock and P. Licence, *ChemPhysChem*, 2015, **16**, 2211-2218.

125. K. R. J. Lovelock, I. J. Villar-Garcia, F. Maier, H.-P. Steinrück and P. Licence, *Chem. Rev.*, 2010, **110**, 5158-5190.

126. D. Yoshimura, T. Yokoyama, T. Nishi, H. Ishii, R. Ozawa, H. Hamaguchi and K. Seki, *J. Electron Spectrosc. Relat. Phenom.*, 2005, **144**, 319-322.

127. K. Kanai, T. Nishi, T. Iwahashi, Y. Ouchi, K. Seki, Y. Harada and S. Shin, *J. Electron Spectrosc. Relat. Phenom.*, 2009, **174**, 110-115.

128. T. Nishi, T. Iwahashi, H. Yamane, Y. Ouchi, K. Kanai and K. Seki, *Chem. Phys. Lett.*, 2008, **455**, 213-217.

129. I. J. Villar-Garcia, S. Fearn, G. F. De Gregorio, N. L. Ismail, F. J. V. Gschwend, A. J. S. McIntosh and K. R. J. Lovelock, *Chem. Sci.*, 2014, **5**, 4404-4418.

130. I. J. Villar-Garcia, S. Fearn, N. L. Ismail, A. J. S. McIntosh and K. R. J. Lovelock, *Chem. Commun.*, 2015, **51**, 5367-5370.

131. J. M. Gottfried, F. Maier, J. Rossa, D. Gerhard, P. S. Schulz, P. Wasserscheid and H.-P. Steinrück, *Z. Phys. Chem.*, 2006, **220**, 1439-1453.

132. C. Kolbeck, M. Killian, F. Maier, N. Paape, P. Wasserscheid and H.-P. Steinrück, *Langmuir*, 2008, **24**, 9500-9507.

133. A. R. Santos, R. K. Blundell and P. Licence, *Phys. Chem. Chem. Phys.*, 2015, **17**, 11839-11847.

134. C. Kolbeck, N. Taccardi, N. Paape, P. S. Schulz, P. Wasserscheid, H.-P. Steinrück and F. Maier, *J. Mol. Liq.*, 2014, **192**, 103-113.

135. C. Kolbeck, N. Paape, T. Cremer, P. S. Schulz, F. Maier, H.-P. Steinrück and P. Wasserscheid, *Chem. Eur. J.*, 2010, **16**, 12083-12087.

136. C. Kolbeck, I. Niedermaier, A. Deyko, K. R. J. Lovelock, N. Taccardi, W. Wei, P. Wasserscheid, F. Maier and H.-P. Steinrück, *Chem. Eur. J.*, 2014, **20**, 3954-3965.

137. T. Hammer, M. Reichelt and H. Morgner, *Phys. Chem. Chem. Phys.*, 2010, **12**, 11070-11080.

138. C. Ridings, V. Lockett and G. Andersson, *Phys. Chem. Chem. Phys.*, 2011, **13**, 17177-17184.

139. K. Nakajima, A. Ohno, H. Hashimoto, M. Suzuki and K. Kimura, *J. Chem. Phys.*, 2010, **133**, 7.

140. A. Ohno, H. Hashimoto, K. Nakajima, M. Suzuki and K. Kimura, *J. Chem. Phys.*, 2009, **130**, 5.

141. X. Paredes, J. Fernandez, A. A. H. Padua, P. Malfreyt, F. Malberg, B. Kirchner and A. S. Pensado, *J. Phys. Chem. B*, 2014, **118**, 731-742.

2. Experimental

2.1 X-ray Photoelectron Spectroscopy

X-ray photoelectron spectroscopy (XPS) is a surface sensitive analytical technique and is possibly the most widely used electron spectroscopy method.[1] Developments made by Kai Siegbahn in the 1960s enabled the measurement of binding energies of core level electrons ejected from a sample *via* X-ray irradiation under ultra-high vacuum (UHV) conditions, and to the present day this technique is valued for its capacity to provide vital information on elemental composition and chemical state of atoms in the near-surface region ($\leq$ 10 nm).[2]

2.1.1 Photoelectric Effect

The basic principle that forms the foundation of XPS is the photoelectric effect. Whereby, in a standard XPS experiment, a sample is irradiated with X-ray photons, which are capable of penetrating many micrometres into the bulk material. On collision with an electron the photon is annihilated with complete energy transfer to the electron. If the energy transferred is sufficient the electron will be ejected from the atom, as illustrated by Figure 2.1.

The attenuation length (average distance travelled between two inelastic events without elastic events) of an emitted photoelectron is dependent on the X-ray energy. For the typical Al Kα X-ray source ($h\nu$ = 1486.6 eV) the subsequent information depth (ID) is approximately 10 nm.[3] Therefore, only photoelectrons emitted in the near-surface region can escape and be detected, thus defining the surface sensitive nature of XPS.

The kinetic energy (KE) of an emitted photoelectron (which has not suffered energy losses from inelastic collisions) can be measured. This value is discrete in nature and is dependent on the energy of the incident X-ray photon ($h\nu$), the binding energy (BE), and the work function of the spectrometer (ϕ_s), as shown by Equation 2.1.

$$KE = h\nu - BE - \phi_S \qquad \mathbf{2.1}$$

The binding energy is measured relative to the Fermi level (highest occupied quantum level) of the sample, and is regarded as the energy gap between the initial and final states of the photoelectron process; its value is both element and orbital specific. The spectrometer work function describes the energy required to remove an electron from the Fermi level to the vacuum level, the spectrometer automatically corrects for this value during analysis (typically ≈ 4.5 eV).[3] Consequently, as KE, hν and ϕ are either known or can be measured, the binding energy can be derived using Equation 2.1.

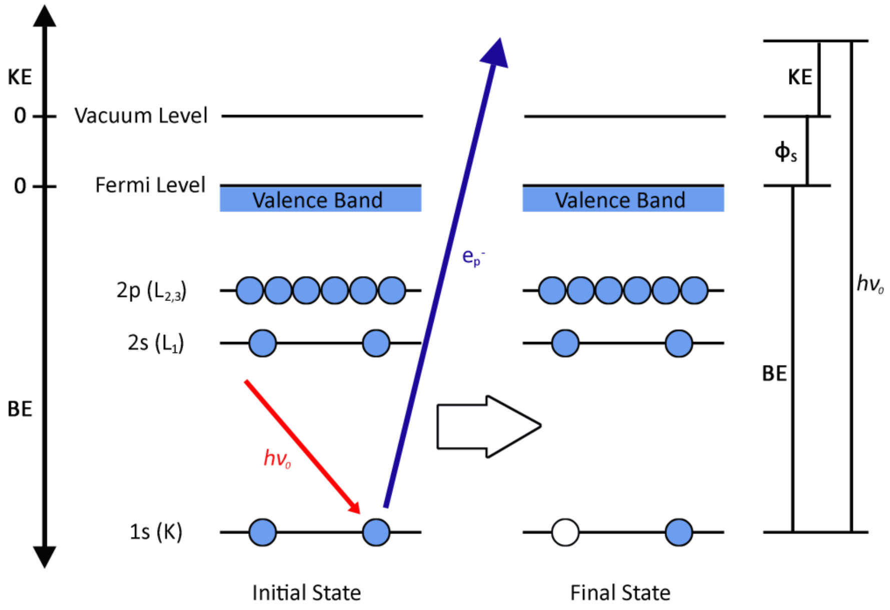

Figure 2.1. Schematic describing the Photoelectric Effect. An X-ray photon of energy ($h\nu_0$) collides with a core level electron in the initial state, thus ejecting it from the atom. This results in a final state with a core hole. The KE of the emitted photoelectron, e_p^-, is related to $h\nu_0$, BE and ϕ_S as described in Equation 2.1.

XPS experiments are generally performed under UHV conditions. This is to minimise gas phase collisions of emitted photoelectrons, which would otherwise result in significant scattering and hence low detection. Additionally, at UHV the impingement rate of gas molecules with the surface is very low, thus promoting a clean surface for analysis. Volatile contaminants, and dissolved gases, present in the sample will also be removed under UHV conditions, thus improving surface purity.[4]

2.1.2 XP Spectrometer Set-up

A schematic of a typical XP spectrometer set-up is shown in Figure 2.2. X-rays are generated by bombarding a metal anode (usually aluminium) with high energy electrons; in this work both aluminium and silver anodes are utilised. The electron bombardment subsequently results in the emission of X-rays of energy characteristic to the source, e.g. Al Kα = 1486.6 eV or Ag Lα’ = 2984.3 eV. Additional radiation including X-ray satellites, Bremsstrahlung radiation and Auger emissions are also produced to a lesser intensity.[1]

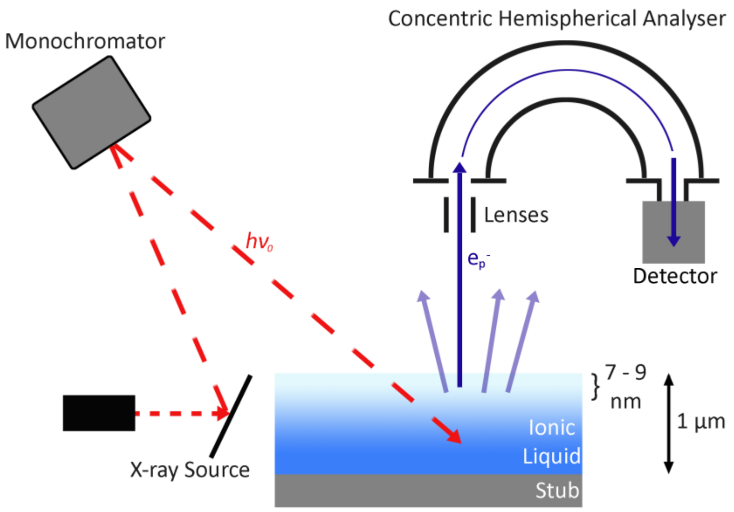

Figure 2.2. Schematic of XP spectrometer set-up.

The line width of the generated X-rays is then reduced by diffraction against a quartz crystal monochromator; with reductions from 0.9 eV to approximately 0.25 eV for Al Kα, and from 2.6 to 1.2 eV for Ag Lα’.[2] Additionally, the monochromator removes any unwanted spectral lines, and focuses the X-rays onto a small spot (down to 10 μm) on the sample surface.[3] The monochromator also provides a greater degree of separation between the sample and source, thereby minimising sample damage from exposure to heat and back-scattered electrons.

Photoelectrons emitted from the sample pass through transfer lenses to the analyser. The most commonly employed analyser is the concentric hemispherical analyser (CHA), in which emitted photoelectrons pass between two concentric plates set at different voltages. Typically, the CHA works in combination with transfer lenses in Fixed Analyser Transmission (FAT) mode. In this mode, the voltage of the concentric plates are fixed for a given photoelectron kinetic energy – known as the pass energy. Before reaching the analyser the photoelectrons must first pass through a series of electrostatic transfer lenses which slow down the photoelectrons to the required pass energy and focus them towards the analyser. Therefore, in order to obtain a photoelectron spectrum, the lens voltages are scanned to focus, sequentially, photoelectrons of varying kinetic energies to the required pass energy. As the pass energy remains constant throughout the energy range, the resolution (in eV) is constant across the entire width of the spectrum.[2]

A typical detector consists of an electron multiplier, to count individual electrons arriving at the detector, and a delay line detector (DLD). The two most common multipliers used are channel electron multipliers and channel plates.

2.1.3 Charge Control and Charge Correction

As discussed in *Section 2.1.1* binding energies are measured relative to the energy of the Fermi level. For conducting samples in electrical contact with the spectrometer the Fermi levels of the sample and spectrometer align. Consequently, positively charged holes created at the sample surface by exiting photoelectrons are quickly dissipated by the flow of electrons from spectrometer to sample.

However, for insulating compounds no such equilibrating mechanism exists, *i.e.* the Fermi levels of the sample and spectrometer are not in alignment. As such, during photoelectron emission, a build-up of positive charge accumulates at the sample surface, thus its potential with respect to the spectrometer changes with time. The result of this sizeable, positive potential difference is the entire XP spectrum to shift to lower kinetic energies (higher apparent binding energies).[5] To compensate for surface charging, charge control methods need to be applied. Charge neutralisation is the most common charge control approach and involves flooding the surface with low energy electrons to neutralise the positive charge.

Generally, charge neutralisation results in overcompensation and the surface will become slightly negatively charged, causing the observed binding energies to subtly shift to lower energies. Consequently, for such samples it is necessary to use charge correction methods (even after charge neutralisation) to obtain an accurate binding energy scale. Typically, charge correction involves calibrating the spectrum by referencing to a photoelectron peak of known binding energy. There are several methods for charge correction, however referencing to an internal standard is the most common as surface charging effects will be experienced equally by the reference and the sample.

Ionic liquids are conducting when in the liquid state; hence, charge control methods (*i.e.* charge neutralisation) are not usually required for liquid ILs. However, as ILs are ionic conductors, rather than electron conductors, they act as insulators in the solid state.[5] Therefore, charge neutralisation must be applied for solid IL samples to prevent surface charging.[6-8]

In order to measure true binding energy values for ILs, the application of charge correction methods is standard for all types of ionic liquid. It has become common practice to charge correct by referencing the spectra to the signal corresponding to the aliphatic carbon atoms ($C_{aliphatic}$ 1s, BE = 285.0 eV) present in most ILs.[5, 8-12]

2.1.4 Surface Cleaning with Argon Sputtering

Due to the highly surface sensitive nature of XPS even small levels of contaminants can have a profound effect on the measured spectra. A problem associated with contaminants is unexpected photoelectron lines which can be excessively intense and/or overlap with photoelectron lines of the sample. This can prevent accurate determination of elemental composition and chemical state analysis of the sample.

If the contamination is surface segregated, argon ion sputtering can be used to etch the surface and remove the contaminant, with typical sputter energies of 0.5 – 5.0 keV. This process involves bombarding the surface with a beam of energetic argon ions. This removes the top few layers of atoms, thus exposing a clean surface that is free of contaminant below.

2.2 The XP spectrum

There are two types of XP spectra that can be measured: survey (or wide) scans and high-resolution scans. For a survey scan photoelectrons emitted from the entire energy range of the spectrometer are recorded, this is typically used to determine sample purity and elemental composition. High-resolution scans focus upon a specific energy region and are used to determine binding energies with higher accuracy.

2.2.1 Survey Scan

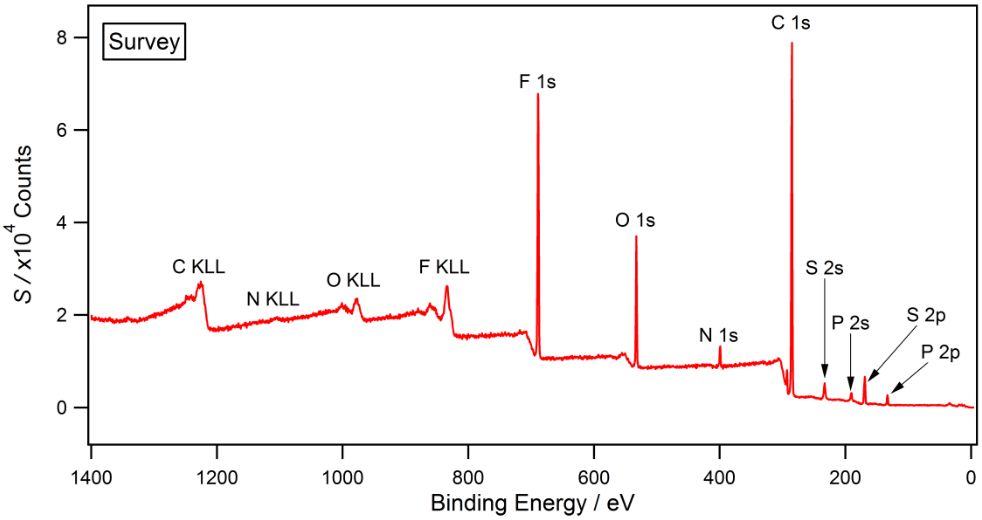

Figure 2.3. Survey (wide) XP spectra of the ionic liquid $[P_{6,6,6,14}][NTf_2]$ acquired with Al Kα X-rays. Charge corrected by referencing the $C_{aliphatic}$ 1s photoelectron emission peak to 285.0 eV.

An example survey scan for the ionic liquid $[P_{6,6,6,14}][NTf_2]$ is presented in Figure 2.3. In this case the spectrum was acquired with the Al Kα X-ray source and the energy range subsequently covers 0 – 1400 eV. The spectrum consists of a series of peaks situated on a background that decreases in a step-like manner after each spectral feature from high to low binding energy. The main photoelectron lines occur in the energy range 30 – 800 eV and are well-defined sharp peaks. Photoelectron binding energies are both element and orbital specific, thus each element has a characteristic set of spectral lines, which can be used for element identification. The exceptions to this are hydrogen and helium, which are not detectable by XPS as their photoelectron cross sections are below XPS detection limits.[1] Photoelectrons which experience energy losses *via* inelastic scattering before escaping the surface contribute to the background signal.

Another spectral feature of the survey scan are Auger peaks, which occur between 800 – 1400 eV in Figure 2.3. These peaks arise from internal atom de-excitation of the core holes produced by photoemission, as illustrated by Figure 2.4. In this example, a K level core hole is “filled” by an L_1 level electron, energy equal to the difference in binding energy of the K and L_1 levels is released and is sufficient to eject an electron from the $L_{2,3}$ level. This is known as a $KL_1L_{2,3}$ transition; however, it should be noted that many other combinations also exist.

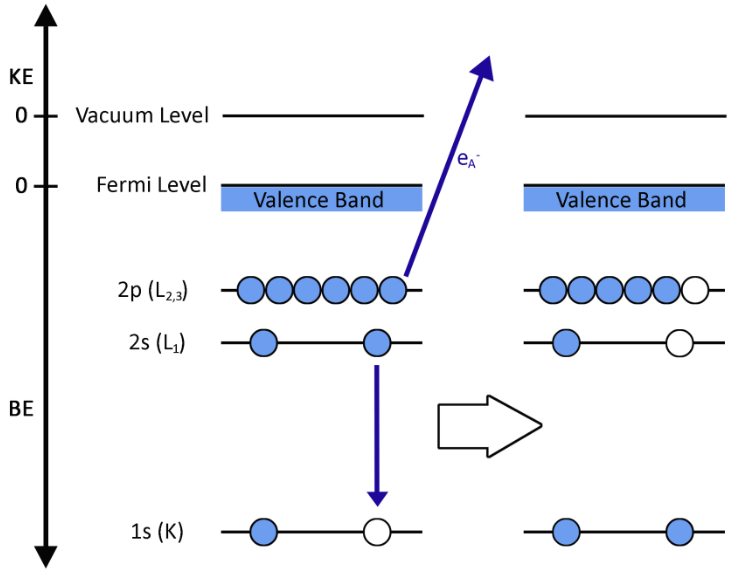

Figure 2.4. Schematic illustrating Auger electron emission (e_A^-) after initial photoionisation. This example illustrates a $KL_1L_{2,3}$ Auger transition. The core hole is filled by an electron “falling” from the L_1 level to K level. Energy liberated is transferred to an electron in the $L_{2,3}$ level, which is ejected from the atom.

The kinetic energy of the emitted Auger electron is only dependent on the energy levels of the element. Subsequently, Auger kinetic energies are characteristic of the emitting atom, and can be used for element identification using the kinetic energy scale.

At binding energies ~ 0 – 30 eV the valence band spectral feature can be seen. This consists of a series of low intensity lines which correspond to photoelectrons emitted from the valence band.

2.2.2 High Resolution Scan

A high resolution scan focuses on a narrow energy range (typically between 10 – 50 eV) which contains a core photoelectron line, as exemplified by the C 1s high resolution scan for $[P_{6,6,6,14}][NTf_2]$ shown in Figure 2.5. In comparison to the survey scan, a smaller energy step size and lower pass energy are applied in combination with longer acquisition times, which significantly improves spectra resolution. Consequently, high resolution spectra enable a greater degree of accuracy in binding energy analysis, which provides vital information on element/component electronic environments.

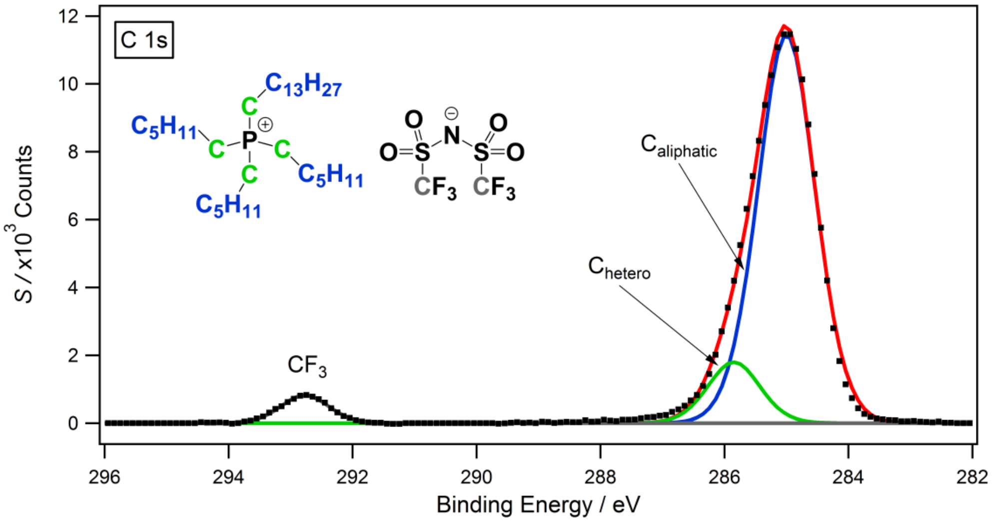

Figure 2.5. C 1s high resolution spectra including component fittings for $[P_{6,6,6,14}][NTf_2]$. Charge corrected by referencing the $C_{aliphatic}$ 1s photoelectron emission peak to 285.0 eV.

As seen from Figure 2.5 it is not always possible to resolve different contributions to the photoelectron emission spectra if they are particularly close in energy. It is, therefore, important to develop fitting models that accurately describe the different chemical environments of an element in order to determine their binding energies. C1s fitting models have previously been described by the University of Nottingham for imidazolium,[5] pyrrolidinium,[13] pyridinium,[14] and guanidinium-based ILs.[15] In this *Thesis* C 1s fitting models for tetraalkylammonium/phosphonium and functionalised ILs have been developed and described (see *Chapter 3 Sections 3.2.3* and *3.3.3*, and *Chapter 5 Section 5.2.2*).

2.2.3 Information from XP spectra

2.2.3.1 Semi-quantitative Analysis

As mentioned previously each element (excluding hydrogen and helium) exhibit at least one core level line in the photoelectron spectrum. The peak positions for these core level lines, when measured on a binding energy scale, are sufficiently unique to enable elemental identification. Therefore, a single survey scan allows complete elemental analysis.[3] Typical survey scan detection limits are 0.1 atomic % for elements with low photoelectron cross-section core levels.

The intensity of any specific photoelectron peak is dependent on its photoelectron cross-section (which in turn is element and orbital specific), consequently a direct comparison of peak areas does not provide useful information on relative atomic concentrations. Therefore, scaling of each photoelectron peak with the empirically derived relative sensitivity factor (RSF) obtained from the Kratos Library is required. This enables the relative atomic concentrations to be determined semi-quantitatively (accuracy 10 – 20 %).

2.2.3.2 Chemical State Analysis

Binding energies obtained from XPS can be regarded as its most valuable output. The measured binding energy of a photoelectron line is a function of the local chemical environment of the atom it originated from. Factors such as type of bonding, oxidation state and surrounding atoms can influence the electron density of an atom, and hence cause a measurable shift in binding energy; this is known as a “chemical shift”.

Typically, a decrease in electron density of an atom, which may be caused by an increase in oxidation state or neighbouring electron withdrawing atoms/groups, generally results in an increase in binding energy. Whereas, increasing electron densities will give rise to lower binding energy values. Photoelectron lines corresponding to different chemical environments of the same element can therefore be distinguished from each other as seen from the C 1s region in Figure 2.5. As discussed previously in *Section 2.2.2* curve fitting may be required to resolve the different components in order to accurately measure their binding energies. The associated error with binding energy measurement is ± 0.1 eV.

2.3 Synthesis of ILs

2.3.1 Materials and Instrumentation

Compounds investigated herein were prepared in our laboratory using modified literature procedures.[16] Chemical precursors were obtained from commercial suppliers and used without further purification unless otherwise stated. Trihexyl(tetradecyl)phosphonium chloride (Cyphos IL 101), Tetraoctylphosphonium bromide (Cyphos 482), and tributyl(methyl)phosphonium methylsulfate (Cyphos IL 108) were obtained from Cytec Industries Inc. Lithium bis(trifluoromethanesulfonyl)imide was obtained from 3M. Tetrakis(triphenylphosphine)palladium(0) 99% was obtained from Acros Organics.

All compounds were dried *in vacuo* ($p \leq 10^{-2}$ mbar) at 50 °C and stored under argon before being characterised by ^{1}H and ^{13}C for all ionic liquids, and ^{31}P-{^{1}H} and ^{19}F-{^{1}H} NMR where appropriate, (recorded at room temperature on a Brucker DPX-400 or DPX-300 spectrometer). Chemical shifts (δ) are reported in parts per million (ppm) with reference to residual traces of protonated solvents in commercial NMR solvents: protonated chloroform (δ_H 7.27) and $CDCl_3$ (δ_C 77.00), and protonated dimethyl sulfoxide (δ_H 2.50) and $(CD_3)_2SO$ (δ_C 39.51). Coupling constants (*J*) are given in Hz and multiplicities were labelled singlet (s), doublet (d), t (triplet), q (quartet), quint (quintet), sext (sextet), sep (septet), dd (double doublet), tt (triple triplet) and m (multiplet). Further characterisation methods also included IR (Perkin Elmer 1600 FT spectrometer); ESI-MS (Brucker MicroTOF 62 spectrometer) and XPS (Kratos

Axis Ultra Spectrometer) for all ILs studied. For syntheses which involved anion exchange chemistries, ion chromatography (Dionex ICS-3000 machine fitted with AS20 analytical column and AG20 guard column) showed that residual halide was below the detection limits of the instrument (~ 10 ppm). TEM measurements were performed using a JEOL 2100F instrument equipped with a Gatan Orius camera with an operating voltage of 200 kV. TEM data was analysed using the Gatan Digital Micrograph software. Holey carbon coated copper TEM grids were used and purchased from Agar Scientific.

2.3.2 XPS Data Collection

Aluminium Source Experiments: XP spectra were recorded using a Kratos Axis Ultra spectrometer employing a focused, monochromated Al Kα source ($h\nu$ = 1486.6 eV), hybrid (magnetic/electrostatic) optics, concentric hemispherical analyser, and a multi-channel plate and delay line detector (DLD) with an X-ray incident angle of 60° (relative to the analyser). X-ray gun power was set to 120 W. Spectra were recorded using an entrance aperture 300 μm × 700 μm with a pass energy of 80 eV and step size 0.5 eV for survey spectra, and pass energy 20 eV and step size 0.1 eV for high resolution spectra. Acquisition times for survey scans and high resolution scans were 1200 s and 600 s respectively.

Silver Source Experiments: XP spectra were recorded using a Kratos Axis Ultra Spectrometer in which the Al Kα source was substituted with a monochromated Ag Lα' source (2984.3 eV) operated at the same X-ray gun power (120 W) with minor adjustments to the gun position and monochromating crystals. All spectra were recorded with an entrance aperture of 300 μm × 700 μm with pass energy of 160 eV and step size 1.0 eV for survey spectra, and pass energy of 40 eV and step size 0.2 eV for high resolution spectra. Acquisition times for surveys scans and high resolution scans were 2400 s and 1200 s respectively.

For both sources binding energy calibration was made using Au $4f_{7/2}$ (83.96 eV), Ag $3d_{5/2}$ (368.21 eV) and Cu $2p_{3/2}$ (932.62 eV). The resolution of the photoelectron detector was based on the Ag $3d_{5/2}$ peak full width half maximum (FWHM), with the values obtained for each source as follows: Al Kα (Ag $3d_{5/2}$ FWHM = 0.55 eV); Ag Lα’ (Ag $3d_{5/2}$ FWHM = 0.90 eV).

Charge neutralisation (used for solid samples only) was applied using a standard Kratos charge neutraliser consisting of a filament, coaxial with the electrostatic and magnetic transfer lenses, and a balance plate which creates a potential between the neutraliser and sample. Charge neutralisation was applied at 1.9 A filament current and 3.3 V balance plate voltage. Sample stubs were earthed *via* the instrument stage using a standard BNC connector.

The preparation method for each sample is dependent on the nature of the material to be analysed, and the type of experiment. *For standard XP experiments*: liquid samples were prepared by placing a small drop (≈ 10 mg) of ionic liquid onto a stainless steel multi-sample bar; solid samples were fixed to the bar using double-sided adhesive tape. *For ARXPS and ERXPS experiments*: A small drop (≈ 10 mg) of a liquid sample was placed on a stainless steel sample bar and cast into a thin film (approx. thickness 0.5 – 1.0 mm). Samples were pre-pumped in a preparative chamber to pressures lower than 1×10^{-6} mbar before transfer to the main analytical chamber. Pressure in the main chamber consistently remained $\leq 1\times 10^{-8}$ mbar during XPS measurements.

2.3.3 XPS Data Analysis

Data was analysed using the CASAXPS (Version 2.3.17 dev 6.6) software. The Al Kα source was used to determine elemental composition using RSFs taken from the Kratos Library (RSF F 1s = 1) and used to determine relative atomic percentages from high-resolution scans of the most intense photoelectron peak for each element. Depending on background shape a two-point linear, Shirley or linear spline background subtraction was performed to measure peak areas. Peaks were fitted using GL (30) lineshapes (70 % Gaussian, 30 % Lorentzian).

For ILs with a long alkyl chain ($n \geq 8$) charge referencing was achieved by setting the experimentally determined binding energy of the aliphatic component ($C_{aliphatic}$) equal to 285.0 eV. For compounds with a short alkyl chain ($n < 8$) charge referencing was achieved by setting the measured binding energy of the cationic heteroatom photoelectron emission peak equal to that for its long chain analogue, *i.e.* N_{cation} 1s for $[N_{4,4,4,1}][NTf_2]$ was set equal to 402.5 eV (where 402.5 eV is the measured binding energy of N_{cation} 1s for $[N_{6,6,6,14}][NTf_2]$). If neither charge referencing method is applicable to the IL investigated it is stated otherwise within the text with an alternative provided.

ARXPS experiments at grazing emission angle ($\theta \geq 70°$) give significantly lower signal intensity than experiments at normal emission angle ($\theta = 0°$). Therefore, to aid visual interpretation of the ARXPS spectra presented, each spectrum recorded $\theta = 80°$ is normalised to the area of the F 1s photoelectron emission peak recorded for the respective ionic liquid at $\theta = 0°$. This peak was selected for normalisation as the F 1s moiety is present in all ILs in the same stoichiometry, and the F 1s peak is easily identifiable with a binding energy well separated from any other photoelectron emission signals. This technique does not affect the relative ratios of different elements within the IL, thus provides a visual comparison of the same region for an IL on changes to emission angle. Therefore, any changes in intensity of an element with emission angle can be observed.

2.3.4 Information Depth for ARXPS and ERXPS

The information depth (ID) can be defined as the depth, within the sample, from which 95.7 % of the measured signal will originate and can be expressed as $ID = 3\lambda_{AL}\cos\theta$. For the lower energy Al Kα X-ray source, ID varies mainly with $\cos\theta$, where θ is the electron emission angle relative to the surface normal. At the kinetic energies measured here (~ 800 – 1400 eV) the attenuation length of photoelectrons in organic compounds is of the order of ~ 3 nm.[17] From this, the ID in each of angle-resolved geometries employed in the ARXPS experiments can be estimated. Therefore, when $\theta = 0°$, ID = 7 – 9 nm (*N.B.* this value is also dependent on the kinetic energy of the escaping photoelectron, and therefore the identity of the element probed) and for $\theta = 80°$, ID = 1 – 1.5 nm. It should be noted that at 80°, 65 % of the signal intensity arises from the uppermost 0.3 – 0.5 nm; this is less than the width of a single molecule for most ILs. An increase in element/component intensity with increasing θ, and thus with increasing surface sensitivity, indicates a higher concentration of this element in the top most layers.

When using the higher energy Ag Lα’ X-ray source for ERXPS studies, a fixed normal emission angle of $\theta = 0°$ is used. Consequently ID can be simplified to ID = $3\lambda_{AL}$, thus ID is solely a function of attenuation length and hence kinetic energy. As a larger kinetic range is investigated ~ 100 – 2800 eV, ID will be very dependent on the kinetic energy of an escaping photoelectron, and hence the core orbital from which it originated. A full description of this technique is provided in *Chapter 4 Section 4.5*.

2.3.5 Ammonium-based ILs – Synthetic Procedures

2.3.5.1 [$N_{6,6,6,14}$]Cl

Trihexyl(tetradecyl)ammonium bromide (3.27 g, 5.97 mmol) was dissolved in methanol (100 ml) and eluted through a column containing Amberlite-IRA400 (Cl) ion-exchange resin (40 g) at a drop rate of 1 ml/min. The solvent was removed and the product was dried *in vacuo* at 50 °C to yield an off-white solid (3.0 g, 100 %). ^{1}H NMR (400 MHz, $CDCl_3$): δ ppm 0.81 – 0.86 (m, 12H), 1.20 – 1.36 (m, 40H), 1.57 – 1.68 (m, 8H), 3.30 – 3.34 (m, 8H); ^{13}C NMR (101 MHz, $CDCl_3$): δ ppm 13.7, 14.0, 22.1, 22.3, 22.5, 25.9, 26.3, 29.0, 29.2, 29.3, 29.5, 31.1, 31.8, 59.0; IR ν max ($CHCl_3$) / cm^{-1} 1246, 1468, 2858, 2929; MS (ESI) positive for $C_{32}H_{68}N$, M^+: calcd 466.5346, found 466.5346.

2.3.5.2 [$N_{6,6,6,14}$][BF_4]

To a stirring solution of trihexyl(tetradecyl)ammonium bromide (2.18 g, 3.98 mmol) in chloroform (15 ml) a solution of sodium tetrafluoroborate (0.6 g, 5.36 mmol) in water (15 ml) was added dropwise at room temperature. The reaction mixture was stirred for 16 h. Chloroform (40 ml) and water (15 ml) was added, and the organic layer was separated and washed with water (6 × 25 ml). The solvent was removed and the product was dried *in vacuo* at 50 °C to yield a white solid (1.72 g, 78 %). ^{1}H NMR (400 MHz, $CDCl_3$): δ ppm 0.86 – 0.90 (m, 12H), 1.25 – 1.34 (m, 40H), 1.54 – 1.66 (m, 8H), 3.15 – 3.20 (m, 8H); ^{13}C NMR (101 MHz, $CDCl_3$): δ ppm 13.8, 14.1, 25.8, 26.2, 29.0, 29.3, 29.4, 29.6, 31.1, 31.9, 58.6; ^{19}F NMR (377 MHz, $CDCl_3$): δ ppm -151.79 (q, *J* = 1.1 Hz), -151.73 (br. s); IR ν max ($CHCl_3$) / cm^{-1} 1059, 1468, 2857, 2929, 2959; MS (ESI) positive for $C_{32}H_{68}N$, M$^+$: calcd 466.5346, found 466.5333.

2.3.5.3 [$N_{6,6,6,14}$][PF_6]

To a stirring suspension of trihexyl(tetradecyl)ammonium bromide (1.85 g, 3.38 mmol) in water (30 ml) an aqueous solution of hexafluorophosphoric acid (60 % w/w, 0.60 ml, 3.92 mmol) was added dropwise using a plastic syringe. The reaction mixture was stirred for 16 h at room temperature. Chloroform (55 ml) was added and the organic layer was separated and washed with water (6 × 25 ml). The solvent was removed and the product was dried *in vacuo* at 50 °C to yield a white, waxy solid (1.96 g, 95 %). ^{1}H NMR (400 MHz, $CDCl_3$): δ ppm 0.86 – 0.91 (m, 12H), 1.26 – 1.34 (m, 40H), 1.54 – 1.65 (m, 8H), 3.12 – 3.16 (m, 8H); ^{13}C NMR (101 MHz, $CDCl_3$): δ ppm 13.8, 14.1, 21.7, 22.3, 22.7, 25.8, 26.1, 29.0, 29.3, 29.4, 29.6, 29.7, 31.0, 31.9, 58.6; ^{31}P NMR (162 MHz, $CDCl_3$): δ ppm -144.38 (spt, *J* = 713 Hz); ^{19}F NMR (377 MHz, $CDCl_3$): δ ppm -72.30 (d, *J* = 713 Hz); IR ν max ($CHCl_3$) / cm^{-1} 848, 1468, 2857, 2929; MS (ESI) positive for $C_{32}H_{68}N$, M$^+$: calcd 466.5346, found 466.5347.

2.3.5.4 [$N_{6,6,6,14}$][OTf]

To a stirring solution of trihexyl(tetradecyl)ammonium bromide (1.80 g, 3.29 mmol) in chloroform (15 ml) a solution of lithium trifluoromethanesulfonate (0.63 g, 4.04 mmol) in water (15 ml) was added dropwise at room temperature. The reaction mixture was stirred for 16 h. Chloroform (40 ml) and water (15 ml) was added, and the organic layer was separated and washed with water (6 × 25 ml). The solvent was removed and the product was dried *in vacuo* at 50 °C to yield a pale yellow, viscous liquid (1.85 g, 91 %). ^{1}H NMR (400 MHz, $CDCl_3$): δ ppm 0.86 – 0.91 (m, 12H), 1.25 – 1.37 (m, 40H), 1.56 – 1.68 (m, 8H), 3.18 – 3.22 (m, 8H); ^{13}C NMR (101 MHz, $CDCl_3$): δ ppm 13.8, 14.1, 21.9, 22.3, 22.6, 25.9, 26.2, 29.0, 29.3, 29.4, 29.6, 31.1, 31.9, 58.8; ^{19}F NMR (377 MHz, $CDCl_3$): δ ppm -78.18; IR ν max ($CHCl_3$) / cm^{-1} 1030, 1164, 1269, 1468, 2857, 2929, 3011; MS (ESI) positive for $C_{32}H_{68}N$, M^+: calcd 466.5346, found 466.5356.

2.3.5.5 [$N_{6,6,6,14}$][NTf_2]

To a stirring solution of trihexyl(tetradecyl)ammonium bromide (1.50 g, 2.74 mmol) dissolved in chloroform (15 ml), a solution of lithium bis(trifluoromethanesulfonyl)imide (0.95 g, 3.30 mmol) in water (15 ml) was added dropwise. The reaction mixture was stirred for 16 h at room temperature. Chloroform (40 ml) and water (15 ml) was added, and the organic layer separated and washed with water (6 × 25 ml). The solvent was removed and the product was dried *in vacuo* at 50 °C to yield a pale yellow, viscous liquid (1.92 g, 94 %). ^{1}H NMR (400 MHz, $CDCl_3$): δ ppm 0.87 – 0.92 (m, 12H), 1.26 – 1.37 (m, 40H), 1.54 – 1.65 (m, 8H), 3.12 – 316 (m, 8H); ^{13}C NMR (101 MHz, $CDCl_3$): δ ppm 13.7, 14.1, 21.8, 22.3, 22.7, 25.8, 26.1, 28.9, 29.3, 29.4, 29.6, 31.0, 31.9, 58.7, 119.8 (q, J = 322 Hz); ^{19}F NMR (377 MHz, $CDCl_3$): δ ppm -78.73; IR ν max ($CHCl_3$) / cm-^{1} 1059, 1137, 1192, 1351, 1468, 1482, 2858, 2929, 2959; MS (ESI) positive for $C_{32}H_{68}N$, M^+: calcd 466.5346, found 466.5349.

2.3.5.6 [$N_{8,8,8,8}$][NTf_2]

To a stirring solution of tetraoctylammonium bromide (2.20 g, 4.02 mmol) in chloroform (15 ml), a solution of lithium bis(trifluoromethanesulfonyl)imide (1.40 g, 4.88 mmol) in water (15 ml) was added dropwise. The reaction mixture was stirred for 16 h at room temperature. Chloroform (40 ml) and water (15 ml) was added, and the organic layer separated and washed with water (6 × 25 ml). The solvent was removed and the product was dried *in vacuo* at 50 °C to yield a pale yellow, viscous liquid (2.88 g, 96 %). ^{1}H NMR (400 MHz, $CDCl_3$): δ ppm 0.87 – 0.90 (m, 12H), 1.22 – 1.43 (m, 40H), 1.54 – 1.65 (m, 8H), 3.11 – 3.15 (m, 8H); ^{13}C NMR (101 MHz, $CDCl_3$): δ ppm 14.0, 21.8, 22.5, 26.1, 28.9, 31.6, 58.7, 120.0 (q, J = 321 Hz); ^{19}F NMR (377 MHz, $CDCl_3$): δ ppm -78.73; IR ν max ($CHCl_3$)/cm^{-1} 1059, 1137, 1192, 1351, 1468, 1482, 2858, 2929, 2959; MS (ESI) positive for $C_{32}H_{68}N$, M^+: calcd 466.5346, found 466.5342.

2.3.5.7 [$N_{4,4,4,4}$][NTf_2]

To a stirring solution of tetrabutylammonium bromide (3.06 g, 9.50 mmol) in dichloromethane (15 ml), a solution of lithium bis(trifluoromethanesulfonyl)imide (4.08 g, 14.2 mmol) in water (15 ml) was added dropwise. The reaction mixture was stirred for 16 h at room temperature. Dichloromethane (75 ml) and water (25 ml) was added, and the organic layer separated and washed with water (6 × 50 ml). The solvent was removed and the product was dried *in vacuo* at 50 °C to yield a white solid (4.70 g, 95 %). ^{1}H NMR (400 MHz, $CDCl_3$): δ ppm 1.00 (t, *J* = 7.3 Hz, 12H), 1.36 – 1.46 (m, 8H), 1.55 – 1.63 (m, 8H), 3.12 – 3.16 (m, 8H); ^{13}C NMR (101 MHz, $CDCl_3$): δ ppm 13.4, 19.4, 24.7, 58.5, 120.0 (q, *J* = 322 Hz); ^{19}F NMR (377 MHz, $CDCl_3$): δ ppm -78.80; MS (ESI) positive for $C_{16}H_{36}N$, M^+: calcd 242.2842, found 242.2839. Data in agreement with reported literature values.[18]

2.3.5.8 [$N_{4,4,4,1}$][NTf_2]

To a stirring solution of tributyl(methyl)ammonium bromide (2.91 g, 10.4 mmol) in chloroform (25 ml) a solution of lithium bis(trifluoromethanesulfonyl)imide (3.58 g, 12.5 mmol) in water (25 ml) was added dropwise at room temperature. The reaction mixture was stirred for 16 h. Chloroform (75 ml) and water (25 ml) was added, and the organic layer separated and washed with water (6 × 50 ml). The solvent was removed and the product was dried *in vacuo* at 50 °C to yield a colourless, viscous liquid (4.53 g, 91 %). ^{1}H NMR (400 MHz, $CDCl_3$): δ ppm 1.00 (t, *J* = 7.3 Hz, 9H), 1.36 – 1.45 (m, 6H), 1.60 – 1.68 (m, 6H), 2.99 (s, 3H), 3.20 (m, 6H); ^{13}C NMR (101 MHz, $CDCl_3$): δ ppm 13.4, 19.4, 24.1, 48.4, 61.7, 119.9 (q, *J* = 321 Hz); ^{19}F NMR (377 MHz, $CDCl_3$): δ ppm -78.90; MS (ESI) positive for $C_{13}H_{30}N$, M^+: calcd 200.2373, found 200.2381. Data in agreement with reported literature values.[19]

2.3.5.9 [$N_{4,4,4,1}$][BF_4]

To a stirring solution of tributyl(methyl)ammonium bromide (2.92 g, 10.4 mmol) in water (20 ml) a solution of sodium tetrafluoroborate (1.70 g, 15.7

mmol) in water was added dropwise. The reaction mixture was stirred vigorously for 16 h at room temperature. Dichloromethane (50 ml) was added, and the organic layer separated and washed with water (6 × 25 ml). The solvent was removed and the product was dried *in vacuo* at 50 °C to yield a white solid (2.14 g, 72 %). ^{1}H NMR (400 MHz, $CDCl_3$): δ ppm 0.97 (t, J = 7.3 Hz, 9H), 1.35 – 1.44 (m, 6H), 1.60 – 1.68 (m, 6H), 3.01 (s, 3H), 3.22 (m, 6H); ^{13}C NMR (101 MHz, $CDCl_3$): δ ppm 13.4, 19.5, 24.0, 48.2, 61.4; ^{19}F NMR (377 MHz, $CDCl_3$): δ ppm -151.25 (q, J = 1.1 Hz), -151.73 (br. s); IR ν max ($CHCl_3$)/cm^{-1} 1061, 1466, 2879, 2938, 2968, 3045; MS (ESI) positive for $C_{13}H_{30}N$, M$^+$: calcd 200.2373, found 200.2379.

2.3.5.10 [$N_{4,4,4,1}$][PF_6]

To a stirring suspension of tributyl(methyl)ammonium chloride (6.84 g, 29.0 mmol) in water (110 ml) an aqueous solution of hexafluorophosphoric acid (60 % w/w, 4.80 ml, 34.8 mmol) was added dropwise using a plastic syringe. The reaction mixture was stirred for 16 h at room temperature. Dichloromethane (150 ml) was added, and the organic layer separated and washed with water (6 × 50 ml). The solvent was removed and the product was dried *in vacuo* at 50 °C to yield a white solid (9.82 g, 98 %). ^{1}H NMR (400 MHz, $CDCl_3$): δ ppm 0.99 (t, J = 7.3 Hz, 9H), 1.36 – 1.45 (m, 6H), 1.61 – 1.69 (m, 6H), 2.97 (s, 3H), 3.16 – 3.21 (m, 6H); ^{13}C NMR (101 MHz, $CDCl_3$): δ ppm 13.4, 19.5, 24.0, 48.2, 61.6; ^{31}P NMR (162 MHz, $CDCl_3$): δ ppm -144.35 (spt, J = 713 Hz); ^{19}F NMR (377 MHz, $CDCl_3$): δ ppm -71.93 (d, J = 713 Hz); MS (ESI) positive for $C_{13}H_{30}N$, M$^+$: calcd 200.2373, found 200.2362. Data in agreement with reported literature values.[20]

2.3.5.11 [$N_{2,2,2,8}$]Br

To a stirring solution of triethylamine (11.8 ml, 84.9 mmol) in ethyl acetate (10 ml), bromooctane (17.6 ml, 101.9 mmol) was added dropwise at room temperature. The reaction mixture was heated to 70 °C and stirred for 60 h. The solvent was removed and the product was dried *in vacuo* to yield a white solid (10.7 g, 43 %). ^{1}H NMR (400 MHz, $CDCl_3$): δ ppm 0.83 (t, J = 7.0 Hz, 3H), 1.22 – 1.36 (m, 19H), 1.61 – 1.69 (m, 2H), 3.22 – 3.26 (m, 2H), 3.47 (q, J

= 7.5 Hz, 6H); ^{13}C NMR (101 MHz, $CDCl_3$): δ ppm 8.0., 13.9, 22.0, 22.4, 26.3, 28.9, 29.0, 31.5, 53.5, 57.4. Data in agreement with reported literature values.[21]

2.3.5.12 [$N_{2,2,2,8}$][NTf_2]

To a stirring solution of triethyl(octyl)ammonium bromide (3.30 g, 11.2 mmol) in water (20 ml), a solution of lithium bis(trifluoromethanesulfonyl)imide (3.90 g, 13.6 mmol) in water (20 ml) was added dropwise. The reaction mixture was stirred for 16 h at room temperature. Dichloromethane (40 ml) was added and the organic layer separated and washed with water (6 × 20 ml). The solvent was removed and the product was dried *in vacuo* to yield a colourless, viscous liquid (5.25 g, 95 %). ^{1}H NMR (400 MHz, $CDCl_3$): δ ppm 0.88 (t, J = 7.0 Hz, 3H), 1.28 – 1.35 (m, 19H), 1.60 – 1.65 (m, 2H), 3.05 – 3.09 (m, 2H), 3.26 (q, J = 7.5 Hz, 6H); ^{13}C NMR (101 MHz, $CDCl_3$): δ ppm 7.3, 14.0, 21.6, 22.5, 26.2, 28.9, 28.9, 31.5, 53.0, 57.2, 119.7 (q, J = 321 Hz) ; ^{19}F NMR (377 MHz, $CDCl_3$): δ ppm -78.88; MS (ESI) positive for $C_{14}H_{32}N$, M^+: calcd 214.2529, found 214.2534. Data in agreement with reported literature values.[21]

2.3.5.13 [$N_{2,2,2,(Et(PEG)2)}$]Br

To a stirring solution of triethylamine (2.30 ml, 16.5 mmol) in ethyl acetate (2.0 ml), 1-bromo-2-(2-ethoxyethoxy)ethane (3.30 ml, 21.7 mmol) was added dropwise at room temperature. The reaction mixture was heated to 75 °C and stirred for 48 h. The solvent was removed and the product was dried *in vacuo* to yield an off-white solid (2.90 g, 57 %). ^{1}H NMR (400 MHz, $CDCl_3$): δ ppm 1.14 (t, J = 7.0 Hz, 3H), 1.36 (t, J = 7.3 Hz, 9H), 3.45 (q, J = 7.0 Hz, 2H), 3.50 – 3.56 (m, 8H), 3.62 – 3.64 (m, 2H), 3.72 – 3.74 (m, 2H), 3.90 – 3.95 (m, 2H); ^{13}C NMR (101 MHz, $CDCl_3$): δ ppm 8.1, 15.1, 54.2, 57.3, 64.5, 66.4, 69.3, 70.6. Data in agreement with reported literature values.[22]

2.3.5.14 [$N_{2,2,2,(Et(PEG)2)}$][NTf_2]

To a stirring solution of triethyl(2-(2-ethoxyethoxy)ethyl)ammonium bromide (2.90 g, 9.70 mmol) in water (10 ml), a solution of lithium bis(trifluoromethanesulfonyl)imide (3.30 g, 11.7 mmol) in water (10 ml) was added dropwise. The reaction mixture was stirred for 16 h at room temperature. Dichloromethane (40 ml) was added and the organic layer separated and washed with water (6 × 20 ml). The solvent was removed and the product was dried *in vacuo* to yield a yellow liquid (3.68 g, 77 %). ^{1}H NMR (400 MHz, $CDCl_3$): δ ppm 1.19 (t, J = 7.0 Hz, 3H), 1.33 (t, J = 7.3 Hz, 9H), 3.35 – 3.44 (m, 8H), 3.51 (q, J = 7.0 Hz, 2H), 3.55 – 3.57 (m, 2H), 3.63 – 3.65 (m, 2H), 3.84 – 3.89 (m, 2H); ^{13}C NMR (101 MHz, $CDCl_3$): δ ppm 7.5, 15.1, 54.0, 56.8, 64.2, 66.5, 69.4, 70.6; ^{19}F NMR (377 MHz, $CDCl_3$): δ ppm -78.85; MS (ESI) positive for $C_{12}H_{28}NO_2$, M^+: calcd 218.2115, found 218.2117. Data in agreement with reported literature values.[22]

2.3.6 Phosphonium-based ILs – Synthetic Procedures

2.3.6.1 [$P_{6,6,6,14}$][BF_4]

Trihexyl(tetradecyl)phosphonium chloride (5.20 g, 10.0 mmol) was suspended in water (15 ml) and a solution of sodium tetrafluoroborate (1.32 g, 12.0 mmol) in water (10 ml) was added dropwise at 0 °C with vigorous stirring. The reaction mixture was allowed to warm to ambient temperature and stirred for 16 h and then extracted with diethyl ether (4 x 25 ml). The combined organic extracts were washed with aqueous 1 % sodium hydroxide solution (2 x 8 ml) followed by water (6 x 50 ml). The solvent was removed and the product was dried *in vacuo* at 50 °C to yield a colourless, viscous liquid which solidified on cooling (5.44 g, 96 %). ^{1}H NMR (400 MHz, $CDCl_3$): δ ppm 0.86 – 0.91 (m, 12H), 1.26 – 1.34 (m, 32H), 1.44 – 1.58 (m, 16H), 2.13 – 2.20 (m, 8H); ^{13}C NMR (101 MHz, $CDCl_3$): δ ppm 13.9, 14.1, 18.7 (d, J = 47.5 Hz), 21.6, 21.7, 22.3, 22.6, 28.9, 29.3, 29.5, 29.6, 30.3 (d, J = 14.6 Hz), 30.7 (d, J = 14.6 Hz), 30.9, 31.9; ^{31}P NMR (162 MHz, $CDCl_3$): δ ppm +32.80; ^{19}F NMR (377 MHz, $CDCl_3$): δ ppm -151.47 (q, J = 1.4 Hz), -151.41 (br. s); MS (ESI) positive for $C_{32}H_{68}P$, M^+: calcd 483.5053, found 483.5039. Data in agreement with reported literature values.[16]

2.3.6.2 [$P_{6,6,6,14}$][PF_6]

Trihexyl(tetradecyl)phosphonium chloride (5.40 g, 10.4 mmol) was suspended in water (60.0 ml) and an aqueous solution of hexafluorophosphoric acid (60 % w/w, 2.0 ml, 13.6 mmol) was added dropwise using a plastic syringe at 0 °C. The reaction mixture was allowed to warm to room temperature and stirred for 16 h then extracted with diethyl ether (4 x 25 ml). The combined organic extracts were washed with an aqueous 1 % sodium hydroxide solution (2 x 8 ml) followed by water (6 x 50 ml). The solvent was removed and the product was dried *in vacuo* at 50 °C to yield a white solid (6.13 g, 94 %). ^{1}H NMR (400 MHz, $CDCl_3$): δ ppm 0.86 – 0.91 (m, 12H), 1.26 – 1.34 (m, 32H), 1.43 – 1.58 (m, 16H), 2.07 – 2.15 (m, 8H); ^{13}C NMR (101 MHz, $CDCl_3$): δ ppm 13.9, 14.1, 18.6 (d, J = 47.6 Hz), 21.4, 21.5, 22.3, 22.7, 28.8, 29.3, 29.5, 29.6, 29.7, 30.2 (d, J = 14.6 Hz), 30.6 (d, J = 14.6 Hz), 30.9, 31.9; ^{31}P NMR (162 MHz, $CDCl_3$): δ ppm +32.81, -144.31 (spt, J = 713 Hz); ^{19}F NMR (377 MHz, $CDCl_3$): δ ppm -72.09 (d, J = 713 Hz); MS (ESI) positive for $C_{32}H_{68}P$, M^+: calcd 483.5053, found 483.5048. Data in agreement with reported literature values.[16]

2.3.6.3 [$P_{6,6,6,14}$][OTf]

To a stirring solution of trihexyl(tetradecyl)phosphonium chloride (6.98 g, 13.4 mmol) in acetone (50 ml) a solution of lithium trifluoromethanesulfonate (2.52 g, 16.2 mmol) in acetone (50 ml) was added dropwise. The reaction mixture was stirred for 16 h at ambient temperature. The solvent was removed and diethyl ether (25 ml) was added, lithium chloride and unreacted lithium trifluoromethanesulfonate were removed by filtration. Diethyl ether (125 ml) was added to the filtrate, and washed with water (6 x 50 ml). The solvent was removed and the product was dried *in vacuo* at 50 °C to yield a colourless, viscous liquid (7.27 g, 86 %). ^{1}H NMR (400 MHz, $CDCl_3$): δ ppm 0.86 – 0.91 (m, 12H), 1.25 – 1.32 (m, 32H), 1.42 – 1.59 (m, 16H), 2.16 – 2.23 (m, 8H); ^{13}C NMR (101 MHz, $CDCl_3$): δ ppm 13.8, 14.1, 18.8 (d, J = 46.8 Hz), 21.6, 21.7, 22.3, 22.6, 28.8, 29.2, 29.3, 29.5, 29.6, 30.3 (d, J = 14.6 Hz), 30.6 (d, J = 14.6 Hz), 30.8, 31.9; ^{31}P NMR (162 MHz, $CDCl_3$): δ ppm +32.84; ^{19}F NMR (377 MHz, $CDCl_3$): δ ppm -78.25; MS (ESI) positive for $C_{32}H_{68}P$, M^+: calcd

483.5053, found 483.5048. Data in agreement with reported literature values.[16]

2.3.6.4 [$P_{6,6,6,14}$][NTf_2]

To a stirring solution of trihexyl(tetradecyl)phosphonium chloride (5.34 g, 10.3 mmol) in acetone (50 ml) a solution of lithium bis(trifluoromethanesulfonyl)imide (3.50 g, 12.2 mmol) in acetone (50 ml) was added dropwise. The reaction mixture was stirred for 16 h at ambient temperature. The solvent was removed and diethyl ether (25 ml) was added, lithium chloride and unreacted lithium bis(trifluoromethanesulfonimide) were removed by filtration. Diethyl ether (125 ml) was added to the filtrate and washed with water (6 x 50 ml). The solvent was removed and the product was dried *in vacuo* at 50 °C to yield a colourless, viscous liquid (7.15 g, 94 %). ^{1}H NMR (400 MHz, $CDCl_3$): δ ppm 0.85 – 0.92 (m, 12H), 1.25 – 1.37 (m, 32H), 1.45 – 1.59 (m, 16H), 2.17 – 2.24 (m, 8H); ^{13}C NMR (101 MHz, $CDCl_3$): δ ppm 13.9, 14.1, 19.0 (d, *J* = 46.8 Hz), 21.6, 21.7, 22.3, 22.6, 28.8, 29.2, 29.3, 29.5, 29.6, 29.6, 30.3 (d, *J* = 14.6 Hz), 30.7 (d, *J* = 14.6 Hz), 30.9, 120.0; ^{31}P NMR (162 MHz, $CDCl_3$): δ ppm +32.99; ^{19}F NMR (377 MHz, $CDCl_3$): δ ppm -78.75; MS (ESI) positive for $C_{32}H_{68}P$, M^+: calcd 483.5053, found 483.5062. Data in agreement with reported literature values.[16]

2.3.6.5 [$P_{8,8,8,8}$][NTf_2]

To a stirring solution of tetraoctylphosphonium bromide (5.00 g, 8.87 mmol) dissolved in chloroform (25 ml), a solution of lithium bis(trifluoromethanesulfonyl)imide (3.05 g, 10.6 mmol) in water (25 ml) was added dropwise. The reaction mixture was stirred for 16 h at ambient temperature. Chloroform (75 ml) and water (25 ml) was added, and the organic layer separated and washed with water (6 x 50 ml). The solvent was removed and the product was dried *in vacuo* to yield a pale yellow liquid (6.72 g, 99 %). ^{1}H NMR (400 MHz, $CDCl_3$): δ ppm 0.87 – 0.90 (m, 12H), 1.24 – 1.37 (m, 32H), 1.42 – 1.55 (m, 16H), 2.08 – 2.15 (m, 8H); ^{13}C NMR (101 MHz, $CDCl_3$): δ ppm 14.0, 18.7 (d, *J* = 46.7 Hz), 21.51, 21.56, 22.5, 28.7, 28.9, 30.5 (d, *J* = 14.6 Hz), 31.6, 119.9 (q, *J* = 321 Hz); ^{31}P NMR (162 MHz,

$CDCl_3$): δ ppm +32.95; ^{19}F NMR (377 MHz, $CDCl_3$): δ ppm -78.75; IR ν max ($CHCl_3$)/cm^{-1} 1060, 1136, 1192, 1378, 2859, 2931, 2958; MS (ESI) positive for $C_{32}H_{68}P$, M$^+$: calcd 483.5053, found 483.5041.

2.3.6.6 [$P_{4,4,4,4}$][NTf_2]

To a stirring solution of tetrabutylphosphonium bromide (1.86 g, 5.49 mmol) dissolved in dichloromethane (15 ml), a solution of lithium bis(trifluoromethanesulfonyl)imide (2.39 g, 8.33 mmol) in water (15 ml) was added dropwise. The reaction mixture was stirred for 16 h at ambient temperature. Dichloromethane (75 ml) and water (25 ml) was added, and the organic layer separated and washed with water (6 x 50 ml). The solvent was removed and the product was dried *in vacuo* to yield a white solid (2.72 g, 92 %). ^{1}H NMR (400 MHz, $CDCl_3$): δ ppm 0.97 (t, *J* = 7.0 Hz, 12H), 1.48 – 1.53 (m, 16H), 2.07 – 2.15 (m, 8H); ^{13}C NMR (101 MHz, $CDCl_3$): δ ppm 13.2, 18.4 (d, *J* = 47.5 Hz), 23.4 (d, *J* = 4.6 Hz), 23.7 (d, *J* = 15.3 Hz), 119.7 (q, *J* = 321 Hz); ^{31}P NMR (162 MHz, $CDCl_3$): δ ppm +33.12; ^{19}F NMR (377 MHz, $CDCl_3$): δ ppm -78.85; MS (ESI) positive for $C_{16}H_{36}P$, M$^+$: calcd 259.2549, found 259.2546. Data in agreement with reported literature values.[23]

2.3.6.7 [$P_{4,4,4,1}$][NTf_2]

To a stirring solution of tributyl(methyl)phosphonium methylsulfate (3.48 g, 10.6 mmol) dissolved in chloroform (25 ml), a solution of lithium bis(trifluoromethanesulfonyl)imide (3.65 g, 12.7 mmol) in water (25 ml) was added dropwise. The reaction mixture was stirred for 16 h at ambient temperature. Chloroform (75 ml) and water (25 ml) was added, and the organic layer was separated and washed with water (6 x 50 ml). The solvent was removed and the product was dried *in vacuo* to yield a colourless, viscous liquid (5.06 g, 96 %). ^{1}H NMR (400 MHz, $CDCl_3$): δ ppm 0.97 (t, *J* = 7.0 Hz, 9H), 1.45 – 1.55 (m, 12H), 1.77 (d, *J* = 13.1 Hz, 3H), 2.08 – 2.16 (m, 6H); ^{13}C NMR (101 MHz, $CDCl_3$): δ ppm 3.9 (d, *J* = 52.2 Hz), 13.2 , 19.9 (d, *J* = 49.1 Hz), 23.3 (d, *J* = 4.6 Hz), 23.6 (*J* = 15.3 Hz), 119.7 (q, *J* = 322 Hz) ; ^{31}P NMR (162 MHz, $CDCl_3$): δ ppm +31.54; ^{19}F NMR (377 MHz, $CDCl_3$): δ ppm -

78.89; IR ν max ($CHCl_3$)/cm^{-1} 1059, 1137, 1191, 1351, 2877, 2936, 2966; MS (ESI) positive for $C_{13}H_{30}P$, M^+: calcd 217.2080, found 217.2084.

2.3.6.8 [$P_{4,4,4,1}$]Cl

Tributyl(methyl)phosphonium methylsulfate (14.3 g, 43.5 mmol) was dissolved in methanol (100 ml) and eluted through a column containing Amberlite-IRA400 (Cl) ion-exchange resin (141 g) at a drop rate of 1 ml/min. The solvent was removed and the product was dried *in vacuo* at 50 °C to yield an off-white solid (9.73 g, 88 %). ^{1}H NMR (300 MHz, $CDCl_3$): δ ppm 0.92 (t, *J* = 7.0 Hz, 9H), 1.44 – 1.55 (m, 12H), 2.06 (d, *J* = 13.6 Hz, 3H), 2.37 – 2.49 (m, 6H); ^{13}C NMR (75 MHz, $CDCl_3$): δ ppm 4.8 (d, *J* = 52.3 Hz), 13.4, 20.1 (d, *J* = 48.9 Hz), 23.6 (d, *J* = 4.6 Hz), 23.7 (d, *J* = 15.5 Hz); ^{31}P NMR (121 MHz, $CDCl_3$): δ ppm +32.01; MS (ESI) positive for $C_{13}H_{30}P$, M^+: calcd 217.2080, found 217.2097. Data in agreement with reported literature values.[24]

2.3.6.9 [$P_{4,4,4,1}$][BF_4]

To a stirring solution of tributyl(methyl)phosphonium methylsulfate (6.54 g, 19.9 mmol) in water (15 ml), a solution of sodium tetrafluoroborate (3.34 g, 30.4 mmol) in water (20 ml) was added dropwise at room temperature. The reaction mixture was stirred for 16 h. Dichloromethane (100 ml) and water (15 ml) was added to the reaction mixture. The organic layer was separated and washed with water (6 x 50 ml). The solvent was removed and the product was dried *in vacuo* at 50 °C to yield a white solid (5.10 g, 90 %). ^{1}H NMR (400 MHz, $CDCl_3$): δ ppm 0.97 (t, *J* = 7.1 Hz, 9H), 1.49 – 1.56 (m, 12H), 1.82 (d, *J* = 13.4 Hz, 3H), 2.14 – 2.22 (m, 6H); ^{13}C NMR (101 MHz, $CDCl_3$): δ ppm 3.7 (d, *J* = 52.9 Hz), 13.3, 19.7 (d, *J* = 49.1 Hz), 23.3 (d, *J* = 4.6 Hz), 23.7 (d, *J* = 15.3 Hz); ^{31}P NMR (162 MHz, $CDCl_3$): δ ppm +32.99; ^{19}F NMR (377 MHz, $CDCl_3$): δ ppm -150.64 (q, *J* = 1.2 Hz), -150.59 (br. s); MS (ESI) positive for $C_{13}H_{30}P$, M^+: calcd 217.2080, found 217.2080. Data in agreement with reported literature values.[25]

2.3.6.10 [$P_{4,4,4,1}$][PF_6]

To a stirring solution of tributyl(methyl)phosphonium methylsulfate (9.06 g, 27.6 mmol) in water (100 ml), an aqueous solution of hexafluorophosphoric acid (60 % w/w, 4.6 ml, 33.1 mmol) was added dropwise using a plastic syringe at 0 °C. The reaction mixture was stirred for 16 h. Chloroform (100 ml) was added to the reaction mixture. The organic layer was separated and washed with water (6 x 50 ml). The solvent was removed and the product was dried *in vacuo* at 50 °C to yield a white solid (9.73 g, 97 %). ^{1}H NMR (300 MHz, $CDCl_3$): δ ppm 0.97 (t, *J* = 7.1 Hz, 9H), 1.45 – 1.56 (m, 12H), 1.76 (d, *J* = 13.3 Hz, 3H), 2.07 – 2.17 (m, 6H); ^{13}C NMR (75 MHz, $CDCl_3$): δ ppm 3.6 (d, *J* = 52.3 Hz), 13.2, 19.7 (d, *J* = 49.4 Hz), 23.3 (d, *J* = 4.6 Hz), 23.7 (d, *J* = 15.5 Hz); ^{31}P NMR (121 MHz, $CDCl_3$): δ ppm +32.81, -144.31 (spt, *J* = 713 Hz); ^{19}F NMR (282 MHz, $CDCl_3$): δ ppm -71.66 (d, *J* = 713 Hz); MS (ESI) positive for $C_{13}H_{30}P$, M^+: calcd 217.2080, found 217.2089. Data in agreement with reported literature values.[26]

2.3.7 Pyrrolidinium-based ILs – Synthetic Procedures

2.3.7.1 [C_8C_1Pyrr]Br

To a stirring solution of 1-methylpyrrolidine (20.0 ml, 188 mmol) in ethyl acetate (15 ml), 1-bromooctane (40.0 ml, 232.0 mmol) was added dropwise at room temperature. The reaction mixture was heated to 40 °C and stirred for 24 h. The solvent was removed and the crude white solid recrystallized from acetonitrile/ethyl acetate and dried *in vacuo* at 50 °C to yield a white solid (33.0 g, 63 %). ^{1}H NMR (400 MHz, $CDCl_3$): δ ppm 0.83 (t, *J* = 7.0 Hz, 3H), 1.19 – 1.38 (m, 10H), 1.69 – 1.77 (m, 2H), 2.23 – 2.30 (m, 4H), 3.27 (s, 3H), 3.59 – 3.63 (m, 2H), 3.75 – 3.86 (m, 4H); ^{13}C NMR (101 MHz, $CDCl_3$): δ ppm 13.9, 21.5, 22.4, 24.0, 26.3, 28.9, 29.1, 31.5, 48.6, 64.1, 64.3; MS (ESI) positive for $C_{13}H_{28}N$, M^+: calcd 198.2216, found 198.2210. Data in agreement with reported literature values.[27]

2.3.7.2 [C_8C_1Pyrr]Cl

1-octyl-1-methylpyrrolidinium bromide (7.20 g, 25.9 mmol) was dissolved in methanol (100 ml) and eluted through a column containing Amberlite-IRA400 (Cl) ion-exchange resin (80 g) at a drop rate of 1 ml/min. The solvent was removed and the product was dried *in vacuo* at 50 °C to yield an off-white solid (5.68 g, 93 %). ^{1}H NMR (300 MHz, $CDCl_3$): δ ppm 0.79 (t, *J* = 7.0 Hz, 3H), 1.16 – 1.36 (m, 10H), 1.63 – 1.74 (m, 2H), 2.17 – 2.28 (m, 4H), 3.23 (s, 3H), 3.53 – 3.58 (m, 2H), 3.71 – 3.84 (m, 4H); ^{13}C NMR (75 MHz, $CDCl_3$): δ ppm 13.9, 21.5, 22.3, 23.9, 26.2, 28.8, 29.0, 31.4, 48.2, 63.9, 64.1; MS (ESI) positive for $C_{13}H_{28}N$, M^+: calcd 198.2216, found 198.2222. Data in agreement with reported literature values.[28]

2.3.7.3 [C_8C_1Pyrr][BF_4]

To a solution of 1-octyl-1-methylpyrrolidinium bromide (6.82 g, 24.5 mmol) in water (25 ml), a solution of sodium tetrafluoroborate (3.24 g, 29.5 mmol) in water (25 ml) was added dropwise. The reaction mixture was stirred overnight at room temperature. Dichloromethane (75 ml) was added and the organic layer separated and washed with water (4 x 50 ml). The solvent was removed and the product was dried *in vacuo* at 50 °C to yield a white solid (6.37 g, 91 %). ^{1}H NMR (400 MHz, $CDCl_3$): δ ppm 0.87 (t, *J* = 7.0 Hz, 3H), 1.26 – 1.35 (m, 10H), 1.70 – 1.78 (m, 2H), 2.22 – 2.28 (m, 4H), 3.06 (s, 3H), 3.31 – 3.35 (m, 2H), 3.48 – 3.60 (m, 4H); ^{13}C NMR (101 MHz, $CDCl_3$): δ ppm 14.0, 21.6, 22.5, 23.8, 26.3, 29.0, 29.0, 31.6, 48.2, 64.3, 64.4; ^{19}F NMR (377 MHz, $CDCl_3$): δ ppm -151.53 (q, *J* = 1.1 Hz), -151.48 (br. s); MS (ESI) positive for $C_{13}H_{28}N$, M^+: calcd 198.2216, found 198.2220. Data in agreement with reported literature values.[27]

2.3.7.4 [C_8C_1Pyrr][PF_6]

To a stirring solution of 1-octyl-1-methylpyrrolidinium bromide (8.10 g, 29.0 mmol) in water (100 ml), an aqueous solution of hexafluorophosphoric acid (60 % w/w, 4.9 ml, 34.9 mmol) was added dropwise using a plastic syringe at 0 °C. The reaction mixture was stirred for 16 h. Dichloromethane (100 ml) was added to the reaction mixture. The organic layer was separated and washed with water (6 x 50 ml). The solvent was removed and the product was dried *in vacuo* at 50 °C to yield a white solid (9.88 g, 90 %). ^{1}H NMR (300 MHz, $CDCl_3$): δ ppm 0.88 (t, *J* = 7.0 Hz, 3H), 1.27 – 1.35 (m, 10H), 1.72 – 1.77 (m, 2H), 2.20 – 2.30 (m, 4H), 3.04 (s, 3H), 3.26 – 3.31 (m, 2H), 3.47 – 3.53 (m, 4H); ^{13}C NMR (75 MHz, $CDCl_3$): δ ppm 14.0, 21.5, 22.5, 23.8, 26.2, 29.0, 31.6, 48.3, 64.4, 64.6; ^{31}P NMR (121 MHz, $CDCl_3$): δ ppm -144.31 (spt, *J* = 713 Hz); ^{19}F NMR (282 MHz, $CDCl_3$): δ ppm -72.09 (d, *J* = 713 Hz); MS (ESI) positive for $C_{13}H_{28}N$, M^+: calcd 198.2216, found 198.2226. Data in agreement with reported literature values.[13]

2.3.7.5 [C_8C_1Pyrr][NTf_2]

To a solution of 1-octyl-1-methylpyrrolidinium bromide (5.82 g, 20.9 mmol) in water (25 ml), a solution of lithium bis(trifluoromethane)sulfonimide (7.21 g, 25.1 mmol) in water (25 ml) was added dropwise. The reaction mixture was stirred overnight at room temperature. Dichloromethane (75 ml) was added and the organic layer separated and washed with water (4 x 50 ml). The solvent was removed and the product was dried *in vacuo* at 50 °C to yield a white solid (9.40 g, 94 %). ^{1}H NMR (400 MHz, $CDCl_3$): δ ppm 0.88 (t, *J* = 7.0 Hz, 3H), 1.28 – 1.35 (m, 10H), 1.70 – 1.78 (m, 2H), 2.25 – 2.28 (m, 4H), 3.04 (s, 3H), 3.27 – 3.32 (m, 2H), 3.49 – 3.56 (m, 4H); ^{13}C NMR (101 MHz, $CDCl_3$): δ ppm 14.0, 21.5, 22.5, 23.8, 26.1, 28.9, 31.5, 48.4, 64.5, 64.8, 86.1, 119.7 (q, *J* = 321 Hz); ^{19}F NMR (377 MHz, $CDCl_3$): δ ppm -78.94; MS (ESI) positive for $C_{13}H_{28}N$, M^+: calcd 198.2216, found 198.2222. Data in agreement with reported literature values.[27]

2.3.7.6 [Et(PEG)$_2$MPyrr]Br

To a stirring solution of 1-methylpyrrolidine (1.80 ml, 17.7 mmol) dissolved in ethyl acetate (1.0 ml) 1-bromo-2-(2-ethoxyethoxy)ethane (3.20 ml, 21.3 mmol) was added dropwise at room temperature. The reaction mixture was heated to 50 °C and stirred for 24 h. The solvent was removed and the product was dried *in vacuo* at 60 °C for 24 h to yield yellow viscous liquid (4.65 g, 93 %). ^{1}H NMR (400 MHz, $CDCl_3$): δ ppm 1.14 (t, *J* = 7.0 Hz, 3H), 2.19 – 2.27 (m, 4H), 3.33 (s, 3H), 3.46 (q, *J* = 7.0 Hz, 2H), 3.51 – 3.53 (m, 2H), 3.62 – 3.65

(m, 2H,), 3.80 – 4.00 (m, 8H); ^{13}C NMR (101 MHz, $CDCl_3$): δ ppm 15.1, 21.3, 48.7, 62.9, 65.3, 65.4, 66.4, 69.3, 70.5; MS (ESI) positive for $C_{11}H_{24}NO_2$, M^+: calcd 202.1802, found 202.1806.

2.3.7.7 [Et(PEG)$_2$MPyrr][NTf$_2$]

To a stirring solution of 1-methyl-1-(2-(2-ethoxyethoxy)ethyl)pyrrolidinium bromide (1.60 g, 5.70 mmol) in water (20 ml) a solution of lithium bis(trifluoromethanesulfonyl)imide (1.95 g, 6.80 mmol) in water (10 ml) was added dropwise at room temperature. The reaction mixture was stirred for 16 h. Dichloromethane (40 ml) was added and the organic layer separated and washed with water (4 x 20 ml). The solvent was removed and the product was dried *in vacuo* at 50 °C for 16 h to yield a pale yellow liquid (2.30 g, 68 %). ^{1}H NMR (400 MHz, $CDCl_3$): δ ppm; 1.19 (t, J = 7.0 Hz, 3H), 2.22 – 2.32 (m, 4H), 3.13 (s, 3H), 3.51 (q, J = 7.0 Hz, 2H), 3.56 – 3.67 (m, 10H), 3.89 – 3.95 (m, 2H); ^{13}C NMR (101 MHz, $CDCl_3$): δ ppm 15.1, 21.4, 48.9, 63.5, 64.9, 65.7, 66.5, 69.3, 70.6, 119.9 (q, J = 321 Hz); ^{19}F NMR (377 MHz, $CDCl_3$): δ ppm -78.92; IR ν max ($CHCl_3$) / cm^{-1} 1059, 1137, 1186, 1352, 1460, 1475, 2879, 2979, 3011; MS (ESI) positive for $C_{11}H_{24}NO_2$, M^+: calcd 202.1802, found 202.1804.

2.3.8 Imidazolium-based ILs – Synthetic Procedures

2.3.8.1 [C$_8$C$_1$Im]Br

To a solution of 1-methylimidazole (7.0 ml, 87.8 mmol) in ethyl acetate (20 ml), 1-bromooctane (20.0 ml, 116 mmol) was added dropwise with stirring at 40 °C. The reaction mixture was stirred at 40 °C for 60 h. The solvent was removed and the crude product recrystallised from acetonitrile/ethyl acetate and dried *in vacuo* at 60 °C to yield a colourless, viscous liquid (19.5 g, 81 %). ^{1}H NMR (400 MHz, DMSO-d_6): δ ppm 0.85 (t, J = 6.8 Hz, 3H), 1.13 – 1.37 (m, 10 H), 1.74 – 1.81 (m, 2H), 3.86 (s, 3H), 4.17 (t, J = 7.2 Hz, 2H), 7.74 – 7.75 (m, 1H), 7.81 – 7.82 (m, 1H), 9.25 (m, 1H); ^{13}C NMR (101 MHz, DMSO-d_6): δ ppm 14.4, 22.5, 26.0, 28.8, 29.0, 29.9, 31.6, 36.3, 49.2, 122.8, 124.1, 137.0; MS (ESI) positive for $C_{12}H_{23}N_2$, M^+: calcd 195.1849, found 195.1856. Data in agreement with reported literature values.[21]

2.3.8.2 $[C_8C_1Im][NTf_2]$

To a stirring solution of 1-methyl-3-octylimidazolium bromide (5.64 g, 20.5 mmol) in water (20 ml) a solution of lithium bis(trifluoromethanesulfonyl)imide (7.06 g, 24.6 mmol) in water (10 ml) was added at room temperature with stirring. The reaction mixture was stirred for 16 h. Dichloromethane (40 ml) was added and the organic layer separated and washed with water (4 x 20 ml). The solvent was removed and product was dried *in vacuo* at 50 °C for 16 h to yield a colourless liquid (9.14 g, 94 %). ^1H NMR (400 MHz, $CDCl_3$): δ ppm 0.88 (t, J = 6.9 Hz, 3H), 1.23 – 1.37 (m, 10H), 1.83 – 1.90 (m, 2H), 3.95 (s, 3H), 4.16 (t, J = 7.5 Hz, 2H), 7.29 – 7.30 (m, 1H), 7.31 – 7.32 (m, 1H), 8.76 (m, 1H); ^{13}C NMR (101 MHz, $CDCl_3$): δ ppm 14.0, 22.5, 26.1, 28.8, 28.9, 30.0, 31.6, 36.3, 50.2, 119.9 (q, J = 322 Hz), 122.2, 123.7 136.1; ^{19}F NMR (377 MHz, $CDCl_3$): δ ppm -79.02; MS (ESI) positive for $C_{12}H_{23}N_2$, M^+: calcd 195.1849, found 195.1963. Data in agreement with reported literature values.[29]

2.3.8.3 $[Et(PEG)_2MIm]Br$

Under an argon atmosphere 1-bromo-2-(2-ethoxyethoxy)ethane (3.30 ml, 21.7 mmol) was added dropwise to 1-methylimidazole (1.40 ml, 17.9 mmol) with stirring at room temperature. After complete addition the temperature was increased to 75 °C and stirred for 96 h. Unreacted starting materials were removed *in vacuo* at 50 °C for 16 h to yield a yellow viscous liquid (5.00 g, 100 %). ^1H NMR (400 MHz, $CDCl_3$): δ ppm 1.16 (t, J = 7.0 Hz, 3H), 3.47 (q, J = 7.0 Hz, 2H), 3.52 – 3.54 (m, 2H), 3.61 – 3.63 (m, 2H), 3.85 – 3.88 (m, 2H), 4.06 (s, 3H), 4.57 – 4.59 (m, 2H), 7.48 – 7.49 (m, 1H), 7.66 – 7.67 (m, 1H), 10.11 (m, 1H); ^{13}C NMR (101 MHz, $CDCl_3$): δ ppm 15.1, 36.6, 49.6, 66.5, 68.8, 69.3, 70.4, 122.8, 123.4, 137.4; MS (ESI) positive for $C_{10}H_{19}N_2O_2$, M^+: calcd 199.1441, found 199.1444.

2.3.8.4 $[Et(PEG)_2MIm][NTf_2]$

To a solution of $[Et(PEG)_2MIm]Br$ (2.04 g, 7.31 mmol) in water (15 ml) a solution of lithium bis(trifluoromethanesulfonyl)imide (2.50 g, 8.60 mmol) in water (15 ml) was added dropwise. The reaction mixture was stirred for 16 h at room temperature. Dichloromethane (50 ml) was added and the organic layer separated and washed with water (4 x 20 ml). The solvent was removed and the product was dried *in vacuo* at 50 °C for 16 h to yield a pale yellow liquid (3.05 g, 88 %). ^{1}H NMR (400 MHz, $CDCl_3$): δ ppm 1.20 (t, *J* = 7.0 Hz, 3H), 3.52 (q, *J* = 7.0 Hz, 2H), 3.55 – 3.58 (m, 2H), 3.63 – 3.65 (m, 2H), 3.82 – 3.85 (m, 2H), 3.93 (s, 3H), 4.34 – 4.37 (m, 2H), 7.27 – 7.28 (m, 1H), 7.50 – 7.51 (m, 1H), 8.76 (m, 1H); ^{13}C NMR (101 MHz, $CDCl_3$): δ ppm 15.1, 36.3, 49.7, 66.5, 68.4, 69.4, 70.3, 119.9 (q, *J* = 321 Hz), 123.0, 123.5, 136.4; ^{19}F NMR (377 MHz, $CDCl_3$): δ ppm -79.02; MS (ESI) positive for $C_{10}H_{19}N_2O_2$, M^+: calcd 199.1441, found 199.1446. Data in agreement with reported literature values.[30]

2.3.8.5 [($F_{13}H_4C_8$)C_1Im]I

To a stirring solution of 1-methylimidazole (0.74 ml, 9.44 mmol) in toluene (2.0 ml) 1-iodo-1*H*,1*H*,2*H*,2*H*-perfluorooctane (2.20 ml, 9.00 mmol) was added dropwise at room temperature. The reaction mixture was stirred and heated at 110 °C for 24 h in darkness. The product was recrystallised from acetonitrile/ethyl acetate/diethyl ether and dried *in vacuo* at 50 °C for 16 h to yield yellow viscous liquid (2.10 g). *N.B. ^{1}H NMR indicated a substantial amount of 1-methylimidazole ~ 40 % which could not be removed via recrystallization, or in vacuo due to the highly viscous nature of the product. Metathesis to [($F_{13}H_4C_8$)C_1Im][NTf_2] resulted in a significantly less viscous product and excess 1-methylimidazole was removed in vacuo at this stage.* ^{1}H NMR (300 MHz, $CDCl_3$): δ ppm 2.88 – 3.05 (m, 2H), 4.09 (s, 3H), 4.83 – 4.87 (t, *J* = 6.7 Hz, 2H), 7.50 – 7.51 (m, 1H), 7.65 – 7.66 (m, 1H), 10.06 (m, 1H); ^{13}C NMR (75 MHz, $CDCl_3$): δ ppm 37.3, 122.8, 123.6, 137.6; ^{19}F NMR (282 MHz, $CDCl_3$): δ ppm -126.30 – -126.15 (m, 2F), -123.29 – -122.70 (m, 4F), -122.04 – -121.67 (m, 2F), -133.52 – -113.28 (m, 2F), -80.88 (tt, *J* = 9.8 Hz, *J* = 2.4 Hz, 3F); MS (ESI) positive for $C_{12}H_{10}F_{13}N_2$, M^+: calcd 429.0636, found 429.0529. Data in agreement with reported literature values.[31]

2.3.8.6 [($F_{13}H_4C_8$)C_1Im][NTf_2]

To a stirring solution of [($F_{13}H_4C_8$)C_1Im]I (2.10 g, 3.78 mmol) dissolved in dichloromethane (15 ml) a solution of lithium bis(trifluoromethanesulfonyl)imide (1.30 g, 4.53 mmol) in water (15 ml) was added dropwise at room temperature. The reaction mixture was stirred for 16 h at room temperature in darkness. Dichloromethane (35 ml) was added and the organic layer separated and washed with water (4 x 25 ml). The solvent was removed and the product was dried *in vacuo* at 50 °C for 16 h to yield pale yellow viscous liquid (1.70 g, 63 %). ^{1}H NMR (400 MHz, DMSO-d_6): δ ppm 2.95 – 3.08 (m, 2H), 3.88 (s, 3H), 4.58 (t, J = 7.1 Hz, 2H), 7.73 – 7.74 (m, 1H), 7.88 – 7.89 (m, 1H), 9.20 (m, 1H); ^{13}C NMR (101 MHz, DMSO-d_6): δ ppm 30.1, 35.8, 41.2, 117.9, 121.1, 122.5, 123.7, 137.2; ^{19}F NMR (377 MHz, DMSO-d_6): δ ppm -125.86 – -125.76 (m, 2F), -123.35 – -123.10 (m, 2F), -122.80 – -122.50 (m, 2F), -121.85 – -121.55 (m, 2F), -113.31 – -113.13 (m, 2F), -80.32 (t, J = 9.8 Hz, 3F), -78.79 (s, 6F); MS (ESI) positive for $C_{12}H_{10}F_{13}N_2$, M^+: calcd 429.0636, found 429.0625. Data in agreement with reported literature values.[31]

2.3.9 Palladium Catalysed Suzuki Cross-Coupling

2.3.9.1 Suzuki Cross-Coupling Reactions

Palladium catalysed Suzuki cross-couplings were performed according to a previously described literature procedure to determine the respective turn-over frequency (TOF) for each system.[32] Under an argon atmosphere a mixture of NaCl (38.0 mg, 0.67 mmol), phenylboronic acid (0.58 g, 4.76 mmol) and [Pd(PPh_3)$_4$] (5.50 mg, 4.76 x 10^{-3}) in 2.00 ml (also weighed) of ionic liquid was stirred at 110 °C. Into this mixture, a solution of Na_2CO_3 (83.0 mg, 0.78 mmol) in water (3.00 ml) and bromobenzene (0.50 ml, 4.76 mmol) were injected. The reaction was allowed to proceed at 110 °C for ten minutes. Immediately after this time the reaction was quenched by immersing the reaction flask in liquid nitrogen. Conversion was determined *via* ^{1}H NMR by integration of the protons *ortho* to the –B(OH)$_2$ group in phenylboronic acid; for each IL a well-defined peak corresponding to the IL was chosen as an internal standard to enable quantification of phenylboronic acid conversion. TOFs were determined using a previously reported method.[32]

2.3.9.2 Model Suzuki Reaction for XPS Analysis

Under an argon atmosphere a mixture of NaCl (12.0 mg, 0.21 mmol), bromobenzene (13.1 μl, 0.125 mmol) and $[Pd(PPh_3)_4]$ (24.0 mg, 2.1×10^{-2} mmol) in 0.25 ml (also weighed) of ionic liquid was stirred at 110 °C. Into this mixture, a solution of Na_2CO_3 (26.0 mg, 0.25 mmol) in water (0.125 μl) was added. Reaction mixture heated at 110 °C with stirring for 3 h. After 3 h mixture was cooled to room temperature and dichloromethane (3.0 ml) added and washed with water (4 × 4.0 ml). Solvent removed and product dried *in vacuo* to yield yellow/orange liquid for analysis by XPS.

2.4 References

1. P. van der Heide, *X-ray Photoelectron Spectroscopy: An Introduction to Principles and Practices*, John Wiley & Sons, New Jersey, 2011.
2. J. F. Watts and J. Wolstenholme, *An Introduction to Surface Analysis by XPS and AES*, John Wiley & Sons Ltd, Great Britain, 1st edn., 2003.
3. D. Briggs and J. T. Grant, *Surface Analysis by Auger and X-ray Photoelectron Spectroscopy*, IM Publications LLP, Manchester, 2003.
4. K. R. J. Lovelock, I. J. Villar-Garcia, F. Maier, H.-P. Steinrück and P. Licence, *Chem. Rev.*, 2010, **110**, 5158-5190.
5. I. J. Villar-Garcia, E. F. Smith, A. W. Taylor, F. L. Qiu, K. R. J. Lovelock, R. G. Jones and P. Licence, *Phys. Chem. Chem. Phys.*, 2011, **13**, 2797-2808.
6. K. R. J. Lovelock, E. F. Smith, A. Deyko, I. J. Villar-Garcia, P. Licence and R. G. Jones, *Chem. Commun.*, 2007, 4866-4868.
7. E. F. Smith, F. J. M. Rutten, I. J. Villar-Garcia, D. Briggs and P. Licence, *Langmuir*, 2006, **22**, 9386-9392.
8. S. Krischok, M. Eremtchenko, M. Himmerlich, P. Lorenz, J. Uhlig, A. Neumann, R. Ottking, W. J. D. Beenken, O. Höfft, S. Bahr, V. Kempter and J. A. Schaefer, *J. Phys. Chem. B*, 2007, **111**, 4801-4806.
9. V. Lockett, R. Sedev, C. Bassell and J. Ralston, *Phys. Chem. Chem. Phys.*, 2008, **10**, 1330-1335.

10. T. Cremer, C. Kolbeck, K. R. J. Lovelock, N. Paape, R. Wölfe, P. S. Schulz, P. Wasserscheid, H. Weber, J. Thar, B. Kirchner, F. Maier and H.-P. Steinrück, *Chem. Eur. J.*, 2010, **16**, 9018-9033.

11. F. Bernardi, J. D. Scholten, G. H. Fecher, J. Dupont and J. Morais, *Chem. Phys. Lett.*, 2009, **479**, 113-116.

12. C. Paun, C. Stere, S. M. Coman, V. I. Parvulescu, P. Goodrich and C. Hardacre, *Catal. Today*, 2008, **131**, 98-103.

13. S. Men, K. R. J. Lovelock and P. Licence, *Phys. Chem. Chem. Phys.*, 2011, **13**, 15244-15255.

14. S. Men, D. S. Mitchell, K. R. J. Lovelock and P. Licence, *ChemPhysChem*, 2015, **16**, 2211-2218.

15. A. R. Santos, R. K. Blundell and P. Licence, *Phys. Chem. Chem. Phys.*, 2015, **17**, 11839-11847.

16. A. Cieniecka-Roslonkiewicz, J. Pernak, J. Kubis-Feder, A. Ramani, A. J. Robertson and K. R. Seddon, *Green Chem.*, 2005, **7**, 855-862.

17. R. F. Roberts, D. L. Allara, C. A. Pryde, N. E. Buchanan and N. D. Hobbins, *Surf. Interface. Anal.*, 1980, **2**, 5-10.

18. R. Arvai, F. Toulgoat, B. R. Langlois, J. Y. Sanchez and M. Medebielle, *Tetrahedron*, 2009, **65**, 5361-5368.

19. E. Bosse, L. Berthon, N. Zorz, J. Monget, C. Berthon, I. Bisel, S. Legand and P. Moisy, *Dalton Trans.*, 2008, 924-931.

20. J. Bresien, S. Ellinger, J. Harloff, A. Schulz, K. Sievert, A. Stoffers, C. Taschler, A. Villinger and C. Zur Taschler, *Angew. Chem. Int. Ed.*, 2015, **54**, 4474-4477.

21. S. L. Desset, S. W. Reader and D. J. Cole-Hamilton, *Green Chem.*, 2009, **11**, 630-637.

22. H. Shirota, H. Fukazawa, T. Fujisawa and J. F. Wishart, *J. Phys. Chem. B*, 2010, **114**, 9400-9412.

23. H. Srour, H. Rouault, C. C. Santini and Y. Chauvin, *Green Chem.*, 2013, **15**, 1341-1347.

24. G. Adamova, R. L. Gardas, M. Nieuwenhuyzen, A. V. Puga, L. P. N. Rebelo, A. J. Robertson and K. R. Seddon, *Dalton Trans.*, 2012, **41**, 8316-8332.

25. M. Picquet, S. Stutzmann, I. Tkatchenko, I. Tommasi, J. Zimmermann and P. Wasserscheid, *Green Chem.*, 2003, **5**, 153-162.

26. M. Rodriguez-Zubiri, S. Anguille and J. J. Brunet, *J. Mol. Catal. A: Chem.*, 2007, **271**, 145-150.

27. M. Guncheva, M. Dimitrov, F. Napoly, M. Draye and B. Andrioletti, *J. Mol. Catal. B: Enzym.*, 2014, **102**, 72-80.

28. G. Cravotto, E. C. Gaudino, L. Boffa, J. M. Leveque, J. Estager and W. Bonrath, *Molecules*, 2008, **13**, 149-156.

29. S. V. Dzyuba and R. A. Bartsch, *ChemPhysChem*, 2002, **3**, 161-166.

30. C. Kolbeck, M. Killian, F. Maier, N. Paape, P. Wasserscheid and H.-P. Steinrück, *Langmuir*, 2008, **24**, 9500-9507.

31. D. Almantariotis, T. Gefflaut, A. A. H. Padua, J. Y. Coxam and M. F. C. Gomes, *J. Phys. Chem. B*, 2010, **114**, 3608-3617.

32. I. J. Villar-Garcia, K. R. J. Lovelock, S. Men and P. Licence, *Chem. Sci.*, 2014, **5**, 2573-2579.

3. XPS of Ammonium and Phosphonium Ionic Liquids

3.1 Introduction

Ionic liquids (ILs) have received heightened interest in recent years due in part to their structural diversity.[1] By simply changing the ions, physicochemical properties such as density, viscosity, melting point and polarity *etc.* can be tuned for specific functions. The ability to predict and fine-tune the properties of an ionic liquid to meet a specific requirement is one of the greatest challenges in the field, and yet if fully achieved would provide an invaluable tool. To predict the bulk behaviour for any given ionic liquid it must first be understood on a molecular level, where changes to the chemical architecture and its impact on cation-anion interactions must be explored both theoretically and experimentally.

Over the past ten years X-ray photoelectron spectroscopy (XPS) has established itself as a robust technique to characterise ionic liquid-based systems,[2] and has provided a wealth of information in areas such as bulk and surface composition,[3-11] *in situ* reaction monitoring,[12, 13] and cation-anion interactions.[10, 14-17] To date investigations into cation-anion interactions have typically been limited to cyclic, nitrogen-based cations, where the effect of the anion on the electronic environment of a common cation has been explored. Additionally, the application of cation-anion interactions to tune a catalytic reaction has recently been described by Men *et al*. in which the anionic tuning of cation-anion interactions was used to modify the catalytic activity of a palladium catalyst in a Suzuki cross-coupling reaction.[18] However, so far, little is known as to the influence of the cation on the electronic environment of the anion.

A particularly interesting sub-set of ionic liquids are those based upon a tetraalkylphosphonium cation; research into these compounds has often been neglected in favour of their nitrogen-based counterparts with particular emphasis on the imidazolium and pyrrolidinium cations.[19] This is likely due to the high cost and air-sensitive nature of the trialkylphosphine starting materials; nevertheless, it has been observed that tetraalkylphosphonium-based ionic liquids can offer superior physico-chemical properties in comparison to their nitrogen-based relatives.[19-21] Furthermore, there are only a few systematic studies that directly investigate the effect of changing the central cationic heteroatom from nitrogen to phosphorus *i.e.* tetraalkylammonium *versus* tetraalkylphosphonium.[22-27] It has been shown that changing the cationic core from nitrogen to phosphorus can have a marked effect upon the physico-chemical properties of ILs;[26] however, little is known about the fundamental cation-anion interactions of these systems.

The work described in this *Chapter* utilises XPS to probe cation-anion interactions for ILs in which the cation is varied (tetraalkylammonium *versus* tetraalkylphosphonium) with common anions to examine the influence of the cationic heteroatom on the electronic environment of the anion, with an aim to determine if a degree of tunability can be achieved *via* the cation.

3.2 XPS of Ammonium Ionic Liquids

3.2.1 Purity and Quantification

XP survey and high resolution scans were used to establish elemental composition and purity for each ionic liquid presented in this study. All expected elements are present with stoichiometry within the expected experimental error (± 20 %). Earlier XPS studies on ionic liquids have highlighted the presence of hydrocarbon- and silicone-based impurities in the near-surface region, which cannot be detected by NMR or other bulk sensitive techniques.[4, 28, 29] A weak O 1s and Si 2p signal was observed in the case of $[N_{6,6,6,14}]Cl$, $[N_{4,4,4,1}][BF_4]$ and $[C_8C_1Pyrr]Cl$, see *Appendix A*; this is likely to be a result of laboratory grease during sample preparation or from double sided tape used for sample mounting, and is not expected to impact upon the recorded binding energies.[4, 30, 31] Surface contaminants, such as grease, can be routinely removed through argon etching, as described within *Chapter 2, Section 2.1.4*. However, this could not be achieved for $[N_{6,6,6,14}]Cl$, $[N_{4,4,4,1}][BF_4]$ and $[C_8C_1Pyrr]Cl$ as irreparable damage to the sample occurred.

There was no evidence of this contaminant in any other ionic liquids used in this study. Furthermore, there is no evidence of metal-based cations or halides that may be carried over from ionic liquid synthesis, particularly anion exchange chemistries. Experimental stoichiometries, calculated from high resolution spectra, for the ammonium and pyrrolidinium ionic liquids investigated are presented in Table 3.1. Experimental stoichiometries are within the typically quoted error of XPS quantification data of ± 20 %, and the majority are well within ± 10 %. Interestingly, larger deviations are seen for the chlorine Cl 2p signal. This could be a result of the small size of the chloride anion, and as such it experiences a dampening effect from the large carbon content of the cations.

Table 3.1. Measured experimental and nominal (in brackets) stoichiometries for ammonium and pyrrolidinium ionic liquids studied in this *Chapter*. [a] Relative sensitivity factors (RSFs) taken from the Kratos Library were used to derive atomic percentages from the most intense photoelectron emission peak for each element *i.e.* C = C 1s, N = N 1s, O = O 1s, F = F 1s, B = B 1s, S = S 2p, P = P 2p and Cl = Cl 2p. Associated experimental error is ± 10 – 20 %. A deviation larger than the experimental error is observed for the chloride photoelectron emission peak, which is discussed in further detail on pg. 73. *N.B.* Hydrogen is undetectable by XPS due its low photoionisation cross-section; consequently reported stoichiometries are determined without consideration of hydrogen content.

	Composition[a] (%)							
Compound	**C**	**N**	**O**	**F**	**B**	**S**	**P**	**Cl**
RSF[4, 32]	0.278	0.477	0.780	1.000	0.159	0.668	0.486	0.891
$[N_{6,6,6,14}]Cl$	95.5 (94.0)	2.3 (2.9)	-	-	-	-	-	2.2 (2.9)
$[N_{6,6,6,14}][BF_4]$	84.0 (84.2)	2.5 (2.6)	-	10.7 (10.5)	2.8 (2.6)	-	-	-
$[N_{6,6,6,14}][PF_6]$	80.5 (80.0)	2.5 (2.5)	-	15.0 (15.0)	-	-	2.0 (2.5)	-
$[N_{6,6,6,14}][OTf]$	80.7 (80.5)	2.4 (2.4)	7.1 (7.3)	7.6 (7.3)	-	2.1 (2.4)	-	-
$[N_{6,6,6,14}][NTf_2]$	70.5 (70.8)	3.9 (4.2)	8.9 (8.3)	12.9 (12.5)	-	3.8 (4.2)	-	-
$[N_{4,4,4,1}][BF_4]$	70.9 (68.4)	4.9 (5.3)	-	18.4 (21.1)	5.8 (5.3)	-	-	-
$[N_{4,4,4,1}][NTf_2]$	52.3 (51.7)	6.6 (6.9)	14.2 (13.8)	20.6 (20.7)	-	6.4 (6.9)	-	-
$[C_8C_1Pyrr]Cl$	88.6 (86.6)	6.2 (6.7)	-	-	-	-	-	5.2 (6.7)
$[C_8C_1Pyrr][BF_4]$	69.5 (68.4)	4.8 (5.3)	-	20.0 (21.1)	5.6 (5.3)	-	-	-
$[C_8C_1Pyrr][NTf_2]$	54.4 (51.7)	6.1 (6.9)	12.5 (13.8)	20.7 (20.7)	-	6.3 (6.9)	-	-

3.2.2 Effect of Alkyl Chain Length

Binding energies can be described as the most important output from XPS analysis as they provide both elemental and chemical information. Small changes in the electronic environment of an element by, for example, a change in chemical bonding or oxidation state will cause a shift in the measured binding energy. This allows both chemical structure and inter-ion interactions to be probed on a molecular level, thus providing vital information on the impact of structural changes on electronic environment and communication between ions. Accordingly, it is of great importance to obtain reliable and reproducible binding energies, thus an appropriate method of charge correction must be applied post data collection. An internal reference method, in which the peak used for referencing is part of the material being analysed, is considered the most accurate approach as charging effects will be experienced equally by both the reference peak and other sample peaks.[30, 33-35]

It is well established for ionic liquids with a long alkyl chain ($n \geq 8$) that reliable charge correction is achieved by setting the experimentally determined binding energy of the aliphatic carbon component ($C_{aliphatic}$ 1s) to a standard reference value, usually 285.0 eV.[10, 30] However, in the case of cations with shorter alkyl chains, *i.e.* $n < 8$, it has been determined that this method is not applicable, as the proximity of the electron-withdrawing ionic head group to the aliphatic carbon influences its electronic environment; therefore it no longer represents a truly aliphatic carbon environment.[30] Consequently, an indirect approach to charge correction of ionic liquids with short alkyl chains must be taken.

A previous study on imidazolium-based ionic liquids has indicated that the length of the alkyl chain has negligible impact on the binding energy of the atoms contained within the imidazolium ring and the anion, thus the binding energies for these atoms can be used as an internal reference for ionic liquids containing the same anion and similar cations. Therefore, it is important to determine if this also holds true for both ammonium- and phosphonium-based ionic liquids to allow reliable charge correction of short alkyl chain systems of this type.

A series of ammonium ionic liquids containing cations with alkyl chains of varying size and a common anion ($[NTf_2]^-$) were investigated to determine the influence of the aliphatic chain on the nitrogen cationic core. To enable reliable comparison of N 1s binding energies, spectra were charge corrected by referencing the F 1s photoelectron peak to 688.7 eV (the measured F 1s binding energy obtained for $[N_{6,6,6,14}][NTf_2]$ where charge correction was achieved by referencing $C_{aliphatic}$ 1s to 285.0 eV). The F 1s photoelectron peak was chosen as for other ionic liquid families it has been seen previously that it remains relatively “stable” in binding energy, *i.e.* within the experimental error of ± 0.1 eV, regardless of the length of the alkyl chain.[10, 16, 30]

Four different cations were investigated comprising $[N_{6,6,6,14}]^+$, $[N_{8,8,8,8}]^+$, $[N_{4,4,4,1}]^+$ and $[N_{4,4,4,4}]^+$. Two peaks in the N 1s high resolution XP spectra were observed in each case (see Figure 3.1). The peak at a higher binding energy (≈ 402.5 eV) corresponds to the more electropositive cationic nitrogen, whereas the peak at lower binding energy (≈ 399.3 eV) corresponds to the electronegative anionic nitrogen. The measured N_{cation} and N_{anion} 1s binding energies for the four ionic liquids are within the experimental error (± 0.1 eV) see Table 3.2 and Figure 3.1; thereby indicating that the length of the alkyl chain has minimal impact on the nitrogen cationic core (and also the anionic nitrogen).

Table 3.2. Experimental binding energies in eV for the ionic liquids studied in this *Chapter*. The associated experimental error is ± 0.1 eV. $[X_{6,6,6,14}]^+$/$[X_{8,8,8,8}]^+$ (where X = N or P) compounds charge corrected by referencing $C_{aliphatic}$ 1s to 285.0 eV unless otherwise stated. $[X_{4,4,4,1}]^+$/$[X_{4,4,4,4}]^+$ (where X = N or P) compounds charge corrected by referencing N_{cation} 1s/P_{cation} $2p_{3/2}$ to the value obtained for the $[X_{6,6,6,14}]^+$ analogue. [a]Compounds charge corrected by referencing F 1s to 688.7 eV, the obtained binding energies were identical to those achieved by alternatively referencing to N_{cation} 1s/P_{cation} $2p_{3/2}$.

Ionic Liquid		**Binding Energy / eV**												
Cation	**Anion**	$C_{aliphatic}$ 1s	C_{inter} 1s	C_{hetero} 1s	N_{cation} 1s	P_{cation} $2p_{3/2}$	C_{anion} 1s	N_{anion} 1s	O 1s	F 1s	B 1s	Cl $2p_{3/2}$	S $2p_{3/2}$	P_{anion} $2p_{3/2}$
$[N_{6,6,6,14}]^+$	Cl^-	285.0	285.6	286.3	402.1	-	-	-	-	-	-	196.6	-	-
$[N_{6,6,6,14}]^+$	$[BF_4]^-$	285.0	285.6	286.5	402.3	-	-	-	-	685.7	194.0	-	-	-
$[N_{6,6,6,14}]^+$	$[PF_6]^-$	285.0	285.7	286.6	402.4	-	-	-	-	686.6	-	-	-	136.4
$[N_{6,6,6,14}]^+$	$[OTf]^-$	285.0	285.7	286.6	402.4	-	292.3	-	531.8	688.3	-	-	168.2	-
$[N_{6,6,6,14}]^+$	$[NTf_2]^-$	285.0	285.7	286.7	402.5	-	292.8	399.3	532.5	688.7	-	-	168.9	-
$[N_{8,8,8,8}]^+$	$[NTf_2]^-$[a]	285.0	285.7	286.7	402.5	-	292.8	399.3	532.5	688.7	-	-	168.8	-
$[N_{4,4,4,4}]^+$	$[NTf_2]^-$[a]	285.1	285.6	286.6	402.5	-	292.8	399.3	532.5	688.7	-	-	168.8	-
$[N_{4,4,4,1}]^+$	$[NTf_2]^-$[a]	285.1	285.6	286.6	402.5	-	292.8	399.3	532.5	688.7	-	-	168.8	-
$[N_{4,4,4,1}]^+$	$[BF_4]^-$	285.0	285.2	286.4	402.3	-	-	-	-	685.7	194.1	-	-	-
$[P_{6,6,6,14}]^+$	Cl^-	285.0	-	285.7	-	132.3	-	-	-	-	-	196.6	-	-
$[P_{6,6,6,14}]^+$	$[BF_4]^-$	285.0	-	285.8	-	132.6	-	-	-	685.7	193.9	-	-	-
$[P_{6,6,6,14}]^+$	$[PF_6]^-$	285.0	-	285.8	-	132.7	-	-	-	686.5	-	-	-	136.3
$[P_{6,6,6,14}]^+$	$[OTf]^-$	285.0	-	285.8	-	132.7	292.3	-	531.9	688.4	-	-	168.2	-
$[P_{6,6,6,14}]^+$	$[NTf_2]^-$	285.0	-	285.9	-	132.7	292.8	399.3	532.5	688.7	-	-	168.8	-
$[P_{8,8,8,8}]^+$	$[NTf_2]^-$[a]	285.0	-	285.8	-	132.7	292.7	399.3	532.5	688.7	-	-	168.8	-
$[P_{4,4,4,4}]^+$	$[NTf_2]^-$[a]	285.2	-	285.7	-	132.7	292.8	399.3	532.5	688.7	-	-	168.8	-
$[P_{4,4,4,1}]^+$	$[NTf_2]^-$[a]	285.1	-	285.6	-	132.7	292.7	399.2	532.4	688.7	-	-	168.8	-
$[P_{4,4,4,1}]^+$	$[BF_4]^-$	285.0	-	285.4	-	132.6	-	-	-	685.5	193.9	-	-	-
$[C_8C_1Pyrr]^+$	Cl^-	285.0	285.5	286.1	402.1	-	-	-	-	-	-	196.9	-	-
$[C_8C_1Pyrr]^+$	$[BF_4]^-$	285.0	285.4	286.5	402.4	-	-	-	-	685.9	194.1	-	-	-
$[C_8C_1Pyrr]^+$	$[NTf_2]^-$	285.0	285.6	286.8	402.7	-	292.9	399.5	532.7	688.8	-	-	169.0	-

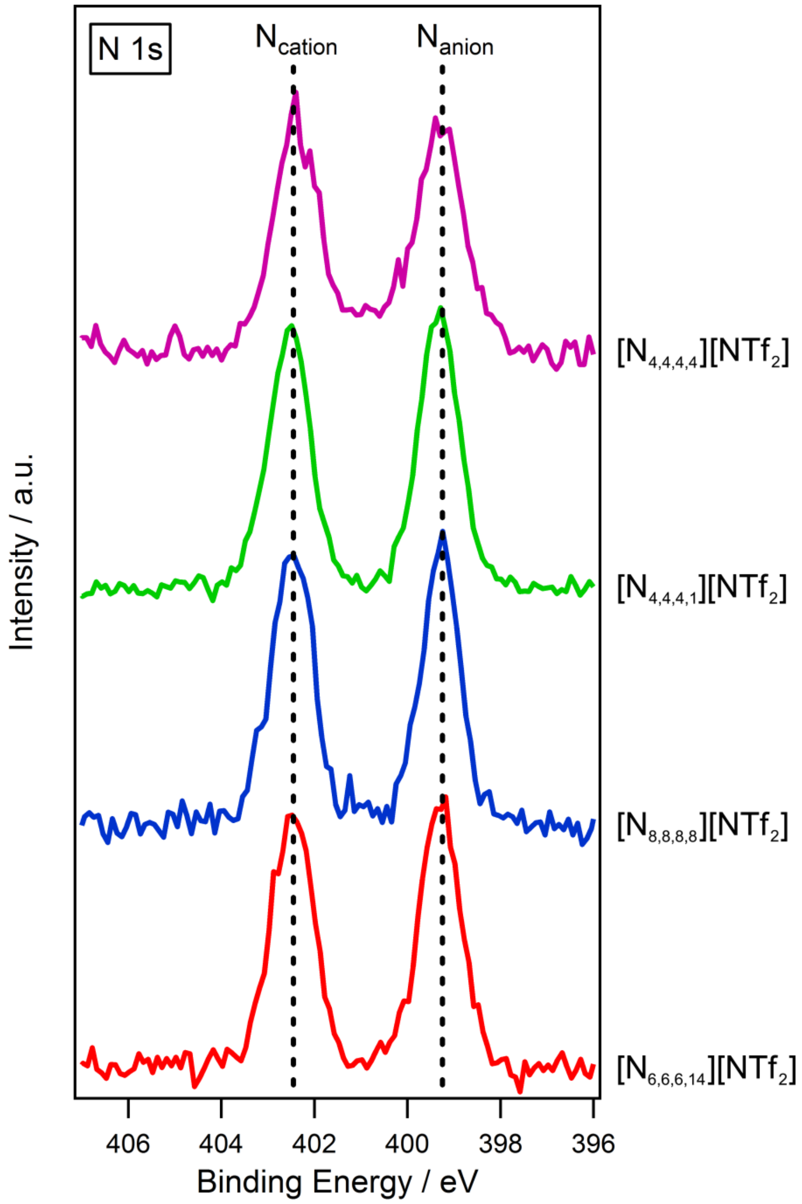

Figure 3.1. N 1s XP spectra for $[N_{6,6,6,14}][NTf_2]$, $[N_{8,8,8,8}][NTf_2]$, $[N_{4,4,4,1}][NTf_2]$ and $[N_{4,4,4,4}][NTf_2]$. Spectra normalised to the area of the F 1s photoelectron emission peak for $[N_{6,6,6,14}][NTf_2]$ and charge corrected by referencing the F 1s photoelectron peak to 688.7 eV.

Consequently, reliable charge correction can be achieved for ammonium cations consisting of short alkyl chains (n < 8) by referencing the binding energy of the N_{cation} 1s peak to the value obtained for its long chain analogue ($n \geq 8$), whereby prior charge correction has been carried out by referencing the $C_{aliphatic}$ 1s peak to 285.0 eV. It must be stressed that this procedure is only valid for a series of ionic liquids containing structurally similar cations and identical anions as it has been seen that cationic binding energy is very dependent upon anion type.[10, 14, 16, 17, 30] The influence of the anion on the cation is to be discussed further in *Section 3.2.4*.

3.2.3 C 1s Fitting Model

The development of fitting models to describe and deconstruct the different electronic environments for each element is particularly important. This is especially relevant to carbon, which has been described as the most important core level in XPS investigations of ionic liquids,[2] as an accurate description of the $C_{aliphatic}$ 1s component is crucial for reliable charge correction and the extraction of accurate binding energies.

Due to the variety and complexity in structure of ionic liquids, C 1s fitting models must be developed on a case-by-case basis, with the aim of developing a fitting model that deconstructs these electronic environments into the minimum number of components possible.[2, 10] C 1s fitting models have been described previously for a range of ionic liquid families including imidazolium,[4-6, 30] pyrrolidinium,[10] pyridinium,[16] and guanidinium.[17] Here this is extended to include the tetraalkylammonium and tetraalkylphosphonium cations.

Upon inspection of the C 1s region for ammonium-based ionic liquids two unresolved peaks for cationic carbon are observed in the binding energy range 284 – 288 eV. An additional peak corresponding to anionic carbon is observed at higher binding energy for ionic liquids containing the anions $[OTf]^-$ and $[NTf_2]^-$. A representative example of the C 1s region for $[N_{6,6,6,14}][NTf_2]$ is shown in Figure 3.2.

Considering the structure of a tetraalkylammonium cation is not dissimilar to that of pyrrolidinium, a three-component model based on that developed for pyrrolidinium cations was used to describe the different electronic environments of cationic carbon. An analysis of the structure of $[N_{6,6,6,14}]^+$ (see structure shown in Figure 3.2) highlights the three plausible electronic environments of carbon.

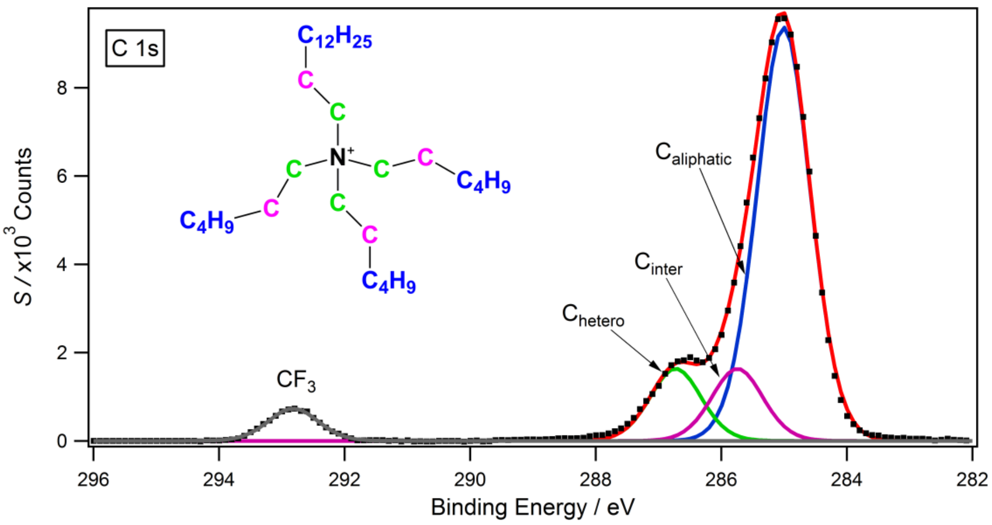

Figure 3.2. High resolution C 1s spectra for $[N_{6,6,6,14}][NTf_2]$ including colour coded component fittings for $C_{aliphatic}$ (blue), C_{inter} (purple), C_{hetero} (green) and CF_3 (grey); fitting envelope (red); counts (black dots) . Charge corrected by referencing $C_{aliphatic}$ 1s photoelectron peak to 285.0 eV.

The carbon directly bound to the nitrogen (C_{hetero}) is expected to have the highest binding energy as it is in closest proximity to the electropositive nitrogen, and thus feels a larger effect of the electron-withdrawing influence of the cationic nitrogen. The next carbon along the chain (C_{inter}) is designated as an "intermediate" carbon environment; here the electron-withdrawing impact of the nitrogen centre is less pronounced, resulting in a slightly lower binding energy. The remaining carbons are essentially aliphatic and give rise to the third contribution, $C_{aliphatic}$, which exhibits the lowest binding energy.

To obtain a satisfactory fit that accurately describes the electronic environment it is necessary to constrain certain parameters. Component areas are constrained to their nominal stoichiometries, *i.e.* for $[N_{6,6,6,14}][NTf_2]$ $C_{aliphatic}$: C_{inter} : C_{hetero} : C_{anion} equates to 6 : 1 : 1: 0.5. The full width at half maximum (FWHM) for C_{hetero} and C_{inter} are set to be equal (and constrained to be between 0.8 and 1.3 eV). The FWHM for $C_{aliphatic}$ is set to be 1.1 times larger than for C_{hetero} as studies on similar ionic liquid systems have characteristically shown the FWHM ratio of $C_{aliphatic}$: C_{hetero} to be 1.1 : 1.[10, 30] The fitting envelope (red trace) shown in Figure 3.2 demonstrates excellent agreement to the experimental spectra (black dots) highlighting the validity of this fitting model. C 1s component fittings for the ammonium ionic liquids investigated in this study are included in *Appendix A*, and are also in agreement with the experimental spectra.

3.2.4 Effect of the Anion

It has been previously established that XPS can be used to probe cation-anion interactions.[10, 14] These earlier studies focus upon the anionic influence on the cationic electronic environment, whereby the effect of various anions on a common cation is investigated. It was demonstrated that the binding energies of C_{hetero} 1s and N_{cation} 1s for imidazolium- and pyrrolidinium-based ionic liquids are dependent upon the basicity - and hence coordination strength - of the anion from correlations made between binding energy and the Kamlet-Taft hydrogen-bond acceptor parameter (β).[10, 14, 30] More recent investigations have also extended this to include pyridinium- and guanidinium- based ionic liquids in which similar behaviour is observed.[16, 17]

The dependence of C_{hetero} 1s and N_{cation} 1s on anion basicity has been attributed to the degree of charge transferred from anion to cation. Ionic liquids containing high basicity anions such as halides show lower C_{hetero} 1s and N_{cation} 1s binding energies, which indicate the cation is in a more electron-rich environment. This is indicative of a significant amount of charge-transfer from anion to cation. Low basicity anions such as $[NTf_2]^-$ give rise to higher C_{hetero} 1s and N_{cation} 1s binding energies signifying that the cation is more electron-poor due to a decrease in the degree of charge transferred.

Here the influence of the anion on the electronic environment of a tetraalkylammonium cation has been investigated for five $[N_{6,6,6,14}][X]$ ionic liquids (where X = Cl^-, $[BF_4]^-$, $[PF_6]^-$, $[OTf]^-$ and $[NTf_2]^-$), a visual representation of anion influence on N_{cation} 1s and C_{hetero} 1s is provided in Figure 3.3.

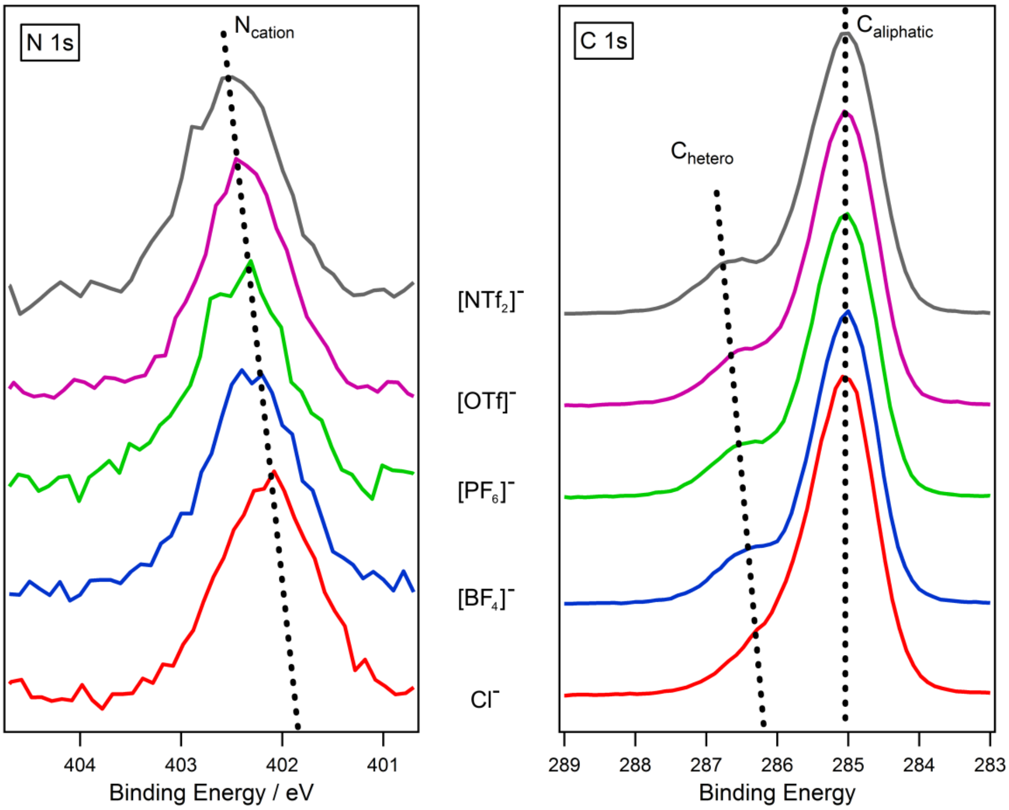

Figure 3.3. N 1s and C 1s high resolution XP spectra for $[N_{6,6,6,14}][X]$ where X = Cl^-, $[BF_4]^-$, $[PF_6]^-$, $[OTf]^-$ and $[NTf_2]^-$. Areas are normalised to the N_{cation} 1s peak for $[N_{6,6,6,14}]Cl$. Spectra are charge corrected by referencing $C_{aliphatic}$ 1s to 285.0 eV. *N.B.* spectra truncated to only show the cation region. Dashed lines are included to indicate binding energy shift (or lack of in the case of $C_{aliphatic}$ 1s) for the N_{cation} 1s and C_{hetero} 1s components.

It can be seen from Figure 3.3 that the measured binding energies (Table 3.2) of N_{cation} 1s and C_{hetero} 1s possess the following trend: $[NTf_2]^-$ > $[OTf]^-$ ≈ $[PF_6]^-$ > $[BF_4]^-$ > Cl^-. This can be interpreted as an increase in charge-transfer with increasing anion basicity, and is in accordance with studies on other ionic liquid families including imidazolium,[14, 30] pyrrolidinium,[10] pyridinium,[16] and guanidinium.[17] Consequently, it seems apparent that the process of charge-transfer from anion to cation (and also its dependence on anion basicity) is general to all systems studied to date.

3.3 XPS of Phosphonium Ionic Liquids

3.3.1 Purity and Quantification

As in the case of ammonium-based ionic liquids, survey and high resolution spectra were used to establish purity and elemental composition for the phosphonium ionic liquids investigated in this study, see Table 3.3 and *Appendix A*.

There was no evidence for the presence of hydrocarbon/silicone contaminants, or metal-based cations and halides carried over from salt metathesis chemistry. Experimental stoichiometries were found to be within the ± 20 % error associated with XPS quantification, and the majority are well within ± 10 %. Similar to ammonium ionic liquids a larger deviation in the chloride signal for $[P_{6,6,6,14}]Cl$ was noted, which is likely a result of the size of the chloride anion as previously mentioned. Additionally the P 2p signal is systematically less than the theoretical value with deviations larger than the experimental error recorded for $[P_{6,6,6,14}][BF_4]$ and $[P_{6,6,6,14}][PF_6]$. It is possible that this may be due to systematic error of the applied relative sensitivity factor for these particular compounds, *i.e.* the RSFs are not ideally suited for these compounds.

Table 3.3. Measured experimental and nominal (in brackets) stoichiometries for phosphonium ionic liquids studied in this work. [a] Relative sensitivity factors (RSFs) taken from the Kratos Library were used to derive atomic percentages from the most intense photoelectron emission peak for each element *i.e.* C = C 1s, N = N 1s, O = O 1s, F = F 1s, B = B 1s, S = S 2p, P = P 2p and Cl = Cl 2p. Associated experimental error is ± 10 – 20 %. A deviation larger than the experimental error is observed for the chloride and phosphorus photoelectron emission peaks, which is discussed in further detail on pg. 83. *N.B.* Hydrogen is undetectable by XPS due its low photoionisation cross-section; consequently reported stoichiometries are determined without consideration of hydrogen content.

	Composition[a] (%)							
Compound	**C**	**N**	**O**	**F**	**B**	**S**	**P**	**Cl**
RSF[4, 32]	0.278	0.477	0.780	1.000	0.159	0.668	0.486	0.891
$[P_{6,6,6,14}]Cl$	95.2 (94.1)	-	-	-	-	-	2.7 (2.9)	2.1 (2.9)
$[P_{6,6,6,14}][BF_4]$	85.3 (84.2)	-	-	10.6 (10.5)	2.2 (2.6)	-	2.0 (2.6)	-
$[P_{6,6,6,14}][PF_6]$	79.9 (80.0)	-	-	16.3 (15.0)	-	-	3.8 (5.0)	-
$[P_{6,6,6,14}][OTf]$	81.3 (80.5)	-	7.4 (7.3)	7.3 (7.3)	-	2.1 (2.4)	2.0 (2.4)	-
$[P_{6,6,6,14}][NTf_2]$	70.8 (70.8)	2.2 (2.1)	8.9 (8.3)	12.6 (12.5)	-	3.9 (4.2)	1.7 (2.1)	-
$[P_{4,4,4,1}][BF_4]$	68.6 (68.4)	-	-	21.3 (21.1)	5.0 (5.3)	-	5.0 (5.3)	-
$[P_{4,4,4,1}][NTf_2]$	52.6 (51.7)	3.5 (3.4)	13.8 (13.8)	20.8 (20.7)	-	6.5 (6.9)	2.8 (3.4)	-

3.3.2 Effect of Alkyl Chain Length

To determine if short chain ($n < 8$) phosphonium cations can be charge corrected utilising a similar method to their ammonium analogues (see *Section 3.2.2*) it must first be understood if the length of the aliphatic chain influences the electronic environment of the phosphorus cationic core.

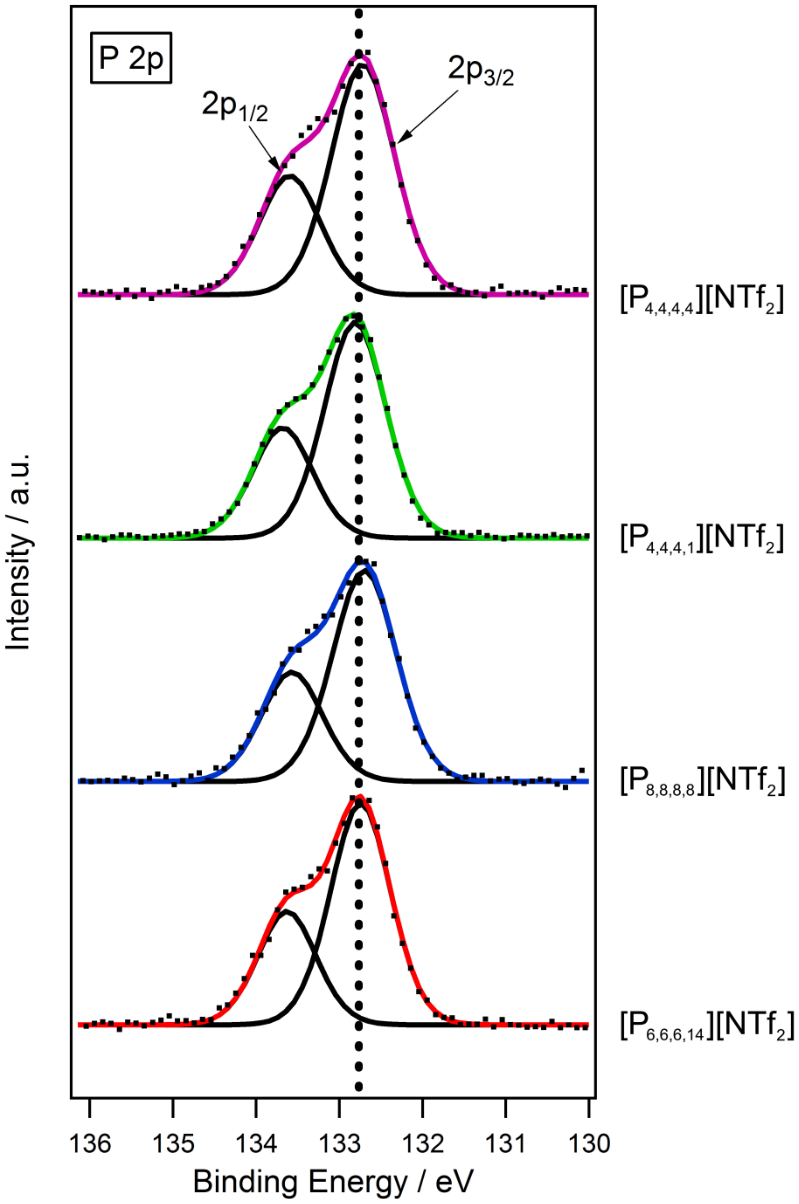

Figure 3.4. P 2p XP spectra for $[P_{6,6,6,14}][NTf_2]$, $[P_{8,8,8,8}][NTf_2]$, $[P_{4,4,4,1}][NTf_2]$ and $[P_{4,4,4,4}][NTf_2]$. Spectra normalised to the area of the F 1s photoelectron emission peak for $[P_{6,6,6,14}][NTf_2]$ and charge corrected by referencing the F 1s photoelectron peak to 688.7 eV.

To achieve this, an analogous series of phosphonium ionic liquids comprising of $[P_{6,6,6,14}][NTf_2]$, $[P_{8,8,8,8}][NTf_2]$, $[P_{4,4,4,1}][NTf_2]$, and $[P_{4,4,4,4}][NTf_2]$ were investigated (Figure 3.4). To enable reliable comparison of P 2p binding energies, spectra were charge corrected by referencing the F 1s photoelectron peak to 688.7 eV (the measured F 1s binding energy obtained for $[P_{6,6,6,14}][NTf_2]$ where charge correction was achieved by referencing $C_{aliphatic}$ 1s to 285.0 eV).

The P 2p region for all compounds studied shows two unresolved peaks arising from splitting of the P 2p peak into a doublet as a result of the spin-orbit coupling effect. Spin-orbit coupling arises from coupling of the magnetic field produced by an electron spinning arounds its own axis (defined by the spin angular momentum quantum number, s, (where $s = \pm 1/2$)) with the magnetic field produced by an electron spinning around its nucleus (defined by the orbital angular momentum quantum number, l) and is described by $j = (l + s)$. Consequently, s levels ($l = 0$) are singlets but all other levels ($l > 0$) give rise to doublet components, see Table 3.4. The relative intensities of the components are given by the ratio of their degeneracies ($2j + 1$).

Table 3.4. Spin-orbit splitting parameters. Where l = orbital angular momentum quantum number, s = spin angular momentum quantum number, and j = total angular momentum quantum number.

Orbital	l	s	j ($l + s$)	Area Ratio ($2j + 1$)
s	0	±1/2	1/2	N/A
p	1	±1/2	1/2, 3/2	1:2
d	2	±1/2	3/2, 5/2	2:3
f	3	±1/2	5/2, 7/2	3:4

Therefore for the P 2p level the ratio of components ($2p_{1/2}$ and $2p_{3/2}$) is statistically defined as 1: 2, which is characteristic for all p-orbitals. The binding energy difference of the P 2p spin-orbit splitting components, ΔBE (P $2p_{1/2} - 2p_{3/2}$), is 0.9 eV.

It can be seen from Figure 3.4 and Table 3.2 that the measured P_{cation} $2p_{3/2}$ binding energies are within the experimental error, thereby indicating that the length of the alkyl chain does not impact upon the phosphorus cationic core. Accordingly, short chain ($n < 8$) phosphonium cations can be charge corrected in a similar manner to their ammonium equivalents, whereby the P_{cation} $2p_{3/2}$ peak is referenced to the value obtained for its long chain ($n \geq 8$) analogue (where prior charge correction has been achieved by referencing $C_{aliphatic}$ 1s to 285.0 eV).

3.3.3 C 1s Fitting Model

The C 1s region for phosphonium ionic liquids differs quite considerably from that of ammonium ionic liquids. It can be seen from the C 1s region for phosphonium ionic liquids that only a single peak with slight asymmetry is observed in the binding energy range 284 – 287 eV, with an additional peak observed at higher binding energy that corresponds to anionic carbon for phosphonium ionic liquids containing an $[OTf]^-$ or $[NTf_2]^-$ anion. A representative example of the C 1s region for $[P_{6,6,6,14}][NTf_2]$ is provided in Figure 3.5.

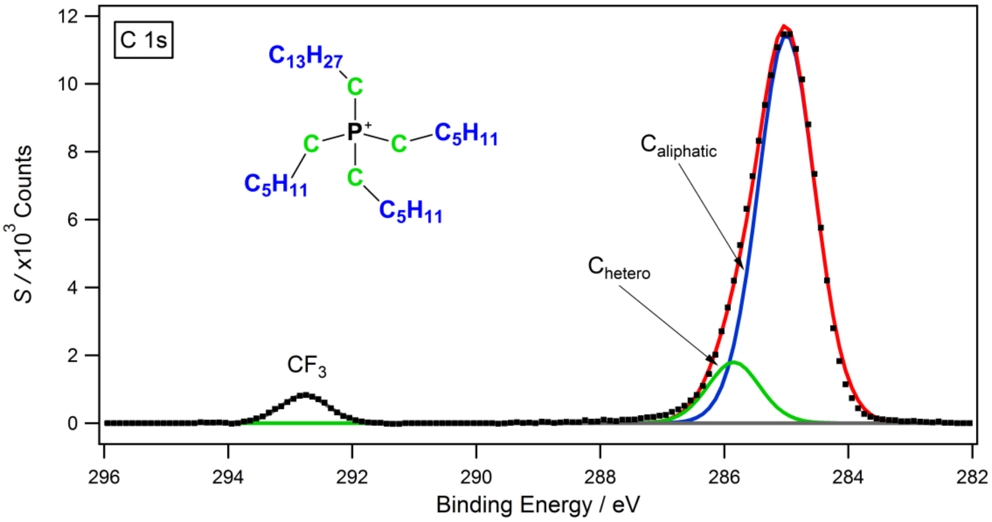

Figure 3.5. High resolution C 1s spectra for $[P_{6,6,6,14}][NTf_2]$ including colour coded component fittings for $C_{aliphatic}$ (blue), C_{hetero} (green) and CF_3 (grey); fitting envelope (red); counts (black dots) . Charge corrected by referencing $C_{aliphatic}$ 1s photoelectron peak to 285.0 eV.

It is apparent that the broad peak in the energy range 284 – 287 eV is distinctly lacking the more obvious shoulder at higher binding energy as seen in the case of the ammonium analogues, see Figure 3.2 and Figure 3.5. Consequently, this peak was fitted using a two component model; the first contribution at higher binding energy arising from the carbon atoms directly bound to the phosphorus (C_{hetero}), with the remaining carbons considered as essentially aliphatic ($C_{aliphatic}$) and occurring at lower binding energy. Parameter constraints were applied in a similar manner to the previously discussed ammonium model, in which component areas were constrained to their nominal stoichiometry *i.e.* for $[P_{6,6,6,14}][NTf_2]$ $C_{aliphatic}$: C_{hetero} : C_{anion} was set to 7 : 1 : 0.5. The FWHM for each component was constrained to be between 0.8 and 1.3 eV, with the FWHM for $C_{aliphatic}$ also set to be 1.1 times larger than for $C_{hetero.}$

A comparison of binding energies (Table 3.2) for the C_{hetero} component of the $[N_{6,6,6,14}]^+$ and $[P_{6,6,6,14}]^+$ cations show that C_{hetero} for $[N_{6,6,6,14}]^+$ is 0.6 - 0.8 eV larger than for the $[P_{6,6,6,14}]^+$ analogue. This can be attributed to the difference in charge density of the nitrogen and phosphorus cationic centres. The smaller atomic radius of nitrogen, in comparison to phosphorus, results in a higher charge density. Consequently, the C_{hetero} carbons for ammonium-based ionic liquids experience a stronger electron-withdrawing effect from the positively charged nitrogen centre which is reflected by a shift to higher binding energy.

Furthermore, from Table 3.2 it can be seen that C_{hetero} binding energies for phosphonium-based ionic liquids are more similar in value to the C_{inter} component for the ammonium analogues. This highlights the weaker electron-withdrawing effect of the phosphorus centre, as a result of its lower charge density, and validates the use of a two-component fitting model to describe the C 1 region for phosphonium-based ionic liquids.

3.3.4 Effect of the Anion

To investigate if phosphonium ionic liquids display a similar anionic dependence on charge transferred from anion to cation five tetraalkylphosphonium ionic liquids of the type $[P_{6,6,6,14}][X]$ (where X = Cl^-, $[BF_4]^-$, $[PF_6]^-$, $[OTf]^-$ and $[NTf_2]^-$) were studied. From Table 3.2 it is seen that the measured binding energies of P_{cation} $2p_{3/2}$ follow the trend $[NTf_2]^- \approx [OTf]^- \approx [PF_6]^- > [BF_4]^- > Cl^-$, this shift is also illustrated by Figure 3.6, thus presenting a similar trend to the tetraalkylammonium analogues.

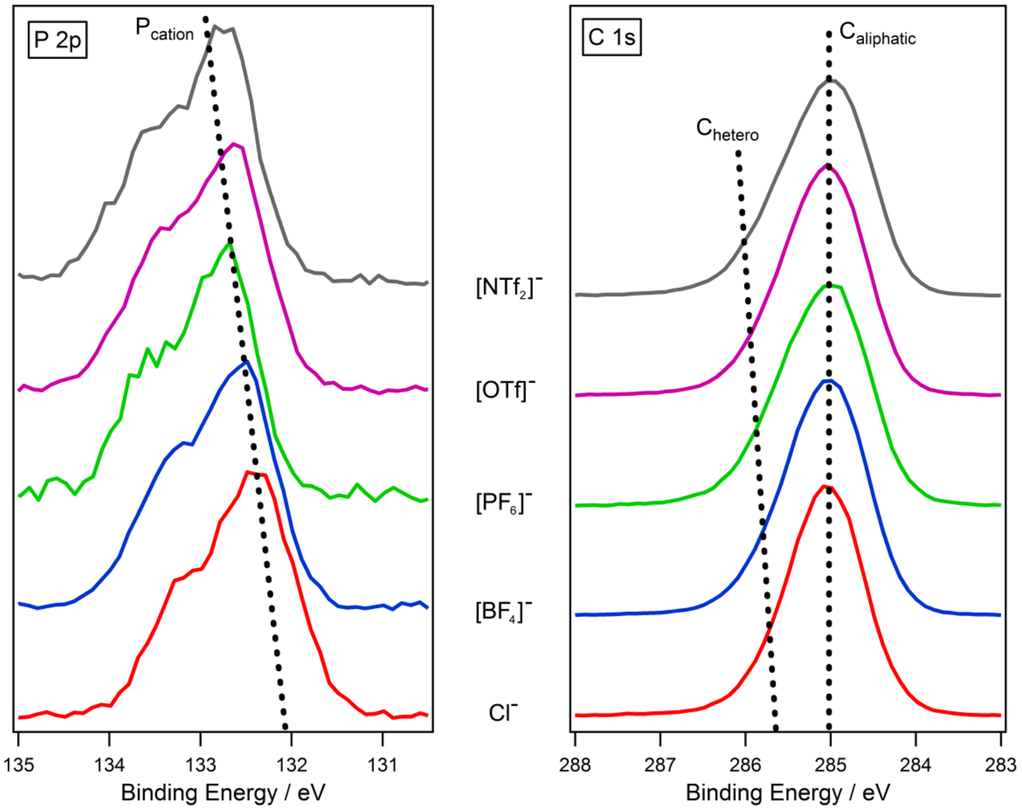

Figure 3.6. P 2p and C 1s high resolution XP spectra for $[P_{6,6,6,14}][X]$ where X = Cl^-, $[BF_4]^-$, $[PF_6]^-$, $[OTf]^-$ and $[NTf_2]^-$. Areas are normalised to the P_{cation} 2p peak for $[P_{6,6,6,14}]Cl$. Spectra are charge corrected by referencing $C_{aliphatic}$ 1s to 285.0 eV. *N.B.* spectra truncated to only show the cation region. Dashed lines are included to indicate binding energy shift (or lack of in the case of $C_{aliphatic}$ 1s) for the P_{cation} $2p_{3/2}$ and C_{hetero} 1s components.

Additionally, the binding energies for the C_{hetero} component display the same pattern as for the P_{cation} $2p_{3/2}$ component, although the shift in C_{hetero} does not appear as obvious as in the case of the ammonium compounds (see Figure 3.3 and Figure 3.6) due to the broad line shape of the respective phosphonium C 1s emission envelope. Nevertheless, the measured C_{hetero} 1s binding energies do present this shift to be outside of the experimental error, and therefore real. Accordingly, phosphonium ionic liquids also exhibit the same anionic dependence on charge-transfer, thereby suggesting this to be an intrinsic property for most ionic liquid systems

A linear correlation of N_{cation} 1s and C_{hetero} 1s binding energies with the Kamlet-Taft β parameter (a measure of hydrogen bond acceptor ability of the anion) has been established for imidazolium-based ionic liquids.[14] However, to date, β has been less extensively studied for ammonium and phosphonium ionic liquids due to the solid nature of many of these compounds at room temperature, thus there are only a select few examples in the literature, which are mainly based on the $[NTf_2]^-$ anion.[36-39] Consequently, a comparison of β with binding energy cannot be made for the compounds investigated in this study due to a restricted dataset of liquid samples, however it is expected that a similar trend to imidazolium-based ionic liquids would be observed.

3.4 Correlation of XPS C 1s fitting model to $^1H/^{13}C$ NMR

As discussed previously in *Section 3.3.3* it is apparent that changing the cationic core from nitrogen to phosphorus has a measurable impact on the electronic environments of the neighbouring carbon atoms of the cation, which may be attributed to the different charge densities of the cationic cores.

This can also be observed by ^1H NMR studies of the $[N_{6,6,6,14}][NTf_2]$ and $[P_{6,6,6,14}][NTf_2]$ ionic liquids. Here it is shown that the hydrogen atoms bound to C_{hetero} occur at highest chemical shift followed by the C_{inter} associated hydrogens, whereas the remaining hydrogen environments resonate further upfield, see Figure 3.7 and Figure 3.8 . The effect of changing the cationic core from nitrogen to phosphorus is clearly presented by the chemical shift for the C_{hetero} hydrogen ($H_{1,\ 1'}$), which occurs at a significantly higher chemical shift of 3.14 ppm for $[N_{6,6,6,14}][NTf_2]$ in comparison to 2.20 ppm for $[P_{6,6,6,14}][NTf_2]$; thereby, illustrating the stronger electron-withdrawing influence of the nitrogen cationic core, in comparison to phosphorus, as a result of its higher charge density.

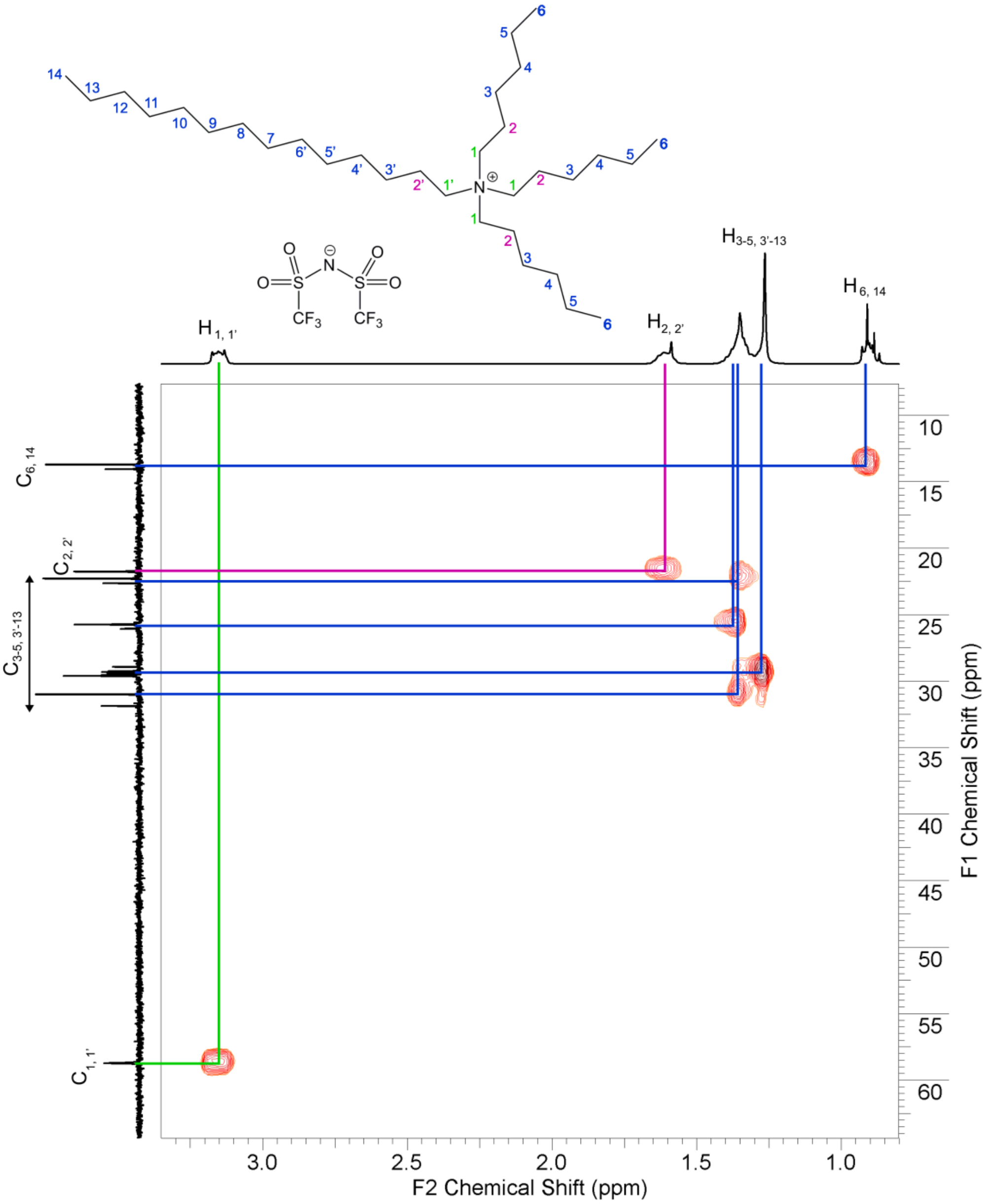

Figure 3.7. 2D ^{1}H-^{13}C HMQC NMR of [N$_{6,6,6,14}$][NTf$_2$]. Spectra truncated to show peaks corresponding to cationic carbon/hydrogen environments. *N.B.* It is important to note that as ^{1}H/^{13}C NMR is more sensitive to differences in electronic environment than XPS a numerical system is used to label the different carbon environments (and their associated hydrogen atoms), see labelled structure above. Therefore the deconstructed carbon NMR environments, with the equivalent XPS notation in brackets, are C$_{1,1'}$ (C$_{hetero}$), C$_{2,2'}$ (C$_{inter}$) and C$_{3\text{-}6,\ 3'\text{-}14}$ (C$_{aliphatic}$).

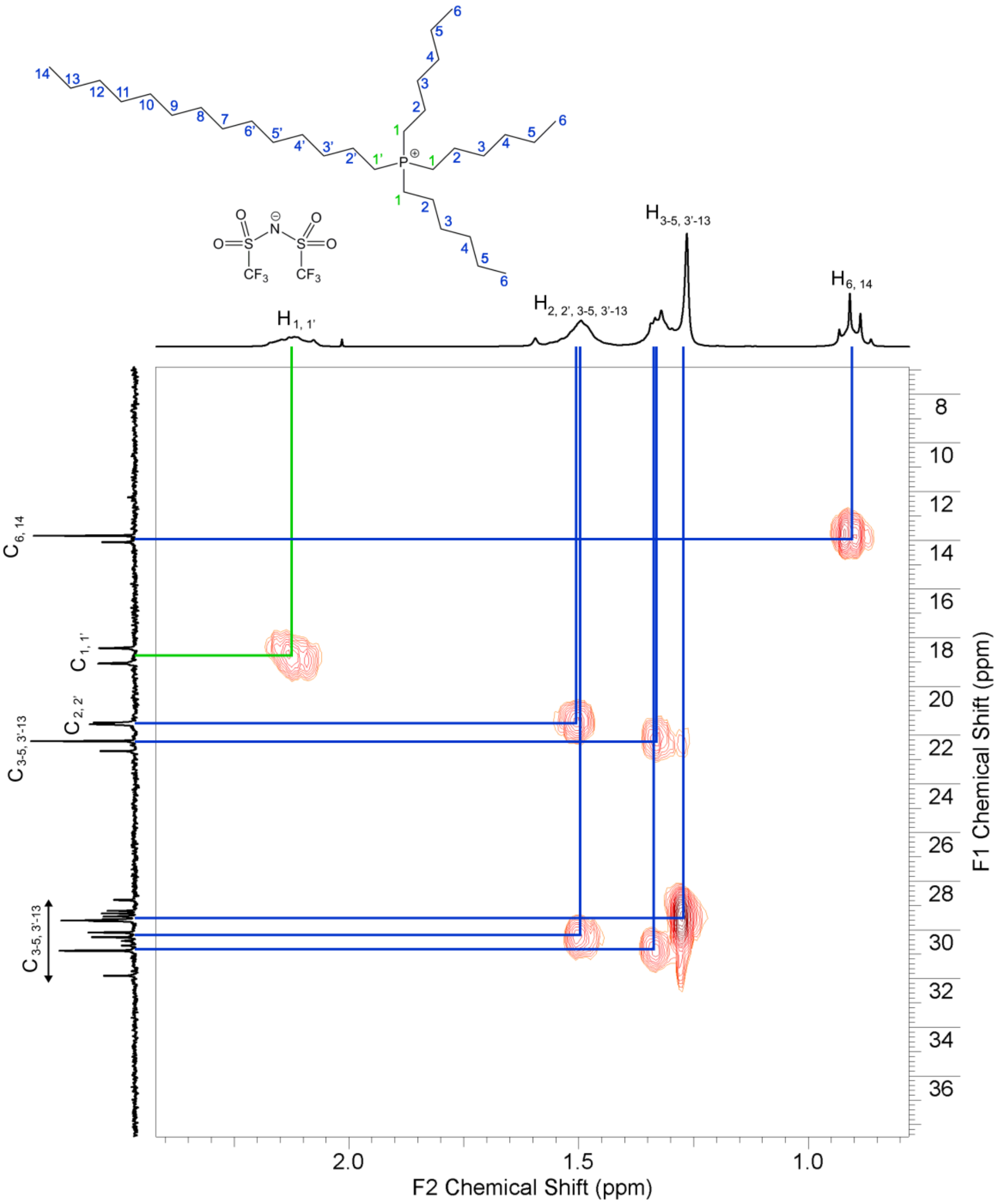

Figure 3.8. 2D ^{1}H-^{13}C HMQC NMR of [$P_{6,6,6,14}$][NTf_2]. Spectra truncated to show peaks corresponding to cationic carbon/hydrogen environments. *N.B.* It is important to note that as ^{1}H/^{13}C NMR is more sensitive to differences in electronic environment than XPS a numerical system is used to label the different carbon environments (and their associated hydrogen atoms), see labelled structure above. Therefore the deconstructed carbon NMR environments, with the equivalent XPS notation in brackets, are $C_{1,1'}$ (C_{hetero}) and $C_{2\text{-}6,\ 2'\text{-}14}$ ($C_{aliphatic}$).

Due to the high carbon content for these ionic liquids their corresponding ^{13}C NMR spectra are particularly convoluted. Subsequently, 2D Heteronuclear Multiple-Quantum Correlation (HMQC) NMR was used to correlate directly bonded carbon-proton nuclei to enable the assignment of the ^{13}C NMR spectra, see Figure 3.7 and Figure 3.8. In the case of $[N_{6,6,6,14}][NTf_2]$ the signal for C_{hetero} $(C_{1,1'})$ has the highest chemical shift (~60 ppm) as would be expected due its close proximity to the electron-withdrawing nitrogen cationic centre. However, for $[P_{6,6,6,14}][NTf_2]$ the C_{hetero} $(C_{1,1'})$ signal is shifted significantly upfield to ~19 ppm presenting itself as a doublet ($^1J_{CP}$ = 46.8 Hz) due to ^{13}C-^{31}P coupling. This abnormally high degree of shielding is likely to be a result of the larger size of phosphorus, whereby the larger phosphorus orbitals induce more complex shielding effects on the carbon atom directly bound to it. This is known as the heavy-atom effect and has been seen previously for carbon atoms directly bound to increasingly heavier halogen and chalcogen atoms.[40-42]

Furthermore, for $[N_{6,6,6,14}][NTf_2]$ the overall trend in carbon chemical shift does not reflect that exhibited by the proton shift (where δ_H $(H_{1,1'}) >$ δ_H $(H_{2,2'})$ $>$ δ_H $(H_{3\text{-}5,\ 3'\text{-}13,}\ H_{6,14})$) as δ_C $(C_{2,2'})$ is shifted further upfield than would be expected. This is a consequence of carbon shifts being strongly affected by additive contributions of substituents in α, β, γ and δ positions.[42, 43] As such carbon NMR does not always provide a reliable indicator of the chemistry of the compound; proton NMR, however, is much less influenced by these effects and provides a better description of the chemical environment. Consequently, a good correlation exists between ^{1}H NMR chemical shifts and XPS C 1s component binding energies, providing further validation for the C 1s fitting models described previously, and illustrating the influence of charge density for the different cationic cores.

3.5 Effect of Cationic Core

3.5.1 $[\mathbf{N_{6,6,6,14}}]^+$ *versus* $[\mathbf{P_{6,6,6,14}}]^+$

As mentioned previously in *Section 3.2.4* cation-anion interactions for a range of ionic liquids have been extensively investigated using XPS. However, to date these studies have been limited to the anionic influence on a common cation. Subsequently, the influence of the cationic core on a common anion is investigated herein.

It is expected that the difference in charge density of the ammonium and phosphonium cationic core will affect the degree of charge-transfer, which would be reflected in the binding energy of the anionic components. It was postulated that a greater degree of charge-transfer would occur for the ammonium cation, as the larger charge density would be more effective in removing excess negative charge from the anion; hence, the binding energies of the anion are expected to indicate a more electron-poor environment in contrast to the phosphonium analogue.

A comparison of binding energies (Table 3.2), however, did not support this assumption. Figure 3.9 illustrates a comparison between [$N_{6,6,6,14}$][BF_4] and [$P_{6,6,6,14}$][BF_4] for all regions. All XP spectra are charge corrected by referencing $C_{aliphatic}$ 1s to 285.0 eV; and are normalised to the area of the F 1s photoelectron emission peak for [$N_{6,6,6,14}$][BF_4] as the number of fluorine atoms are equivalent for both samples. It can be seen that the binding energies of the anionic components are identical, within the error of experiment (± 0.1 eV), for example the F 1s component for [$N_{6,6,6,14}$][BF_4] and [$P_{6,6,6,14}$][BF_4] is 685.7 eV in each instance (Figure 3.9 and Table 3.2). This is also true for the B 1s component where binding energies are 194.0 eV and 193.9 eV for [$N_{6,6,6,14}$][BF_4] and [$P_{6,6,6,14}$][BF_4] respectively. The P 2s photoelectron emission peak is also observed in the B 1s XP spectrum for [$P_{6,6,6,14}$][BF_4] at a lower binding energy of 190.4 eV.

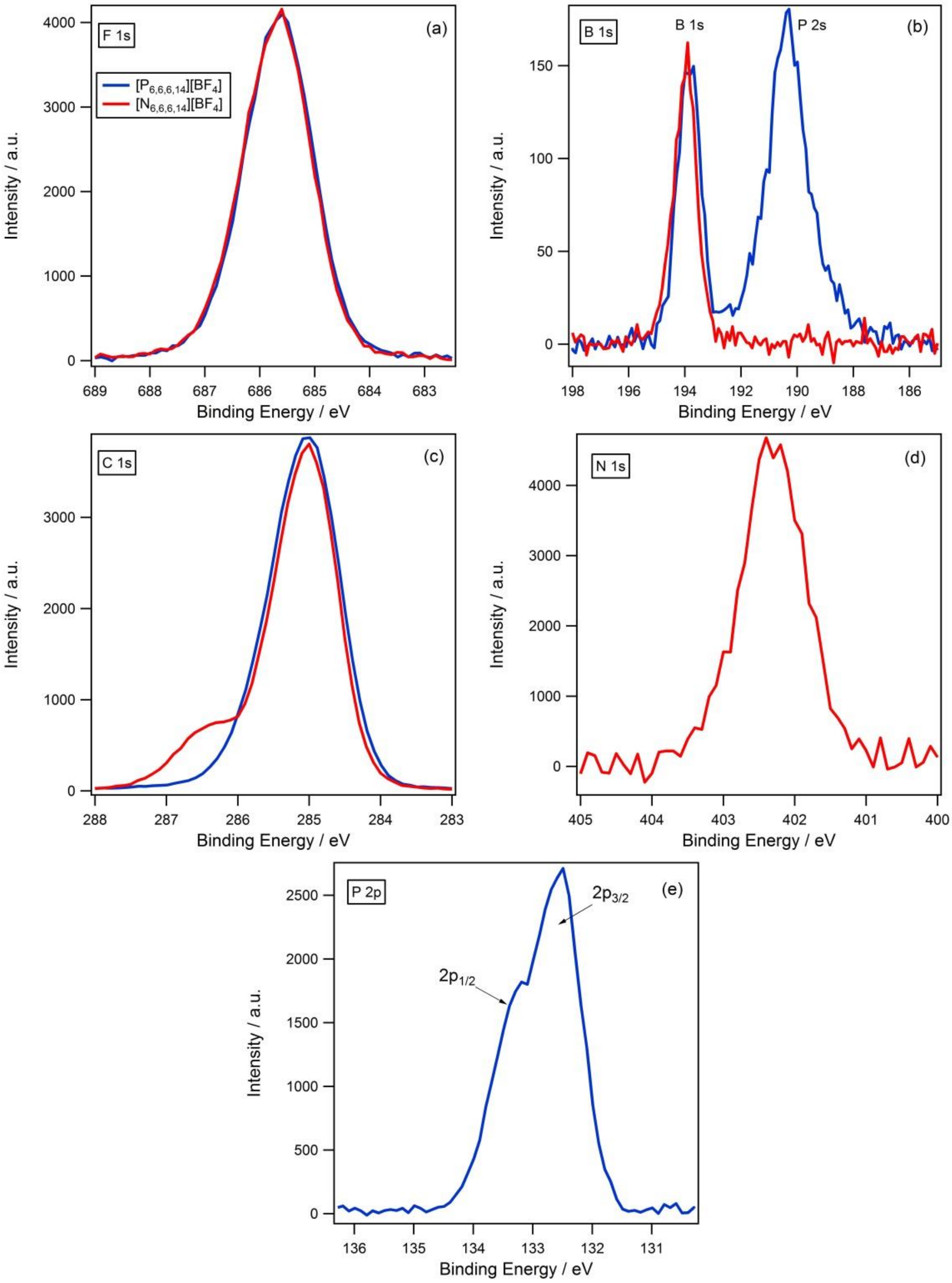

Figure 3.9. XP spectra of $[N_{6,6,6,14}][BF_4]$ and $[P_{6,6,6,14}][BF_4]$ for: (a) F 1s, (b) B 1s, (c) C 1s, (d) N 1s and (e) P 2p. Areas normalised to area of F 1s peak for $[N_{6,6,6,14}][BF_4]$. Spectra were charge corrected by setting $C_{aliphatic}$ 1s = 285.0 eV.

The anionic component binding energies for a range of anions of varying size and basicity, including Cl^-, $[PF_6]^-$, $[OTf]^-$ and $[NTf_2]^-$, also match within the experimental error for the $[N_{6,6,6,14}]^+$ and $[P_{6,6,6,14}]^+$ cations. This suggests that the anion cannot experience the difference in charge density of the cation, and it is proposed that the long alkyl chains are wrapped around the cationic centre effectively shielding it from the anion. This is in agreement with measurements on the enthalpy of vaporisation at 298 K, $\Delta_{vap}H_{298}$, for $[P_{6,6,6,14}][BF_4]$, which describe how the experimentally determined van der Waals contribution is significantly smaller than the theoretical value, it is suggested that parts of the alkyl chain close to the phosphorus are unavailable for van der Waals bonding with adjacent species due to shielding from the outer parts of the chain.[44] In contrast, molecular dynamics simulations indicate that the alkyl chains are in a fully stretched conformation, with a small degree of bending for longer chains ($n > 6$) and no evidence of coiling or wrapping.[45, 46]

It should be noted that although the anion is shielded from the difference in charge density of the two different cations, it is not shielded from experiencing a positive charge completely. In this way, the "wrapping" of the aliphatic chains has little impact on the actual ability of the anion to transfer charge, and hence a shift in binding energy of the cationic core is seen for anions of different basicity as mentioned previously in *Sections 3.2.4* and *3.3.4*.

3.5.2 $[N_{4,4,4,1}]^+$ *versus* $[P_{4,4,4,1}]^+$

In the previous section it was determined for ammonium and phosphonium cations with long alkyl chains that there is no difference in binding energy of the anionic components for a variety of different anions. To test whether the length of the alkyl chain impacts on cation-anion interactions and the ability of the anion to experience the difference in charge density of the cationic centres, a series of short chain analogues were investigated where the cation size has been reduced to $[N_{4,4,4,1}]^+$ and $[P_{4,4,4,1}]^+$. A visual comparison between $[N_{4,4,4,1}][BF_4]$ and $[P_{4,4,4,1}][BF_4]$ for all regions is shown in Figure 3.10.

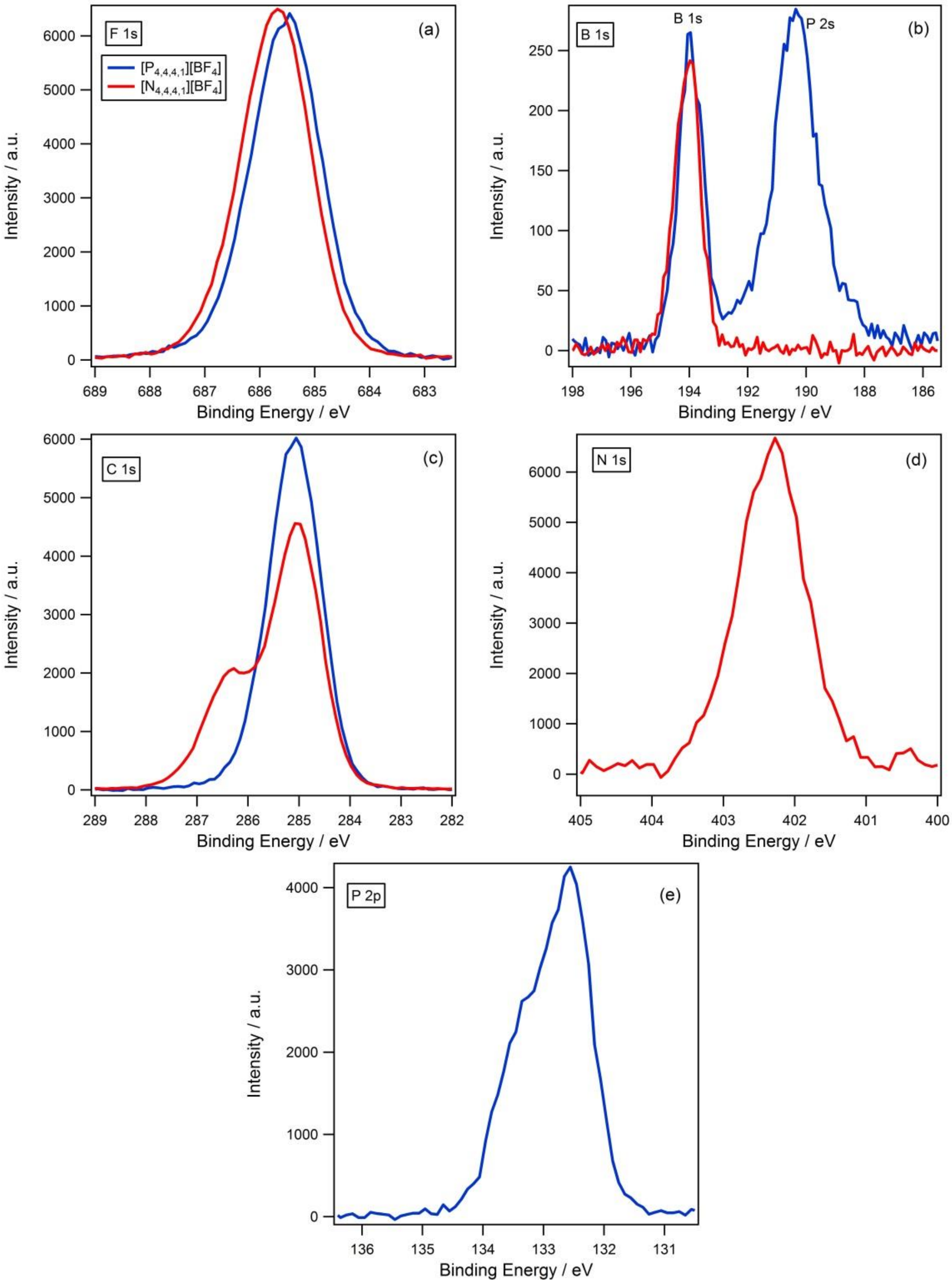

Figure 3.10. XP spectra of $[N_{4,4,4,1}][BF_4]$ and $[P_{4,4,4,1}][BF_4]$ for: (a) F 1s, (b) B 1s, (c) C 1s, (d) N 1s and (e) P 2p. Areas normalised to area of F 1s peak for $[N_{4,4,4,1}][BF_4]$. $[N_{4,4,4,1}][BF_4]$ XP spectra charge corrected by setting N_{cation} 1s to 402.3 eV. $[P_{4,4,4,1}][BF_4]$ XP spectra charge corrected by setting P_{cation} $2p_{3/2}$ to 132.6 eV

The F 1s binding energy for $[N_{4,4,4,1}][BF_4]$ is 0.2 eV higher than for $[P_{4,4,4,1}][BF_4]$ (Figure 3.10 and Table 3.2), this being at the upper limit of the accepted experimental error (and slightly larger, at 0.22 eV) is taken to suggest that the shift is real. A similar shift of 0.2 eV is also seen for the B 1s binding energy (Table 3.2), however due to the larger energy range used in Figure 3.10b to accommodate the P 2s peak it is less obvious than that of the F 1s photoelectron peak.

As the B 1s and F 1s binding energies are higher for $[N_{4,4,4,1}]^+$ relative to $[P_{4,4,4,1}]^+$ this is indicative that the boron and fluorine atoms are more electron-poor for $[N_{4,4,4,1}]^+$, which suggests a greater degree of charge-transfer occurs for the ammonium-based ionic liquid. This supports the initial hypothesis that charge-transfer should be more significant for ammonium-based ionic liquids due to the larger charge density of the cationic core relative to the phosphonium analogue. Additionally, it indicates that reducing the length of the alkyl chain allows for a more open structure of the cation which permits the anion to experience the difference in charge density of the cationic centre.

It should be noted that for $[N_{4,4,4,1}][NTf_2]$ and $[P_{4,4,4,1}][NTf_2]$ only a small shift (~ 0.1 eV) to a higher binding energy is observed for the anionic components of $[N_{4,4,4,1}]^+$ relative to $[P_{4,4,4,1}]^+$ (Table 3.2). This is within the experimental error so no real conclusion can be made; however, as $[NTf_2]^-$ is poorly co-ordinating it is likely that it participates in charge-transfer to a very small degree, hence little or no difference is observed when comparing the different cationic centres. Furthermore, comparison could not be made between the $[N_{4,4,4,1}]^+$ and $[P_{4,4,4,1}]^+$ cations when coupled with the highly basic Cl^- anion. This was due to the instability of $[N_{4,4,4,1}]Cl$ under the X-ray beam, which resulted in irregularities in peak line shape, thus reliable binding energies could not be obtained for this ionic liquid.

Fabris *et al*. found that a trioctylmethylphosphonium ($[P_{8,8,8,1}]^+$) cation coupled with a methylcarbonate ($[MeOCOO]^-$) or hydrogen carbonate ($[HOCOO]^-$) anion exhibited stronger basicity than its ammonium counterparts and other conventional basic catalysts, and as a result was a more efficient catalyst for Michael reactions.[47] This could support the assertions made from the work described here, as the high basicity of $[P_{8,8,8,1}][MeOCOO]$ and $[P_{8,8,8,1}][HOCOO]$ may arise from a smaller degree of charge-transfer occurring from anion to cation; consequently the anion is more electron-rich thus the electrons are more available for donation. In contrast, a higher degree of charge-transfer occurs for the ammonium analogues and inorganic bases as a result of the larger charge density of the cationic centre, hence basicity is reduced as electron density is less available for donation.

It is still unclear at this time how the charge-transfer phenomenon is mediated. Previous studies on 1-alkyl-3-methylimidazolium systems have shown a correlation between anion basicity and hydrogen-bonding at the C-2 position, and also with N_{cation} 1s and C 1s binding energy.[14] However, upon methylation of the C-2 position (hence decreasing the hydrogen-bonding contribution) an anion-dependent shift of the N_{cation} 1s and C 1s binding energies is still observed at a similar magnitude as the non-methylated analogues.[14] This indicates that charge-transfer cannot solely be mediated through hydrogen-bonding, which is especially relevant in the case of tetraalkylammonium and phosphonium ILs as the proton alpha to the heteroatom is even less available due to steric hindrance of the long alkyl chains. This suggests charge-transfer is also highly dependent on the coulombic interaction of the cation and anion.

3.6 Influence of Cation Conformational Flexibility

As discussed in *Section 3.5* it was seen that changing the cationic core from nitrogen to phosphorus for long chain systems, *i.e.* $[N_{6,6,6,14}]^+$ *versus* $[P_{6,6,6,14}]^+$, had minimal impact on charge-transfer due to a perceived hydrocarbon-based shielding of the cationic core. In an effort to reduce the effect of hydrocarbon-based shielding of the heteroatom, a second series of experiments were conducted where the alkyl components are pruned back, *i.e.* $[N_{4,4,4,1}]^+$ *versus* $[P_{4,4,4,1}]^+$, and it was found that changing the cationic core from nitrogen to phosphorus does indeed influence the degree of charge-transfer, with an increase in charge-transfer shown for ammonium ILs.

Here the concept of hydrocarbon-based shielding of the cationic core, and its impact upon cation-anion interactions, is explored further by comparison of a relatively unconstrained $[N_{6,6,6,14}]^+$ cation with a conformationally constrained $[C_8C_1Pyrr]^+$ cation. Whereby, the degree of charge-transfer is assessed for a common anion, in which anions of varying size and basicity are investigated, including the Cl^-, $[BF_4]^-$ and $[NTf_2]^-$ anions.

The 1-octyl-1-methylpyrrolidinium and trihexyl(tetradecyl)ammonium cations are structurally very similar; however, a large proportion of the alkyl chain for $[C_8C_1Pyrr]^+$ is effectively "pinned back" in a 5-membered heterocyclic ring. Subsequently, the nitrogen core is expected to be more exposed than in the case of $[N_{6,6,6,14}]^+$ in which the central nitrogen is shielded by a layer of conformationally flexible long-chain hydrocarbon. Crystallographic data reported by Adamova *et al.*[21] supports this assertion since they describe the $N\cdots Cl$ distance for $[N_{2,2,2,2}]Cl$ as significantly longer than for $[C_3C_1Pyrr]Cl$. This is attributed to the fact that the presence of strained rings around the central nitrogen atom for $[C_3C_1Pyrr]Cl$ allows a closer approach of the halide anion.[21]

On consideration of the Coulomb potential, the interaction energy of two point charges is inversely proportional to separation distance. Consequently, the closer two point charges are to each other the stronger the interaction between them. Therefore, it is anticipated that a greater degree of charge-transfer will occur in the case of the constrained $[C_8C_1Pyrr]^+$ cation due to a stronger interaction with the anion, which would be reflected in the measured binding energy values for the anionic components.

The high resolution XP spectra for all elemental regions for $[N_{6,6,6,14}]Cl$ and $[C_8C_1Pyrr]Cl$ are presented in Figure 3.11. To enable a visual comparison between the samples, spectra were normalised to the intensity of the Cl 2p photoelectron emission for $[N_{6,6,6,14}]Cl$, as both samples contain chlorine atoms in the same stoichiometric quantity. Consequently, the different stoichiometries of carbon for each cation are clearly evidenced by the significantly more intense C 1s spectra for $[N_{6,6,6,14}]Cl$ in comparison to $[C_8C_1Pyrr]Cl$, where the stoichiometric carbon content for $[N_{6,6,6,14}]^+$ is ~ × 2.5 larger than for $[C_8C_1Pyrr]^+$.

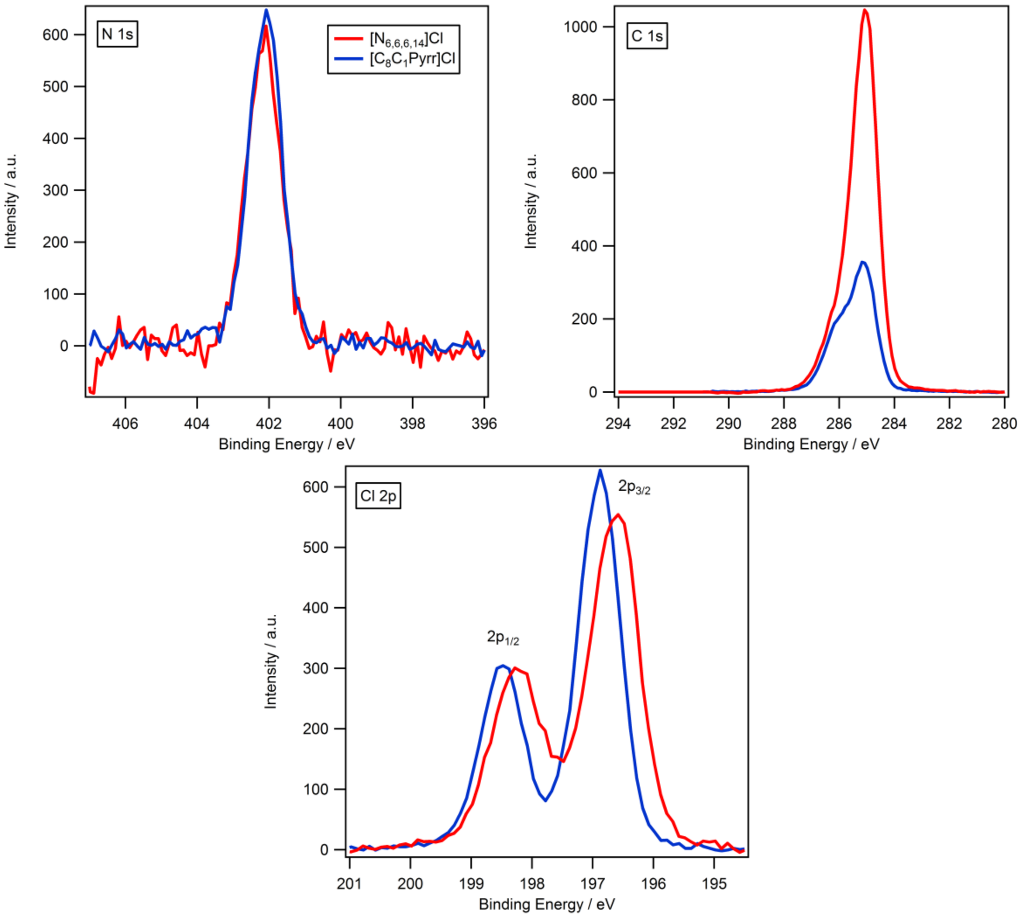

Figure 3.11. XP spectra for all regions for the ionic liquids $[N_{6,6,6,14}]Cl$ (red) and $[C_8C_1Pyrr]Cl$ (blue). Spectra were charge corrected by setting $C_{aliphatic}$ 1s = 285.0 eV and normalised to the area of the Cl 2p photoelectron peak for $[N_{6,6,6,14}]Cl$.

Additionally, from Figure 3.11 and Table 3.2 it can be seen that the measured binding energies for N_{cation} 1s, $C_{aliphatic}$ 1s, C_{inter} 1s and C_{hetero} 1s are identical within the experimental the error (± 0.1 eV). However, a 0.3 eV shift to higher binding energy is observed for the Cl $2p_{3/2}$ component of $[C_8C_1Pyrr]Cl$, this is greater than the experimental error and indicates a noticeable change in the electronic environment of the anion, which is attributed to the availability of the cationic core.

It should be noted that due to spin-orbit coupling the Cl 2p photoelectron line is split into a doublet with a ratio of 1: 2 ($2p_{1/2}$: $2p_{3/2}$). This is an inherent property of p-orbital photoelectron lines and does not indicate two different electronic environments of chlorine. It is observed that ΔBE (Cl $2p_{1/2} - 2p_{3/2}$) is 1.6 eV for each cation, this consistency reinforces that a true shift is observed and is not the result of other processes such as beam damage. A small broadening of the Cl 2p component peaks is observed for $[N_{6,6,6,14}]Cl$ with an observed FWHM = 0.98 eV, in comparison to 0.82 eV for $[C_8C_1Pyrr]Cl$. This is likely to be indicative of small differences in surface charging of the samples.

The increase in binding energy of the Cl $2p_{3/2}$ (and $2p_{1/2}$) component for $[C_8C_1Pyrr]Cl$, relative to $[N_{6,6,6,14}]Cl$, suggests that the chloride anion is less electron rich when partnered with the 1-octyl-1-methylpyrrolidinium cation and indicates a greater degree of charge-transfer from anion to cation for this ionic liquid. This supports the proposed hydrocarbon-based shielding of the cationic core, from the anion, for cations containing long alkyl chains such as $[N_{6,6,6,14}]Cl$.

A similar trend is also observed when comparing the F 1s high resolution spectra for $[C_8C_1Pyrr][BF_4]$ and $[N_{6,6,6,14}][BF_4]$ (Table 3.2 and Figure 3.12), in which a 0.2 eV shift is observed. The B 1s component also shifts slightly to higher binding energy by 0.1 eV for the $[C_8C_1Pyrr]^+$ cation, however this is within the experimental error and suggests that the cationic structure has minimal impact on the electronic environment of the central boron atom. This may simply be the result of the inversely proportional relationship between interaction energy and separation distance, *i.e.* the fluorine atoms are closer to the cationic core and experience a stronger interaction, whereas the increased distance to the boron atom results in a weaker interaction.

Furthermore, point charges calculated by de Andrade *et al.*[48] and Tsuzuki *et al.*[49] indicate that the negative charge of the $[BF_4]^-$ anion is distributed across the four fluorine atoms, which could provide justification for the fact that changes in charge-transfer are more noticeable in the F 1s binding energies.

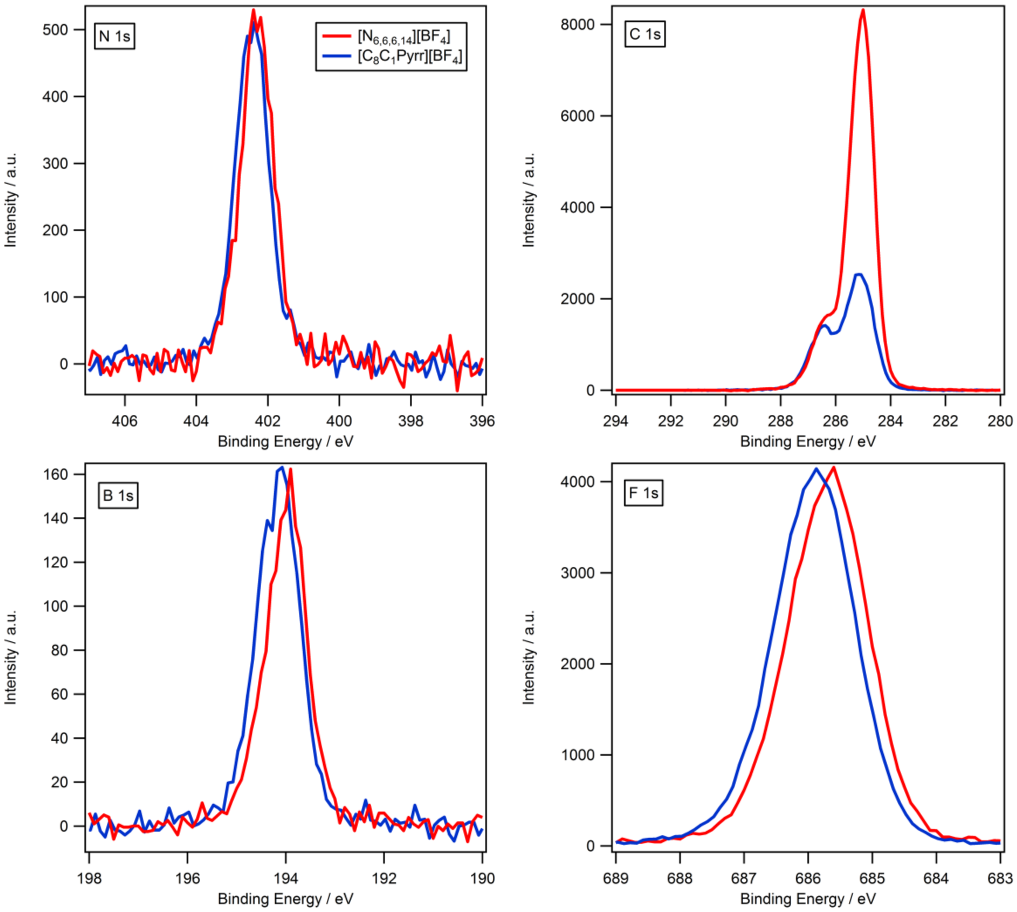

Figure 3.12. XP spectra for all regions for the ionic liquids $[N_{6,6,6,14}][BF_4]$ and $[C_8C_1Pyrr][BF_4]$. Spectra were charge corrected by setting $C_{aliphatic}$ 1s = 285.0 eV and normalised to the area of the F 1s photoelectron peak for $[N_{6,6,6,14}][BF_4]$.

It has been previously shown that there is a strong correlation between the degree of charge-transfer and the solvatochromically determined hydrogen-bond basicity (β) of the anion; whereby high basicity anions such as halides transfer a significant amount of charge, with the opposite true for low basicity anions such as $[NTf_2]^-$.[10, 14] This could also provide an explanation for the smaller difference in F 1s binding energy (0.2 eV) than the observed Cl $2p_{3/2}$ shift (0.3 eV), as the $[BF_4]^-$ anion naturally transfers less charge than the Cl^- anion. To date, solvatochromic parameters have been extensively reported for the 1-alkyl-3-methylimidazolium-based ionic liquids, whereas significantly fewer have been reported for 1-alkyl-1-methylpyrrolidinium and tetraalkylammonium-based ILs.[10, 39] Subsequently, a comparison of the Kamlet-Taft (β) parameter with the N_{cation} 1s binding energy cannot be made in this study, although an analogous trend to the imidazolium based systems would be expected.

A comparison of binding energies for $[C_8C_1Pyrr][NTf_2]$ and $[N_{6,6,6,14}][NTf_2]$ indicate that the anionic components all match within the experimental error excluding O 1s and N 1s (Table 3.2 and Figure 3.13). The O 1s and N 1s binding energies are shifted to higher binding energy by 0.2 eV for $[C_8C_1Pyrr][NTf_2]$ in comparison to $[N_{6,6,6,14}][NTf_2]$. Examination of point charges determined by Hunt *et al*,.[50] Canongia Lopes *et al*.,[51] and Tsuzuki *et al.*[49] demonstrate that the negative charge is mainly distributed across the oxygen and nitrogen atoms of the $[NTf_2]^-$ anion. Therefore, it is likely that the electronic environment and hence binding energies of these atoms will be most affected by changes to electron density, which can be seen in this study.

Interestingly, the cationic nitrogen peak is also shifted 0.2 eV higher for $[C_8C_1Pyrr][NTf_2]$ relative to $[N_{6,6,6,14}][NTf_2]$ which indicates that the electronic environment of N_{cation} for $[N_{6,6,6,14}][NTf_2]$ is significantly more electron-rich than $[C_8C_1Pyrr][NTf_2]$.

To explain this observation the charge-transfer ability of the anion must be considered. It has been established that the N_{cation} 1s binding energy follows the trend $[NTf_2]^- > [BF_4]^- > Cl^-$, which corresponds to an increase in charge-transfer with increasing anion basicity;[14] thus, the electronic environment of N_{cation} is more electron-poor when coupled with the $[NTf_2]^-$. Consequently, a stronger electron-releasing effect of the aliphatic chain will be induced for ionic liquids containing an $[NTf_2]^-$ anion.

Considering that the $[N_{6,6,6,14}]^+$ cation has a substantially larger aliphatic contribution than $[C_8C_1Pyrr]^+$, it seems reasonable that the N_{cation} environment for $[N_{6,6,6,14}][NTf_2]$ experiences a stronger inductive effect from the surrounding alkyl chains causing a subsequent shift to lower binding energy.

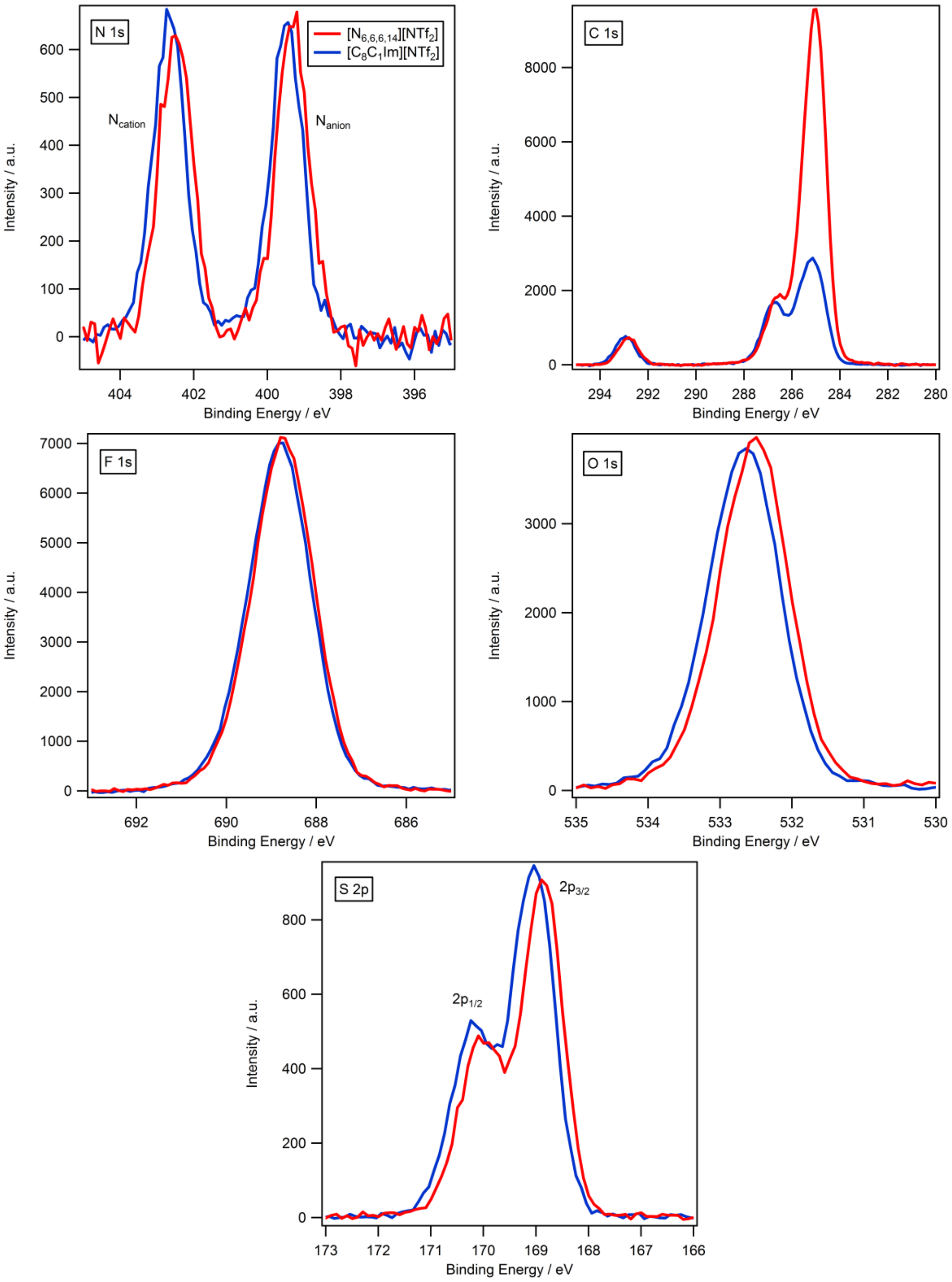

Figure 3.13. XP spectra for all regions for the ionic liquids $[N_{6,6,6,14}][NTf_2]$ and $[C_8C_1Pyrr][NTf_2]$. Spectra were charge corrected by setting $C_{aliphatic}$ 1s = 285.0 eV and normalised to the area of the F 1s photoelectron peak for $[N_{6,6,6,14}][NTf_2]$.

In conclusion, the electronic environment of the anion is dependent upon cationic structure, with an increase in charge-transfer from anion to cation achieved for the more constrained structure of a 1-octyl-1-methylpyrrolidinium cation. This provides evidence for a hydrocarbon-based shielding of the cationic core for cations containing long-alkyl chains, which subsequently impacts upon cation-anion interactions.

3.7 Conclusions

In this *Chapter* the high purity of various tetraalkylammonium and phosphonium ionic liquids has been confirmed with a description of binding energies and multi-component fitting models. Furthermore, a robust C 1s peak fitting model has been developed and described for both the tetraalkylammonium and tetraalkylphosphonium families of ionic liquid. A method for charge correction of short alkyl chain ($n < 8$) cations has also been discussed and it was established that reliable charge correction is achieved through referencing the N_{cation} 1s/P_{cation} $2p_{3/2}$ binding energy of the cationic core to the value obtained for its long chain ($n \geq 8$) analogue (which has prior to been charge corrected by referencing $C_{aliphatic}$ 1s to 285.0 eV) *N.B.* anion must be identical in each case.

Evidence for the different charge densities of the ammonium and phosphonium cationic cores has also been provided through XPS and NMR measurements, and the effect this has on cation-anion interactions has been investigated by XPS. For long chain systems, *i.e.* $[N_{6,6,6,14}]^+$ *versus* $[P_{6,6,6,14}]^+$, it appears that changing the cation core has minimal impact on the electronic environment of the anion due to a perceived shielding effect of the long alkyl chains. In an effort to reduce the effect of hydrocarbon based shielding of the heteroatom, a second series of experiments were conducted where the alkyl components are pruned back, hence allowing a more clear investigation of the role of the heteroatom based charge carrier. A decrease in alkyl chain length to $[N_{4,4,4,1}]^+$ and $[P_{4,4,4,1}]^+$ indicates that changing the cation core from nitrogen to phosphorus does indeed influence the electronic environment of the anion; with an increase in charge-transfer shown for ammonium ILs.

Further evidence for the concept of hydrocarbon-based shielding of the cationic core was provided through a comparison of a conformationally flexible $[N_{6,6,6,14}]^+$ cation with a constrained $[C_8C_1Pyrr]^+$ cation. Here, it was observed that the electronic environment of the anion is dependent on cation structure, with an increase in charge-transfer from anion to cation achieved for the more constrained 1-octyl-1-methylpyrrolidinium cation. This not only furthers our understanding of inter-ion interactions of ILs, but also provides a step towards being able to predict how changing the different components of an ionic liquid will impact on their respective electronic environments, a step that is key to developing the ability to tune an ionic liquid system to meet a specific function.

3.8 References

1. P. Wasserscheid and T. Welton, *Ionic Liquids in Synthesis*, Wiley-VCH, Weinham, 2nd edn., 2008.

2. K. R. J. Lovelock, I. J. Villar-Garcia, F. Maier, H.-P. Steinrück and P. Licence, *Chem. Rev.*, 2010, **110**, 5158-5190.

3. J. M. Gottfried, F. Maier, J. Rossa, D. Gerhard, P. S. Schulz, P. Wasserscheid and H.-P. Steinrück, *Z. Phys. Chem.*, 2006, **220**, 1439-1453.

4. E. F. Smith, F. J. M. Rutten, I. J. Villar-Garcia, D. Briggs and P. Licence, *Langmuir*, 2006, **22**, 9386-9392.

5. C. Kolbeck, T. Cremer, K. R. J. Lovelock, N. Paape, P. S. Schulz, P. Wasserscheid, F. Maier and H.-P. Steinrück, *J. Phys. Chem. B*, 2009, **113**, 8682-8688.

6. K. R. J. Lovelock, C. Kolbeck, T. Cremer, N. Paape, P. S. Schulz, P. Wasserscheid, F. Maier and H.-P. Steinrück, *J. Phys. Chem. B*, 2009, **113**, 2854-2864.

7. F. Maier, T. Cremer, C. Kolbeck, K. R. J. Lovelock, N. Paape, P. S. Schulz, P. Wasserscheid and H.-P. Steinrück, *Phys. Chem. Chem. Phys.*, 2010, **12**, 1905-1915.

8. V. Lockett, R. Sedev, C. Bassell and J. Ralston, *Phys. Chem. Chem. Phys.*, 2008, **10**, 1330-1335.

9. V. Lockett, R. Sedev, S. Harmer, J. Ralston, M. Horne and T. Rodopoulos, *Phys. Chem. Chem. Phys.*, 2010, **12**, 13816-13827.

10. S. Men, K. R. J. Lovelock and P. Licence, *Phys. Chem. Chem. Phys.*, 2011, **13**, 15244-15255.

11. S. Men, B. B. Hurisso, K. R. J. Lovelock and P. Licence, *Phys. Chem. Chem. Phys.*, 2012, **14**, 5229-5238.

12. C. Kolbeck, I. Niedermaier, N. Taccardi, P. S. Schulz, F. Maier, P. Wasserscheid and H.-P. Steinrück, *Angew. Chem. Int. Ed.*, 2012, **51**, 2610-2613.

13. I. Niedermaier, C. Kolbeck, N. Taccardi, P. S. Schulz, J. Li, T. Drewello, P. Wasserscheid, H.-P. Steinrück and F. Maier, *ChemPhysChem*, 2012, **13**, 1725-1735.

14. T. Cremer, C. Kolbeck, K. R. J. Lovelock, N. Paape, R. Wölfe, P. S. Schulz, P. Wasserscheid, H. Weber, J. Thar, B. Kirchner, F. Maier and H.-P. Steinrück, *Chem. Eur. J.*, 2010, **16**, 9018-9033.

15. I. J. Villar-Garcia, K. R. J. Lovelock, S. Men and P. Licence, *Chem. Sci.*, 2014, **5**, 2573-2579.

16. S. Men, D. S. Mitchell, K. R. J. Lovelock and P. Licence, *ChemPhysChem*, 2015, **16**, 2211-2218.

17. A. R. Santos, R. K. Blundell and P. Licence, *Phys. Chem. Chem. Phys.*, 2015, **17**, 11839-11847.

18. S. Men, K. R. J. Lovelock and P. Licence, *RSC Adv.*, 2015, **5**, 35958-35965.

19. K. J. Fraser and D. R. MacFarlane, *Aust. J. Chem.*, 2009, **62**, 309-321.

20. R. E. Del Sesto, C. Corley, A. Robertson and J. S. Wilkes, *J. Organomet. Chem.*, 2005, **690**, 2536-2542.

21. G. Adamova, R. L. Gardas, M. Nieuwenhuyzen, A. V. Puga, L. P. N. Rebelo, A. J. Robertson and K. R. Seddon, *Dalton Trans.*, 2012, **41**, 8316-8332.

22. K. Tsunashima and M. Sugiya, *Electrochem. Commun.*, 2007, **9**, 2353-2358.

23. K. Tsunashima, E. Niwa, S. Kodama, M. Sugiya and Y. Ono, *J. Phys. Chem. B*, 2009, **113**, 15870-15874.

24. H. Shirota, H. Fukazawa, T. Fujisawa and J. F. Wishart, *J. Phys. Chem. B*, 2010, **114**, 9400-9412.

25. H. Y. Lee, H. Shirota and E. W. Castner, *J. Phys. Chem. Lett.*, 2013, **4**, 1477-1483.

26. P. J. Carvalho, S. P. M. Ventura, M. L. S. Batista, B. Schröder, F. Gonçalves, J. Esperança, F. Mutelet and J. A. P. Coutinho, *J. Chem. Phys.*, 2014, **140**, 64505-64505.

27. L. K. Scarbath-Evers, P. A. Hunt, B. Kirchner, D. R. MacFarlane and S. Zahn, *Phys. Chem. Chem. Phys.*, 2015, **17**, 20205-20216.

28. E. F. Smith, I. J. Villar Garcia, D. Briggs and P. Licence, *Chem. Commun.*, 2005, 5633-5635.

29. K. R. J. Lovelock, E. F. Smith, A. Deyko, I. J. Villar-Garcia, P. Licence and R. G. Jones, *Chem. Commun.*, 2007, 4866-4868.

30. I. J. Villar-Garcia, E. F. Smith, A. W. Taylor, F. L. Qiu, K. R. J. Lovelock, R. G. Jones and P. Licence, *Phys. Chem. Chem. Phys.*, 2011, **13**, 2797-2808.

31. A. W. Taylor, S. Men, C. J. Clarke and P. Licence, *RSC Adv.*, 2013, **3**, 9436-9445.

32. C. D. Wagner, L. E. Davis, M. V. Zeller, J. A. Taylor, R. H. Raymond and L. H. Gale, *Surf. Interface Anal.*, 1981, **3**, 211-225.

33. D. Briggs and J. T. Grant, *Surface Analysis by Auger and X-ray Photoelectron Spectroscopy*, IM Publications LLP, Manchester, 2003.

34. R. T. Lewis and M. A. Kelly, *J. Electron Spectrosc. Relat. Phenom.*, 1980, **20**, 105-115.

35. A. Cros, *J. Electron Spectrosc. Relat. Phenom.*, 1992, **59**, 1-14.

36. A. Jelicic, N. Garcia, H. G. Lohmannsroben and S. Beuermann, *Macromolecules*, 2009, **42**, 8801-8808.

37. N. D. Khupse and A. Kumar, *J. Phys. Chem. B*, 2010, **114**, 376-381.

38. S. Coleman, R. Byrne, S. Minkovska and D. Diamond, *Phys. Chem. Chem. Phys.*, 2009, **11**, 5608-5614.

39. P. G. Jessop, D. A. Jessop, D. B. Fu and L. Phan, *Green Chem.*, 2012, **14**, 1245-1259.

40. L. Laitem, L. Christiaens and M. Renson, *Org. Magn. Res.*, 1980, **13**, 319-322.

41. G. C. Levy, *Topic in Carbon-13 NMR Spectroscopy*, John Wiley & Sons, New York, 1974.

42. F. W. Wehrli, A. P. Marchand and S. Wehrli, *Interpretation of Carbon-13 NMR Spectra*, John Wiley & Sons, Chichester, 2nd edn., 1983.

43. J. Clayden, N. Greeves, S. Warren and P. Wothers, *Organic Chemistry*, Oxford University Press Inc United States, 2001.

44. A. Deyko, S. G. Hessey, P. Licence, E. A. Chernikova, V. G. Krasovskiy, L. M. Kustov and R. G. Jones, *Phys. Chem. Chem. Phys.*, 2012, **14**, 3181-3193.

45. L. Gontrani, O. Russina, F. Lo Celso, R. Caminiti, G. Annat and A. Triolo, *J. Phys. Chem. B*, 2009, **113**, 9235-9240.

46. X. M. Liu, Y. L. Zhao, X. C. Zhang, G. H. Zhou and S. J. Zhang, *J. Phys. Chem. B*, 2012, **116**, 4934-4942.

47. M. Fabris, V. Lucchini, M. Noe, A. Perosa and M. Selva, *Chem. Eur. J.*, 2009, **15**, 12273-12282.

48. J. de Andrade, E. S. Boes and H. Stassen, *J. Phys. Chem. B*, 2002, **106**, 13344-13351.

49. S. Tsuzuki, H. Tokuda, K. Hayamizu and M. Watanabe, *J. Phys. Chem. B*, 2005, **109**, 16474-16481.

50. P. A. Hunt, I. R. Gould and B. Kirchner, *Aust. J. Chem.*, 2007, **60**, 9-14.

51. J. N. Canongia Lopes, J. Deschamps and A. A. H. Padua, *J. Phys. Chem. B*, 2004, **108**, 2038-2047.

4. Depth Profiling of Ammonium and Phosphonium Ionic Liquids: An ARXPS and ERXPS Study

4.1 Introduction

The relatively new topic of ionic liquid (IL) surface science has experienced rapid growth during recent years. As such, a multitude of ultra-high vacuum techniques have been used to probe the IL/vacuum interface, including laboratory and synchrotron X-ray photoelectron spectroscopy (XPS),[1-7] ultraviolet photoelectron spectroscopy (UPS),[8-12] metastable impact electron spectroscopy (MIES),[9, 10, 13] low energy ion scattering (LEIS),[14-17] Rutherford backscattering (RBS),[18-20] and neutral impact collision ion scattering spectroscopy (NICISS).[21-23] To date, the vast majority of these studies have focused on cyclic nitrogen-containing cations, particularly the 1-alkyl-3-methylimidazolium family, whereas acyclic cations including tetraalkylammonium and tetraalkylphosphonium have been somewhat overlooked despite their potential use in a wide range of existing applications including heterogeneous catalysis, gas capture/separation, and nanoparticle formation. Clearly, the structure of the IL/vacuum interface plays a crucial role for many of these applications; therefore, it is necessary to understand how changes to the component ions can influence the IL surface, and consequently impact their chemistry-based applications. XPS has been shown to be a robust and powerful tool for the analysis and characterisation of ionic liquid surface structure, and has provided many significant contributions in the area of bulk and surface composition.[1-7, 21, 24-26]

With the advent of commercially available harder/high energy X-ray sources – such as Ag Lα’ – Energy-resolved XPS (ERXPS) is expected to attract considerable interest over the coming years. Although ERXPS is not a new technique, it has previously required the use of synchrotron X-ray sources, which can be costly and time-limited. Consequently, the improved accessibility offered by high energy laboratory-based sources provides a new means to conduct ERXPS studies on ionic liquids. This has several advantages over currently existing depth profiling techniques. Firstly, no geometry change to the sample is required, as in the case of angle-resolved XPS (ARXPS), thus enabling repeated analysis of a consistently level surface thereby minimising error caused by physical shifting of the sample. Secondly, depth profiling data can be obtained from a single experiment as opposed to repeated experiments in which the emission angle is altered (ARXPS) or photon-energy varied (synchrotron-based ERXPS); thus minimising X-ray exposure and hence sample damage.

Lastly, higher energy core orbitals can be probed, elucidating further information concerning ionic liquid electronic environments, which is imperative to understanding ionic liquids at a molecular level. Accordingly, the work herein provides the first description of a high energy Ag Lα' source for XPS depth profile analysis and characterisation for a variety ionic liquids.

Previous depth profiling studies on ionic liquid systems have used ARXPS, with few examples of ERXPS (*N.B.* limited to synchrotron sources). These investigations are again predominantly concerned with the 1-alkyl-3-methylimidazolium cation, [1, 2, 4, 25, 26] with only a handful of ARXPS studies addressing the structurally distinct pyrrolidinium cation.[5, 26] Nevertheless, through these investigations a robust set of design rules have been established for the IL/vacuum interface of 1-alkyl-3-methylimidazolium-based ionic liquids, in which, for sufficient chain length ($n \geq 4$), the alkyl chains are projected towards the vacuum forming an aliphatic overlayer, with a polar sublayer of positively and negatively charged head groups residing underneath.[1, 2, 4, 25, 26] This set of design rules also appears to hold true for the 1-alkyl-1-methylpyrrolidinium analogues;[5, 26] however, it would be unreasonable to simply assume that other structurally diverse cations such as the acyclic tetraalkylammonium and tetraalkylphosphonium would also follow this trend. Subsequently, the work described in this *Chapter* directly addresses this gap in knowledge to further understand the role of the cation on the structure of the IL/vacuum interface.

In summary, the aim of this work is to understand how the cation can influence the structure of the IL/vacuum interface through depth profiling investigations on ILs with cations of varying structural diversity, including the lesser-studied tetraalkylammonium and tetraalkylphosphonium cations. This is achieved utilising the highly surface sensitive XPS techniques: ARXPS and ERXPS, to probe differences in the bulk and surface compositions for the ionic liquids investigated. Furthermore, through a comparison of binding energies obtained *via* both the Al Kα and Ag Lα' X-ray sources validation for using the Ag Lα' source to obtain robust and reliable chemical state analysis of ionic liquids has been provided, as well as characterising previously undetectable core level photoelectron emissions.

4.2 High Energy XPS: The Ag Lα' X-ray Source

4.2.1 Intensity and Broadening of Photoelectron Peaks

The main, and most important, difference between the Al Kα (hν = 1486.6 eV) and Ag Lα' (2984.3 eV) sources are their respective energies, whereby the energy of the Ag Lα' X-rays are approximately twice that of the Al Kα X-rays. For each source the same spectrometer set-up is used in each case, with only minor adjustments to the X-ray gun position and the quartz crystal monochromator.

The same quartz crystal monochromator is permitted for use with each source as an integer number of Al Kα and Ag Lα' X-ray wavelengths (0.834 nm and 0.415 nm respectively) equate to the spacing between the quartz (1010) planes (0.425 nm) at an angle close to 78.5°.[27] The Bragg diffraction criterion specifies that for constructive interference of reflected photons to occur they must satisfy the conditions outlined in the Bragg equation shown below, where n = order of diffraction, λ = wavelength, d = crystal spacing, and θ = angle of diffraction.

$$n\lambda = 2d\sin\theta \qquad \textbf{4.1}$$

Consequently, the Bragg diffraction criteria is satisfied to first order for Al Kα and second order for Ag Lα' (as the wavelength for Ag Lα' is half that of Al

Kα). The combination of Bragg diffraction and a slight concavity of the quartz crystal results in a focused X-ray beam at the sample surface, see Figure 4.1.

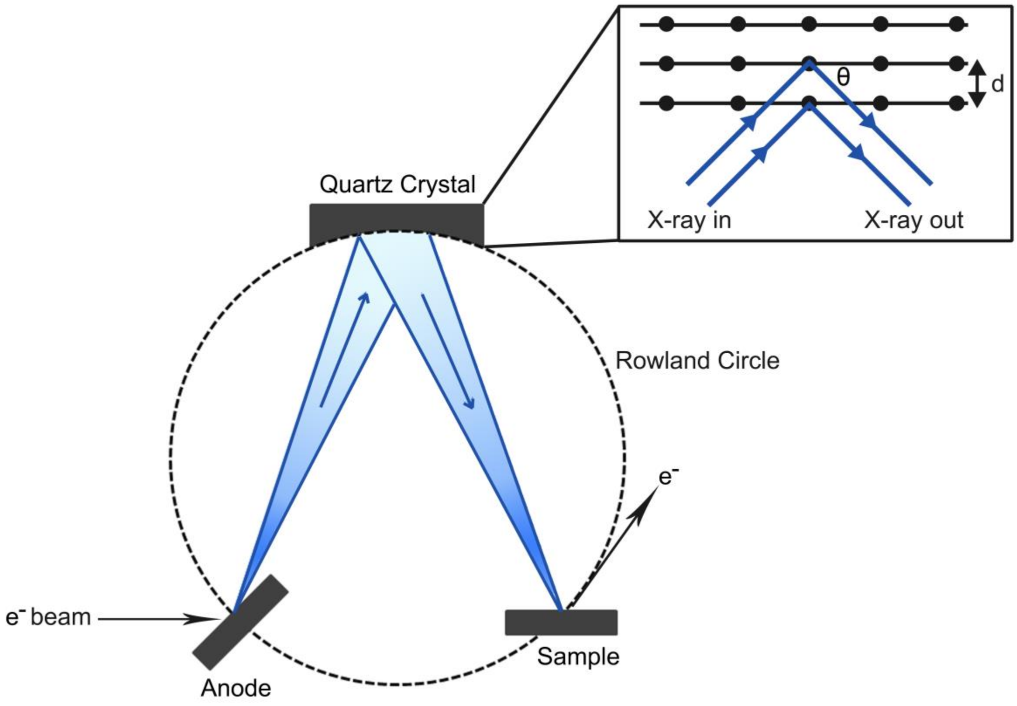

Figure 4.1. Schematic illustrating the XPS monochromator geometry in which X-rays generated at the anode are reflected off quartz crystal and focused at the sample. The inset describes the Bragg diffraction criterion for constructive interference of the scattered X-rays.

With increasing order of diffraction a wider energy distribution of the respective X-ray beam will result *i.e.* X-ray linewidth will increase with diffraction order. Consequently, as Ag Lα' X-rays satisfy second order diffraction conditions a larger linewidth of ~1.2 eV occurs in comparison to ~ 0.2 – 0.3 eV for Al Kα.[27] As such, the photoelectron peaks obtained using the Ag Lα' X-ray source are typically broader than when obtained using the Al Kα source. For example, when using the Ag $3d_{5/2}$ peak to determine energy resolution a full width half maximum (FWHM) of < 0.55 eV is obtained using the Al Kα source in comparison to 0.9 eV for Ag Lα'. This is also exemplified in Figure 4.2, which shows a visual comparison of the high resolution spectra obtained with each X-ray source for all regions for $[N_{4,4,4,1}][NTf_2]$. It can be seen that the FWHM for the photoelectron peaks detected with the Ag Lα' source are typically 0.1 eV larger than those obtained with the Al Kα source.

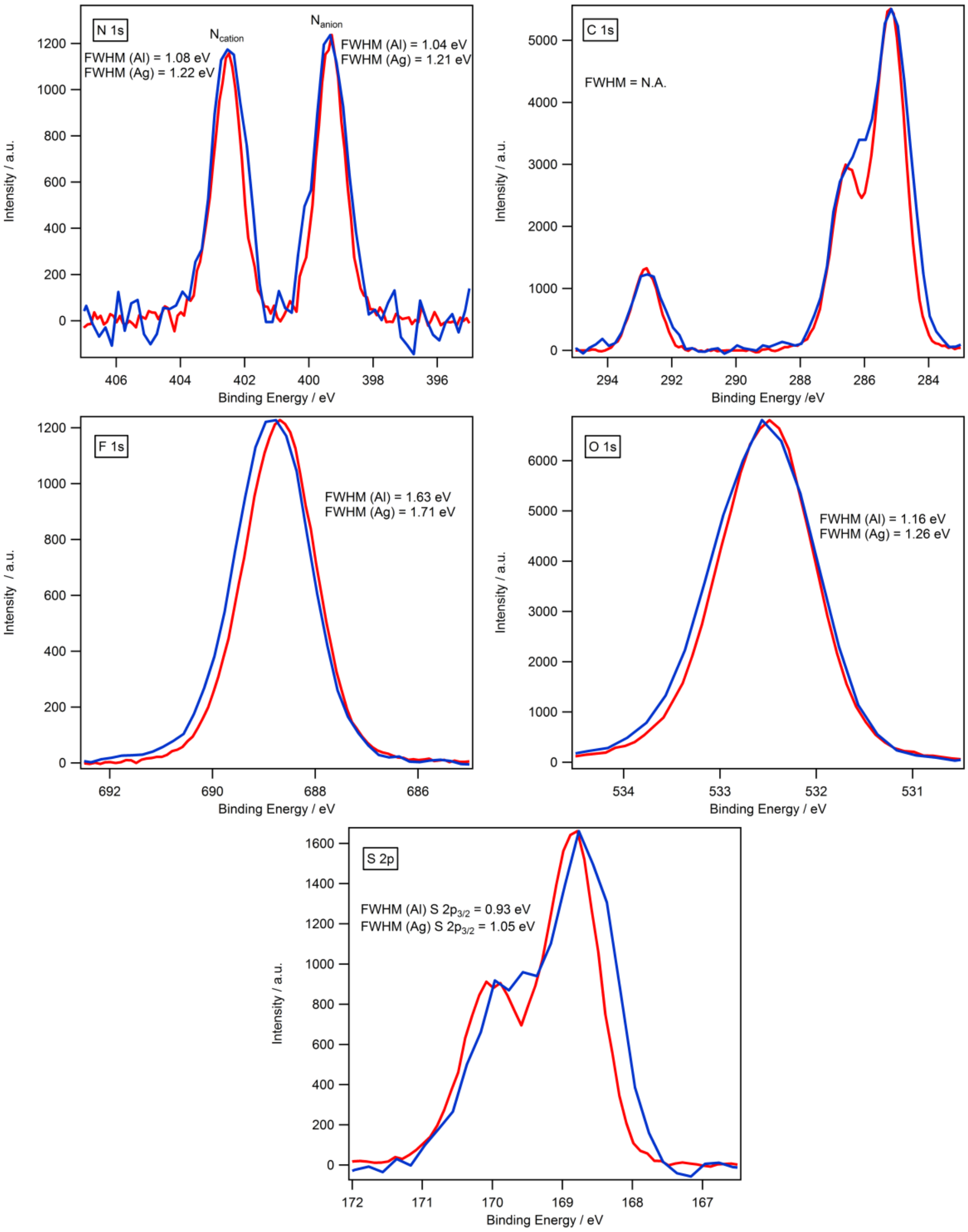

Figure 4.2. Comparison of XP spectra obtained with Ag Lα' source (blue) and Al Kα source (red) for all regions for $[N_{4,4,4,1}][NTf_2]$. Spectra charge corrected by referencing N$_{cation}$ 1s = 402.5 eV and normalised to the intensity of the respective photoelectron peak obtained using the Al Kα X-ray source.

The FWHM for the C 1s regions are not stated as the C 1s spectra consists of several components, consequently the FWHM of the respective components are dependent on the constraints used in the fitting model. However, a slight broadening in line shape can be observed for the Ag Lα' C 1s region in Figure 4.2.

Due to the broader line shape of photoelectron emissions resulting from the Ag Lα' source the FWHM constraints for the C 1s fitting model have to be slightly modified. The fitting model is followed exactly as previously described for the Al Kα source, see *Chapter 3 Sections 3.2.3* and *3.3.3*, however the FWHM is constrained to be between 0.8 – 1.5 eV instead of 0.8 – 1.3 eV.

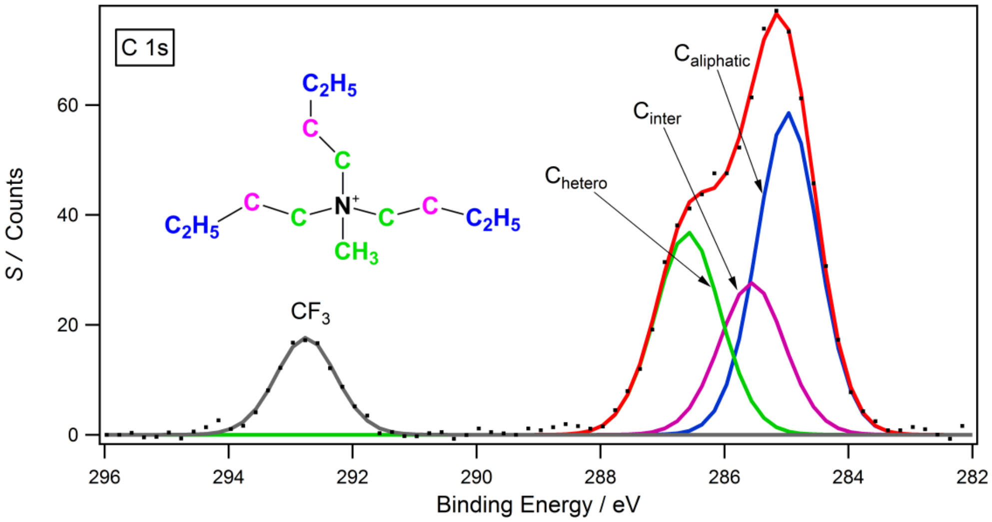

Figure 4.3. High resolution C 1s spectra obtained with the Ag Lα' source for $[N_{4,4,4,1}][NTf_2]$ including colour coded component fittings for $C_{aliphatic}$ (blue), C_{inter} (purple), C_{hetero} (green) and CF_3 (grey); fitting envelope (red); counts (black dots). Charge corrected by referencing N_{cation} 1s = 402.5 eV.

A representative example of the C 1s fitting model for $[N_{4,4,4,1}][NTf_2]$ is provided in Figure 4.3. The fitting envelope (red trace) demonstrates excellent agreement to the experimental spectra (black dots) highlighting the validity of the fitting model. C 1s component fittings for all ionic liquids investigated with the Ag Lα' X-ray source are included in *Appendix B*, and are also in good agreement with the experimental spectra.

Additionally, an increase in order of diffraction is also accompanied by a significant decrease in X-ray beam intensity. Consequently, the signal intensity when using the Ag Lα' source is considerably reduced in comparison to the Al Kα source, as demonstrated by the unnormalised C 1s spectra for $[N_{4,4,4,1}][NTf_2]$ obtained from each source in Figure 4.4. As a result longer acquisition times have to be employed when using the Ag Lα' X-ray source to obtain spectra comparable in quality to the Al Kα source, see *Chapter 2*

Section 2.3.2 for details. Furthermore, in order to obtain a visual comparison of spectra obtained from the two different sources an appropriate normalisation procedure must be applied.

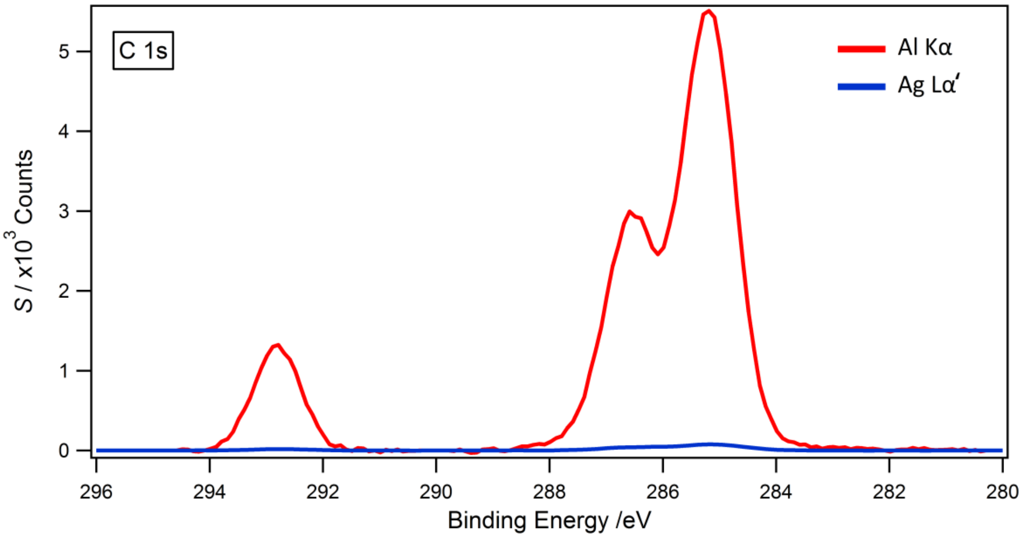

Figure 4.4. Comparison of C 1s high resolution spectra intensity for $[N_{4,4,4,1}][NTf_2]$ obtained with Ag Lα' source (blue) and Al Kα (red). Spectra charge corrected by referencing N_{cation} 1s = 402.5 eV

4.2.2 Energy Range

The kinetic energy of an emitted photoelectron is dependent on the energy of the incident radiation. Consequently, on consideration of the Einstein equation shown below – where KE = kinetic energy, hν = energy of incident radiation, BE = binding energy, and Φ_S = spectrometer work function – the binding energy of a photoelectron peak should not change between X-ray sources.

$$KE = h\nu - BE - \Phi_S \qquad \textbf{4.2}$$

This is clearly seen by a comparison of survey spectra for $[N_{4,4,4,1}][NTf_2]$ obtained with the Al Kα and Ag Lα' sources between the energy range 0 – 1400 eV (Figure 4.5). Additionally, due to the higher energy of the Ag Lα' X-rays, which is approximately twice that of Al Kα radiation, a broader energy range of photoelectron emissions can be observed, thus core orbitals of higher binding energy can be detected *i.e.* the S 1s photoelectron emission at ≈ 2500 eV.

In contrast, Auger electron emissions have a kinetic energy that is independent to the energy of the incident radiation as they arise from internal atom de-excitation. As a binding energy scale is used in an XP spectrum for the analysis of photoelectron emissions, the apparent "binding energy" of the Auger emissions will vary as the energy of the X-ray source is changed. This is clearly exhibited by Figure 4.5 where the Auger emissions using the Al Kα source occur between 800 – 1400 eV, whereas the same Auger emissions occur at 2300 – 2800 eV using the Ag Lα' source. As only photoelectron emissions are analysed in this study the binding energy scale is used throughout.

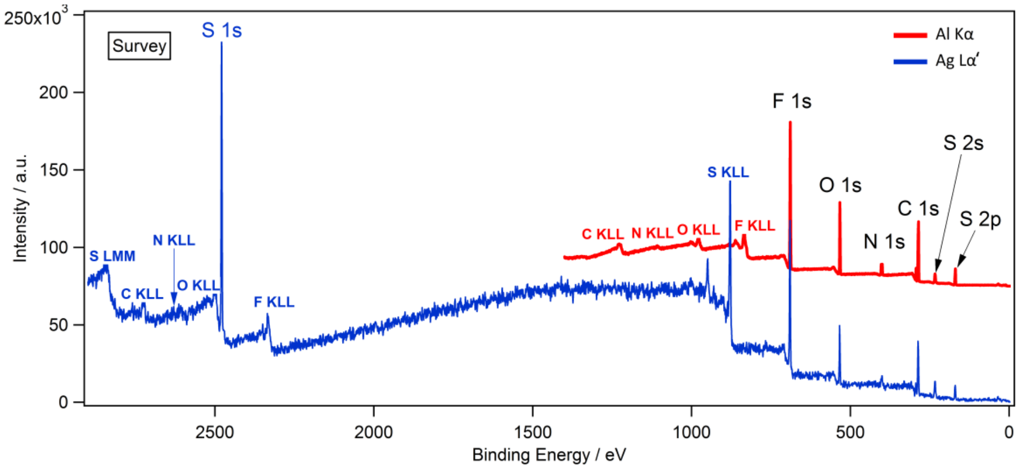

Figure 4.5. Survey XP spectra for $[N_{4,4,4,1}][NTf_2]$ using Al Kα and Ag Lα' X-ray sources; showing photoelectron emissions detected by both sources (black labels); Auger emissions for Al source (red labels); Auger and photoelectron emissions for Ag source (blue labels). Spectra normalised to intensity of the F 1s photoelectron emission peak obtained using the Al Kα source.

The dependency of the kinetic energy for any given photoelectron emission on the energy of the incident radiation also has implications on the depth of the sample probed. For example, radiation of higher energy will result in a higher kinetic energy of the emitted photoelectron. In turn, this results in a longer attenuation length, and hence a greater probability of it escaping from deeper within the sample. As such the Ag Lα' source can probe deeper within a sample, in comparison to Al Kα radiation, thereby elucidating further information on the bulk structure of ionic liquids.

It should be noted that in order to calculate XPS sensitivity factors for a particular analyser, it is necessary to determine its efficiency for focusing and discriminating electrons as a function of their energy, also known as the transmission function.[28] Relative sensitivity factors (RSFs) for the softer Al Kα source, *i.e.* for photoelectron kinetic energies in the range 0 – 1500 eV, are well-defined in the literature enabling elemental quantification.[29, 30] In contrast, for the harder Ag Lα' source no sensitivity factors or transmission function protocol currently exists for photoelectron kinetic energies in the range 1500 – 2900 eV. Consequently, for depth profiling experiments using the Ag Lα' X-ray source a qualitative approach is utilised and is discussed further in *Section 4.5*.

4.2.3 Binding Energy Analysis

A comparison of binding energies obtained with the Ag Lα' and Al Kα source has been made. These investigations were carried out upon a series of structurally diverse ammonium and phosphonium ionic liquids comprising of the cations $[C_8C_1Pyrr]^+$, $[N_{4,4,4,1}]^+$, $[N_{6,6,6,14}]^+$, $[P_{4,4,4,1}]^+$ and $[P_{6,6,6,14}]^+$. In addition, the corresponding anions comprising Cl^-, $[PF_6]^-$ and $[NTf_2]^-$ were chosen such that a range of sizes and basicity were covered, and importantly they all include an element that has higher energy core orbitals which can only be detected with the higher energy Ag Lα' source *i.e.* the Cl 1s, P 1s and S 1s photoelectron emissions.

4.2.3.1 Chloride-based ILs

A clear difference in sample stability under the high energy Ag Lα' X-ray beam was observed for the five chloride-based ionic liquids investigated. Unsurprisingly, due to its instability under the lower energy Al Kα X-rays, $[N_{4,4,4,1}]Cl$ exhibited irreparable sample damage under the high energy Ag Lα' X-rays. Furthermore, its long chain analogue $[N_{6,6,6,14}]Cl$ also exhibited the same behaviour, and consequently reliable binding energies could not be obtained in either case due to considerable line broadening and irregularities in line shape. Interestingly, the cyclic pyrrolidinium displayed an increased stability towards the high energy Ag Lα' X-rays, thus allowing the extraction of reliable binding energies in this instance. However, after prolonged exposure to the X-ray beam, increasing signs of sample damage were observed, as illustrated by the Cl 2p region shown in Figure 4.6. Here the effects of beam damage can be observed after around three hours by a loss in peak line shape and broadening of the photoelectron emission peak. After, eight hours this has progressed further such that the original Cl 2p photoelectron line possesses an obvious shoulder in the binding energy range 200 – 202 eV, indicating more than one electronic environment of chlorine is present. A similar effect is also seen in the spectra for other elemental regions of this ionic liquid. As the ammonium-based chloride samples investigated are high melting solids, the observed change in spectra as a function of beam exposure, is likely due to the accumulation of actinic degradant on the sample surface.

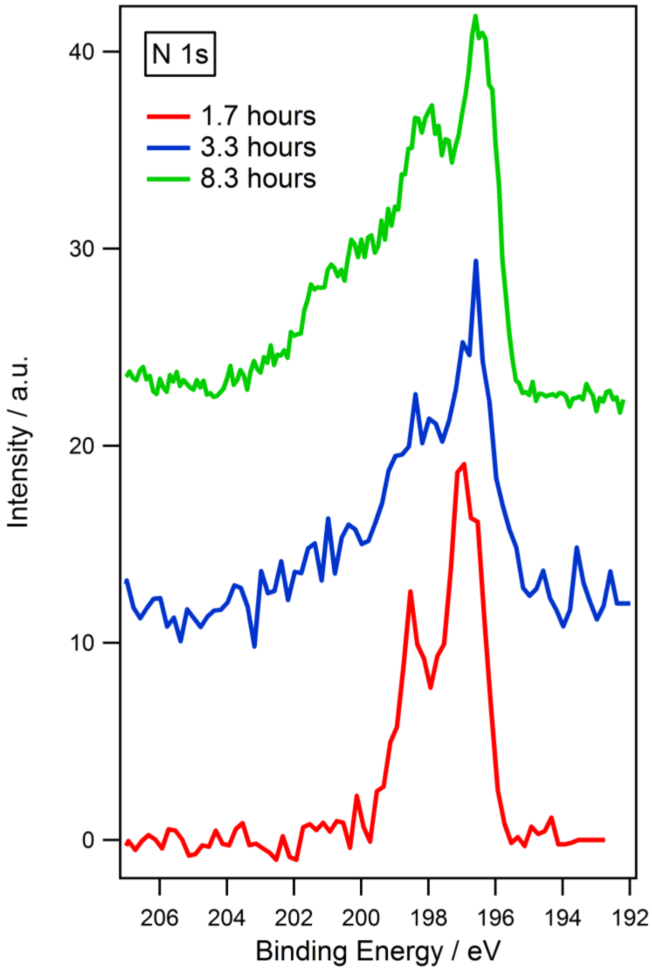

Figure 4.6. Cl 2p region for [C_8C_1Pyrr]Cl as a function of exposure time to Ag Lα’ X-ray radiation.

In contrast to their ammonium analogues the phosphonium ionic liquids investigated remained robust against beam damage. This mirrors the reported cationic influence on thermal and electrochemical stability for these ionic liquids in which the order of stability is tetraalkylphosphonium > 1-alkyl-1-methylpyrrolidinium > tetraalkylammonium.[31-39]

The measured binding energies for the chloride ionic liquids which were not affected immediately by beam damage are presented in Table 4.1, with comparison made to binding energies obtained with the Al Kα source. Excellent agreement is seen for binding energies obtained in the range 0 – 1400 eV for the two X-ray sources as they match within the experimental error of ± 0.1 eV.

Table 4.1. Experimental binding energies in eV for the chloride-based ionic liquids studied in this *Chapter*. The associated experimental error is ± 0.1 eV. $[C_8C_1Pyrr]Cl$ and $[P_{6,6,6,14}]Cl$ charge corrected by referencing $C_{aliphatic}$ 1s to 285.0 eV. $[P_{4,4,4,1}]Cl$ charge corrected by referencing P_{cation} $2p_{3/2}$ to the value obtained for $[P_{6,6,6,14}]Cl$ using the same X-ray source.

	Ionic Liquid		**Binding Energy / eV**							
	Cation	**Anion**	$C_{aliphatic}$ 1s	C_{inter} 1s	C_{hetero} 1s	N_{cation} 1s	P_{cation} 1s	P_{cation} $2p_{3/2}$	Cl 1s	Cl $2p_{3/2}$
Ag Lα’	$[C_8C_1Pyrr]^+$	Cl^-	285.0	285.5	286.2	402.0	-	-	2819.5	196.9
	$[P_{6,6,6,14}]^+$	Cl^-	285.0	-	285.7	-	2146.8	132.2	2819.6	196.5
	$[P_{4,4,4,1}]^+$	Cl^-	284.8	-	285.4	-	2146.7	132.2	2819.5	196.5
Al Kα	$[C_8C_1Pyrr]^+$	Cl^-	285.0	285.5	286.1	402.1	-	-	-	196.9
	$[P_{6,6,6,14}]^+$	Cl^-	285.0	-	285.7	-	-	132.3	-	196.6
	$[P_{4,4,4,1}]^+$	Cl^-	284.8	-	285.2	-	-	132.3	-	196.6

Additionally, binding energies for the higher energy Cl 1s and P 1s core orbitals have been characterised with values of ≈ 2820 eV and 2147 eV respectively.

Furthermore, inspection of the [$P_{4,4,4,1}$]Cl survey spectra - obtained with both the Al and Ag X-ray sources - highlighted the presence of silicon and oxygen surface contaminants in each case, see Figure 4.7. This is likely due to contamination by laboratory grease during synthesis or from the double-sided tape used in sample mounting (solids only) and is unlikely to influence the measured binding energies.[29, 40, 41] Interestingly, it can be seen from Figure 4.7 that the higher energy Ag source can be used to detect the Si 1s photoelectron emission at ≈ 1840 eV. It is apparent that the Si 1s peak is considerably more intense than the Si 2s and 2p peaks, which are barely visible at energies of 153 eV and 100 eV respectively, due to the different orbital cross-sections. This illustrates that the Ag Lα' X-ray source could provide a greater sensitivity and means of detection for silicon based surface contaminants in future studies.

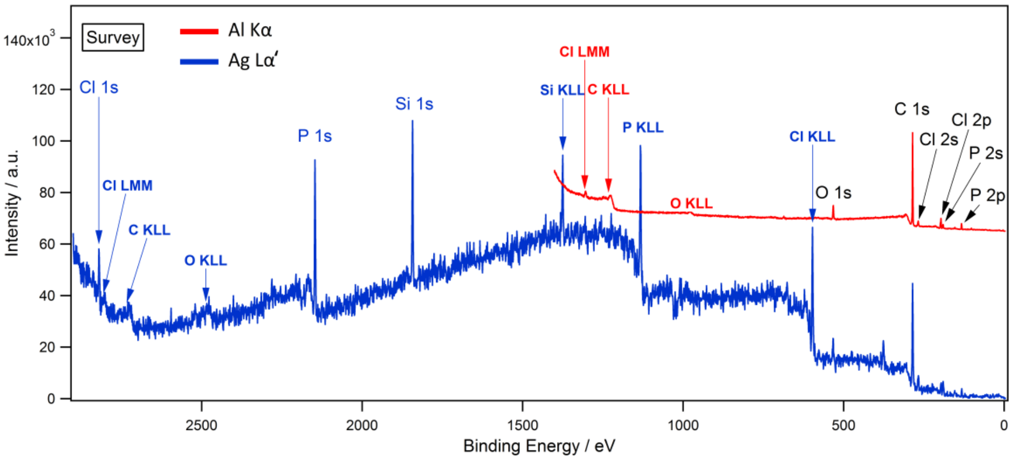

Figure 4.7. Survey XP spectra for [$P_{4,4,4,1}$]Cl using Al Kα and Ag Lα' X-ray sources; showing photoelectron emissions detected by both sources (black labels), Auger emissions for Al source (red labels), Auger and photoelectron emissions for Ag source (blue labels). Spectra normalised to intensity of the C 1s photoelectron emission peak obtained using the Al Kα source.

4.2.3.2 Hexafluorophosphate-based ILs

In contrast to the chloride-based ionic liquids the hexafluorophosphate series did not present any effects of beam damage. The measured binding energies are presented in Table 4.2, with comparison made to those obtained with the Al Kα source. It should be noted that reliable binding energies could not be obtained for the P 2p region for $[P_{6,6,6,14}][PF_6]$ and $[P_{4,4,4,1}][PF_6]$ due to very poor resolution of the photoelectron emission peaks, see *Appendix B*; consequently charge correction was achieved for $[P_{4,4,4,1}][PF_6]$ by referencing the P_{cation} 1s photoelectron peak to the value obtained for $[P_{6,6,6,14}][PF_6]$ (where prior charge correction was achieved by referencing $C_{aliphatic}$ 1s = 285.0 eV).

Overall, good agreement between the two X-ray sources was observed for binding energies in the range 0 - 1400 eV, with the majority of measured values within the experimental error (± 0.1 eV). Small discrepancies larger than the experimental error were seen for the carbon components C_{inter} in the case of $[N_{6,6,6,14}][PF_6]$, and C_{hetero} in $[P_{4,4,4,1}][PF_6]$. However, as these values depend upon a fitting model, which may introduce a larger degree of error, these differences are not significant. Interestingly, the measured binding energy of the F 1s photoelectron emission appears to be systematically ~ 0.2 eV higher than that measured using the Al Kα source. However, as this shift is on the upper limit of experimental error no absolute conclusion can yet be made on this difference.

Table 4.2. Experimental binding energies in eV for the hexafluorophosphate-based ionic liquids studied in this *Chapter*. The associated experimental error is ± 0.1 eV. $[C_8C_1Pyrr][PF_6]$, $[N_{6,6,6,14}][PF_6]$ and $[P_{6,6,6,14}][PF_6]$ charge corrected by referencing $C_{aliphatic}$ 1s to 285.0 eV. $[N_{4,4,4,1}][PF_6]$/ $[P_{4,4,4,1}][PF_6]$ charge corrected by referencing N_{cation} 1s/ P_{cation} $2p_{3/2}$ to the value obtained for $[N_{6,6,6,14}][PF_6]$/ $[P_{6,6,6,14}][PF_6]$ using the same X-ray source, unless otherwise stated. [a]charge correction achieved by referencing P_{cation} 1s to the value obtained for $[P_{6,6,6,14}][PF_6]$. *Poor resolution of P 2p signal, thus reliable binding energy could not be obtained.

	Ionic Liquid		**Binding Energy / eV**								
	Cation	**Anion**	$C_{aliphatic}$ 1s	C_{inter} 1s	C_{hetero} 1s	N_{cation} 1s	P_{cation} 1s	P_{cation} $2p_{3/2}$	F 1s	P_{anion} 1s	P_{anion} $2p_{3/2}$
Ag Lα’	$[C_8C_1Pyrr]^+$	$[PF_6]^-$	285.0	285.6	286.6	402.6	-	-	686.9	2152.2	136.4
	$[N_{6,6,6,14}]^+$	$[PF_6]^-$	285.0	286.0	286.5	402.4	-	-	686.7	2152.1	136.3
	$[N_{4,4,4,1}]^+$	$[PF_6]^-$	285.0	285.4	286.5	402.4	-	-	686.7	2152.0	136.3
	$[P_{6,6,6,14}]^+$	$[PF_6]^-$	285.0	-	286.0	-	2147.0	*	686.7	2151.9	*
	$[P_{4,4,4,1}]^{+a}$	$[PF_6]^-$	285.0	-	285.3	-	2147.0	*	686.6	2151.9	*
Al Kα	$[C_8C_1Pyrr]^{+42}$	$[PF_6]^-$	285.0	285.5	286.7	402.5	-	-	686.6	-	136.6
	$[N_{6,6,6,14}]^+$	$[PF_6]^-$	285.0	285.7	286.6	402.4	-	-	686.5	-	136.4
	$[N_{4,4,4,1}]^+$	$[PF_6]^-$	284.9	285.4	286.5	402.4	-	-	686.5	-	136.3
	$[P_{6,6,6,14}]^+$	$[PF_6]^-$	285.0	-	285.8	-	-	132.7	686.5	-	136.3
	$[P_{4,4,4,1}]^+$	$[PF_6]^-$	285.0	-	285.6	-	-	132.7	686.6	-	136.4

4.2.3.3 Bis(trifluoromethanesulfonyl)imide-based ILs

As with the hexafluorophosphate series, the ionic liquids containing the $[NTf_2]^-$ anion did not show any indication of beam damage. In addition, there was no evidence of contaminants such as laboratory grease, and all peaks in the survey spectra could be assigned to elements within the respective ionic liquids, highlighting the high purity for this particular series of ionic liquids, see *Appendix B.* Furthermore, as these compounds were in their liquid state at room temperature they emitted superior photoelectron flux in comparison to the chloride- and hexafluorophosphate-based analogues. This enabled the measurement of high quality spectra with excellent resolution.

The measured binding energies for both sources display excellent agreement with values within the experimental error (± 0.1 eV), see Table 4.3. As seen previously for the $[PF_6]^-$ compounds, the measured binding energy of the F 1s photoelectron peak is ~ 0.2 eV higher for the XP spectra obtained with the Ag Lα' source, (*Section 4.2.3.2*).

Consequently, the Ag Lα' X-ray source provides robust chemical state analysis for a variety of ionic liquids, as well as the characterisation of previously inaccessible higher energy core orbitals such as Si 1s, Cl 1s, P 1s and S 1s. The added value of the high energy Ag Lα' X-ray source, however, is its ability to provide another approach to depth profiling based on detecting two different core photoelectron emissions (which have a large difference in binding energy) from the same element.

As the five bis(trifluoromethanesulfonyl)imide-based ionic liquids in this study were free of contaminants; displayed high stability; and were in the liquid state at room temperature, they were investigated further in a depth profiling study to determine the influence of the cation on the ionic liquid/vacuum interface, this is discussed in detail in the following sections.

Table 4.3. Experimental binding energies in eV for the bis(trifluoromethanesulfonyl)imide-based ionic liquids studied in this *Chapter*. The associated experimental error is ± 0.1 eV. $[C_8C_1Pyrr][NTf_2]$, $[N_{6,6,6,14}][NTf_2]$ and $[P_{6,6,6,14}][NTf_2]$ charge corrected by referencing $C_{aliphatic}$ 1s to 285.0 eV. $[N_{4,4,4,1}][NTf_2]$/ $[P_{4,4,4,1}][NTf_2]$ charge corrected by referencing N_{cation} 1s/ P_{cation} $2p_{3/2}$ to the value obtained for $[N_{6,6,6,14}][NTf_2]$/ $[P_{6,6,6,14}][NTf_2]$ using the same X-ray source

	Ionic Liquid		**Binding Energy / eV**											
	Cation	**Anion**	$C_{aliphatic}$ 1s	C_{inter} 1s	C_{hetero} 1s	N_{cation} 1s	P_{cation} 1s	P_{cation} $2p_{3/2}$	C_{anion} 1s	N_{anion} 1s	O 1s	F 1s	S 1s	S $2p_{3/2}$
Ag Lα’	$[C_8C_1Pyrr]^+$	$[NTf_2]^-$	285.0	285.8	286.8	402.7	-	-	292.9	399.5	532.8	689.0	2478.5	168.9
	$[N_{6,6,6,14}]^+$	$[NTf_2]^-$	285.0	285.8	286.8	402.5	-	-	292.9	399.4	532.6	688.9	2478.4	168.8
	$[N_{4,4,4,1}]^+$	$[NTf_2]^-$	285.0	285.5	286.6	402.5	-	-	292.8	399.3	532.5	688.8	2478.2	168.7
	$[P_{6,6,6,14}]^+$	$[NTf_2]^-$	285.0	-	285.9	-	2147.2	132.6	292.8	399.4	532.6	688.9	2478.4	168.7
	$[P_{4,4,4,1}]^+$	$[NTf_2]^-$	285.1	-	285.6	-	2147.1	132.6	292.7	399.3	532.5	688.8	2478.3	168.6
Al Kα	$[C_8C_1Pyrr]^+$	$[NTf_2]^-$	285.0	285.6	286.8	402.7	-	-	292.9	399.5	532.7	688.8	-	169.0
	$[N_{6,6,6,14}]^+$	$[NTf_2]^-$	285.0	285.7	286.7	402.5	-	-	292.8	399.3	532.5	688.7	-	168.9
	$[N_{4,4,4,1}]^+$	$[NTf_2]^-$	285.1	285.4	286.6	402.5	-	-	292.8	399.3	532.5	688.7	-	168.8
	$[P_{6,6,6,14}]^+$	$[NTf_2]^-$	285.0	-	285.9	-	-	132.7	292.8	399.3	532.5	688.7	-	168.8
	$[P_{4,4,4,1}]^+$	$[NTf_2]^-$	285.1	-	285.6	-	-	132.7	292.7	399.2	532.4	688.6	-	168.8

4.3 Depth Profiling: Surface Sensitivity and Information Depth

The surface sensitivity of XPS experiments is influenced by two main factors: i) electron emission angle, θ and ii) the attenuation length, $\lambda_{AL,}$ of the emitted photoelectrons (*N.B.* this value is also dependent upon the photoelectron kinetic energy). A measure of surface sensitivity is provided by the information depth (ID) which is defined as the depth at which 95.7 % of the signal originates; the dependence of ID upon θ and λ_{AL} is shown by Equation 4.3.

$$\mathrm{ID} = 3\lambda_{AL}\cos\theta \qquad \textbf{4.3}$$

It should be noted that definitions for inelastic mean free path (λ_{IMFP}) and attenuation length (λ_{AL}) are often used interchangeably in the literature. Herein, λ_{IMFP} is defined as the average distance travelled by an electron of a specific energy between two inelastic events, with elastic scattering included. Whereas, λ_{AL} is defined as the average distance travelled by an electron of a specific energy between two inelastic events without elastic scattering. Consequently, λ_{AL} is used to describe depth, rather than λ_{IMFP}, as it does not include elastic scattering events which can cause an overestimated depth, and is typically 20 % smaller than λ_{IMFP}.[43, 44]

Subsequently, there are two methods with which to alter the surface sensitivity of an XPS experiment: (1) Angle-Resolved XPS (ARXPS), based on varying the detection angle (θ) of the emitted photoelectrons and (2) Energy-Resolved XPS (ERXPS), utilising the dependence of λ_{AL} on the kinetic energy of the emitted photoelectron.

4.3.1 Angle-Resolved XPS

Of the two methods ARXPS is the most commonly employed to obtain a depth profile for ionic liquid systems. Typically, the lower energy Al Kα X-ray source is used due to its higher signal intensity, and ID varies chiefly with θ. The emission angle, θ, can be varied with respect to the surface normal by rotation of the sample stage with respect to the concentric hemispherical analyser (CHA), as illustrated by the schematic in Figure 4.8.

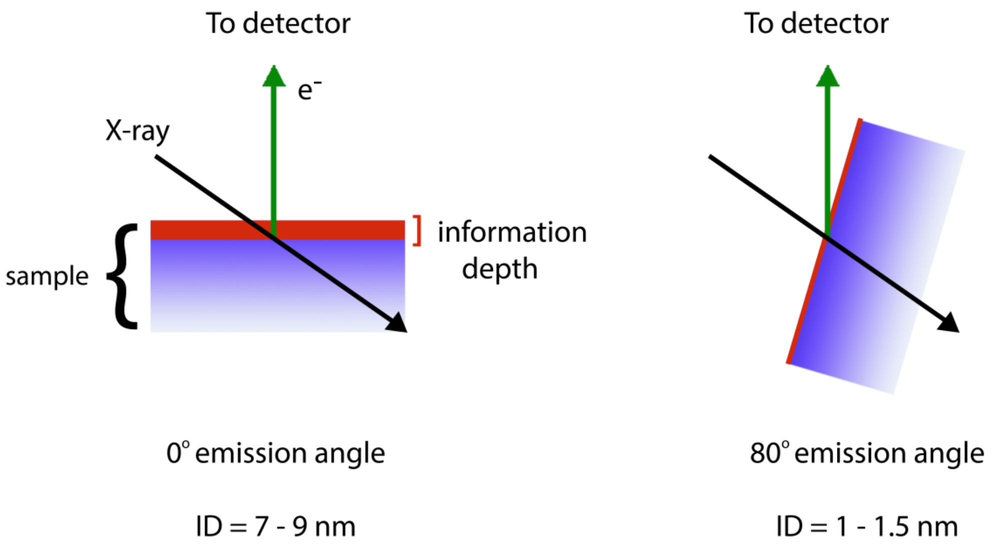

Figure 4.8. Schematic detailing the influence of sample geometry on information depth when recording XP spectra at normal emission angle, θ = 0° (left); and at grazing emission angle, θ = 80° (right).

By increasing the emission angle the distance that an emitted photoelectron must travel through the sample is increased, thus only photoelectrons that have escaped from a shallower depth are detected. At the kinetic energies measured here using the Al Kα source (~ 800 – 1400 eV) the attenuation length of photoelectrons in organic compounds is of the order ~ 3 nm.[45] From this, the ID for each of the angle-resolved geometries employed in the ARXPS experiments can be estimated. Subsequently, at a normal emission angle (θ = 0°) ID is between 7 – 9 nm, and on increasing emission angle to 70° then 80° the measured ID changes to 2 – 3 nm and 1 – 1.5 nm respectively.[46] At θ = 80°, approximately 65 % of the measured signal arises from the topmost 0.3 – 0.5 nm of the sample; this is smaller than the size of most IL ions, highlighting the high degree of surface sensitivity this technique provides.

In a typical ARXPS experiment a series of spectra are recorded in the "bulk sensitive" geometry, where θ = 0°, and with increasing emission angle to more "surface sensitive" geometries *i.e.* 70° ≤ θ ≤ 85°. For a homogeneous and isotropic arrangement of ions in an ionic liquid, identical core photoelectron intensities would be observed for all emission angles. However, a preferential increase in a core photoelectron emission intensity with increasing θ, and thus increasing surface sensitivity, indicates a higher surface concentration for the respective element/component in comparison to the bulk.

4.3.2 Energy-Resolved XPS

In the case of ERXPS the dependence of λ_{AL} on the kinetic energy of the emitted photoelectron is exploited in order to depth profile a sample. Unlike ARXPS, a fixed geometry is employed with a normal emission angle of $\theta = 0°$. Consequently, ID can be simplified to ID = $3\lambda_{AL}$, thus ID is solely a function of attenuation length and hence kinetic energy.

This can be achieved in two ways. Firstly, by looking at spectra of the same core photoelectron emission but changing the energy of the incident radiation, thereby varying photoelectron kinetic energy, and hence the depth which is probed. Typically this procedure requires the use of synchrotron radiation sources as they can provide high intensity X-ray photons that can be tuned across a broad range of energies. The most surface sensitive mode for synchrotron depth profiling experiments are at a photon energy about 50 eV higher than the binding energy of the core level photoelectron emission examined, in which the surface layer probed is around several atoms thick.[26]

The second ERXPS approach can be accomplished by looking at two different core photoelectron emissions from the same element produced using the same X-ray source. Importantly, the binding energy difference – and consequently, the kinetic energy difference – between the two photoelectron emissions must be sufficiently large, therefore high energy X-ray sources such as Ag Lα’ are required to detect core levels of higher energy.

In contrast to ARXPS there are only few reported examples of using ERXPS to probe the IL/vacuum interface, and these have been limited to variable-photon energy experiments which require a synchrotron source.[25, 26] Although many synchrotron facilities exist, obtaining time on them can be limited and also expensive. Herein, an alternative approach of utilising a high energy laboratory Ag Lα’ X-ray source for the depth profiling of a series of bis(trifluoromethanesulfonyl)imide-based ionic liquids is described.

4.4 ARXPS of Ammonium and Phosphonium Ionic Liquids

XP spectra have been obtained at two emission angles, 0° and 80°, with respect to the surface normal for all five bis(trifluoromethanesulfonyl)imide-based ionic liquids, *i.e.* [C_8C_1Pyrr][NTf_2], [$N_{4,4,4,1}$][NTf_2], [$P_{4,4,4,1}$][NTf_2], [$N_{6,6,6,14}$][NTf_2] and [$P_{6,6,6,14}$][NTf_2], using the Al Kα X-ray source. Experimental stoichiometries were determined from the high resolution scans for each element and are presented in Table 4.4.

Stoichiometries determined at the electron emission angle $\theta = 0°$ (ID = 7 – 9 nm) agree very well to the nominal stoichiometry and are within the experimental error for all ionic liquids studied and are well within ± 10 % for the majority. It can be seen that the experimental O 1s stoichiometry is systematically lower than the nominal value. This suggests that the RSF, taken from the Kratos Library, for this element is not ideally suited for the compounds under investigation. Similar deviations in stoichiometry have been reported elsewhere.[3, 5, 26] As this investigation is on changes in stoichiometric ratio with respect to emission angle, small deviations in RSF values have minimal impact on the conclusions made.

Table 4.4. Quantitative analysis of the XP spectra for ionic liquids studied with ARXPS. Experimental and nominal stoichiometries (in number of atoms) are given for all constituent elements of the ionic liquids. The experimental values are obtained from XP spectra at θ = 0° and 80°. Associated experimental error is ± 10 - 20 %.

	Cation						Anion				
	Element	$C_{aliphatic}$ 1s	C_{hetero} 1s	C_{inter} 1s	N_{cation} 1s	P_{cation} 2p	C_{anion} 1s	N_{anion} 1s	O 1s	S 2p	F 1s
	RSF	0.278	0.278	0.278	0.477	0.486	0.278	0.477	0.780	0.668	1.000
$[C_8C_1Pyrr][NTf_2]$	Nominal	**6**	**4**	**3**	**1**	**-**	**2**	**1**	**4**	**2**	**6**
	0°	6.4	4.3	3.2	0.9	-	2.1	0.9	3.5	1.9	5.8
	80°	9.3	3.5	2.3	0.9	-	1.8	0.8	3.3	2.2	5.0
$[N_{4,4,4,1}][NTf_2]$	Nominal	**6**	**4**	**3**	**1**	**-**	**2**	**1**	**4**	**2**	**6**
	0°	6.3	4.2	3.2	1.0	-	2.1	0.9	3.5	1.9	5.8
	80°	7.8	4.0	2.9	0.9	-	2.0	0.8	3.2	2.1	5.3
$[P_{4,4,4,1}][NTf_2]$	Nominal	**9**	**4**	**-**	**-**	**1**	**2**	**1**	**4**	**2**	**6**
	0°	9.3	4.1	-	-	0.8	2.1	1.0	3.7	1.9	6.1
	80°	9.6	3.8	-	-	1.2	1.9	0.9	2.5	2.3	5.8
$[N_{6,6,6,14}][NTf_2]$	Nominal	**24**	**4**	**4**	**1**	**-**	**2**	**1**	**4**	**2**	**6**
	0°	24.8	4.1	4.1	0.9	-	2.1	0.9	3.3	1.9	5.8
	80°	25.2	4.1	4.1	0.7	-	2.1	0.7	3.1	2.7	5.3
$[P_{6,6,6,14}][NTf_2]$	Nominal	**28**	**4**	**-**	**-**	**1**	**2**	**1**	**4**	**2**	**6**
	0°	28.7	4.1	-	-	0.9	2.1	1.1	3.4	2.0	5.7
	80°	28.9	3.8	-	-	1.2	1.8	1.1	3.4	2.2	5.6

Previous ARXPS studies upon 1,3-dialkylimidazolium ionic liquids have shown a significant increase in intensity of the $C_{aliphatic}$ 1s component with increasing emission angle, providing evidence for an enrichment of alkyl chains at the outer surface.[1, 2, 4, 6, 7, 25, 26] A systematic investigation into this effect as a function of alkyl chain length has also shown that the degree of surface enrichment increases with the length of the alkyl chain.[2, 4, 47]

In this study, the surface enrichment of alkyl carbon for a variety of tetraalkylammonium and tetraalkylphosphonium cations, including the 1-octyl-1-methylpyrrolidinium cation, is investigated using an empirical surface enrichment factor, *SE*, first described by Kolbeck *et al.* in the study of imidazolium-based systems.[6] *SE* is defined as the ratio of the $C_{aliphatic}$ 1s component at 80° (ID = 1 – 1.5 nm) to that at 0° (ID = 7 – 9 nm), *i.e.* representative of the nominal value). Consequently, an *SE* value of 1.0 would indicate no surface enrichment of the alkyl chains.

For $[C_8C_1Pyrr][NTf_2]$ an *SE* value of 1.45 was obtained indicating a significant degree of surface enrichment of the alkyl chains, this is also illustrated by comparison of the C 1s photoelectron emission spectra obtained at 0° and 80° in Figure 4.9 (*N.B.* to aid visual interpretation of the presented XP spectra a normalisation procedure was applied, see *Chapter 2 Section 2.3.3* for details). This behaviour is in accordance with previous ARXPS reports on pyrrolidinium and imidazolium ionic liquids.[2, 4, 5, 26] Furthermore, the reported *SE* factor for the imidazolium analogue, $[C_8C_1Im][NTf_2]$, is comparable at a value of 1.52.[6] This suggests that the surface enrichment behaviour of pyrrolidinium- and imidazolium-based ionic liquids is very similar.

A decrease in *SE* is observed for $[N_{4,4,4,1}][NTf_2]$ where *SE* = 1.24 indicating that surface enrichment of alkyl carbon is less for this cation in comparison to $[C_8C_1Pyrr][NTf_2]$. As this cation contains the same amount of alkyl carbon as $[C_8C_1Pyrr][NTf_2]$ (see Table 4.4) and yet does not show the same degree of carbon surface enrichment, it is indicative that not all four of the alkyl chains for $[N_{4,4,4,1}][NTf_2]$ point towards the vacuum at the IL surface.

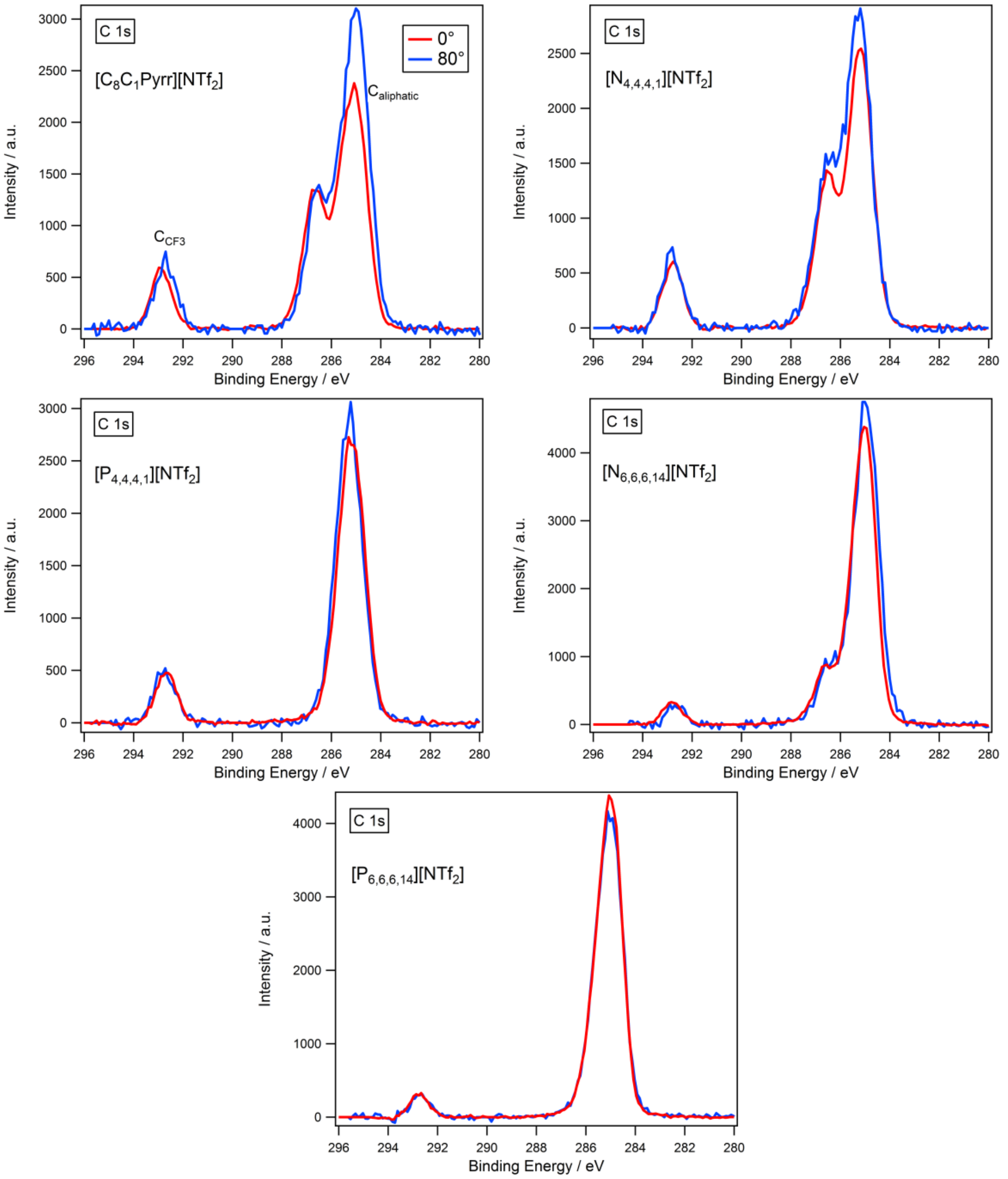

Figure 4.9. High resolution XP spectra of the C 1s region for the five bis(trifluoromethanesulfonyl)imide-based ionic liquids studied in this *Chapter*, recorded at 0° (red) and 80° (blue) electron emission angle, θ, with respect to the surface normal. $[C_8C_1Pyrr][NTf_2]$, $[N_{6,6,6,14}][NTf_2]$ and $[P_{6,6,6,14}][NTf_2]$ spectra charge corrected by referencing $C_{aliphatic}$ 1s to 285.0 eV. $[N_{4,4,4,1}][NTf_2]$ and $[P_{4,4,4,1}][NTf_2]$ spectra were charge corrected by referencing N_{cation} 1s/P_{cation} $2p_{3/2}$ to the value obtained for $[N_{6,6,6,14}][NTf_2]$/$[P_{6,6,6,14}][NTf_2]$. Spectra recorded at θ = 80° normalised to the area of the F 1s photoelectron emission peak recorded for the respective ionic liquid at θ = 80°.

Remarkably, the *SE* values for the compounds $[P_{4,4,4,1}][NTf_2]$, $[N_{6,6,6,14}][NTf_2]$ and $[P_{6,6,6,14}][NTf_2]$ show almost negligible surface enrichment of alkyl carbon with *SE* values of 1.03, 1.02 and 1.01. This is particularly surprising for the

$[N_{6,6,6,14}]^+$ and $[P_{6,6,6,14}]^+$ cations which contain a considerably large amount of aliphatic carbon. A visual comparison of the C 1s photoelectron emission at 0° and 80° for each ionic liquid studied is presented in Figure 4.9, highlighting the differences in surface enrichment for each cation.

Previously, *Chapter 3* described an XPS study on tetraalkylammonium and tetraalkylphosphonium ionic liquids which investigated the influence of the cation on anionic binding energies, in which a perceived hydrocarbon-based shielding of the cationic core for long chain cations, *i.e.* $[N_{6,6,6,14}]^+$ and $[P_{6,6,6,14}]^+$, was observed. It was proposed this was due to the long alkyl chains wrapping around the cationic core rather than being fully extended. Furthermore, it was observed that the hydrocarbon-based shielding could be reduced through a decrease in alkyl chain length or conformational restriction *i.e.* using cyclic analogues such as $[C_8C_1Pyrr][NTf_2]$. The results obtained in this ARXPS study fully support this assertion as the lack of surface enrichment of alkyl carbon for $[N_{6,6,6,14}][NTf_2]$, $[P_{6,6,6,14}][NTf_2]$ and $[P_{4,4,4,1}][NTf_2]$ strongly suggest that the alkyl chains are indeed wrapped around the cation core for these cations. Also, in accordance with the studies described in *Chapter 3*, the effect of hydrocarbon-based shielding is clearly diminished for the cations $[C_8C_1Pyrr][NTf_2]$ and $[N_{4,4,4,1}][NTf_2]$ as evidenced by an increase in surface enrichment of alkyl carbon for these ionic liquids.

In comparison to the large surface enrichment of carbon observed for $[C_8C_1Pyrr][NTf_2]$ where a 50 % increase in the $C_{aliphatic}$ signal is seen, more subtle effects are seen for the anionic components. Here, a small decrease of ~ 15 % is seen in the F 1s and C_{anion} 1s signals, with a corresponding ~15 % increase in the S 2p signal, Table 4.4. It is proposed that this is the result of an orientation preference of the anion (which is situated beneath the aliphatic carbon overlayer) such that the $–CF_3$ groups are pointed towards the bulk ionic liquid, away from the vacuum. A similar trend is also seen for the anionic components of the other ionic liquids studied. This supports the synchrotron-based XPS studies conducted by Lockett *et al.*[26] in which they suggest the anion, on average, has a *cis* configuration with both $–CF_3$ groups facing the bulk. A further study by Men *et al.*[5] on a homologous series of ionic liquids of the type [C_nC_1Pyrr][NTf_2] also supports this conclusion. It should be stressed that due to the liquid state of the samples, a fluid and dynamic nature exists as a result of molecular tumbling, thus the data obtained represents an average of the true situation at any time. Additionally, as this possible orientation preference of the anion exhibits a considerably smaller effect on the ionic liquid near-surface region, in comparison to carbon surface enrichment, it is not the primary focus of this ARXPS study.

Information on the relative position of the cationic head group (X; where X = N_{cation} 1s or P_{cation} 2p) to the anionic head group (N_{anion} 1s) can be obtained by measuring the change in elemental ratio for each with electron emission angle, see Table 4.5. It can be seen for the pyrrolidinium and ammonium ionic liquids that there is very little change in ratio with emission angle indicating that cation and anion are at approximately the same distance from the interface. Interestingly for the phosphonium ionic liquids, [$P_{4,4,4,1}$][NTf_2] and [$P_{6,6,6,14}$][NTf_2], an increase in X / N_{anion} from 0.8 to 1.3 and 1.1 respectively is observed suggesting that the cation is located slightly above the anion at the surface.

Table 4.5. Elemental ratio of cationic head group X (where X = N_{cation} 1s or P_{cation} 2p) to anionic head group (N_{anion} 1s) at $\theta = 0°$ and 80° with an associated error of ± 5 %.

	Elemental Ratios	
Ionic Liquid	X / N_{anion} 0°	X / N_{anion} 80°
[C_8C_1Pyrr][NTf_2]	1.00	1.13
[$N_{4,4,4,1}$][NTf_2]	1.11	1.13
[$P_{4,4,4,1}$][NTf_2]	0.80	1.33
[$N_{6,6,6,14}$][NTf_2]	1.00	1.00
[$P_{6,6,6,14}$][NTf_2]	0.82	1.09

In summary, [C_8C_1Pyrr][NTf_2] and [$N_{4,4,4,1}$][NTf_2] display similar behaviour at the ionic liquid/vacuum interface as previously recorded in the literature for imidazolium ionic liquids of the type [C_nC_1Im][X], whereby the surface is constructed of an alkyl chain overlayer, with a sublayer of charge-bearing head groups residing underneath. However, for [$N_{6,6,6,14}$][NTf_2], [$P_{6,6,6,14}$][NTf_2] and [$P_{4,4,4,1}$][NTf_2] a different picture emerges, in which minimal surface ordering is present indicating a homogeneous distribution of carbons atoms in the near-surface and the bulk. This provides further evidence for the wrapping of the aliphatic chains around the cationic core for these cationic systems. It is proposed that the "wrapping" effect occurs as a result of extensive van der Waals interactions existing between the four alkyl chains.

It is unclear at this time as to why $[P_{4,4,4,1}][NTf_2]$ also displays evidence for wrapping of the alkyl chains around the cationic core, unlike its short chain ammonium analogue ($[N_{4,4,4,1}][NTf_2]$). However, a recent study by Scarbath-Evers *et al.*[48] has indicated a higher flexibility of bond angles and dihedral angles for phosphonium ionic liquids,[48] for this reason it is conceivable that the wrapping of alkyl chains around the cationic core is more likely for the short chain phosphonium cation.

It is postulated that extensive van der Waals interactions between the four aliphatic chains may be the cause for their wrapping around the cation core; in an attempt to provide further evidence for this, variable-temperature ARXPS (VT-ARXPS) experiments were conducted. It is proposed that heating the sample could provide enough energy to weaken the van der Waals interactions between the four chains, which would result in an "unwrapping" of the chains and their subsequent projection towards the vacuum phase. This would be detected through an increase in surface enrichment of the aliphatic carbon component by ARXPS.

To investigate this the ionic liquid $[P_{6,6,6,14}][NTf_2]$ was initially chosen for investigation. Sample heating was achieved *in situ* through heating *via* the sample stage. Due to software limitations of the XP spectrometer when heating the stage, the emission angle was restricted to an upper limit of 75°, rather than the 80° geometry used in previous experiments; however, a high surface sensitivity is retained at this geometry, with an approximate ID = 1.5 – 2 nm, thus any change in carbon surface enrichment would still be detectable. Thus with the emission angle fixed at 75°, XP spectra were recorded at room temperature, 50 °C, 70 °C and 150 °C and the experimental stoichiometries were determined, see Table 4.6.

Table 4.6. Quantitative analysis of the XP spectra for ionic liquids studied with VT-ARXPS. Experimental and nominal stoichiometries (in number of atoms) are given for all constituent elements of the ionic liquids. The experimental values are obtained from XP spectra at θ = 75°. Associated experimental error is ± 10 - 20 %.

	Cation						Anion				
	Element	$C_{aliphatic}$ 1s	C_{hetero} 1s	C_{inter} 1s	N_{cation} 1s	P_{cation} 2p	C_{anion} 1s	N_{anion} 1s	O 1s	S 2p	F 1s
	RSF	0.278	0.278	0.278	0.477	0.486	0.278	0.477	0.780	0.668	1.000
$[P_{6,6,6,14}][NTf_2]$	Nominal	**28**	**4**	**-**	**-**	**1**	**2**	**1**	**4**	**2**	**6**
	R.T.	28.0	4.3	-	-	0.8	2.2	0.8	3.8	1.7	6.4
	50 °C	28.0	4.4	-	-	0.9	2.2	0.8	3.5	1.7	6.5
	70 °C	28.2	4.1	-	-	0.8	2.1	0.9	3.7	1.7	6.6
	150 °C	28.8	3.8	-	-	0.8	1.9	0.8	3.8	1.7	6.3
$[N_{6,6,6,14}][NTf_2]$	Nominal	**24**	**4**	**4**	**1**	**-**	**2**	**1**	**4**	**2**	**6**
	R.T.	24.3	4.2	4.2	0.8	-	2.1	0.7	3.6	1.9	6.1
	150 °C	24.9	3.9	3.9	1.1	-	2.0	0.9	3.6	2.0	5.8
$[P_{4,4,4,1}][NTf_2]$	Nominal	**9**	**4**	**-**	**-**	**1**	**2**	**1**	**4**	**2**	**6**
	R.T.	9.8	4.4	-	-	1.0	2.2	1.1	3.2	2.0	5.3
	150 °C	9.9	4.4	-	-	1.0	2.2	1.1	3.4	2.0	5.0

An upper temperature limit of 150 °C was set to avoid distillation of ionic liquids into the vacuum chamber as decomposition (and slow distillation) for various ammonium and phosphonium ionic liquids has been to seen to occur between 200 - 300 °C (pressure 6 mbar).[49] It is seen from Table 4.6 that with increasing temperature there is negligible change in all elemental and component intensities, the consistency of the value for the $C_{aliphatic}$ 1s component indicates that no change in surface enrichment occurred. $[P_{4,4,4,1}][NTf_2]$ and $[N_{6,6,6,14}][NTf_2]$ were also investigated by VT-ARXPS with comparison made at room temperature and 150 °C. As with $[P_{6,6,6,14}][NTf_2]$ there is negligible change in experimental stoichiometry with temperature for these ionic liquids. Consequently, a potential “unwrapping” of the aliphatic chains could not be observed through this investigation. This could be due to the energy requirements to dissociate the aliphatic chains from each other, *i.e.* higher temperatures required, or it is possible that by increasing the temperature the resultant increase in motion of the component ions and their constituents prevents surface ordering.

4.5 ERXPS of Ammonium and Phosphonium Ionic Liquids

As previously mentioned in *Section 4.3.2* a depth profile of an element within an ionic liquid can be obtained if two core photoelectron emissions from that element can be detected, most importantly they must also have a wide separation in energy. By using the higher energy Ag Lα’ X-ray source photoelectron emissions at higher binding energy can be detected, Figure 4.5. This technique, termed ERXPS, was therefore used to obtain a depth profile for the sulfur atom of the $[NTf_2]^-$ anion through comparison of the S 1s and S 2p photoelectron peaks for the ionic liquids: $[C_8C_1Pyrr][NTf_2]$, $[N_{4,4,4,1}][NTf_2]$, $[P_{4,4,4,1}][NTf_2]$, $[N_{6,6,6,14}][NTf_2]$ and $[P_{6,6,6,14}][NTf_2]$. It is important to note that no geometry change to the sample is required, *i.e.* all spectra are recorded at fixed emission angle θ = 0°, consequently any error introduced by a change in geometry is removed.

This approach is based on the fact that the depth from which a photoelectron is able to escape is dependent on the kinetic energy of the photoelectron. A higher kinetic energy will allow the photoelectron to travel for a longer distance in the sample without experiencing energy loss through collisions *i.e.* it has a longer attenuation length, $\lambda_{AL.}$

From Table 4.3 the binding energies for S 2p and S 1s core orbitals for all ionic liquids studied are respectively ≈ 169 eV and 2478 eV. This corresponds to kinetic energies of S 2p ≈ 2816 eV and S 1s ≈ 507 eV. Consequently, a photoelectron emitted from the S 2p orbital has a greater probability of escaping from deeper in the sample than an S 1s photoelectron. The NIST Electron Inelastic-Mean-Free-Path Database was used to estimate λ_{AL} for S 2p and S 1s photoelectrons for each ionic liquid to give approximate values of 5.3 nm and 1.4 nm respectively.[50] This was achieved by using the database to first calculate the inelastic mean free path (λ_{IMFP}) for each ionic liquid using the TPP-2M method. This calculation can only be carried out up to a kinetic energy of 2000 eV. Consequently, extrapolation of the obtained data set up to 3000 eV is required to obtain an estimate λ_{IMFP} in the energy range 2000 – 3000 eV. The resultant plots of λ_{IMFP} *versus* kinetic energy for each ionic liquid are presented in Figure 4.10.

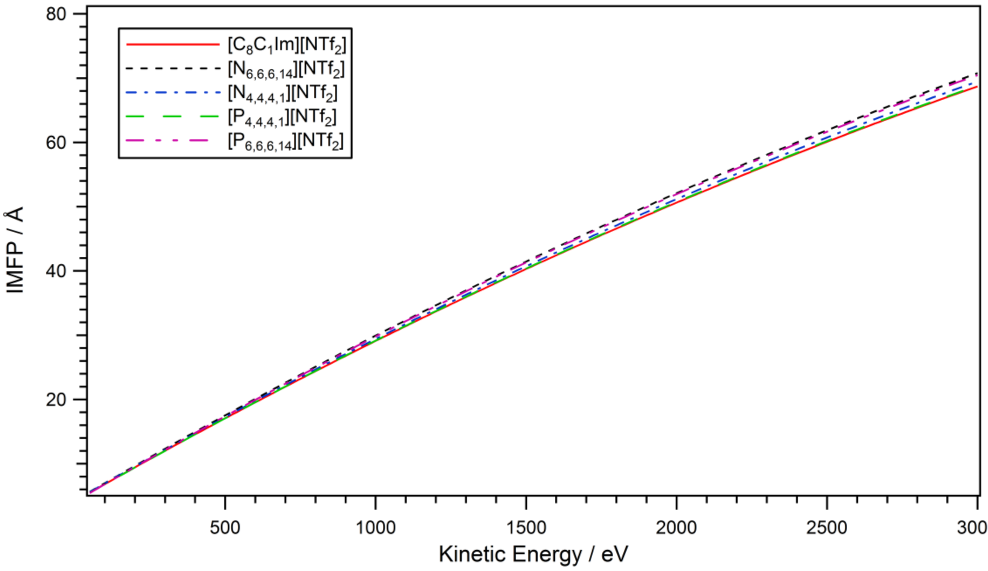

Figure 4.10. Calculated λ_{IMFP} values for the kinetic energy range 50 – 3000 eV for all five ionic liquids studied using the TPP-2M method.

The attenuation length is typically 20 % smaller than the calculated inelastic mean free path as it does not include elastic scattering events;[43, 44] subsequently, this is accounted for in the estimation of λ_{AL} in this work. Figure 4.11 provides a representative example of this procedure for $[N_{4,4,4,1}][NTf_2]$. This shows a plot of the calculated λ_{IMFP} for the energy range 50 – 3000 eV (solid line), and the estimated λ_{AL} (dashed line) – which is 80 % of λ_{IMFP}. The corresponding λ_{AL} values can then be determined for the required kinetic energies.

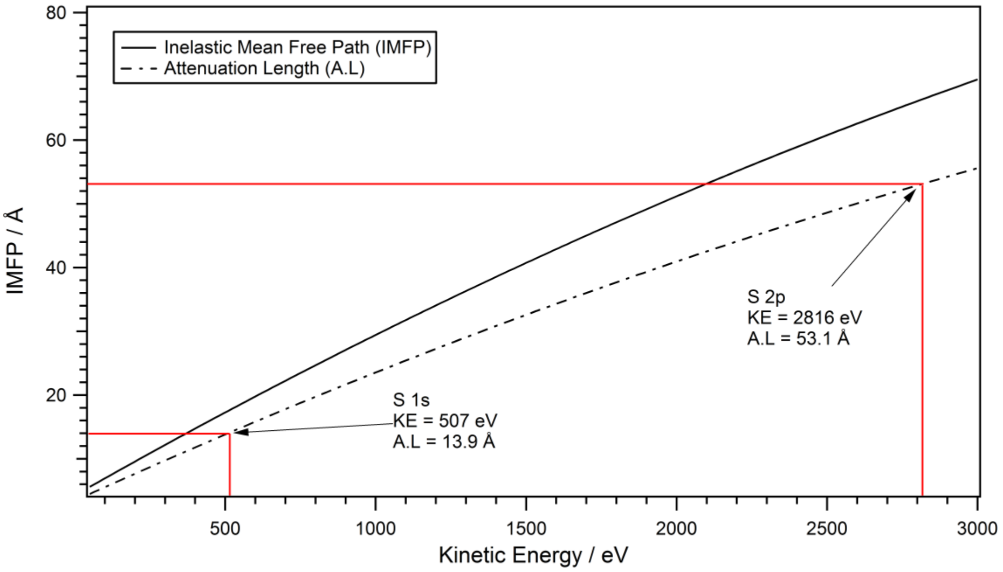

Figure 4.11. Plot describing the calculated λ_{IMFP} (solid black line) and estimated λ_{AL} (dashed line) for $[N_{4,4,4,1}][NTf_2]$. Highlighting the λ_{AL} values obtained for S 1s and S 2p photoelectrons.

The λ_{IMFP} and λ_{AL} values obtained for each ionic liquid are presented in Table 4.7. It can be seen that the values are consistent between compounds and are therefore not sensitive to the ionic liquid.

Table 4.7. λ_{IMFP} and λ_{AL} values for the S 2p and S 1s photoelectrons for all five $[NTf_2]^-$ ionic liquids.

	S 2p		S 1s	
	λ_{IMFP} (nm)	λ_{AL} (nm)	λ_{IMFP} (nm)	λ_{AL} (nm)
$[C_8C_1Im][NTf_2]$	6.6	**5.3**	1.7	**1.4**
$[N_{6,6,6,14}][NTf_2]$	6.8	**5.4**	1.8	**1.4**
$[N_{4,4,4,1}][NTf_2]$	6.6	**5.3**	1.7	**1.4**
$[P_{4,4,4,1}][NTf_2]$	6.6	**5.3**	1.7	**1.4**
$[P_{6,6,6,14}][NTf_2]$	6.7	**5.4**	1.8	**1.4**

As this technique uses a fixed geometry of the sample *i.e.* an emission angle where $\theta = 0°$, ID can be expressed as ID = $3\lambda_{AL}$. The information depths for the required photoelectron emissions were obtained using the calculated λ_{AL} values to give an S 1s ID = 4.2 nm and S 2p ID = 15.9 nm. Consequently, the S 2p signal gives a "bulk sensitive" representation of the sulfur concentration in the sample, in contrast to the S 1s signal which gives a "surface sensitive" representation.

Due to the different cross-sections of the two sulfur orbitals (S 2p and S 1s), and hence different RSF values, a direct comparison of peak areas does not provide quantitative information on sulfur surface enrichment within a sample. To achieve this, the area ratio of S 2p : S 1s must first be determined for a homogeneously disordered ionic liquid sample, this can then be used to construct the currently unknown RSF for the S 1s peak by multiplication of the known S 2p RSF by the appropriate factor (obtained from the area ratio of S 2p : S 1s). Once attained the S 1s and S 2p signals can be quantified and directly compared for any sample, thus providing a measure of sulfur surface enrichment. However, as previously discussed many ionic liquids show significant surface ordering and therefore do not contain a homogeneous distribution of ions, thus the confirmation of an appropriate ionic liquid standard is currently underway.

As such, in this work a qualitative approach is used to determine differences in sulfur surface enrichment between samples. By comparison of the peak area ratio of S 2p : S 1s between different samples a relative depth profile can be obtained, whereby the area for S 2p is effectively constant (as it is representative of the bulk) and the area for S 1s will vary with surface enrichment of sulfur, thus affecting the ratio of S 2p : S 1s accordingly for each sample. Therefore a comparison of this ratio between different samples will show any differences with respect to sulfur surface enrichment relative to each other; this method is illustrated by the schematic presented in Figure 4.12 .

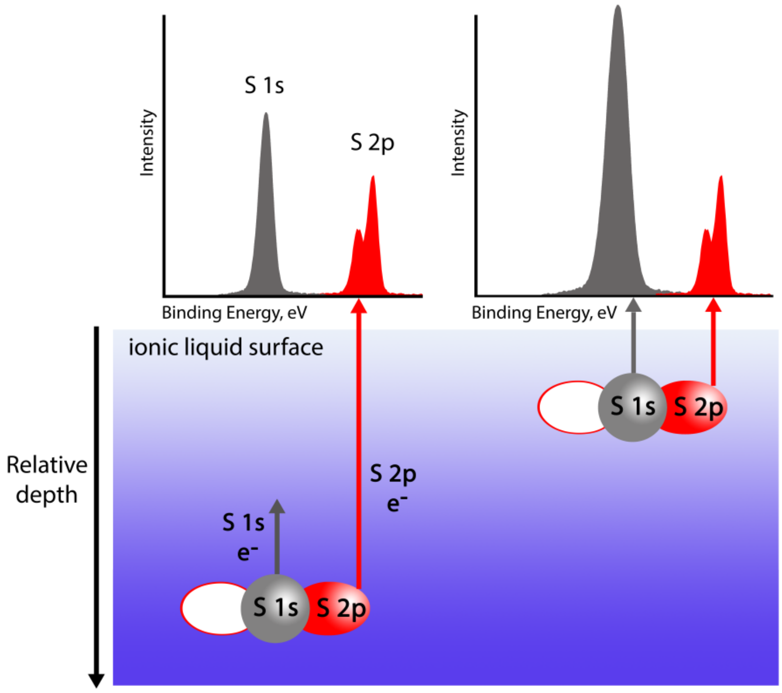

Figure 4.12. Schematic representation illustrating the influence of depth of the sulfur atom from the $[NTf_2]^-$ anion on the corresponding S 1s and S 2p photoelectron emission intensities. The higher kinetic energy of an emitted S 2p photoelectron results in a higher probability of its escape from within the bulk (ID = 15.9 nm), thus the intensity the S 2p photoelectron emission signal remains constant regardless of the depth of the emitting sulfur atom. In contrast, the lower kinetic energy of an emitted S 1s photoelectron reduces its probability of escape from within the bulk (ID = 4.2 nm). Consequently, the change in intensity of the S 1s photoelectron emission peak provides information on the surface concentration of sulfur, *i.e.* high sulfur surface concentration increases the S 1s signal, whereas low sulfur surface concentration decreases the S 1s signal (relative to S 2p).

The S 2p and S 1s peak areas for each of the ionic liquids studied were measured from the respective survey spectra with an average taken for three different positions on the sample to obtain the peak area ratio as presented in Table 4.8.

Table 4.8. Ratio of S 2p to S 1s photoelectron emission peak area for the ionic liquids studied in this work. Areas measured from survey spectra with an associated error of ± 5 %

Ionic Liquid	Photoelectron emission peak area S 2p : S 1s
$[N_{4,4,4,1}][NTf_2]$	1 : 20.5
$[C_8C_1Pyrr][NTf_2]$	1 : 17.7
$[P_{4,4,4,1}][NTf_2]$	1 : 14.1
$[N_{6,6,6,14}][NTf_2]$	1 : 13.9
$[P_{6,6,6,14}][NTf_2]$	1 : 13.8

It is apparent that the concentration of the $[NTf_2]^-$ anion in the near-surface region appears highly dependent on the structure of the cation. A greater surface presence of sulfur is observed for $[N_{4,4,4,1}][NTf_2]$ as the ratio of S 1s to S 2p is largest, this is closely followed by $[C_8C_1Pyrr][NTf_2]$. In contrast, the ionic liquids $[N_{6,6,6,14}][NTf_2]$, $[P_{6,6,6,14}][NTf_2]$ and $[P_{4,4,4,1}][NTf_2]$ all have a similar S 2p : S 1s ratio which is significantly lower than the values obtained for $[N_{4,4,4,1}][NTf_2]$ and $[C_8C_1Pyrr][NTf_2]$, thus corresponding to a decrease in surface concentration of the sulfur atom of the $[NTf_2]^-$ anion. It is interesting how this difference in behaviour mirrors the trend observed in the angle-resolved studies on these ionic liquids as discussed previously in *Section 4.4*.

An explanation for the differences in surface concentration of the $[NTf_2]^-$ anion in the near-surface region can be provided through considering the difference in ordering at the ionic liquid/vacuum interface for these ionic liquids. As mentioned in *Section 4.4* for the ionic liquids $[N_{4,4,4,1}][NTf_2]$ and $[C_8C_1Pyrr][NTf_2]$ the surface is constructed of an alkyl chain overlayer, with a sublayer of charge-bearing head groups residing underneath, an illustration for the surface structure is provided in Figure 4.13. Therefore, the observed sulfur enrichment by ERXPS for these ionic liquids may arise through detection of the polar sublayer of charged head groups which reside underneath the alkyl overlayer.

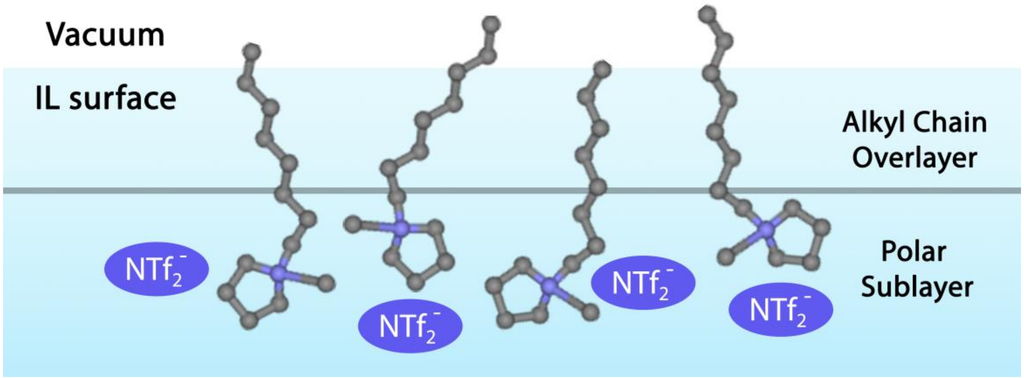

Figure 4.13. Schematic illustrating the surface structure for [C_8C_1Pyrr][NTf_2] and [$N_{4,4,4,1}$][NTf_2], using [C_8C_1Pyrr][NTf_2] as a representative example.

However, in the case of [$N_{6,6,6,14}$][NTf_2], [$P_{6,6,6,14}$][NTf_2] and [$P_{4,4,4,1}$][NTf_2] ARXPS indicated that no such ordering occurs at the IL/vacuum interface and a homogeneous distribution of ions exists. This is supported by a reduction of the S 2p : S 1s ratio, which indicates a reduction in surface concentration of sulfur, and hence a greater proportion of the sulfur signal arises from the bulk. Furthermore, as both ARXPS and ERXPS studies on these ionic liquids provide evidence for a homogeneous distribution of ions, they could be used in future studies as an appropriate reference sample to estimate the currently unknown S 1s RSF. This would enable quantitative data on sulfur surface enrichment to be obtained through future ERXPS investigations. RSFs were not extracted for the ionic liquids in this study as the current dataset is limited to ammonium and phosphonium ILs of the [NTf_2]$^-$ variety, thus the resultant RSFs may not be applicable to other cations and anions. Therefore it is important for robust testing against a variety of ionic liquids, alongside using other techniques to confirm the homogeneous nature of the ILs discussed above, before extracting and reporting RSF values.

Overall, the data obtained with ERXPS is not only supportive to ARXPS, but also additive to it. It is apparent that the surface ordering of the [NTf_2]$^-$ anion is very dependent on cation structure, in which sulfur surface enrichment occurs for [$N_{4,4,4,1}$][NTf_2] and [C_8C_1Pyrr][NTf_2], and in corroboration with ARXPS it provides further evidence for the wrapping of alkyl chains around the cationic core for long chain ammonium and phosphonium systems.

4.6 Conclusions

Two depth profiling techniques (ARXPS and ERXPS) have been used to probe the cationic influence on the structure of the ionic liquid/vacuum interface. An ARXPS study has shown that the degree of aliphatic carbon surface enrichment is dependent on the type of cation used, whereby it is largest for constrained or short chain ammonium cations. However, in the case of long chain ammonium and phosphonium systems (and also a short chain phosphonium analogue) minimal surface ordering is observed, providing further evidence for the wrapping of aliphatic chains around the cationic core in these systems, resulting in a homogeneous distribution of ions.

Additionally, the first use of an Ag Lα’ X-ray source for ionic liquid analysis has been described. A comparison of binding energies obtained with this source against the Al Kα source has been made and indicate that the Ag Lα’ source also provides robust chemical state analysis for ionic liquids, alongside characterising higher energy core photoelectron emissions *i.e.* Cl 1s, P 1s, S 1s and Si 1s.

Furthermore, the use of the Ag Lα’ X-ray source to provide another depth profiling technique, ERXPS, to measure the depth profile of the sulfur atom of the $[NTf_2]^-$ anion has been demonstrated. A cationic dependence on surface ordering of the anion was shown, with similar trends observed as to those obtained through ARXPS. It was found that both depth profiling techniques were supportive and additive to each other and provide evidence for a hydrocarbon-based shielding of the cationic core for cations of the type $[N_{6,6,6,14}]^+$, $[P_{6,6,6,14}]^+$, and $[P_{4,4,4,1}]^+$, in contrast to $[C_8C_1Pyrr]^+$ and $[N_{4,4,4,1}]^+$ where the alkyl chains are extended away from the cationic core.

4.7 References

1. C. Kolbeck, T. Cremer, K. R. J. Lovelock, N. Paape, P. S. Schulz, P. Wasserscheid, F. Maier and H.-P. Steinrück, *J. Phys. Chem. B*, 2009, **113**, 8682-8688.

2. K. R. J. Lovelock, C. Kolbeck, T. Cremer, N. Paape, P. S. Schulz, P. Wasserscheid, F. Maier and H.-P. Steinrück, *J. Phys. Chem. B*, 2009, **113**, 2854-2864.

3. C. Kolbeck, M. Killian, F. Maier, N. Paape, P. Wasserscheid and H.-P. Steinrück, *Langmuir*, 2008, **24**, 9500-9507.

4. F. Maier, T. Cremer, C. Kolbeck, K. R. J. Lovelock, N. Paape, P. S. Schulz, P. Wasserscheid and H.-P. Steinrück, *Phys. Chem. Chem. Phys.*, 2010, **12**, 1905-1915.

5. S. Men, B. B. Hurisso, K. R. J. Lovelock and P. Licence, *Phys. Chem. Chem. Phys.*, 2012, **14**, 5229-5238.

6. C. Kolbeck, A. Deyko, T. Matsuda, F. T. U. Kohler, P. Wasserscheid, F. Maier and H.-P. Steinrück, *ChemPhysChem*, 2013, **14**, 3726-3730.

7. C. Kolbeck, I. Niedermaier, A. Deyko, K. R. J. Lovelock, N. Taccardi, W. Wei, P. Wasserscheid, F. Maier and H.-P. Steinrück, *Chem. Eur. J.*, 2014, **20**, 3954-3965.

8. D. Yoshimura, T. Yokoyama, T. Nishi, H. Ishii, R. Ozawa, H. Hamaguchi and K. Seki, *J. Electron Spectrosc. Relat. Phenom.*, 2005, **144**, 319-322.

9. O. Höfft, S. Bahr, M. Himmerlich, S. Krischok, J. A. Schaefer and V. Kempter, *Langmuir*, 2006, **22**, 7120-7123.

10. T. Iwahashi, T. Nishi, H. Yamane, T. Miyamae, K. Kanai, K. Seki, D. Kim and Y. Ouchi, *J. Phys. Chem. C*, 2009, **113**, 19237-19243.

11. T. Nishi, T. Iwahashi, H. Yamane, Y. Ouchi, K. Kanai and K. Seki, *Chem. Phys. Lett.*, 2008, **455**, 213-217.

12. A. Ulbrich, M. Reinmoller, W. J. D. Beenken and S. Krischok, *ChemPhysChem*, 2012, **13**, 1718-1724.

13. S. Krischok, M. Eremtchenko, M. Himmerlich, P. Lorenz, J. Uhlig, A. Neumann, R. Ottking, W. J. D. Beenken, O. Höfft, S. Bahr, V. Kempter and J. A. Schaefer, *J. Phys. Chem. B*, 2007, **111**, 4801-4806.

14. S. Caporali, U. Bardi and A. Lavacchi, *J. Electron Spectrosc. Relat. Phenom.*, 2006, **151**, 4-8.

15. A. Kauling, G. Ebeling, J. Morais, A. Padua, T. Grehl, H. H. Brongersma and J. Dupont, *Langmuir*, 2013, **29**, 14301-14306.

16. I. J. Villar-Garcia, S. Fearn, G. F. De Gregorio, N. L. Ismail, F. J. V. Gschwend, A. J. S. McIntosh and K. R. J. Lovelock, *Chem. Sci.*, 2014, **5**, 4404-4418.

17. I. J. Villar-Garcia, S. Fearn, N. L. Ismail, A. J. S. McIntosh and K. R. J. Lovelock, *Chem. Commun.*, 2015, **51**, 5367-5370.

18. K. Nakajima, A. Ohno, M. Suzuki and K. Kimura, *Nucl. Instrum. Methods Phys. Res. Sect. B.*, 2009, **267**, 605-609.

19. K. Nakajima, A. Ohno, H. Hashimoto, M. Suzuki and K. Kimura, *J. Chem. Phys.*, 2010, **133**, 7.

20. K. Nakajima, M. Miyashita, M. Suzuki and K. Kimura, *J. Chem. Phys.*, 2013, **139**, 8.

21. T. Hammer, M. Reichelt and H. Morgner, *Phys. Chem. Chem. Phys.*, 2010, **12**, 11070-11080.

22. C. Ridings, V. Lockett and G. Andersson, *Phys. Chem. Chem. Phys.*, 2011, **13**, 17177-17184.

23. C. Ridings, G. G. Warr and G. G. Andersson, *Phys. Chem. Chem. Phys.*, 2012, **14**, 16088-16095.

24. F. Maier, J. M. Gottfried, J. Rossa, D. Gerhard, P. S. Schulz, W. Schwieger, P. Wasserscheid and H.-P. Steinrück, *Angew. Chem. Int. Ed.*, 2006, **45**, 7778-7780.

25. V. Lockett, R. Sedev, C. Bassell and J. Ralston, *Phys. Chem. Chem. Phys.*, 2008, **10**, 1330-1335.

26. V. Lockett, R. Sedev, S. Harmer, J. Ralston, M. Horne and T. Rodopoulos, *Phys. Chem. Chem. Phys.*, 2010, **12**, 13816-13827.

27. P. van der Heide, *X-ray Photoelectron Spectroscopy: An Introduction to Principles and Practices*, John Wiley & Sons, New Jersey, 2011.

28. J. Carrazza and V. Leon, *Surf. Interface Anal.*, 1991, **17**, 225-229.

29. E. F. Smith, F. J. M. Rutten, I. J. Villar-Garcia, D. Briggs and P. Licence, *Langmuir*, 2006, **22**, 9386-9392.

30. C. D. Wagner, L. E. Davis, M. V. Zeller, J. A. Taylor, R. H. Raymond and L. H. Gale, *Surf. Interface Anal.*, 1981, **3**, 211-225.

31. C. Maton, N. De Vos and C. V. Stevens, *Chem. Soc. Rev.*, 2013, **42**, 5963-5977.

32. K. Tsunashima, E. Niwa, S. Kodama, M. Sugiya and Y. Ono, *J. Phys. Chem. B*, 2009, **113**, 15870-15874.

33. C. J. Bradaric, A. Downard, C. Kennedy, A. J. Robertson and Y. H. Zhou, *Green Chem.*, 2003, **5**, 143-152.

34. J. A. Vega, J. F. Zhou and P. A. Kohl, *J. Electrochem. Soc.*, 2009, **156**, A253-A259.

35. J. S. Luo, O. Conrad and I. F. J. Vankelecom, *J. Mater. Chem.*, 2012, **22**, 20574-20579.

36. D. R. MacFarlane, S. A. Forsyth, J. Golding and G. B. Deacon, *Green Chem.*, 2002, **4**, 444-448.

37. J. L. Anderson, J. Ding, T. Welton and D. W. Armstrong, *J. Am. Chem. Soc.*, 2002, **124**, 14247-14254.

38. H. Tokuda, K. Ishii, M. Susan, S. Tsuzuki, K. Hayamizu and M. Watanabe, *J. Phys. Chem. B*, 2006, **110**, 2833-2839.

39. P. Wasserscheid and T. Welton, *Ionic Liquids in Synthesis*, Wiley-VCH, Weinham, 2nd edn., 2008.

40. I. J. Villar-Garcia, E. F. Smith, A. W. Taylor, F. L. Qiu, K. R. J. Lovelock, R. G. Jones and P. Licence, *Phys. Chem. Chem. Phys.*, 2011, **13**, 2797-2808.

41. A. W. Taylor, S. Men, C. J. Clarke and P. Licence, *RSC Adv.*, 2013, **3**, 9436-9445.

42. S. Men, K. R. J. Lovelock and P. Licence, *Phys. Chem. Chem. Phys.*, 2011, **13**, 15244-15255.

43. J. F. Watts and J. Wolstenholme, *An Introduction to Surface Analysis by XPS and AES*, John Wiley & Sons Ltd, Great Britain, first edition edn., 2003.

44. D. Briggs and J. T. Grant, *Surface Analysis by Auger and X-ray Photoelectron Spectroscopy*, IM Publications LLP, Manchester, 2003.

45. R. F. Roberts, D. L. Allara, C. A. Pryde, N. E. Buchanan and N. D. Hobbins, *Surf. Interface. Anal.*, 1980, **2**, 5-10.

46. K. R. J. Lovelock, I. J. Villar-Garcia, F. Maier, H.-P. Steinrück and P. Licence, *Chem. Rev.*, 2010, **110**, 5158-5190.

47. H.-P. Steinrück, *Phys. Chem. Chem. Phys.*, 2012, **14**, 5010-5029.

48. L. K. Scarbath-Evers, P. A. Hunt, B. Kirchner, D. R. MacFarlane and S. Zahn, *Phys. Chem. Chem. Phys.*, 2015, **17**, 20205-20216.

49. M. J. Earle, J. Esperanca, M. A. Gilea, J. N. Canongia Lopes, L. P. N. Rebelo, J. W. Magee, K. R. Seddon and J. A. Widegren, *Nature*, 2006, **439**, 831-834.

50. C. J. Powell and A. Jablonski, *NIST Electron Inelastic-Mean-Free-Path- Database - Version 1.2*, National Institute of Standards and Technology, Gaithersburg, MD, 2010.

5. XPS of Functionalised Ionic Liquids

5.1 Introduction

Ionic liquids (ILs) are often referred to as "*designer solvents*" due to that fact that by simply changing the component ions chemical and physical properties can be altered to suit a specific function.[1] Furthermore, an additional degree of tunability can also be obtained *via* functionalisation of either the cationic or anionic components; typically this is applied to impart a particular type of reactivity or property, and has led to a sub-set of ILs known as task-specific ionic liquids (TSILs).[2, 3] TSILs have been prepared for a range of applications including CO_2 capture,[4, 5] metal extraction,[6, 7] transition metal catalysis,[8] biomass dissolution,[9] and surfactant synthesis.[10]

Previously, in *Chapter 3* the influence of the cation on charge-transfer was reported, with focus on substituting the central charge carrier from nitrogen to phosphorus in a series of structurally related, and conformationally constrained quaternary salts. It was noted that the nature of the cation did indeed impact on the magnitude of charge-transfer, and consequentially the bulk electronic environment of the liquid itself. In this *Chapter*, this level of analysis is extended a step further by investigating the influence of additional functionality embedded within the alkyl side chains of the cations themselves. Subsequently, the impact of two classes of commonly employed functional substituents – polyether and perfluorinated alkyls – is probed using X-ray photoelectron spectroscopy (XPS). The influence of these substituents on the physico-chemical properties of ILs is well documented,[11, 12] however little is known about their effect on inter-ion interactions and local electronic environments of ILs. As such, the investigations described here are designed to probe local tuning of the inductive effect of the substituent groups. The XPS spectra of these materials, particularly the charge carrier regions, is compared to non-functionalised analogues to reveal the influence of functionalisation, and consequently any impact on the magnitude of charge-transfer from anion to cation.

Ionic liquids have found particular application as solvents for transition metal catalysis including, but not limited to, hydrogenation,[13, 14] hydroformylation,[15] oxidation,[16] and Pd-catalysed cross-coupling reactions.[17-20] In particular, a "non-innocent" nature has been observed for imidazolium-based ILs utilised as solvents in various Pd cross-coupling reactions, in which enhancements in activity are attributed to the formation of a palladium-imidazolylidene complex, see Figure 5.1.[18, 20, 21]

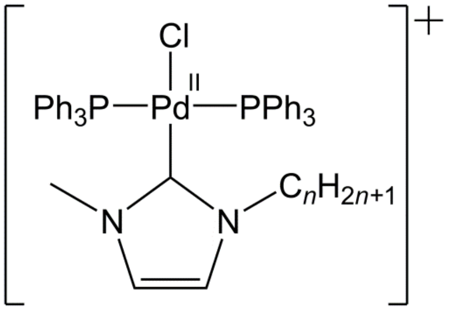

Figure 5.1. Structure of palladium-imidazolylidene complex formed *in situ* under Suzuki cross-coupling conditions using ionic liquids of type [C_nC_1Im][X] as the solvent.

A recent XPS study by Men *et al.* has demonstrated that the electronic environment, and hence catalytic activity, of the palladium-imidazolylidene complex in the Pd-catalysed Suzuki reaction can be tuned *via* anion exchange.[22] Consequently, it is of considerable interest to understand how functionalisation of the cation may also impact on an IL-based catalytic system. Herein, turn-over frequencies (TOFs) for polyether-functionalised ILs are examined in a well-studied catalytic system – the palladium catalysed Suzuki cross-coupling. The measured TOFs are then compared to those measured in a series of benchmark reactions carried out in non-functionalised ILs.

5.2 Effect of Functionalisation on IL Electronic Environment

As described in *Chapter 3*, XPS studies of cation-anion interactions have shown a strong correlation between binding energy of the cationic heteroatom (and also the carbon component directly bonded to it) and anion basicity.[23-27] This is interpreted as a measure of the degree of charge transferred from anion to cation. Highly basic anions, such as halides, transfer a significant amount of electron density to the cation; however, less basic anions, such as $[NTf_2]^-$, transfer notably less.

Furthermore, a study by Villar-Garcia *et al*. on ionic liquids of the type $[C_nC_1Im][X]$ (where $n = 2 – 12$) for a variety of anions has shown that the binding energy of the $C_{aliphatic}$ 1s component, as a function of chain length, is also anion dependent.[28] This effect can only be seen for short alkyl chain lengths where $n < 8$; for larger alkyl chain length, *i.e.* $n \geq 8$, the $C_{aliphatic}$ 1s binding energy is not significantly influenced by anion type. The relative $C_{aliphatic}$ 1s shift follows the trend $[NTf_2]^- > [TfO]^- \approx [N(CN)_2]^- \approx [BF_4]^- > [PF_6]^- > Cl^- \approx Br^-$; where, in fact, Cl^- and Br^- show no significant shift in $C_{aliphatic}$ 1s binding energy at all, see Figure 5.2.[28]

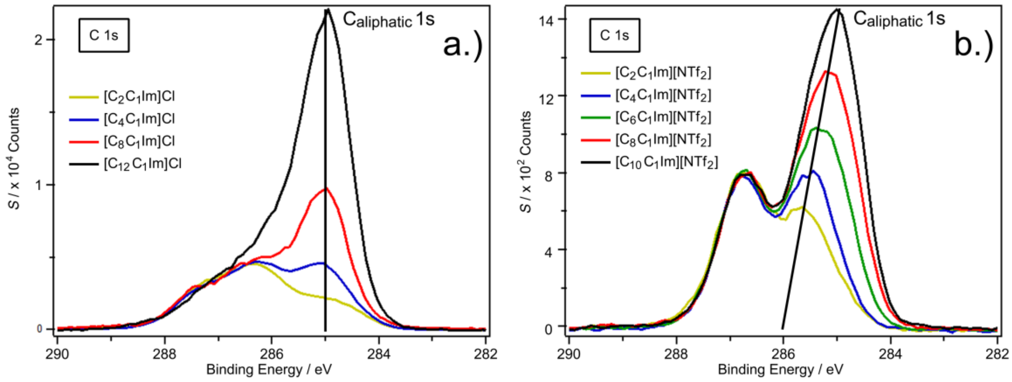

Figure 5.2. C 1s XP spectra for a.) $[C_nC_1Im]Cl$ (where $n = 2 – 12$) and b.) $[C_nC_1Im][NTf_2]$ (where $n = 2 – 10$) showing the anion dependent shift in binding energy of the $C_{aliphatic}$ 1s component for varying alkyl chain lengths.[28] $[C_nC_1Im]Cl$ spectra charge corrected by referencing N_{cation} 1s = 401.7 eV, and $[C_nC_1Im][NTf_2]$ spectra charge corrected by referencing N_{cation} 1s = 402.1 eV. Spectra normalised to area of respective N_{cation} 1s peak.

This may be rationalised as a consequence of two sets of interactions: (1) the magnitude of charge-transfer from anion to cation, and (2) the inductive effect of the aliphatic chain. Subsequently, for high basicity anions, such as Cl^-, a large degree of charge-transfer occurs from anion to cation, as such the cationic nitrogen is more electron-rich and the inductive effect of the alkyl chain is minimised, hence the $C_{aliphatic}$ 1s binding energy remains effectively constant. In contrast, for low-basicity anions, such as $[NTf_2]^-$ charge-transfer from anion to cation is minimal; thus, the cationic nitrogen is more electron-poor causing a larger inductive influence of the alkyl chain, which results in an observable shift in $C_{aliphatic}$ binding energy. A schematic illustrating the anionic influence on these two different contributions is provided in Figure 5.3.

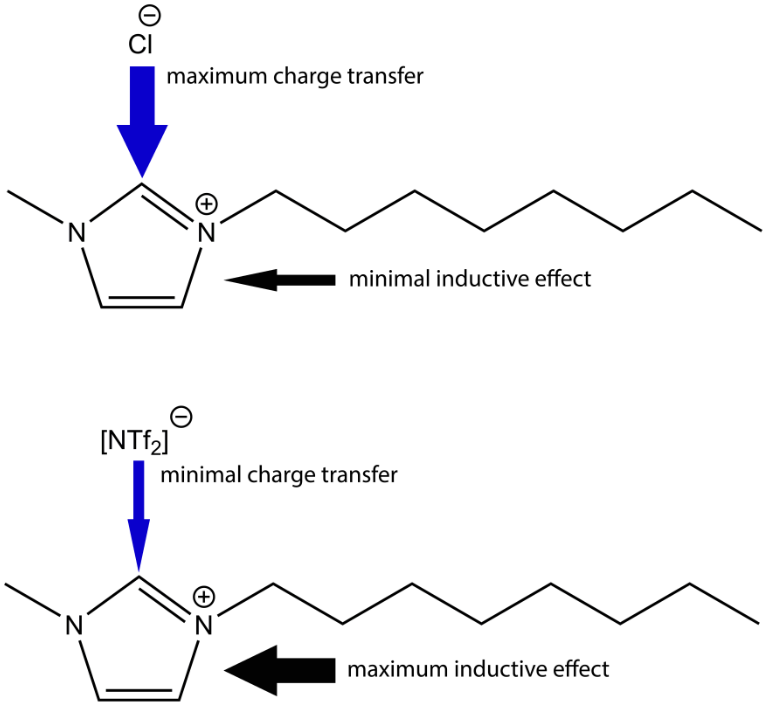

Figure 5.3. Schematic illustrating the influence of the anion on the magnitude of charge-transfer from anion to cation (blue arrow) and inductive effect (black arrow) for a high basicity anion (top structure) and a low basicity anion (bottom structure).

Here, the influence of cation functionalisation on both sets of interactions is investigated. A series of ionic liquids comprising a variety of cationic head-groups, and containing either polyether or perfluorinated functionalities, were investigated by XPS with comparison made to their non-functionalised analogues. The $[NTf_2]^-$ anion was chosen for analysis as it does not participate in significant charge-transfer from anion to cation; consequently, the inductive effect of the aliphatic chain is most significant for this anion. As such it is proposed that disruption to the inductive contribution *via* cation functionalisation may impact charge-transfer from anion to cation to a greater degree, which would be reflected in the binding energy of the anionic components.

5.2.1 Purity and Synthesis

The functionalised ILs in this study were synthesised in a similar manner to their non-functionalised analogues *i.e.* N-alkylation of a nitrogen base (1-methylimidazole, 1-methylpyrrolidine or triethylamine) with a functionalised alkyl halide (1-bromo-2-(2-ethoxyethoxy)ethane or 1-iodo-1*H*,1*H*,2*H*,2*H*-perfluorooctane) followed by anion metathesis, see *Chapter 2 Section 2.3*. Interestingly, the expected product for N-alkylation between triethylamine with 1-iodo-1*H*,1*H*,2*H*,2*H*-perfluorooctane could not be isolated. Instead ^{1}H and ^{13}C NMR analysis on the white solid recovered from the reaction mixture indicated the formation of the protic salt, $[HN_{2,2,2}]I$, see Figure 5.4. This was further supported by the lack of any signal in the recorded ^{19}F NMR spectrum. Similarly, for the reaction between 1-methylpyrrolidine and 1-iodo-1*H*,1*H*,2*H*,2*H*-perfluorooctane the expected N-alkylation product was not recovered due to formation of the analogous protic salt, $[HC_1Pyrr]I$.

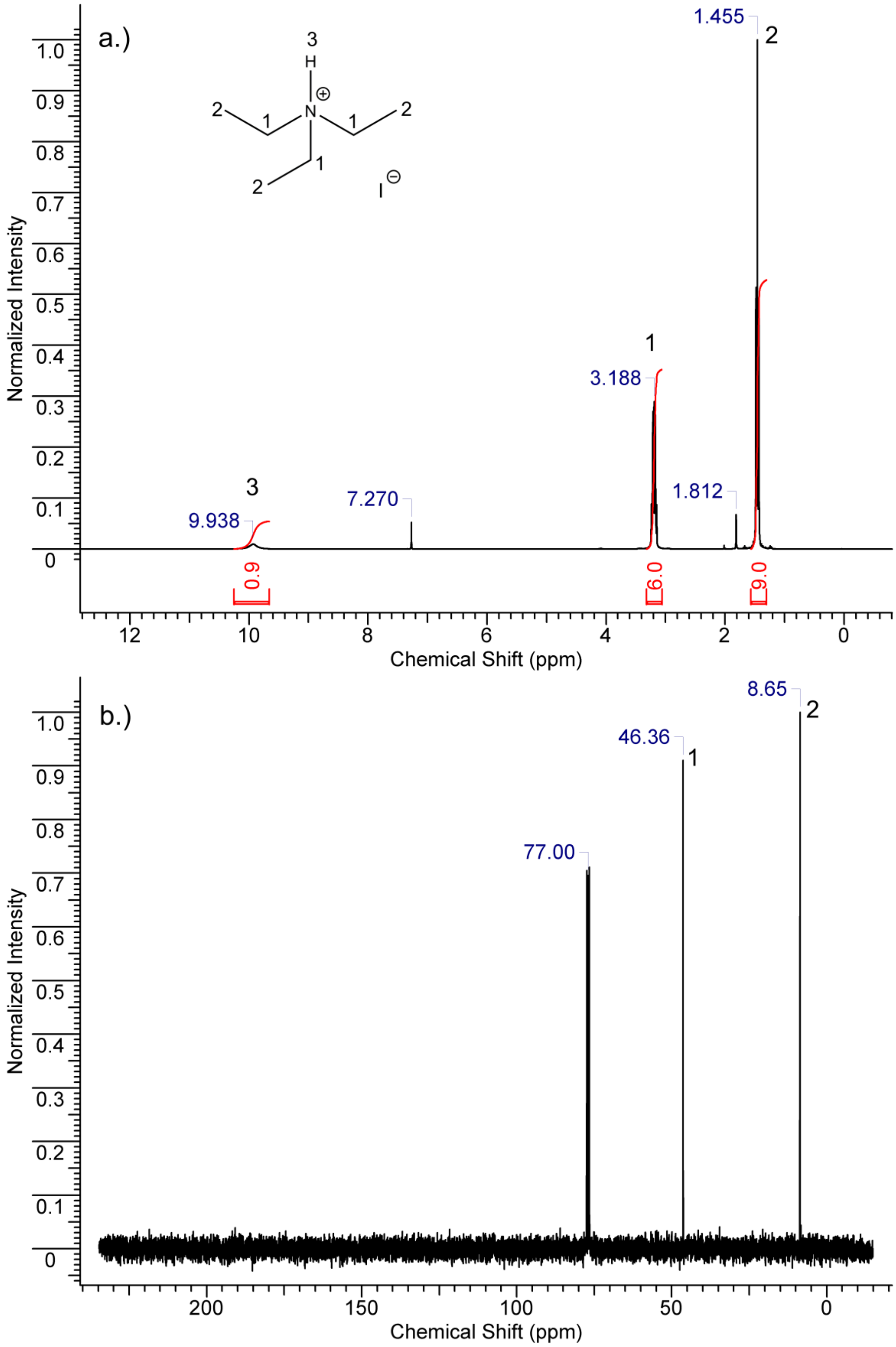

Figure 5.4. ^{1}H NMR (a) and ^{13}C NMR (b) of product ($[HN_{2,2,2}]I$) isolated from reaction between triethylamine and 1-iodo-1*H*,1*H*,2*H*,2*H*-perfluorooctane recorded at frequencies of 300 MHz and 75.5 MHz respectively in chloroform-d. The signals at chemical shifts 1.81 and 7.27 ppm in the ^{1}H NMR spectrum are assigned to water and chloroform respectively.

This is consistent with previous reports in the literature on the propensity of fluoroalkyl iodides with a –CH_2CH_2– spacer to undergo elimination reactions, rather than S_N2 substitution, in the presence of bases such as potassium hydroxide, sodium methoxide and various alkylamines;[29-31] a schematic illustrating this process is provided in Figure 5.5.

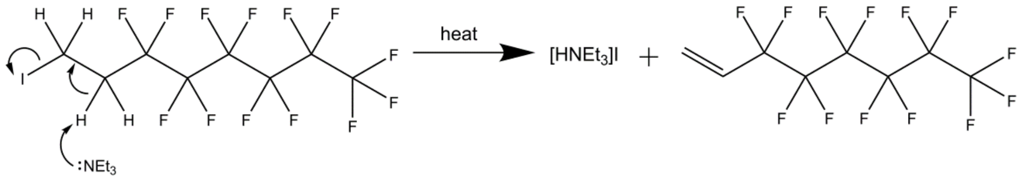

Figure 5.5. Elimination reaction that occurs between triethylamine and 1-iodo-1*H*,1*H*,2*H*,2*H*-perfluorooctane to form the protic elimination salt $[HN_{2,2,2}]I$.

When 1-methylimidazole is used as the nucleophile the dominant process is S_N2, rather than elimination, to form the expected perfluoro-functionalised ionic liquid, $[(F_{13}H_4C_8)C_1Im][NTf_2]$. This difference in reactivity can be attributed to the basicity for each nucleophile. The pK_{aH} values for triethylamine and 1-methylpyrrolidine are 10.7 and 10.6 respectively.[32, 33] In comparison, 1-methylimidazole has a lower pK_{aH} of 7.1,[34] thus is considerably less basic, and favours the S_N2 pathway over elimination. This is supported by reports of functionalisation with perfluorinated alkyl chains using similarly soft bases such as phosphines (PEt_3, $pK_{aH} = 8.7$) *via* the S_N2 reaction.[35, 36]

Consequently, in this investigation comparison was made between the non-functionalised IL and its polyether and perfluorinated analogues for the imidazolium cationic head group only. In the case of the ammonium and pyrrolidinium ILs comparison was restricted to the non-functionalised and polyether functionalised equivalents.

XP survey and high resolution scans using the Al Kα source were used to establish elemental composition and purity for each IL presented in this study. It was seen that all expected elements are present and the stoichiometry within the experimental error, see Table 5.1 and *Appendix C*. For each IL there was no evidence for the presence of silicon-based contaminants, metal based cations and/or halides that may be carried over from IL synthesis.

Table 5.1. Measured experimental and nominal (in brackets) stoichiometries for ionic liquids studied in this *Chapter*. [a] Relative sensitivity factors (RSFs) taken from the Kratos Library were used to derive atomic percentages from the most intense photoelectron emission peak for each element *i.e.* C = C 1s, N = N 1s, O = O 1s, F = F 1s, S = S 2p. Associated experimental error is ± 10 – 20 %. *N.B.* Hydrogen is undetectable by XPS due its low photoionisation cross-section; consequently reported stoichiometries are determined without consideration of hydrogen content.

	Composition^{a} (%)				
Compound	**C**	**N**	**O**	**F**	**S**
RSF[37, 38]	0.278	0.477	0.780	1.000	0.668
$[C_8C_1Im][NTf_2]$	51.9 (48.3)	10.1 (10.3)	12.1 (13.8)	19.3 (20.7)	6.6 (6.9)
$[Et(PEG)_2MIm][NTf_2]$	43.3 (41.4)	10.7 (10.3)	18.7 (20.7)	21.2 (20.7)	6.1 (6.9)
$[(F_{13}H_4C_8)C_1Im][NTf_2]$	34.3 (33.3)	6.8 (7.1)	8.3 (9.5)	46.4 (45.3)	4.3 (4.8)
$[C_8C_1Pyrr][NTf_2]$	54.2 (51.7)	6.5 (6.9)	12.3 (13.8)	20.7 (20.7)	6.3 (6.9)
$[Et(PEG)_2MPyrr][NTf_2]$	47.9 (44.8)	6.5 (6.9)	18.7 (20.7)	20.4 (20.7)	6.6 (6.9)
$[N_{2,2,2,8}]$ $[NTf_2]$	55.5 (53.3)	6.0 (6.7)	11.7 (13.3)	20.8 (20.0)	5.9 (6.7)
$[N_{2,2,2,(Et(PEG)2)}][NTf_2]$	44.4 (47.0)	6.2 (6.7)	18.6 (20.0)	20.1 (20.0)	5.8 (6.7)

5.2.2 C 1s Region

In *Chapter 3, Section 3.2.3* the importance of developing fitting models that deconstruct the different electronic environments for the carbon region was described. Clearly, the introduction of additional functionality into the alkyl side chain will increase the complexity of the carbon photoelectron emission envelope. Consequently, an appropriate fitting model must be developed for each functionalised IL to describe the influence of functionality on the various carbon electronic environments.

Here, carbon fitting models developed for each cationic head group studied, *i.e.* imidazolium, pyrrolidinium and ammonium, are described with comparison made between the various functionalities.

5.2.2.1 Imidazolium-based ILs

Fitting models for the C 1s region of non-functionalised imidazolium-based ionic liquids of the type [C_nC_1Im][X] have been extensively reported in the literature.[28, 37, 39-41] Two different models, named after the groups who developed them, have been proposed: (1) the Licence model (used in this investigation) and (2) the Maier model.[42]

The development of two different models is a consequence of the different XPS instruments employed by both groups. The Kratos set-up utilised by the Licence group (and consequently used in this work) consists of a monochromated Al Kα source with an energy resolution of 0.55 eV (FWHM for Ag $3d_{5/2}$). In comparison, for the non-monochromated set-up utilised by Maier and co-workers a particular line width is not given, but an overall energy resolution of 0.9 eV is reported.[42] Consequently, due to the improved energy resolution of the set-up utilised by Licence and co-workers the resultant C 1s spectra can be deconstructed to a greater extent.

Component fitting, using the Licence model,[28, 37] for the C 1s spectra obtained for [C_8C_1Im][NTf_2] is shown in Figure 5.6a. The peak at ~ 293 eV corresponds to carbon from the [NTf_2]$^-$ anion, and the two partially resolved peaks in the binding energy range 284 – 288 eV correspond to cationic carbon.

Five components were used to describe the different carbon environments contained in $[C_8C_1Im][NTf_2]$. The peak at ~285.0 eV is fitted with one component ($C_{aliphatic}$), the peak at ~286 – 288 eV is fitted with three components ($C_{6,7}$; $C_{4,5}$; C_2) and the peak at ~293 eV is fitted with one component CF_3.

Analysis of the chemical structure is used to determine the order of binding energy for the components C_2; $C_{4,5}$; $C_{6,7}$; and $C_{aliphatic}$. C_2 occurs at highest binding energy as it is positioned between two electron-withdrawing nitrogen atoms. This is followed by the $C_{4,5}$ component, in which the carbon atoms are directly bound to one nitrogen atom. $C_{4,5}$ is expected to occur at higher binding energy relative to $C_{6,7}$ as the $C_{4,5}$ carbon atoms are part of the positively charged imidazolium ring. $C_{aliphatic}$ exhibits the lowest binding energy as the carbons contributing to this component are essentially aliphatic.

To obtain a satisfactory fit that accurately describes the electronic environment appropriate parameter constraints were implemented. This consists of constraining component areas to their nominal stoichiometry. For $[C_8C_1Im][NTf_2]$ it is expected that the component ratio of $CF_3 : C_2 : C_{4,5} : C_{6,7} : C_{aliphatic}$ would be 2 : 1 : 2 : 2 : 7. However, it is necessary to account for intensity losses due to shake-up/shake-off phenomena in atoms involved in conjugated bonding, in this example the C_2 and $C_{4,5}$ environments.

Shake-up is a consequence of excitation of a valence electron from a π orbital to an unoccupied π^* orbital after photoelectron emission. Consequently, the kinetic energy of the emitted photoelectron is lowered, and it does not contribute to the main photoelectron line, but rather forms a satellite peak at higher binding energy.[43] Similarly, in shake-off valence electrons are ionised, *i.e.* excited into the continuum state. No apparent signal is observed in the case of shake-off as the energy for this transition is disperse, subsequently the emitted photoelectron loses most of its kinetic energy and contributes to the inelastic baseline. Shake-up and shake-off collectively lead to a 20 % loss in intensity of the main photoelectron line.[37, 43]

Taking shake-up/shake-off into consideration, the component area constraints for CF_3 : C_2 : $C_{4,5}$: $C_{6,7}$: $C_{aliphatic}$ were set to 2 : 0.8 : 1.6 : 2 : 7. Additionally, the FWHM for C_2, $C_{4,5}$ and $C_{6,7}$ were set to be equal (and constrained to be between 0.8 and 1.3 eV). The FWHM for $C_{aliphatic}$ is separately constrained as it has been shown to produce a broader signal.[28, 37] As expected, it is seen from Figure 5.6a that the fitting envelope (red trace) demonstrates excellent agreement to the experimental spectra (black dots) for $[C_8C_1Im][NTf_2]$.

In Figure 5.6b it is seen that the C 1s peak lineshape alters significantly with polyether-functionalisation for the compound $[Et(PEG)_2MIm][NTf_2]$ in comparison to the non-functionalised $[C_8C_1Im][NTf_2]$. Therefore, an appropriate fitting model for $[Et(PEG)_2MIm][NTf_2]$ was developed. Previous studies on polyether-functionalised ILs have shown that the binding energy for a carbon atom bound to oxygen is very similar to a carbon atom in a C–N bond.[39, 41, 44] Using this assumption, the carbon atoms of the polyether chain directly bound to oxygen (C_8, C_{10}, C_{11} and C_{13}) were considered to be in a similar electronic environment to the carbon atoms bound to nitrogen outside the imidazolium ring (C_6 and C_7) (see Figure 5.6b) with the single remaining carbon (C_{14}) of the chain considered as essentially aliphatic. Each peak was fitted with the same number of components as for $[C_8C_1Im][NTf_2]$, *i.e.* one component for the peak at ~ 285.0 eV; three components for the peak at 286 – 288 eV; and one component for the peak at ~293 eV. However, changes to the nominal stoichiometry of each component were accounted for such that CF_3 : C_2 : $C_{4,5}$: $C_{6,7,8,10,11,13}$: $C_{14(aliphatic)}$ was set to 2 : 0.8 : 1.6 : 6 : 1. FWHM constraints were applied in a similar fashion as for $[C_8C_1Im][NTf_2]$. From Figure 5.6b it is seen that the fitting envelope (red trace) demonstrates excellent agreement to the experimental spectra (black dots), highlighting the validity of this fitting model.

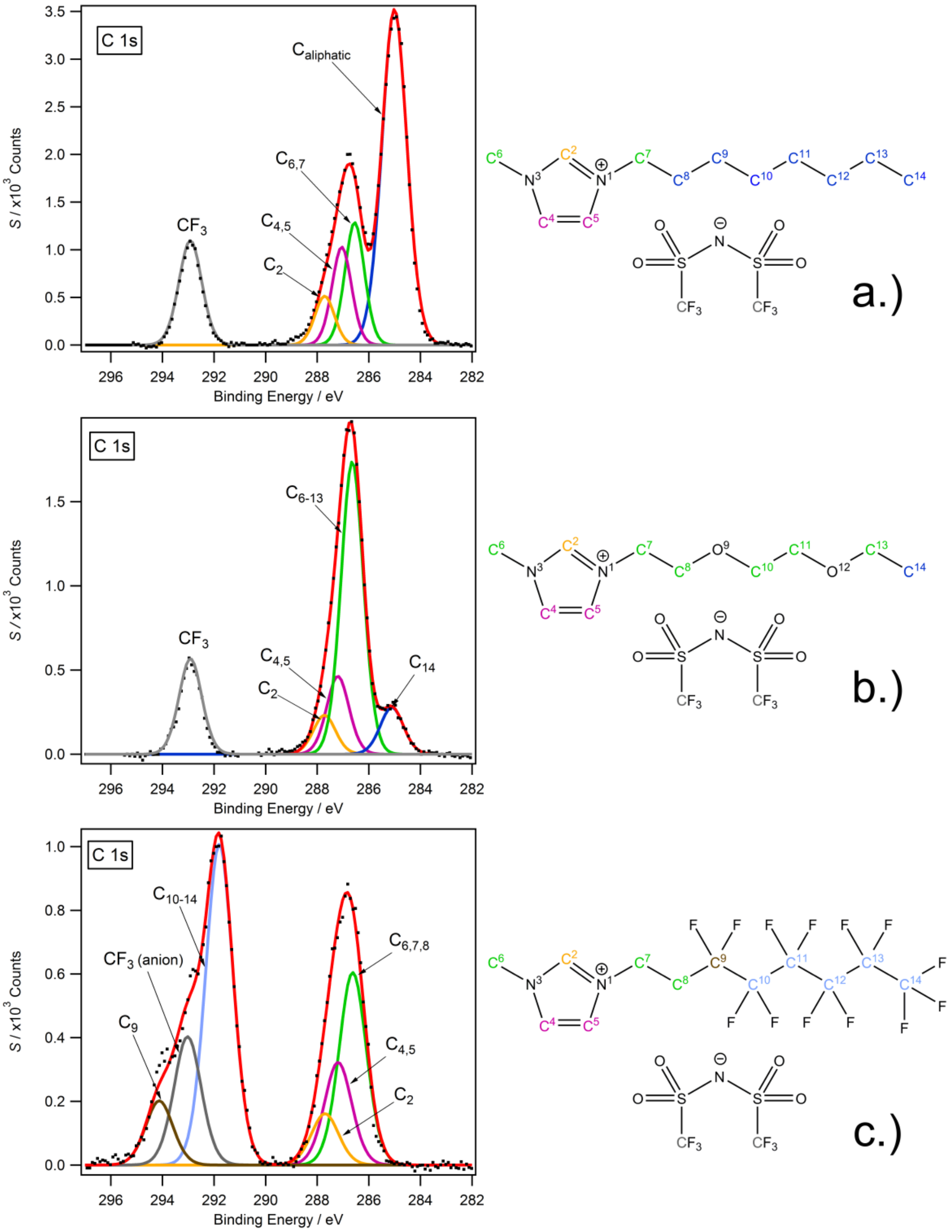

Figure 5.6. C 1s spectra with colour-coded component fittings; fitting envelope (red); counts (black dots); and corresponding structures for (a) $[C_8C_1Im][NTf_2]$ (b) $[Et(PEG)_2MIm][NTf_2]$ and (c) $[(F_{13}H_4C_8)C_1Im][NTf_2]$. Charge correction achieved by referencing the S $2p_{3/2}$ component to 169.0 eV (value obtained from $[C_8C_1Im][NTf_2]$ where prior charge correction achieved by referencing $C_{aliphatic}$ 1s to 285.0 eV).

On functionalisation with a perfluorinated chain further complexity in the carbon photoelectron emission envelope is seen, Figure 5.6c. Here it is seen that the peak corresponding to anionic carbon of the $[NTf_2]^-$ ion is co-incident with a broader photoelectron emission envelope between 290 – 295 eV due to the various fluorinated carbon environments contained in the cation.

A possible fitting model for [$(F_{13}H_4C_8)C_1$Im][NTf_2] was developed, with the structure in Figure 5.6c showing the different carbon environments that are proposed. It is suggested that the C_8 carbon atom is in a similar electronic environment to the $C_{6,7}$ carbon atoms, which implies the electron-withdrawing influence of the neighbouring perfluorinated chain on C_8 is similar in magnitude to that of the positively-charged imidazolium ring for $C_{6,7}$. The remaining carbons of the perfluorinated chain are split into two components C_9 and $C_{10\text{-}14}$. The C_9 environment is positioned at higher binding energy relative to $C_{10\text{-}14}$ due to its closer proximity to the positively-charged imidazolium ring. From Figure 5.6c it is seen that the fitting envelope (red trace) demonstrates good agreement to the experimental spectra (black dots) indicating this to be a plausible fitting model to describe [$(F_{13}H_4C_8)C_1$Im][NTf_2].

5.2.2.2 Pyrrolidinium-based ILs

The C 1s fitting model for non-functionalised pyrrolidinium-based ionic liquids has been previously described in *Chapter 3 Section 3.2.3*. For the purposes of this section a brief review is provided. For the ionic liquid [C_8C_1Pyrr][NTf_2] the C 1s envelope is fitted with four components: the peak at ~293 eV is fitted with one component corresponding to anionic carbon in the [NTf_2]$^-$ ion; and the two partially resolved peaks in the energy range 284 -288 eV are fitted with three components corresponding to the different cationic carbon environments. The order in binding energy of the cationic components is rationalised as follows, the carbon directly bound to the nitrogen (C_{hetero}) is expected to have the highest binding energy as it will experience a stronger electron-withdrawing effect of the cation core. The next carbon along the chain (C_{inter}) experiences this to a lesser degree and is consequently lower in binding energy. The remaining carbon environment is considered essentially aliphatic and exhibits the lowest binding energy. Component areas are constrained to their nominal stoichiometry, *i.e.* CF_3 : C_{hetero} : C_{inter} : $C_{aliphatic}$ equates to 2 : 4 : 3 : 6. The FWHM for C_{hetero} and C_{inter} are set to be equal (and constrained to be between 0.8 and 1.3 eV), and the FWHM for $C_{aliphatic}$ set to be 1.1 times larger than for C_{hetero}. Figure 5.7a shows excellent agreement between the experimental spectra (black dots) and the fitting envelope (red trace) as previously described in the literature.[24]

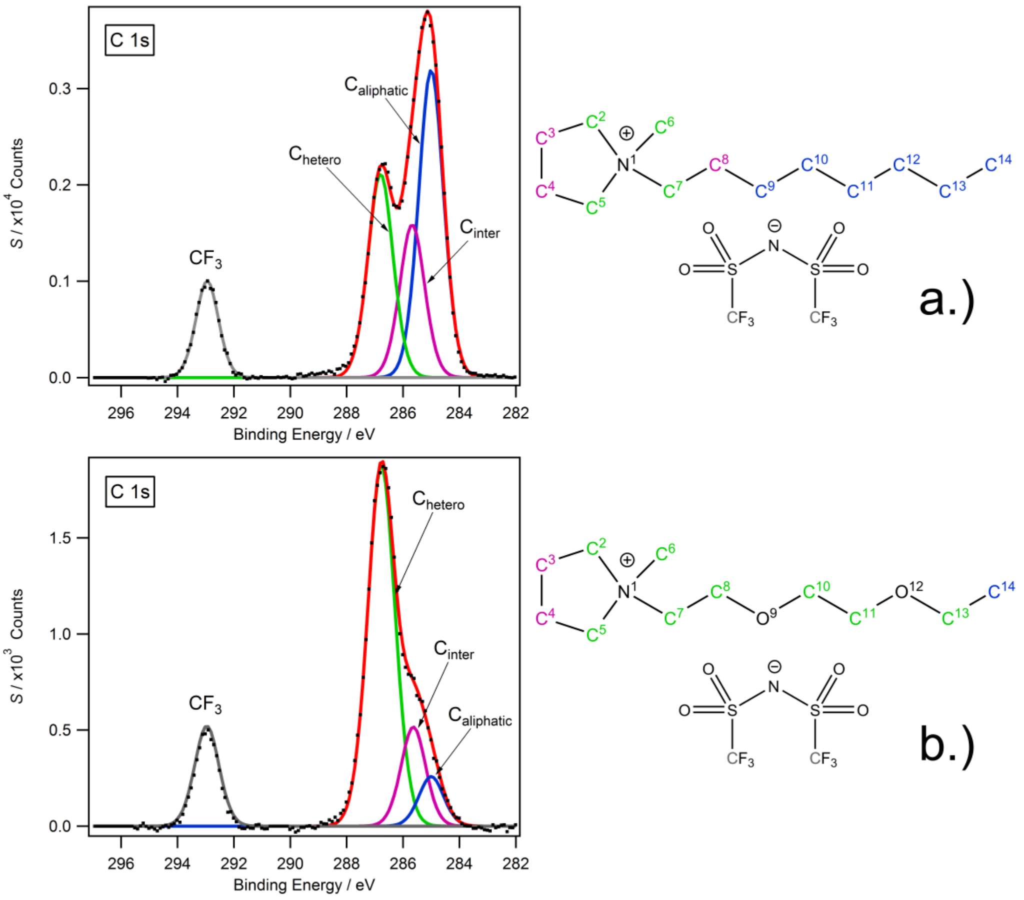

Figure 5.7. C 1s spectra with colour-coded component fittings; fitting envelope (red); counts (black dots); and corresponding structures for (a) [C_8C_1Pyrr][NTf_2] and (b) [Et(PEG)$_2$MPyrr][NTf_2]. Charge correction achieved by referencing the S $2p_{3/2}$ component to 169.0 eV (value obtained from [C_8C_1Pyrr][NTf_2] where prior charge correction achieved by referencing $C_{aliphatic}$ 1s to 285.0 eV).

As seen previously with imidazolium-based ILs, polyether functionalisation resulted in a significant change to the measured C 1s spectrum in the region 284 -288 eV, see Figure 5.7b. The assumption that carbon bound to oxygen has a similar binding energy to carbon bound to nitrogen was also applied. Accordingly, the carbon atoms directly bound to oxygen in the polyether chain (C_8, C_{10}, C_{11} and C_{13}) were considered to be equivalent to the carbon atoms bound to the nitrogen cationic core (C_2, C_5, C_6 and C_7), collectively forming the C_{hetero} component.

Interestingly, the best fit was obtained if the C_{14} carbon atom was fit as a separate component, and considered as essentially aliphatic, rather than considering it to be similar to the $C_{3,4}$ (C_{inter}) environment. This implies that the electron-withdrawing influence of an oxygen atom on a carbon atom in the β-position (relative to oxygen) is weaker than the equivalent situation in which the oxygen is replaced by a positively-charged nitrogen cationic core. Subsequently, the component areas for CF_3 : C_{hetero} : C_{inter} : $C_{aliphatic}$ were set to 2 : 8 : 2 : 1.

5.2.2.3 Ammonium-based ILs

As mentioned in *Chapter 3 Section 3.2.3* the fitting model used for non-functionalised pyrrolidinium ionic liquids was also applied to their tetraalkylammonium analogues. For the ionic liquid $[N_{2,2,2,8}][NTf_2]$ the only changes to the model were the appropriate modifications to the component areas to describe the different carbon environments contained in the cation. As such the component areas for CF_3 : C_{hetero} : C_{inter} : $C_{aliphatic}$ were constrained to 2 : 4 : 4 : 6 as shown by the structure in Figure 5.8a.

Additionally, due to the similarity in structure for pyrrolidinium and ammonium ILs only slight modifications to the model for polyether-functionalised pyrrolidinium ionic liquids were needed to describe the C 1s region for $[N_{2,2,2,(Et(PEG2))}][NTf_2]$. Here the $[N_{2,2,2,(Et(PEG2))}][NTf_2]$ component areas for CF_3 : C_{hetero} : C_{inter} : $C_{aliphatic}$ were set to 2 : 8 : 3 : 1, see Figure 5.8b. It was again seen that the best fit was achieved by setting the C_9 carbon environment as a separate component, $C_{aliphatic}$.

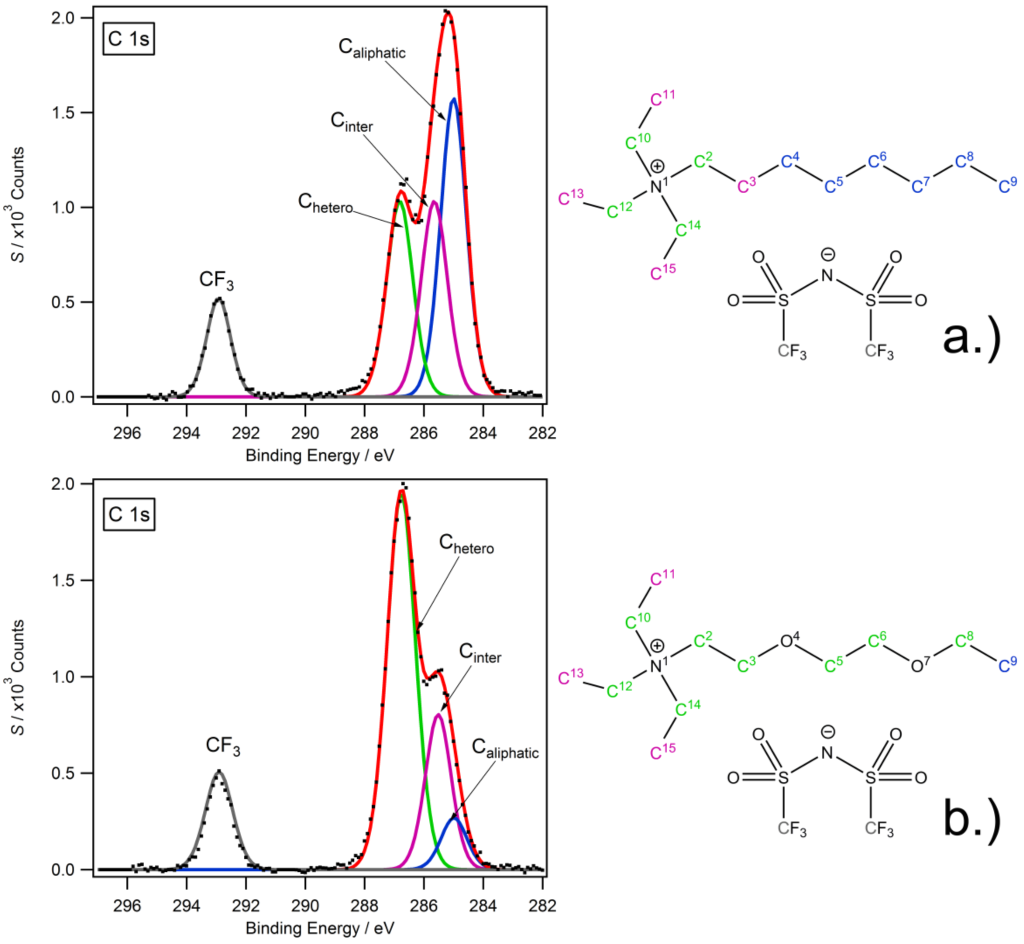

Figure 5.8. C 1s spectra with colour-coded component fittings; fitting envelope (red); counts (black dots); and corresponding structures for (a) $[N_{2,2,2,8}][NTf_2]$ and (b) $[N_{2,2,2,(Et(PEG2))}][NTf_2]$. Charge correction achieved by referencing the S $2p_{3/2}$ component to 169.0 eV (value obtained from $[N_{2,2,2,8}][NTf_2]$ where prior charge correction was achieved by referencing $C_{aliphatic}$ 1s to 285.0 eV).

5.2.3 Binding Energy Analysis

To determine if functionalisation of the alkyl chain does indeed influence the degree of charge transferred from anion to cation, a comparison of binding energies for the functionalised ILs *versus* their non-functionalised analogues was made. To enable reliable comparison between compounds an appropriate charge-referencing procedure must be used.

Relatively simple non-functionalised ILs, *i.e.* $[C_8C_1Im][NTf_2]$, $[C_8C_1Pyrr][NTf_2]$ and $[N_{2,2,2,8}][NTf_2]$, can be charge referenced directly using an established internal reference method of setting the observed $C_{aliphatic}$ 1s component to 285.0 eV, as described in *Chapter 3 Section 3.2.2*.[28] However, from the C 1s spectra described in *Section 5.2.2*, it is clear this method is inappropriate for use in the case of compounds which do not contain large aliphatic side chains, *i.e.* when $n < 8$, or if the substituent chain contains substantive functionality which may perturb the electronic contribution.

It has been previously shown, for ionic liquids of the type $[C_nC_1Im][NTf_2]$, that the binding energy of elements associated with the anion, *i.e.* F 1s, O 1s, and S $2p_{3/2}$ in the case of $[NTf_2]^-$, are insensitive to structural changes in the periphery of the cation.[28] Consequently, these photoelectron emission lines can be used as an indirect method of charge referencing through extracting their absolute values from a standard sample, *e.g.* $[C_8C_1Im][NTf_2]$, which has been charge-referenced using direct methods (*i.e.* setting $C_{aliphatic}$ 1s to 285.0 eV). Considering that perfluorinated and polyether functionalised ionic liquids contain fluorine and oxygen in multiple environments respectively, the S $2p_{3/2}$ component was selected for internal charge referencing. Using imidazolium-based ILs as a representative example this procedure is outlined as follows; charge referencing of $[C_8C_1Im][NTf_2]$ is achieved by setting $C_{aliphatic}$ 1s to 285.0 eV, and the binding energy for the S $2p_{3/2}$ component is extracted, the S $2p_{3/2}$ binding energy for $[Et(PEG)_2MIm][NTf_2]$ and $[(F_{13}H_4C_8)C_1Im][NTf_2]$ is then set equal to that of $[C_8C_1Im][NTf_2]$. This procedure is also used for charge-referencing the pyrrolidinium- and ammonium-based ionic liquids, where $[C_8C_1Pyrr][NTf_2]$ and $[N_{2,2,2,8}][NTf_2]$ are the respective standards. The measured binding energies for each IL investigated are presented in Table 5.2 (*N.B.* due to the complexity and variety of carbon contained in the functionalised side chain, the reported carbon components are limited to those that contain carbon atoms directly bound to the cationic charge carrier).

Table 5.2. Experimental binding energies in eV for the ionic liquids studied in this *Chapter*. The associated experimental error is ± 0.1 eV. $[C_8C_1Im][NTf_2]$, $[C_8C_1Pyrr][NTf_2]$ and $[N_{2,2,2,8}][NTf_2]$ charge referenced by setting $C_{aliphatic}$ 1s to 285.0 eV. Perfluorinated and polyether functionalised ionic liquids charge referenced by setting the binding energy of the S $2p_{3/2}$ component equal to their non-functionalised analogue. [a]Carbon atoms C_8, C_{10}, C_{11} and C_{13} also included in this component, see Figure 5.6 for details. [b]Carbon atom C_8 also included in this component, see Figure 5.6 for details.

Ionic Liquid		**Binding Energy / eV**										
Cation	**Anion**	C_2 1s	$C_{4,5}$ 1s	$C_{6,7}$ 1s	C_{hetero} 1s	C_{inter} 1s	N_{cation} 1s	C_{anion} 1s	N_{anion} 1s	F 1s	O 1s	S $2p_{3/2}$
$[C_8C_1Im]^+$	$[NTf_2]^-$	287.7	287.1	286.6	-	-	402.1	292.9	399.5	688.8	532.7	169.0
$[Et(PEG)_2MIm]^+$	$[NTf_2]^-$	287.7	287.2	286.6[a]	-	-	402.1	292.9	399.5	688.8	532.8	169.0
$[(F_{13}H_4C_8)C_1Im]^+$	$[NTf_2]^-$	287.7	287.2	286.6[b]	-	-	402.2	293.0	399.5	689.0	532.7	169.0
$[C_8C_1Pyrr]^+$	$[NTf_2]^-$	-	-	-	286.8	285.7	402.7	292.9	399.5	688.8	532.7	169.0
$[Et(PEG)_2MPyrr]^+$	$[NTf_2]^-$	-	-	-	286.8	285.7	402.7	293.0	399.5	688.8	532.8	169.0
$[N_{2,2,2,8}]^+$	$[NTf_2]^-$	-	-	-	286.8	285.7	402.5	292.9	399.4	688.8	532.6	169.0
$[N_{2,2,2,(Et(PEG)2)}]^+$	$[NTf_2]^-$	-	-	-	286.8	285.5	402.6	292.9	399.4	688.8	532.7	169.0

Somewhat surprisingly, the measured binding energy for all components (for each family of cationic head group) showed remarkable consistency, with all but two values being within acceptible experimental error (± 0.1 eV). Thereby demonstrating the dominance of the anion in setting the electronic nature of the ionic liquid.

On closer inspection of the imidazolium-based ionic liquids, the only difference of note is a 0.2 eV shift in the F 1s photoelectron emission peak for $[(F_{13}H_4C_8)C_1Im][NTf_2]$ when compared to both $[C_8C_1Im][NTf_2]$ and $[Et(PEG)_2MIm][NTf_2]$. Figure 5.9 illustrates all regions for the imidazolium-based ILs investigated. It is seen from the F 1s region that a single broad peak exists for each IL. In the case of $[(F_{13}H_4C_8)C_1Im][NTf_2]$ this is accompanied by modest peak broadening (FWHM = 1.70 eV) when compared to both $[C_8C_1Im][NTf_2]$ (FWHM = 1.65 eV) and $[Et(PEG)_2MIm][NTf_2]$ (FWHM = 1.64 eV). This broadening is consistent with a relative increase in the number of discrete chemical states of fluorine for $[(F_{13}H_4C_8)C_1Im][NTf_2]$, and is likely to contribute to the observed shift in binding energy of 0.2 eV.

Furthermore, it can be seen from the O 1s region that a single broad peak is observed for each IL, with measured binding energies all within experimental error, see Figure 5.9 and Table 5.2. This data indicates that the oxygen atoms of the polyether chains in $[Et(PEG)_2MIm][NTf_2]$ are in a similar electronic environment to the oxygen atoms bound to sulfur in the $[NTf_2]^-$ anion. This is also observed for the pyrrolidinium- and ammonium-based analogues investigated; see Figure 5.10 and Figure 5.11.

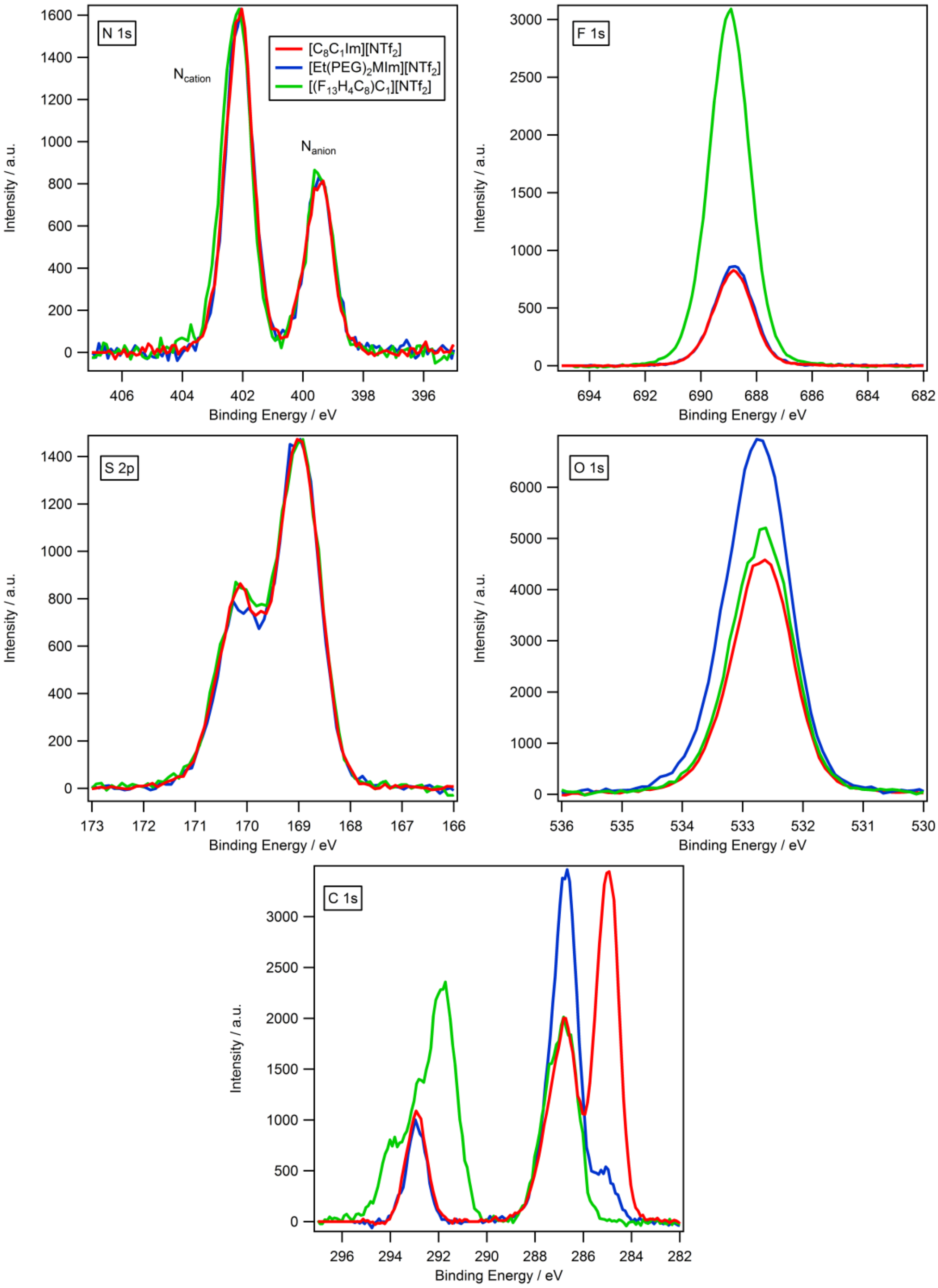

Figure 5.9. XP spectra for [C_8C_1Im][NTf_2] (red trace), [Et(PEG)$_2$MIm][NTf_2] (blue trace) and [($F_{13}H_4C_8$)C_1Im][NTf_2] (green trace). Intensities normalised to the intensity of the N_{cation} 1s peak for [C_8C_1Im][NTf_2], therefore peak areas are representative of the elemental composition of each compound. Charge correction achieved by referencing the S $2p_{3/2}$ component to 169.0 eV.

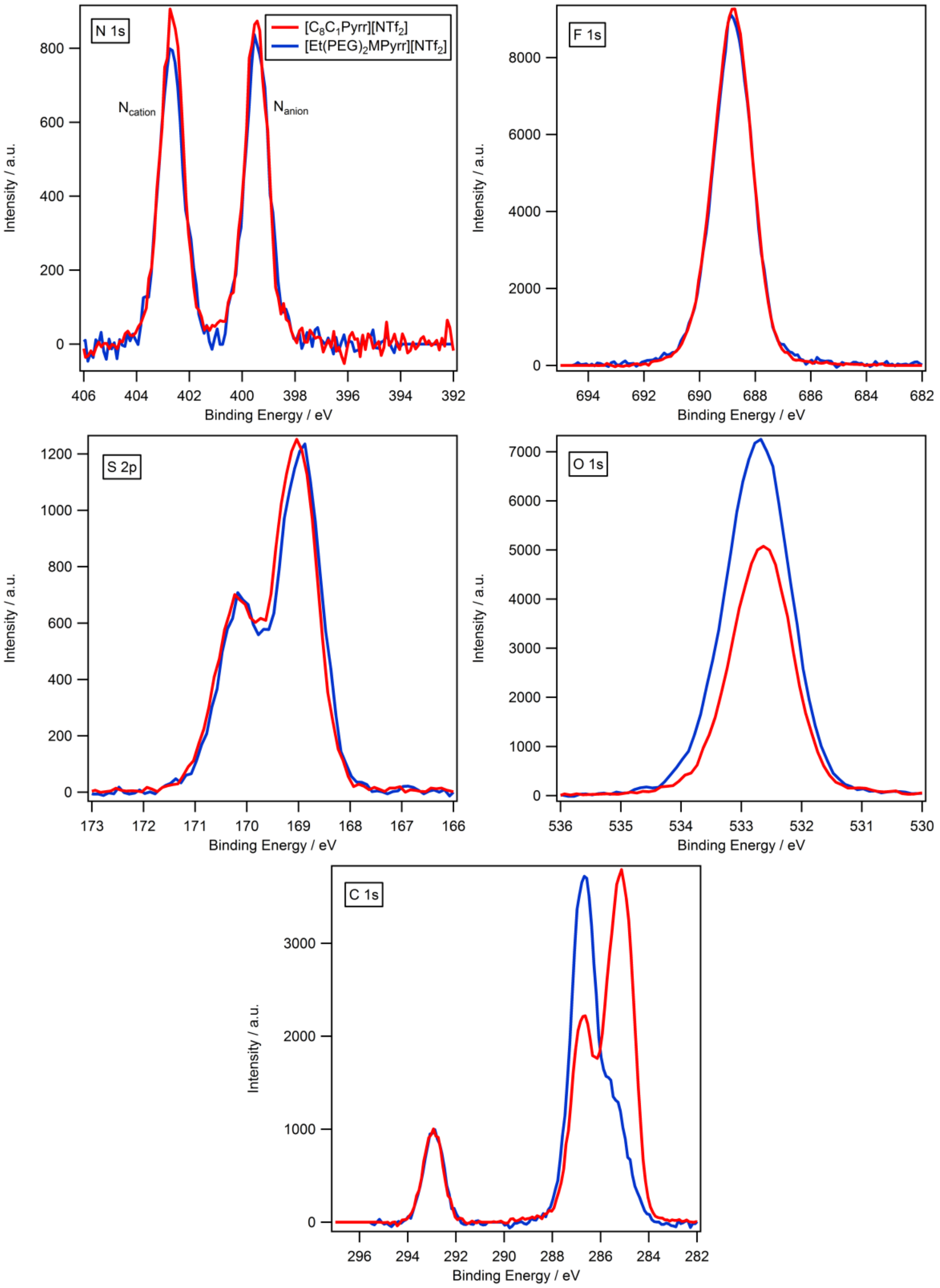

Figure 5.10. XP spectra for [C_8C_1Pyrr][NTf_2] (red trace) and [Et(PEG)$_2$MPyrr][NTf_2] (blue trace). Intensities normalised to the intensity of the N_{cation} 1s peak for [C_8C_1Pyrr][NTf_2], therefore peak areas are representative of the elemental composition of each compound. Charge correction achieved by referencing the S $2p_{3/2}$ component to 169.0 eV.

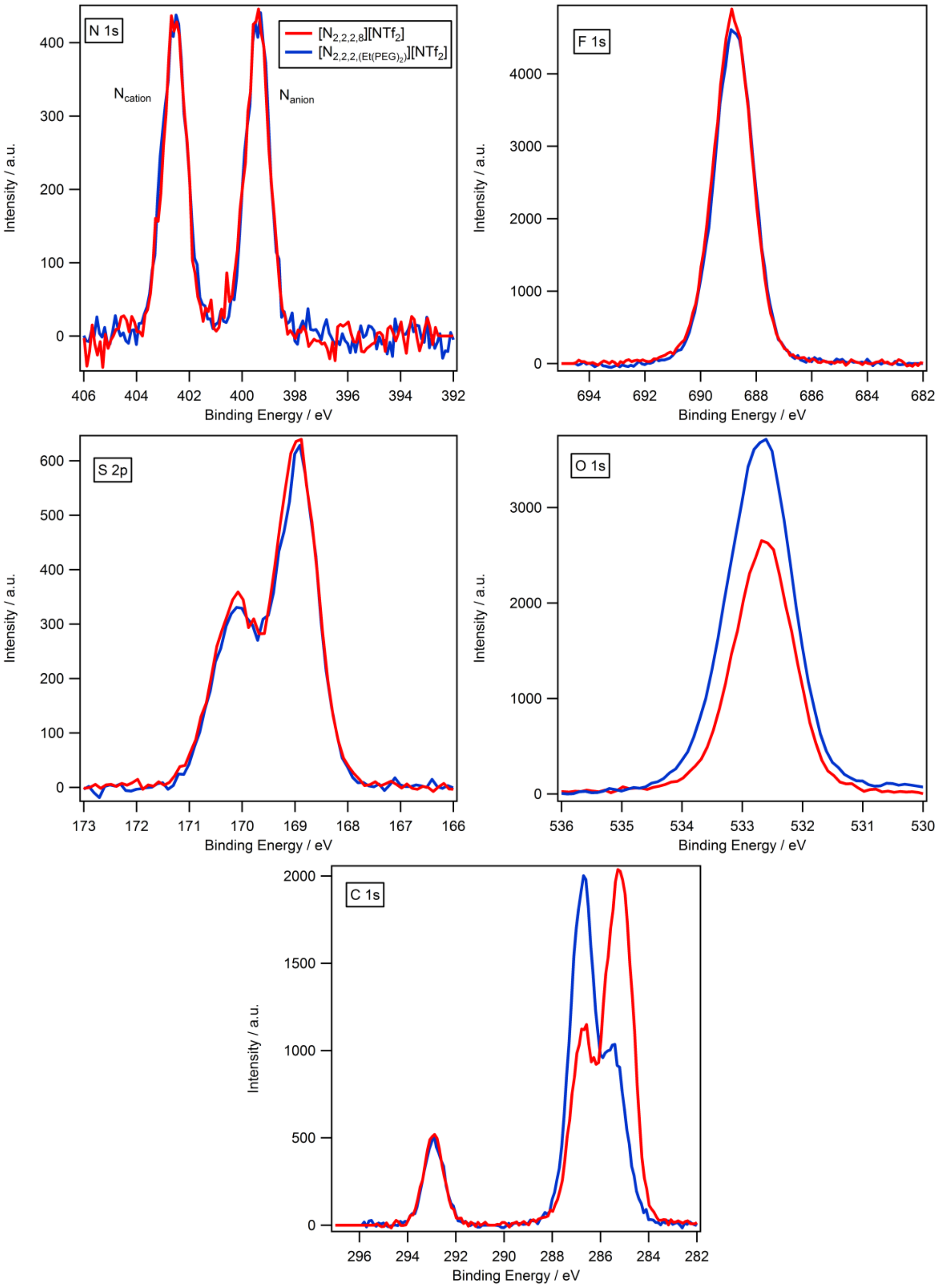

Figure 5.11. XP spectra for [N$_{2,2,2,8}$][NTf$_2$] (red trace) and [N$_{2,2,2,(Et(PEG)2)}$][NTf$_2$] (blue trace). Intensities normalised to the intensity of the N$_{cation}$ 1s peak for [N$_{2,2,2,8}$][NTf$_2$], therefore peak areas are representative of the elemental composition of each compound. Charge correction achieved by referencing the S 2p$_{3/2}$ component to 169.0 eV.

For each cationic head group minimal change is seen in the binding energies for N$_{cation}$ 1s and the carbon components directly bound to the cationic core with increasing functionalisation of the alkyl chain. Clearly, the inductive influence of the peripheral side chain has negligible effect on the cationic head group. Furthermore, measured binding energies for all anionic components equally remain consistent. This is indicative that charge-transfer from anion to cation is also unaffected. Consequently, it can be concluded that by XPS cation-anion interactions are not greatly influenced by functionalisation of the alkyl chain as the ionic head groups appear electronically identical.

5.3 Palladium Catalysed Suzuki Cross-Coupling

It has been previously shown that the Suzuki cross-coupling reaction of aryl halides with boronic acid (Figure 5.12), typically using $[Pd(PPh_3)_4]$ as a catalyst, shows an enhanced reaction rate when performed in ionic liquids of the type $[C_nC_1Im][X]$ in comparison to traditional molecular solvents.[45] This has been attributed to the *in situ* formation of an air stable, catalytically active palladium-imidazolylidene complex, see Figure 5.1.[18, 20, 46, 47] Several techniques have been used to detect this species in solution including NMR spectroscopy,[46] ESI-MS,[22, 46] and XPS;[22, 25] the crystal structure of the respective complex for a $[C_4C_1Im][BF_4]$-based catalytic system has also been successfully achieved.[46]

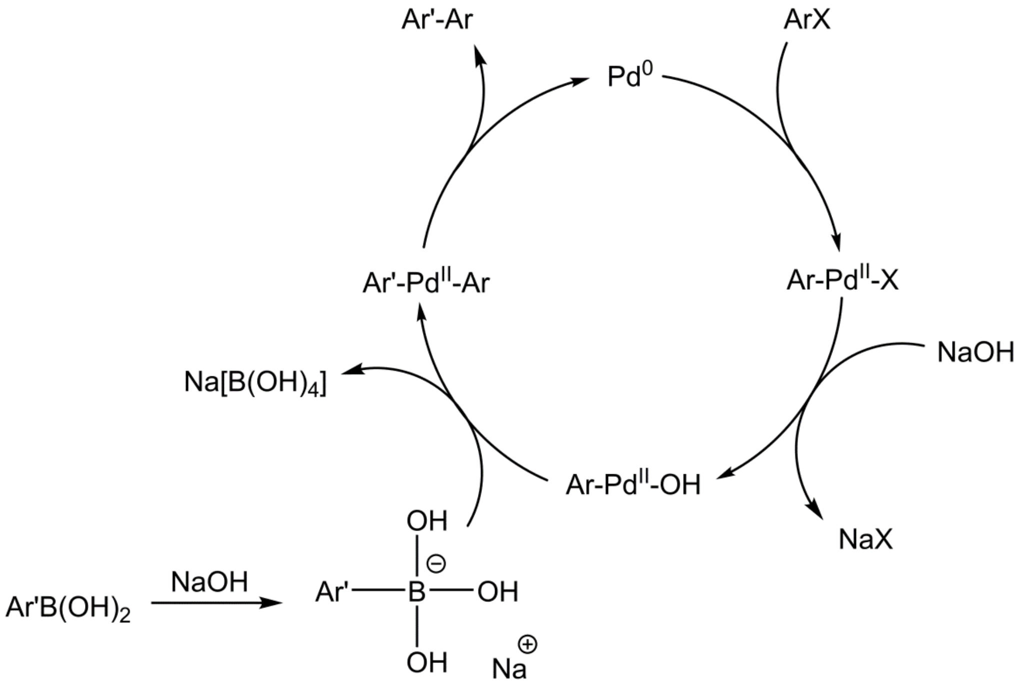

Figure 5.12. Catalytic cycle for Suzuki cross-coupling reaction of an aryl halide with aryl boronic acid. Ligands that co-ordinate to palladium are omitted for clarity.

A recent XPS investigation by Men *et al.* into the formation of the palladium-imidazolylidene complex in ILs of the type $[C_8C_1Im][X]$ (where X = $[OAc]^-$, Cl^-, $[BF_4]^-$, $[OTf]^-$ and $[NTf_2]^-$) has shown the Pd $3d_{5/2}$ binding energy of the palladium complex to be dependent on anion type.[22] It is seen that the Pd binding energy follows the trend $[NTf_2]^- > [OTf]^- \sim [BF_4]^- > Cl^- > [OAc]^-$. A lower binding energy corresponds to an increase in electron density of the cationic head group, indicating significant charge-transfer from anion to cation, which results in a more electron-rich Pd centre; this is seen for high basicity anions such as Cl^- and $[OAc]^-$. However, the reverse is true for low basicity anions such as $[NTf_2]^-$, which do not transfer a significant amount of charge to the cationic head group; consequently, the Pd centre is more electron deficient in comparison. Due to the difference in catalytic performance between $[Pd(PPh_3)_4]$ and the palladium-imidazolylidene complex generated in a $[BF_4]^-$ based ionic liquid, it was proposed that a more electron poor palladium centre would be more catalytically active.[22]

Subsequently, the authors investigated the impact of anion basicity on tuning the catalytic reaction; whereby, ^1H NMR was used to determine the TOF for systems comprising the $[C_8C_1Im]^+$ cation coupled with anions of varying basicity. A correlation between Pd $3d_{5/2}$ binding energy and TOF was indeed observed, in which the least basic $[C_8C_1Im][NTf_2]$ exhibited the highest reaction rate (and Pd binding energy), followed by $[C_8C_1Im][BF_4]$ (intermediate basicity) and then $[C_8C_1Im][OAc]$ (highest basicity).[22] Therefore, reaction rate appears dependent on the basicity of the ionic liquid anion, and hence the electronic environment of the IL.

In this section it is investigated whether the reaction rate for this system can be improved further through the cation of the ionic liquid. From *Section 5.2.3* it is apparent that structural modification to the alkyl side chain of the cation appears to have minimal impact on the electronic environment of the ionic liquid, however in the case of polyether functionalised ionic liquids the oxygen atoms of the polyether side chain could provide chelation sites which may influence the catalytic activity of the Pd centre of the palladium-imidazolylidene complex.

5.3.1 Influence of the Cation on Reaction Rate

The palladium catalysed Suzuki cross-coupling of bromobenzene and phenylboronic acid, see Figure 5.13, was performed in both $[C_8C_1Im][NTf_2]$ and $[Et(PEG)_2MIm][NTf_2]$ using the procedure described by Men *et al.*[22] to determine their respective TOFs from ^{1}H NMR spectroscopy, and is described in *Chapter 2 Section 2.3.9.1*.

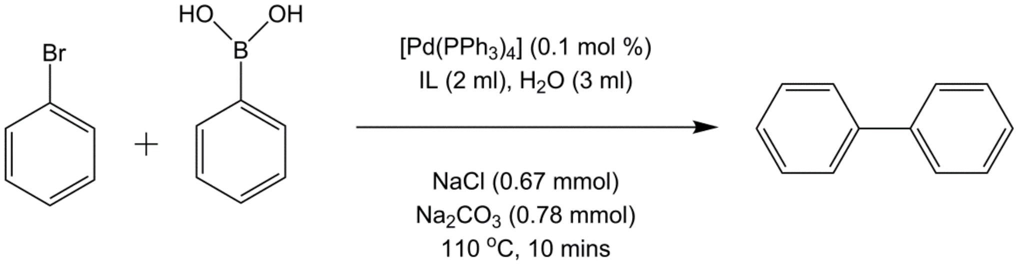

Figure 5.13. Reaction scheme for Suzuki cross-coupling of bromobenzene and phenylboronic acid.

Conversion was obtained from ^{1}H NMR through integration of the peak corresponding to the protons *ortho* to the $–B(OH)_2$ group in phenylboronic acid, as their chemical shift (δ_H ~ 8.3 ppm) is well separated from the other proton environments of the reaction mixture which resonate further upfield. For each IL used, a well-defined peak corresponding to the IL was chosen as an internal standard to enable quantification of phenylboronic acid conversion. Additionally, it is assumed that no side-reactions occurred during the reaction, and that starting materials are only converted to the desired product. NMR analysis indicates this assumption is valid as all peaks can be assigned to starting material, product or solvent. TOF can then be determined using the following equation:

$$\mathrm{TOF} = \frac{\text{mol of starting material converted}}{\text{mol of catalyst} \times \text{time}} \qquad \mathbf{5.1}$$

5.3.1.1 $[C_8C_1Im][NTf_2]$ *versus* $[Et(PEG)_2MIm][NTf_2]$

Interestingly, a distinct series of colour changes occurred during the reaction for $[C_8C_1Im][NTf_2]$ and $[Et(PEG)_2MIm][NTf_2]$. The reaction mixture for the non-functionalised $[C_8C_1Im][NTf_2]$ remained pale yellow throughout;

however, in the case of the polyether functionalised [Et(PEG)$_2$MIm][NTf$_2$] the reaction mixture turned black after five minutes. On analysis of the respective TOFs for each system, see Table 5.3, it is seen that a high catalytic activity is not only retained, but also shows a modest increase for the polyether functionalised system with a TOF = 4971 h^{-1} in comparison to [C$_8$C$_1$Im][NTf$_2$] (TOF = 4709 h^{-1}).

Table 5.3. Turnover frequencies (reported as an average of three separate reactions) for Suzuki cross-coupling of bromobenzene and phenylboronic acid in various ionic liquid solvents and determined from conversion of phenylboronic acid *via* ^{1}H NMR.

Ionic Liquid	**TOF / h^{-1} (error %)**
[C$_8$C$_1$Im][NTf$_2$]	4709 (± 2 %)
[Et(PEG)$_2$MIm][NTf$_2$]	4971 (± 1 %)
[C$_8$C$_1$Pyrr][NTf$_2$]	4007 (± 1 %)
[Et(PEG)$_2$MPyrr][NTf$_2$]	4939 (± 1 %)

Stabilisation of palladium nanoparticles (Pd-NPs) by various nitrile-functionalised ionic liquids has previously been seen;[48-50] therefore, it is possible that the observed increase in catalytic activity using [Et(PEG)$_2$MIm][NTf$_2$] as the solvent is from the formation of Pd-NPs, which are stabilised by the ether linkages contained in the peripheral side chain of the cation. Earlier work by Yang *et al*. has also indicated an increase in product yield for Suzuki cross-coupling reactions run in ether-functionalised ILs, however until now the nature of the palladium catalysts has been unclear.[51]

Subsequently, this was investigated further using transmission electron microscopy (TEM) to determine the presence of nanoparticles in both the non-functionalised and the polyether functionalised systems. In each case the reaction was quenched after five minutes and a small sample removed for analysis.

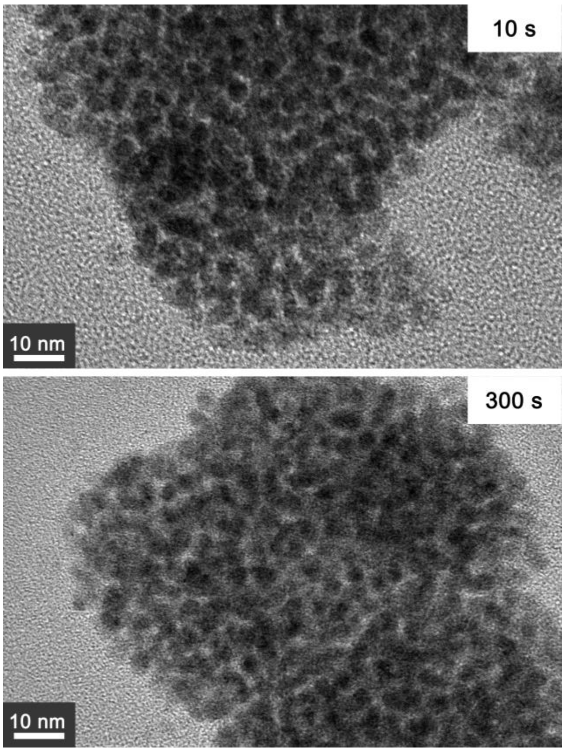

Figure 5.14. TEM micrographs showing palladium nanoparticles extracted from the [Et(PEG)$_2$MIm][NTf$_2$] Suzuki cross-coupling reaction mixture. The images were taken after an exposure time of 10 s (upper image) and 300 s (lower image) to the electron beam. It should be noted that although the sample shifts under the electron beam the size and number of nanoparticles does not show a significant increase.

An abundance of Pd-NPs is indeed observed in the [Et(PEG)$_2$MIm][NTf$_2$] Suzuki cross-coupling reaction mixture. It was seen that the sample was stable to electron beam exposure at 200 kV as there was no evidence of growth in size or number of nanoparticles as a function of exposure time, see Figure 5.14.

The nanoparticles display a uniform size distribution between 3 – 4 nm, and an interplanar spacing of 0.242 nm is clearly seen at high magnification (as labelled in Figure 5.15) which is consistent with Pd (111) planes.

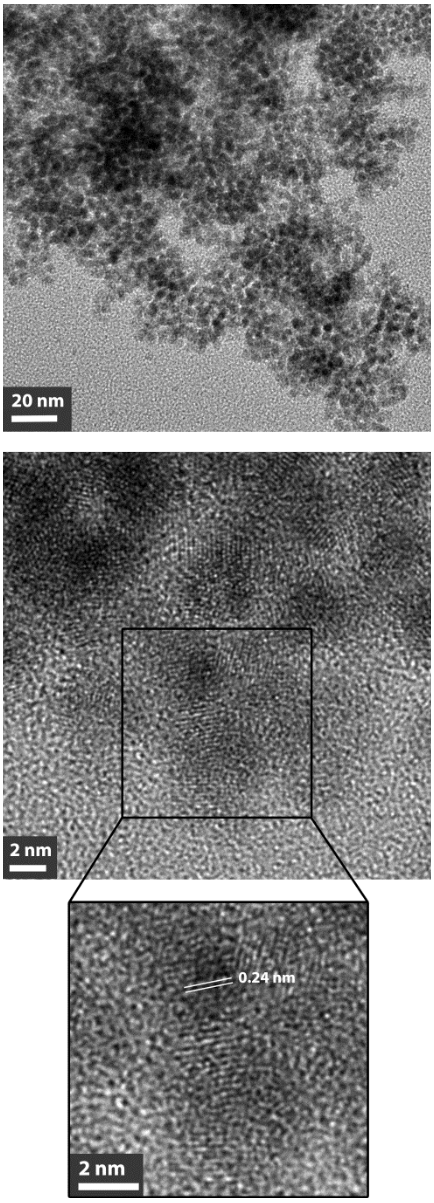

Figure 5.15. TEM micrographs showing palladium nanoparticles in the [Et(PEG)$_2$MIm][NTf$_2$] Suzuki cross-coupling reaction mixture, an interplanar spacing of 0.242 nm is observed and is consistent with Pd (111) planes.

TEM analysis of the [C$_8$C$_1$Im][NTf$_2$] Suzuki cross-coupling reaction mixture exhibited considerably fewer nanoparticles. A region of small, irregular shaped nanoparticles were observed as highlighted in Figure 5.16. However, these were only visible after a few minutes of exposure to the electron beam; additionally, the number of nanoparticles was seen to increase with further beam exposure. It is thought that these nanoparticles are formed from beam damage, *i.e.* reduction of the palladium-imidazolylidene complex *via* the high energy electron beam, and are consequently not present in the reaction mixture.

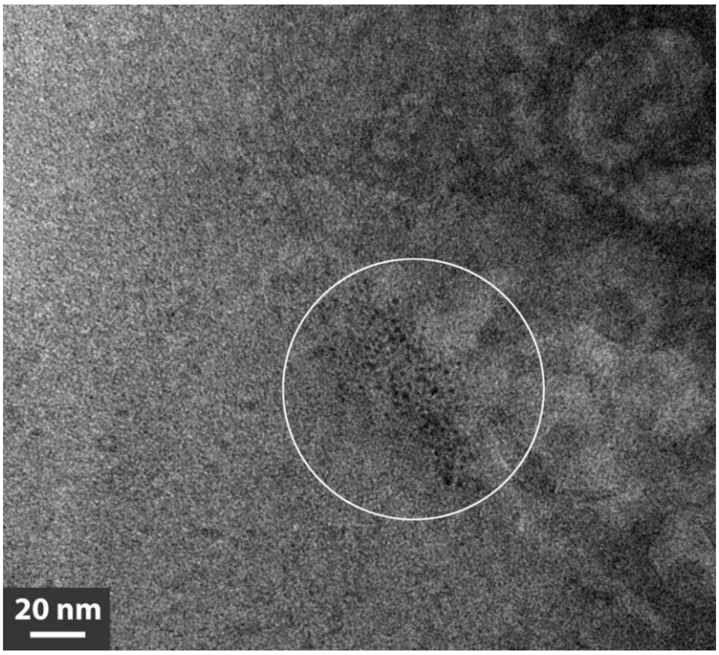

Figure 5.16. TEM micrograph of the $[C_8C_1Im][NTf_2]$ Suzuki cross-coupling reaction mixture. A region of small, irregular shaped nanoparticles is highlighted within the white circle.

In accordance with literature reports it is apparent that Suzuki cross-coupling in the non-functionalised ionic liquid, $[C_8C_1Im][NTf_2]$, is not likely to be mediated through nanoparticular catalysis. In contrast, for $[Et(PEG)_2MIm][NTf_2]$ there is clear evidence of nanoparticle formation; however, it is not clear whether catalysis is enhanced *via* palladium nanoparticles, the respective palladium-imidazolylidene complex or both. Consequently, XPS and ESI-MS were used to determine if the palladium-imidazolylidene complex can indeed form under Suzuki cross-coupling conditions when using $[Et(PEG)_2MIm][NTf_2]$ as the solvent.

The detection limits for XPS analysis are generally around 0.1 atomic % for survey scans and 0.01 % for high resolution scans, although this value can vary for different elements. In a typical catalytic reaction the concentration of palladium is too low for detection by XPS. This is exemplified by the Suzuki cross-coupling conditions described in *Section 5.3.1*; when using $[C_8C_1Im][NTf_2]$ as the ionic liquid solvent in this system the Pd concentration is ~ 3.2×10^{-3} atomic %. Consequently, for XPS analysis a “model” Suzuki system, in which the palladium concentration is ~ 0.1 atomic %, was used to prepare the palladium containing IL solutions, as previously described in the literature.[22] This involved heating a mixture of NaCl (12 mg, 0.21 mmol), bromobenzene (13.1 µl, 0.125 mmol), $[Pd(PPh_3)_4]$ (24 mg, 0.021 mmol) and Na_2CO_3 (26 mg, 0.25 mmol) in the appropriate ionic liquid (0.25 ml) and water (3 ml) at 110 °C for 3 hours – see *Chapter 2 Section 2.3.9* for full details. It should be noted that phenylboronic acid was not added to ensure the reaction did not turn over.

Interestingly, for both $[C_8C_1Im][NTf_2]$ and $[Et(PEG)_2MIm][NTf_2]$ a pale yellow solution is formed in each case, which remained stable to heating at 110 °C, with no observable change in colour or indication of nanoparticle formation. The Pd 3d high resolution scan for each ionic liquid solution is presented in Figure 5.17. It is seen that the Pd 3d peak is split into a doublet due to spin-orbit coupling with an area ratio of 2 : 3 ($3d_{3/2}$: $3d_{5/2}$) where ΔBE (Pd $3d_{3/2}$ – Pd$3d_{5/2}$) = 5.3 eV for each ionic liquid in accordance with the literature.[22] The measured Pd $3d_{5/2}$ binding energies are within the experimental error with values of 338.6 eV and 338.7 eV for the $[C_8C_1Im][NTf_2]$ and $[Et(PEG)_2MIm][NTf_2]$ solutions respectively. This is consistent with the Pd $3d_{5/2}$ binding energy for palladium in the +2 oxidation state, and more specifically with the palladium-imidazolylidene complex.[22] Additionally, there is no evidence in either sample for palladium present in the (0) oxidation state, which would occur at a lower binding energy of ~ 336 eV. XP spectra for the other elemental regions of the Pd-containing solutions were also found to be identical to those obtained for the corresponding pure IL samples (see *Appendix C*), indicating that the Pd solute does not affect the electronic environment of the bulk ionic liquid in either case.

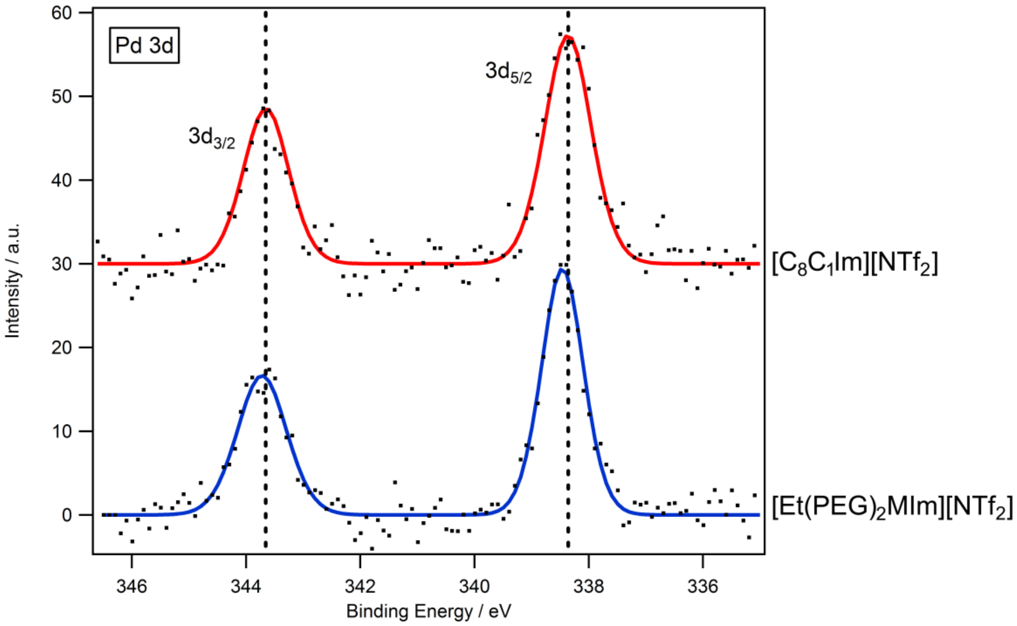

Figure 5.17. Pd 3d spectra for palladium-containing ionic liquid solutions formed in $[C_8C_1Im][NTf_2]$ (red trace) and $[Et(PEG)_2MIm][NTf_2]$ (blue trace). Spectra charge corrected by referencing S $2p_{3/2}$ to 169.0 eV and normalised to intensity of the F 1s peak for $[C_8C_1Im][NTf_2]$. Dashed lines represent the binding energies of Pd $3d_{3/2}$ and Pd $3d_{5/2}$ components for the $[C_8C_1Im][NTf_2]$ palladium-containing solution to provide visual guide lines.

ESI-MS was also used to confirm the formation of the palladium-imidazolylidene complex for both $[C_8C_1Im][NTf_2]$ and $[Et(PEG)_2MIm][NTf_2]$. In each instance excellent agreement is seen between the measured spectra and the theoretical isotope pattern; see Figure 5.18 and Figure 5.19.

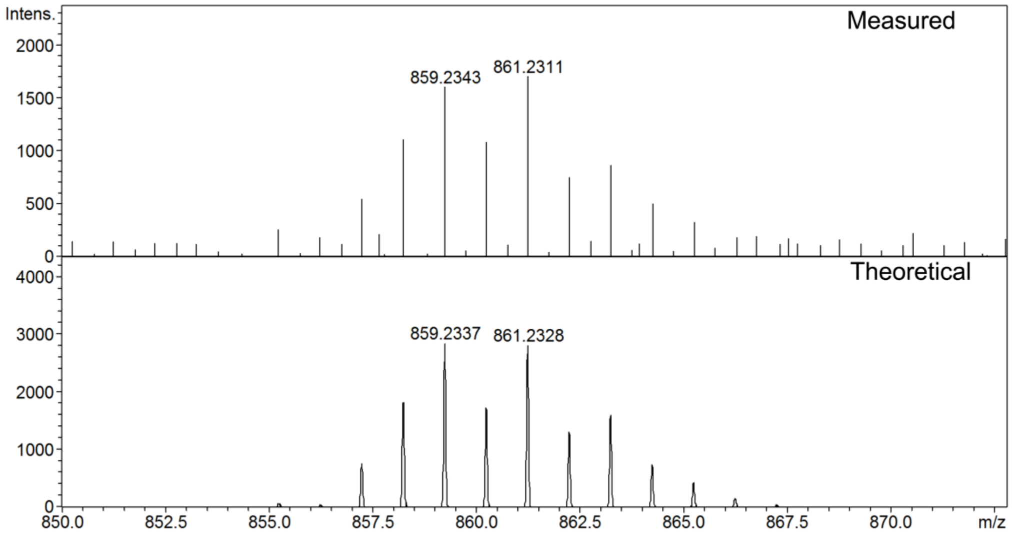

Figure 5.18. Measured and theoretical ESI-MS spectra for the palladium-imidazolylidene complex formed in [C_8C_1Im][NTf_2].

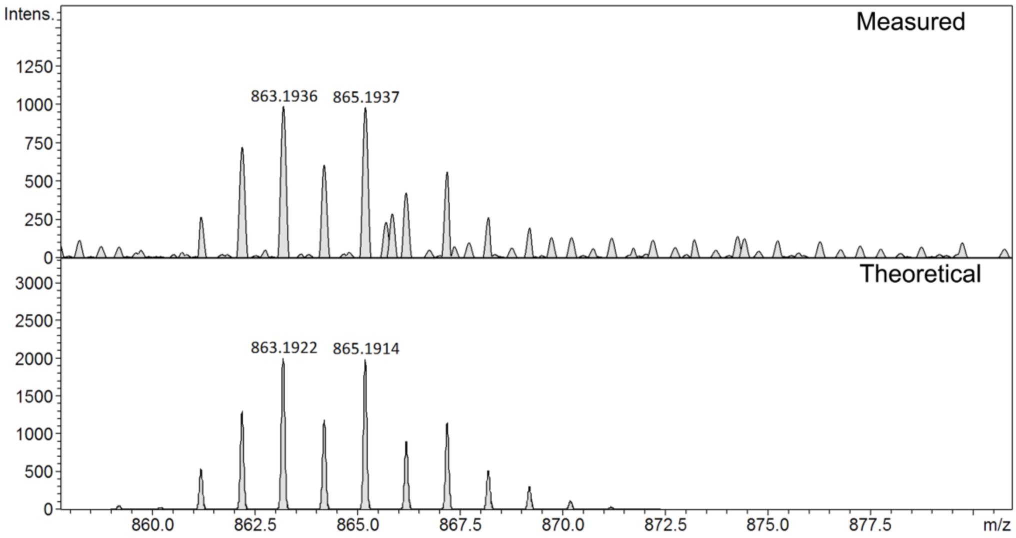

Figure 5.19. Measured and theoretical ESI-MS spectra for the palladium-imidazolylidene complex formed in [Et(PEG)$_2$MIm][NTf_2].

Consequently, it can be seen for both [C_8C_1Im][NTf_2] and [Et(PEG)$_2$MIm][NTf_2] that the palladium-imidazolylidene complex does indeed form in each case, in the absence of the phenylboronic acid starting material, and remains stable for extended periods of time under heating and vacuum conditions. However, in the presence of phenylboronic acid and with subsequent reaction turn-over, nanoparticle formation is observed for [Et(PEG)$_2$MIm][NTf_2] only. This suggests an *in situ* reduction of the palladium-imidazolylidene complex to palladium nanoparticles for

[Et(PEG)$_2$MIm][NTf$_2$], which is attributed to Pd-NP stabilisation *via* the ether linkages of the alkyl chain.

5.3.1.2 Comparison to Pyrrolidinium ILs

In the previous section it is suggested that functionalising the cation can influence the nature of catalysis, *i.e.* in the case of simple, non-functionalised imidazolium ILs molecular catalysis dominates, whereas for polyether-functionalised ILs nanoparticle-mediated catalysis occurs. To investigate this further, two control reactions were carried out using an alternative pair of non-functionalised and polyether-functionalised ILs, this time based on pyrrolidinium charge carriers, *i.e.* [C$_8$C$_1$Pyrr][NTf$_2$] and [Et(PEG)$_2$MPyrr][NTf$_2$]. Through using a pyrrolidinium charge carrier, which cannot form carbenes, the formation of a complex equivalent to the palladium-imidazolylidene complex is not possible; thus, elucidating further information on the influence of polyether chains on catalysis.

The observed TOF for the Suzuki cross-coupling reaction in the ionic liquid [C$_8$C$_1$Pyrr][NTf$_2$] exhibits a dramatic decrease to 4007 h^{-1} (Table 5.3), confirming that the presence of either an imidazolium moiety or polyether functionality is necessary for an increased catalytic rate.

For the ionic liquid [Et(PEG)$_2$MPyrr][NTf$_2$], however, there is the potential for nanoparticle stabilisation through the polyether functionality, and a noticeable formation of a black solution was observed as the reaction proceeded indicating the presence of Pd-NPs. The high TOF for this system reflects this with a value of 4939 h^{-1} (Table 5.3), and is comparable in value to the analogous polyether-functionalised imidazolium-based ionic liquid system. Additionally, a most striking comparison is made between [Et(PEG)$_2$MPyrr][NTf$_2$] and [C$_8$C$_1$Im][NTf$_2$] as similar TOFs are obtained in each case (Table 5.3). This indicates that it is not a synergistic effect between the imidazolium-head group and a polyether chain which increases catalytic activity, *i.e.* either an imidazolium head group or a polyether chain is necessary for a higher catalytic activity; however, both together do not lead to a significant improvement. This result is strongly indicative that Pd-NPs are formed and stabilised in polyether-functionalised ionic liquids during the course of the Suzuki reaction and contribute to the increased TOFs that are observed.

In summary, it has been observed that changing the structure of an IL can change the nature of the palladium catalytic species, which is determined by the functionality within the cation. For a simple non-functionalised imidazolium ionic liquid, $[C_8C_1Im][NTf_2]$, a molecular palladium catalyst is formed and the reaction proceeds at high TOF. The introduction of polyether functionality in the IL also gives rise to a catalytically active solution; however, it is proposed that the catalyst is nanoparticular. Careful insight into the nature of the ionic liquid, and specifically the interaction that it may have with a catalytic (or pre-catalytic) solute can clearly offer a degree of control that should be considered in the design of reactive systems involving ionic liquids.

5.4 Conclusions

In this *Chapter* XPS has been used to investigate a variety of functionalised ILs with comparison made to their non-functionalised analogues. All compounds were synthesised to high purity and robust C 1s peak fitting models for the functionalised ionic liquids were developed. The subsequent comparison of the different C 1s electronic environments, with pre-existing models for the non-functionalised ILs, highlighted the influence of increasing functionalisation on the complexity of the C 1s photoelectron emission envelope.

Additionally, it was observed that functionalisation of the cation alkyl side chain with polyether and perfluorinated groups had negligible impact on the degree of charge transferred from anion to cation. Therefore, disruption to the inductive influence of the alkyl side chain by the inclusion of electron-withdrawing groups appears to have minimal impact on cation-anion interactions; consequently, the electronic environment of the charge-bearing head groups appear identical for each cationic family of ionic liquids.

The introduction of functionalisation into the cationic structure of ILs employed as solvents in the palladium catalysed Suzuki cross-coupling was also examined. A moderate increase in TOF was observed for polyether functionalised ILs, in comparison to an established system utilising $[C_8C_1Im][NTf_2]$ as the solvent (in which catalytic activity is associated with a palladium-imidazolylidene complex). The measured increase in reaction productivity was linked to the nature, and type of catalytic species present in solution *i.e.* the formation and stabilisation of Pd-NPS in polyether functionalised ILs. This highlights the implications of cation structure on the catalytic species formed, and that indeed the nature of catalysis can even be changed, *via* the cation, from molecular to nanoparticular catalysis in this system. As such this work demonstrates the ability to tune ionic liquids in order to dramatically alter and improve their role within catalytic systems, and presents a step towards designer catalysis.

5.5 References

1. M. J. Earle and K. R. Seddon, *Pure Appl. Chem.*, 2000, **72**, 1391-1398.
2. J. H. Davis, K. J. Forrester and T. Merrigan, *Tetrahedron Lett.*, 1998, **39**, 8955-8958.
3. J. H. Davis, *Chem. Lett.*, 2004, **33**, 1072-1077.
4. E. D. Bates, R. D. Mayton, I. Ntai and J. H. Davis, *J. Am. Chem. Soc.*, 2002, **124**, 926-927.
5. Z. Z. Yang, Y. N. Zhao and L. N. He, *RSC Adv.*, 2011, **1**, 545-567.
6. A. E. Visser, R. P. Swatloski, W. M. Reichert, R. Mayton, S. Sheff, A. Wierzbicki, J. H. Davis and R. D. Rogers, *Chem. Commun.*, 2001, 135-136.
7. A. E. Visser, R. P. Swatloski, W. M. Reichert, R. Mayton, S. Sheff, A. Wierzbicki, J. H. Davis and R. D. Rogers, *Environ. Sci. Technol.*, 2002, **36**, 2523-2529.
8. R. J. C. Brown, P. J. Dyson, D. J. Ellis and T. Welton, *Chem. Commun.*, 2001, 1862-1863.
9. N. Kimizuka and T. Nakashima, *Langmuir*, 2001, **17**, 6759-6761.
10. T. L. Merrigan, E. D. Bates, S. C. Dorman and J. H. Davis, *Chem. Commun.*, 2000, 2051-2052.

11. S. K. Tang, G. A. Baker and H. Zhao, *Chem. Soc. Rev.*, 2012, **41**, 4030-4066.

12. A. B. Pereiro, J. M. M. Araujo, S. Martinho, F. Alves, S. Nunes, A. Matias, C. M. M. Duarte, L. P. N. Rebelo and I. M. Marrucho, *ACS Sustainable Chem. Eng.*, 2013, **1**, 427-439.

13. P. A. Z. Suarez, J. E. L. Dullius, S. Einloft, R. F. DeSouza and J. Dupont, *Polyhedron*, 1996, **15**, 1217-1219.

14. Y. Chauvin, L. Mussmann and H. Olivier, *Angew. Chem. Int. Ed.*, 1995, **34**, 2698-2700.

15. T. Welton, *Coord. Chem. Rev.*, 2004, **248**, 2459-2477.

16. C. E. Song and E. J. Roh, *Chem. Commun.*, 2000, 837-838.

17. D. E. Kaufmann, M. Nouroozian and H. Henze, *Synlett*, 1996, 1091-&.

18. A. J. Carmichael, M. J. Earle, J. D. Holbrey, P. B. McCormac and K. R. Seddon, *Org. Lett.*, 1999, **1**, 997-1000.

19. W. P. Chen, L. J. Xu, C. Chatterton and J. L. Xiao, *Chem. Commun.*, 1999, 1247-1248.

20. F. McLachlan, C. J. Mathews, P. J. Smith and T. Welton, *Organometallics*, 2003, **22**, 5350-5357.

21. L. J. Xu, W. P. Chen and J. L. Xiao, *Organometallics*, 2000, **19**, 1123-1127.

22. S. Men, K. R. J. Lovelock and P. Licence, *RSC Adv.*, 2015, **5**, 35958-35965.

23. T. Cremer, C. Kolbeck, K. R. J. Lovelock, N. Paape, R. Wölfe, P. S. Schulz, P. Wasserscheid, H. Weber, J. Thar, B. Kirchner, F. Maier and H.-P. Steinrück, *Chem. Eur. J.*, 2010, **16**, 9018-9033.

24. S. Men, K. R. J. Lovelock and P. Licence, *Phys. Chem. Chem. Phys.*, 2011, **13**, 15244-15255.

25. I. J. Villar-Garcia, K. R. J. Lovelock, S. Men and P. Licence, *Chem. Sci.*, 2014, **5**, 2573-2579.

26. S. Men, D. S. Mitchell, K. R. J. Lovelock and P. Licence, *ChemPhysChem*, 2015, **16**, 2211-2218.

27. A. R. Santos, R. K. Blundell and P. Licence, *Phys. Chem. Chem. Phys.*, 2015, **17**, 11839-11847.

28. I. J. Villar-Garcia, E. F. Smith, A. W. Taylor, F. L. Qiu, K. R. J. Lovelock, R. G. Jones and P. Licence, *Phys. Chem. Chem. Phys.*, 2011, **13**, 2797-2808.

29. C. S. Rondestvedt, *J. Org. Chem.*, 1977, **42**, 1985-1990.

30. N. O. Brace, L. W. Marshall, C. J. Pinson and G. Vanwingerden, *J. Org. Chem.*, 1984, **49**, 2361-2368.

31. H. B. Alhanash and A. K. Brisdon, *J. Fluorine Chem.*, 2013, **156**, 152-157.

32. V. Frenna, N. Vivona, G. Consiglio and D. Spinelli, *J. Chem. Soc., Perkin Trans. 2*, 1985, 1865-1868.

33. A. Dahlen and G. Hilmersson, *J. Am. Chem. Soc.*, 2005, **127**, 8340-8347.

34. Y. Nozaki, F. R. N. Gurd, R. F. Chen and J. T. Edsall, *J. Am. Chem. Soc.*, 1957, **79**, 2123-2129.

35. B. W. Kail, L. M. Pérez, S. D Zarić, A. J. Millar, C. G. Young, M. B. Hall and P. Basu, *Chem. Eur. J.*, 2006, **12**, 7501-7509.

36. J. J. Tindale and P. J. Ragogna, *Chem. Commun.*, 2009, 1831-1833.

37. E. F. Smith, F. J. M. Rutten, I. J. Villar-Garcia, D. Briggs and P. Licence, *Langmuir*, 2006, **22**, 9386-9392.

38. C. D. Wagner, L. E. Davis, M. V. Zeller, J. A. Taylor, R. H. Raymond and L. H. Gale, *Surf. Interface Anal.*, 1981, **3**, 211-225.

39. K. R. J. Lovelock, C. Kolbeck, T. Cremer, N. Paape, P. S. Schulz, P. Wasserscheid, F. Maier and H.-P. Steinrück, *J. Phys. Chem. B*, 2009, **113**, 2854-2864.

40. C. Kolbeck, T. Cremer, K. R. J. Lovelock, N. Paape, P. S. Schulz, P. Wasserscheid, F. Maier and H.-P. Steinrück, *J. Phys. Chem. B*, 2009, **113**, 8682-8688.

41. F. Maier, T. Cremer, C. Kolbeck, K. R. J. Lovelock, N. Paape, P. S. Schulz, P. Wasserscheid and H.-P. Steinrück, *Phys. Chem. Chem. Phys.*, 2010, **12**, 1905-1915.

42. K. R. J. Lovelock, I. J. Villar-Garcia, F. Maier, H.-P. Steinrück and P. Licence, *Chem. Rev.*, 2010, **110**, 5158-5190.

43. D. Briggs and J. T. Grant, *Surface Analysis by Auger and X-ray Photoelectron Spectroscopy*, IM Publications LLP, Manchester, 2003.

44. C. Kolbeck, M. Killian, F. Maier, N. Paape, P. Wasserscheid and H.-P. Steinrück, *Langmuir*, 2008, **24**, 9500-9507.

45. C. J. Mathews, P. J. Smith and T. Welton, *Chem. Commun.*, 2000, 1249-1250.

46. C. J. Mathews, P. J. Smith, T. Welton, A. J. P. White and D. J. Williams, *Organometallics*, 2001, **20**, 3848-3850.

47. C. H. Yang, C. C. Tai, Y. T. Huang and I. W. Sun, *Tetrahedron*, 2005, **61**, 4857-4861.

48. D. B. Zhao, Z. F. Fei, T. J. Geldbach, R. Scopelliti and P. J. Dyson, *J. Am. Chem. Soc.*, 2004, **126**, 15876-15882.

49. Z. F. Fei, D. B. Zhao, D. Pieraccini, W. H. Ang, T. J. Geldbach, R. Scopelliti, C. Chiappe and P. J. Dyson, *Organometallics*, 2007, **26**, 1588-1598.

50. Y. G. Cui, I. Biondi, M. Chaubey, X. Yang, Z. F. Fei, R. Scopelliti, C. G. Hartinger, Y. D. Li, C. Chiappe and P. J. Dyson, *Phys. Chem. Chem. Phys.*, 2010, **12**, 1834-1841.

51. X. Yang, Z. F. Fei, T. J. Geldbach, A. D. Phillips, C. G. Hartinger, Y. D. Li and P. J. Dyson, *Organometallics*, 2008, **27**, 3971-3977.

6. Concluding Remarks

The influence of changing the anion on cation-anion interactions, structural organisation and physicochemical properties of ionic liquids (ILs) is extensively reported within the literature. The cationic influence, however, is considerably less understood, with the majority of investigations focused on the ubiquitous 1-3-dialkylimidazolium cation. This *Thesis* directly addresses this gap in knowledge through utilising X-ray Photoelectron Spectroscopy (XPS) to gather vital information on how cation structure can influence fundamental interactions within IL systems. Additionally, an example of how seemingly subtle changes to cation structure can significantly influence IL-metal based catalysis has been provided.

It is, perhaps, paradoxical that tetraalkylammonium and tetraalkylphosphonium ILs receive less interest from the scientific community, in comparison to imidazolium-based ILs, and yet experience extensive industrial use. As such this *Thesis* is an important expansion to these classes of ILs, and provides a step towards understanding structure-property relationships between these particular compounds. Fundamental investigations into the electronic environment of tetraalkylammonium and tetraalkylphosphonium ILs have revealed subtle cationic effects on cation-anion interactions. Whereby, for cations containing long alkyl chains, the cation core (*i.e.* ammonium *versus* phosphonium) has minimal effect on the electronic environment of the anion, due to a proposed hydrocarbon shielding effect. However, for cations containing shorter alkyl chain lengths, or conformational restriction, hydrocarbon shielding is diminished; consequently, the role of charge carrier can be seen, whereby charge-transfer from anion to cation is more pronounced for the more charge dense ammonium cation.

In order to understand surface-based applications of ILs it is crucial to first understand their surface structure, with the ultimate goal of developing design rules such that the structure for any given IL can be predicted. Currently, the accepted design rules that describe the IL/vacuum interface are limited to imidazolium-based ILs. The work described in this *Thesis* sets the foundations for developing design rules that accurately describe the surface structure for ILs consisting of tetraalkylammonium and tetraalkylphosphonium cations. For the first time a high energy, laboratory-based X-ray source (Ag Lα') has been used to conduct depth profiling investigations using Energy-resolved XPS (ERXPS); which, in combination with traditional Angle-resolved XPS (ARXPS) studies, supports the concept of hydrocarbon based shielding of the cationic core for quaternary ammonium and phosphonium cations containing long alkyl chains.

Consequently, the added value of the Ag Lα' source has clearly been demonstrated through its convenience and accessibility in providing a complementary depth profiling technique which yields detailed information on differences between the bulk and surface structure. Limitations to this technique, however, have been recognised; firstly, the reduced intensity of the Ag Lα' line (in comparison to Al Kα) requires longer acquisition times promoting an increased risk of sample damage. Secondly, depth profiling is restricted to compounds containing elements with high energy (BE > 1400 eV) photoelectron emissions (e.g. in this work, S 1s, P 1s and Cl 1s); as such, information regarding many commonly used cations and anions (e.g. $[C_nC_1Im]^+$, $[C_nC_1Pyrr]^+$, $[N_{R,R,R,R}]^+$ and $[BF_4]^-$) is unattainable.

In addition to the effect of changing the cationic core, the influence of cation functionalisation was also investigated with a view to enable fine-tuning of cation-anion interactions *via* electron-withdrawing substituents embedded within the alkyl side chain. Binding energy analysis from XPS indicated that cation functionalisation with perfluorinated and polyether chains had minimal influence on charge-transfer from anion to cation, and the electronic environment of the ionic head groups remains identical to their non-functionalised analogues. Despite this, cation functionalisation has a clear and significant effect on the palladium catalysed Suzuki cross-coupling reaction; in which the nature of catalysis can be changed *via* cation functionalisation with a polyether chain. This highlights the highly complex (and sometimes unpredictable) nature of IL-transition metal systems, and provides a step towards fully understanding the structure-property relationships of ILs to enable the development of wholly tuneable systems.

In summary, this *Thesis* provides new insight to the field of Ionic Liquids by investigating the influence of cation structure in the areas of cation-anion interactions, structural organisation and catalysis; and consequently provides valuable information on the often overlooked tetraalkylammonium and tetraalkylphosphonium cations.

Appendix A: XP Spectra for Chapter 3

Survey and fitted high resolution spectra for neat ammonium-, phosphonium- , and pyrrolidinium-based ionic liquids studied in *Chapter 3* using the Al Kα X-ray source are presented in Figures A1.1 – A1.9, Figures A2.1 – A2.9 and Figures A3.1 – A3.3 respectively.

C 1s high resolution spectra were fitted according to the models described within *Chapter 3*. Cl 2p, P 2p and S 2p high resolution spectra were fitted taking into account spin-orbit coupling; whereby the area ratio of $2p_{1/2}$:$2p_{3/2}$ components are set to 1:2. The O 1s and S 2p high resolution spectra for ionic liquids containing the $[OTf]^-$ and $[NTf_2]^-$ anion are affected by shake up/off phenomena and a 4 % intensity loss (per oxygen/sulfur atom involved in double bonding) was taken into account when calculating atomic percentages for these elements.

For ILs containing a long aliphatic chain ($n \geq 8$) spectra are charge corrected using an established internal reference method of setting the $C_{aliphatic}$ 1s component to 285.0 eV. For ILs comprising short aliphatic chains ($n < 8$) an indirect means of charge correction is applied; in which, spectra are charge corrected by referencing the binding energy of the cationic head group, N 1s/P $2p_{3/2,}$ to the value obtained for its long-chain analogue. A full description of this procedure is provided within *Chapter 3*.

A1 XP Spectra – Ammonium-based ILs

Figure A1.1. XP spectra with component fittings for [$N_{6,6,6,14}$]Cl. *N.B.* O 1s signal detected in survey scan indicating trace amount of surface contaminant present – this is likely to be the result of laboratory grease/double-sided mounting tape – and is not expected to affect the recorded binding energies.

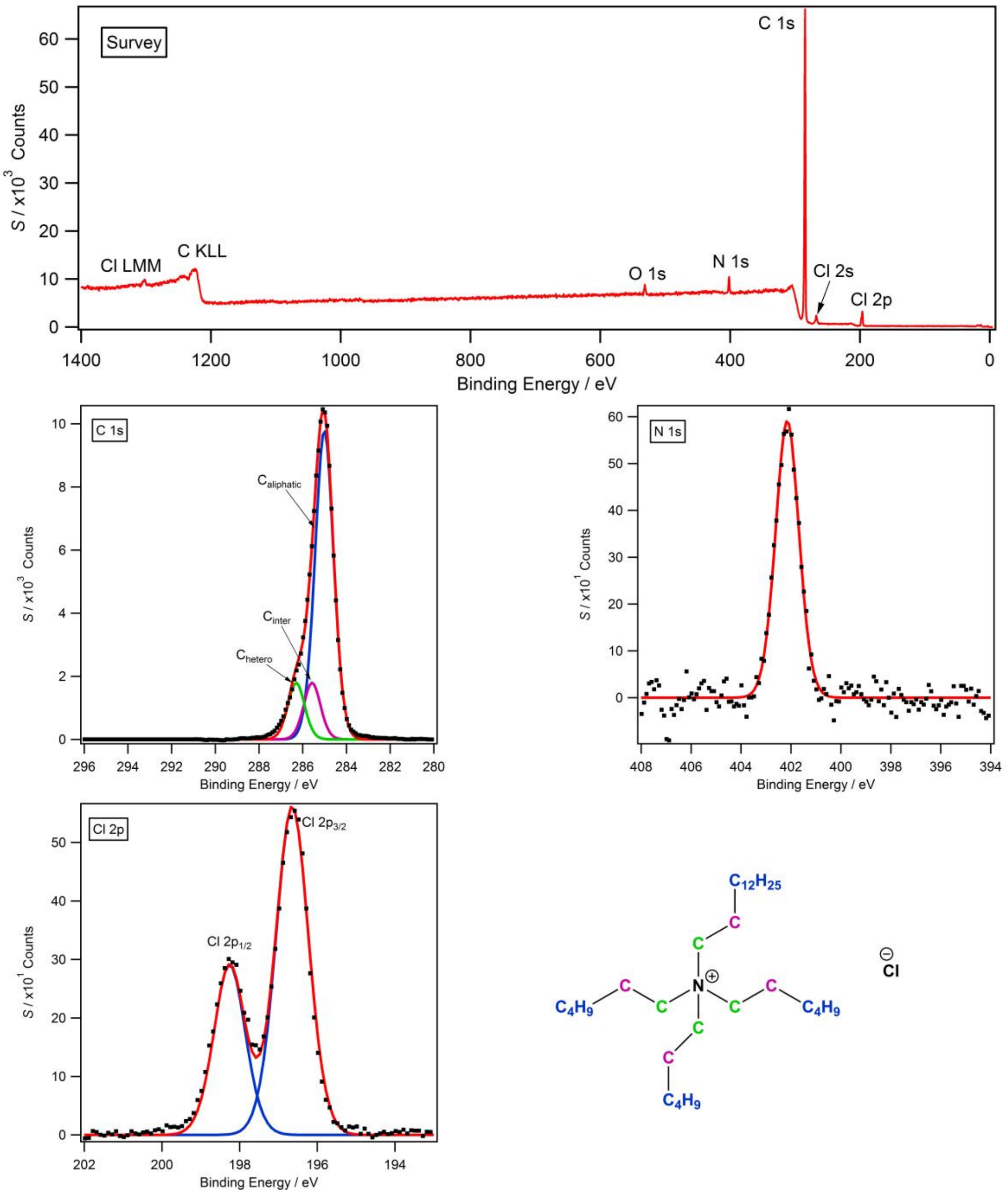

Figure A1.2. XP spectra with component fittings for [$N_{6,6,6,14}$][BF_4].

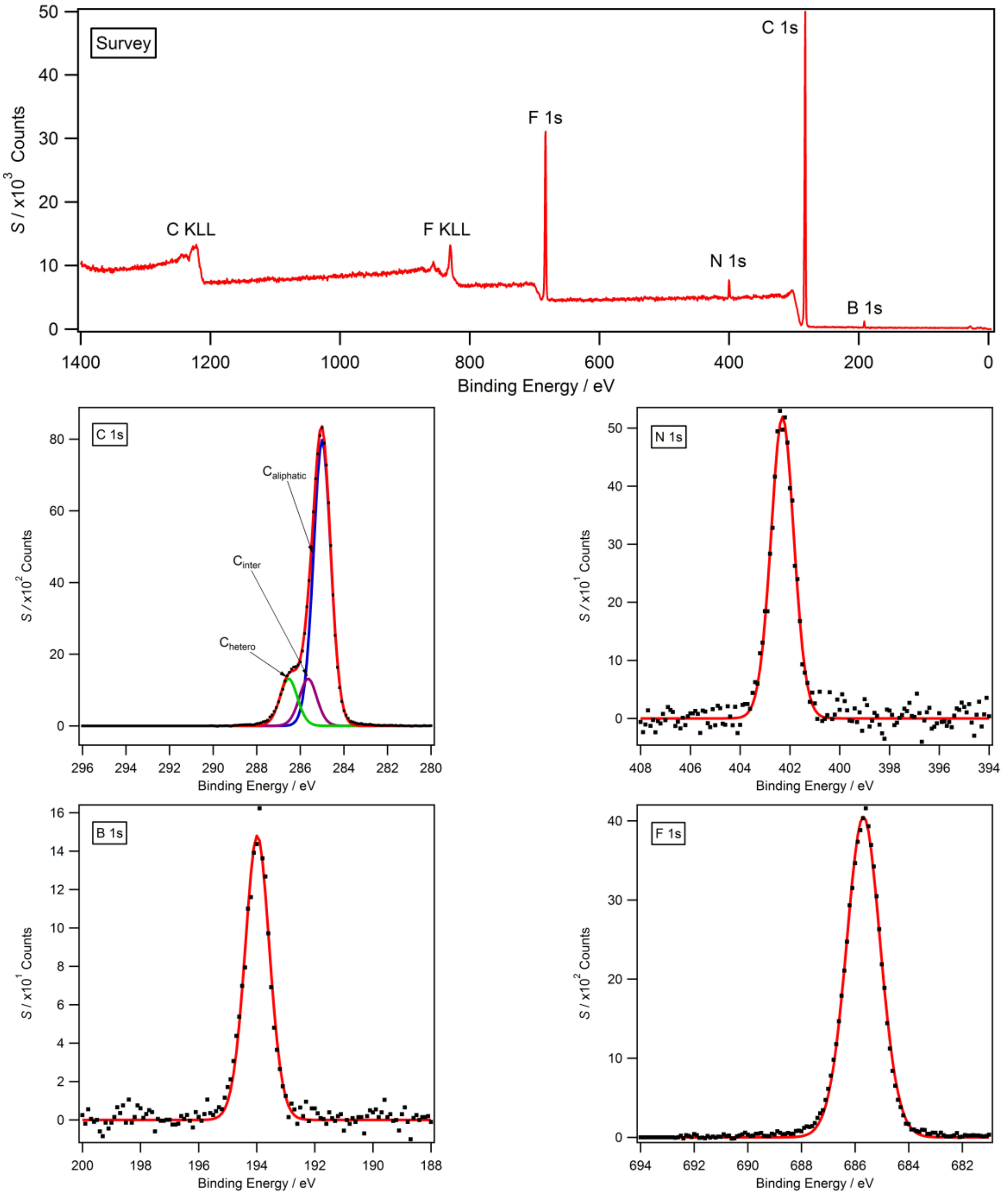

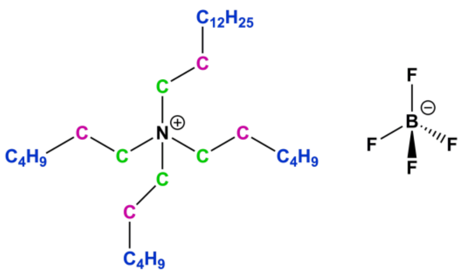

Figure A1.3. XP spectra with component fittings for [$N_{6,6,6,14}$][PF_6].

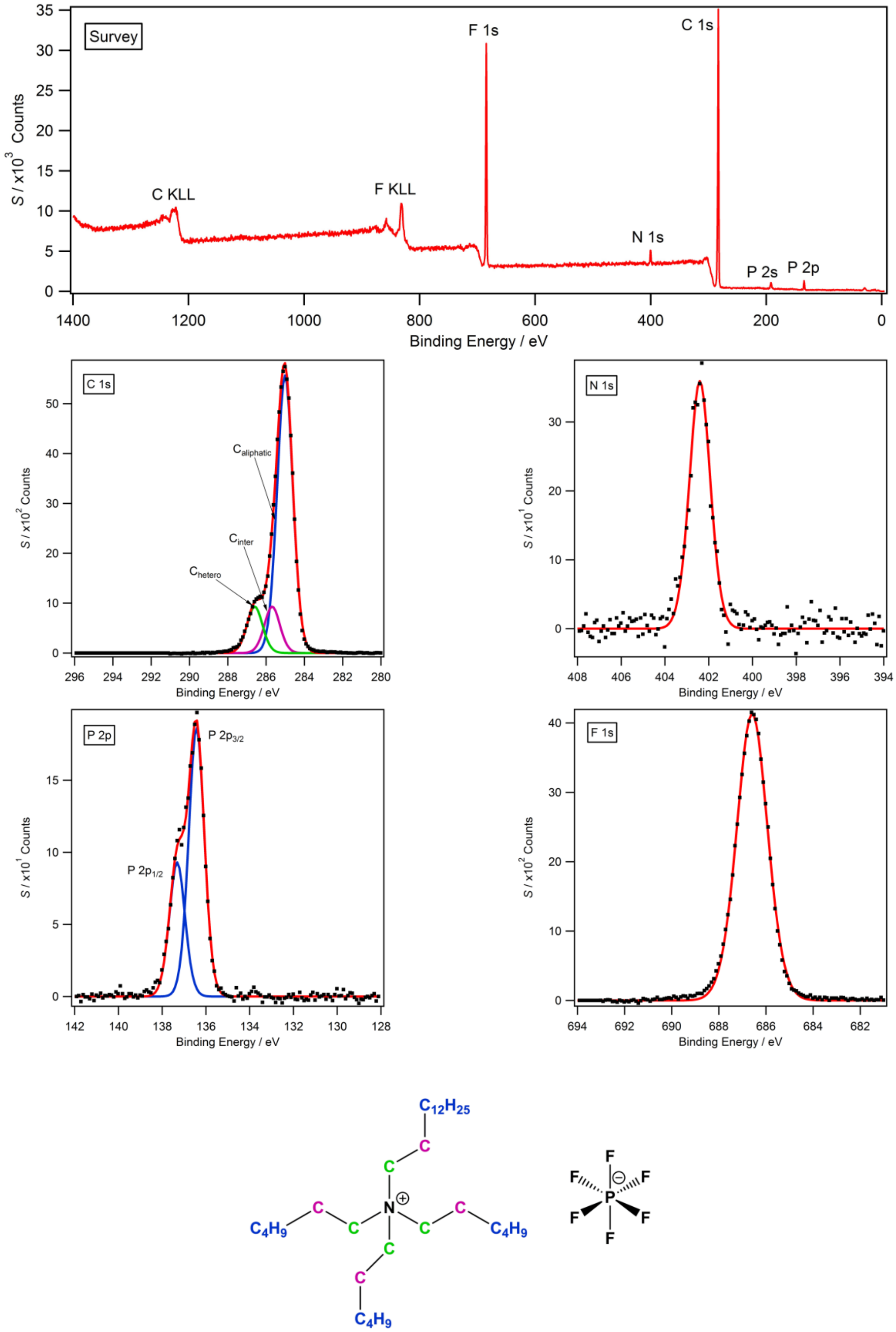

Figure A1.4. XP spectra with component fittings for [$N_{6,6,6,14}$][OTf].

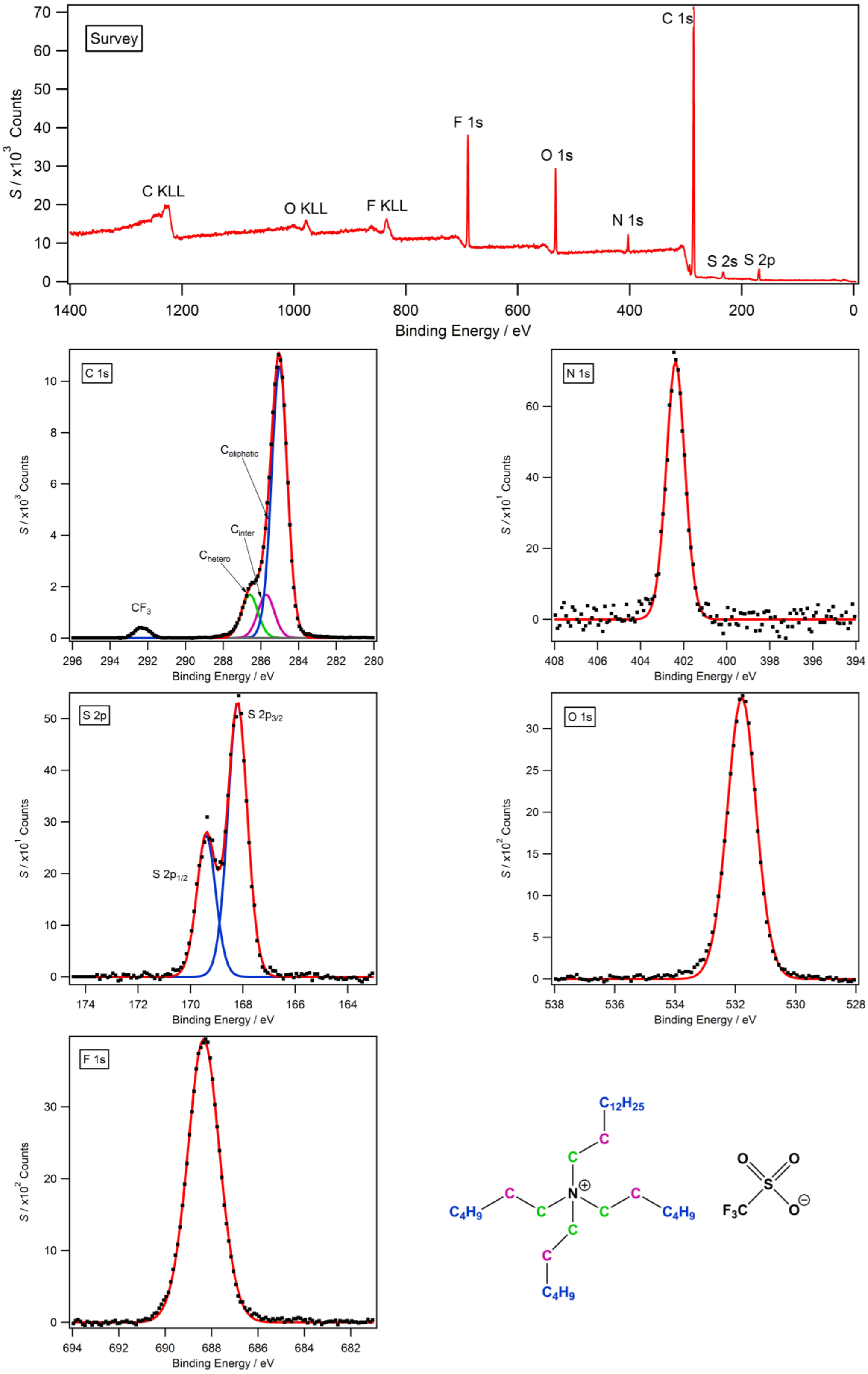

Figure A1.5. XP spectra with component fittings for $[N_{6,6,6,14}][NTf_2]$.

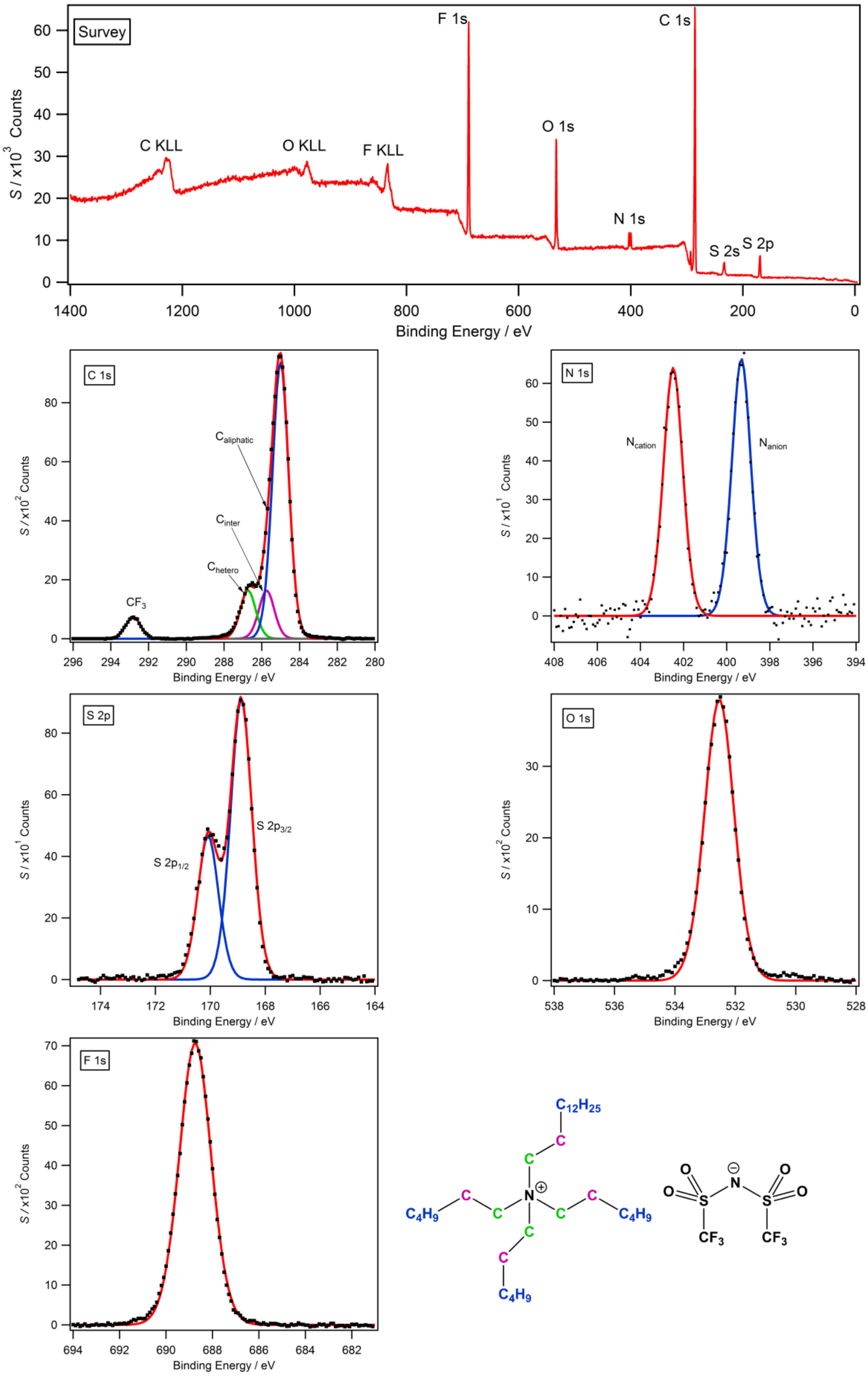

Figure A1.6. XP spectra with component fittings for [$N_{8,8,8,8}$][NTf_2].

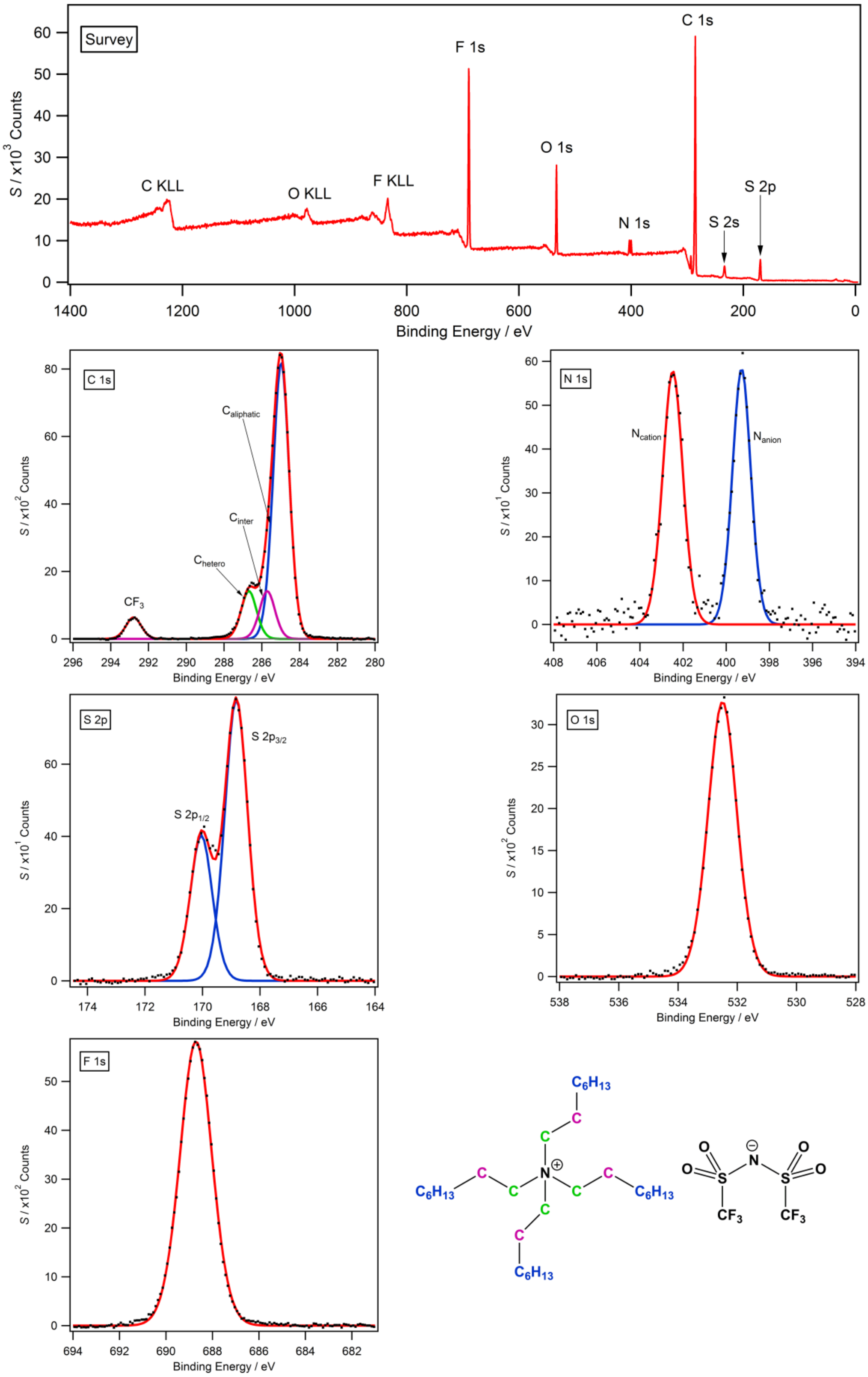

Figure A1.7. XP spectra with component fittings for $[N_{4,4,4,4}][NTf_2]$.

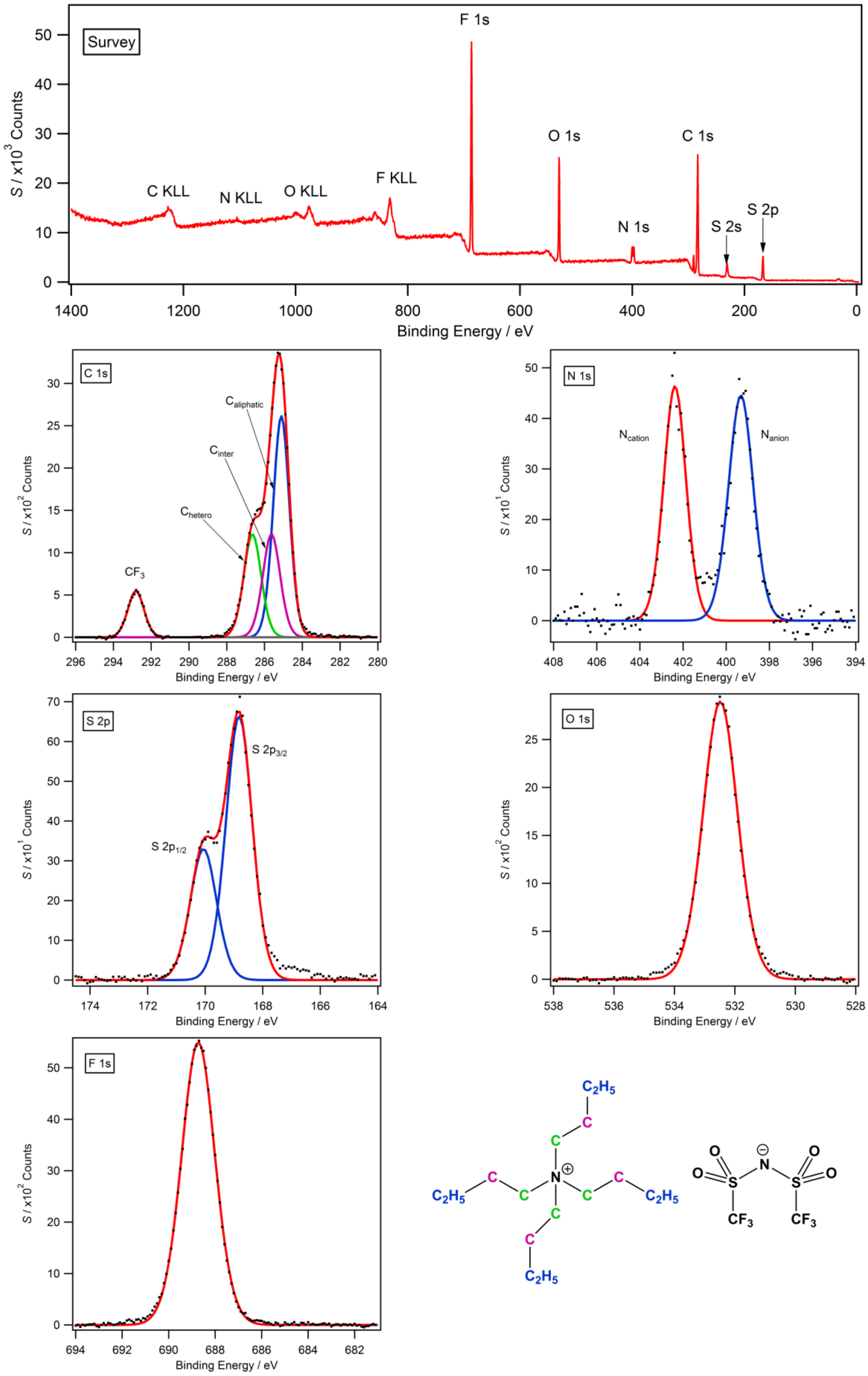

Figure A1.8. XP spectra with component fittings for [$N_{4,4,4,1}$][NTf_2].

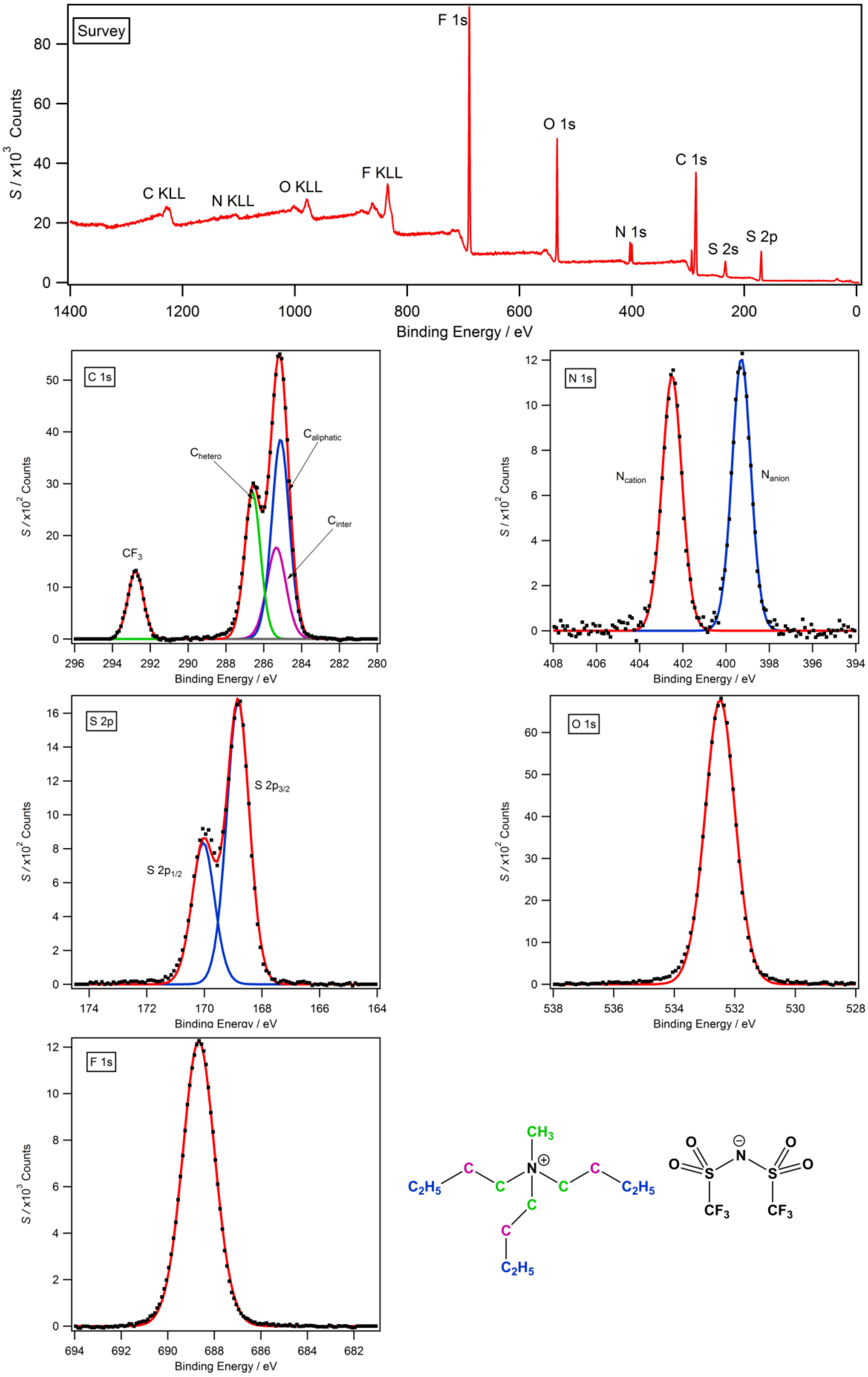

Figure A1.9. XP spectra with component fittings for [$N_{4,4,4,1}$][BF_4]. *N.B.* O 1s and Si 1s signals detected in survey scan indicating trace amount of surface contaminant present – this is likely to be the result of laboratory grease/double-sided mounting tape – and is not expected to affect the recorded binding energies.

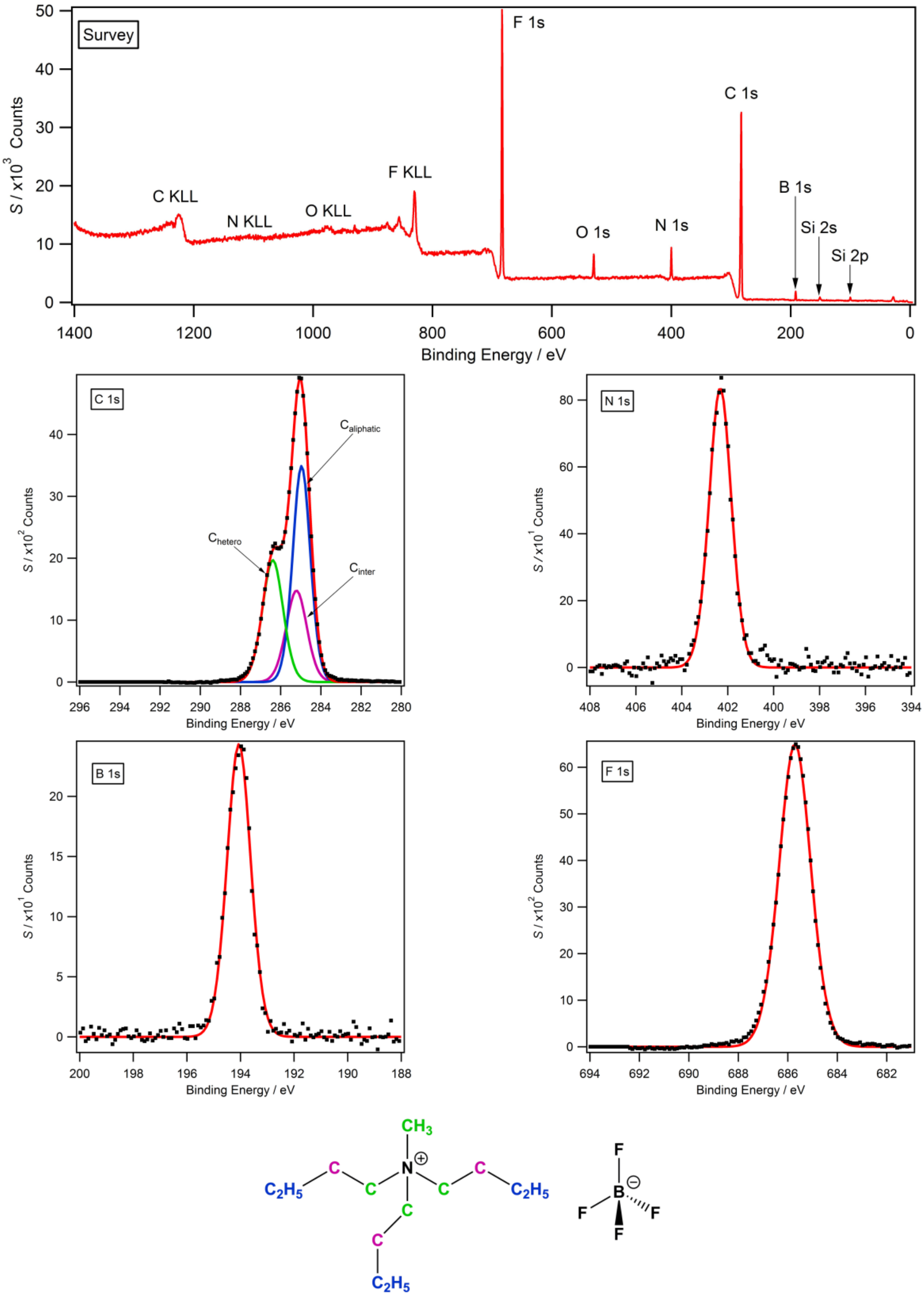

A2 XP Spectra – Phosphonium-based ILs

Figure A2.1. XP spectra with component fittings for [$P_{6,6,6,14}$]Cl.

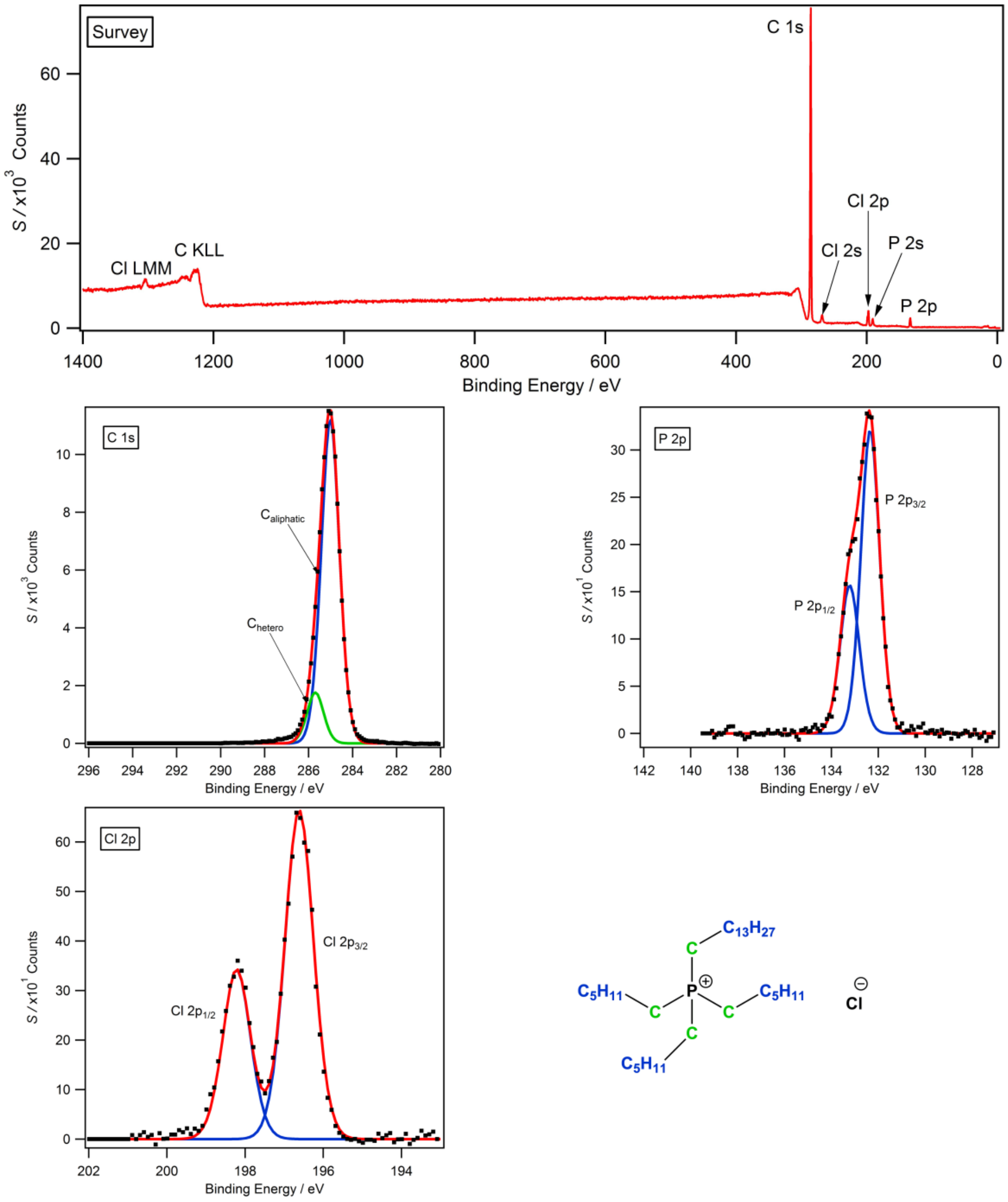

Figure A2.2. XP spectra with component fittings for [$P_{6,6,6,14}$][BF_4].

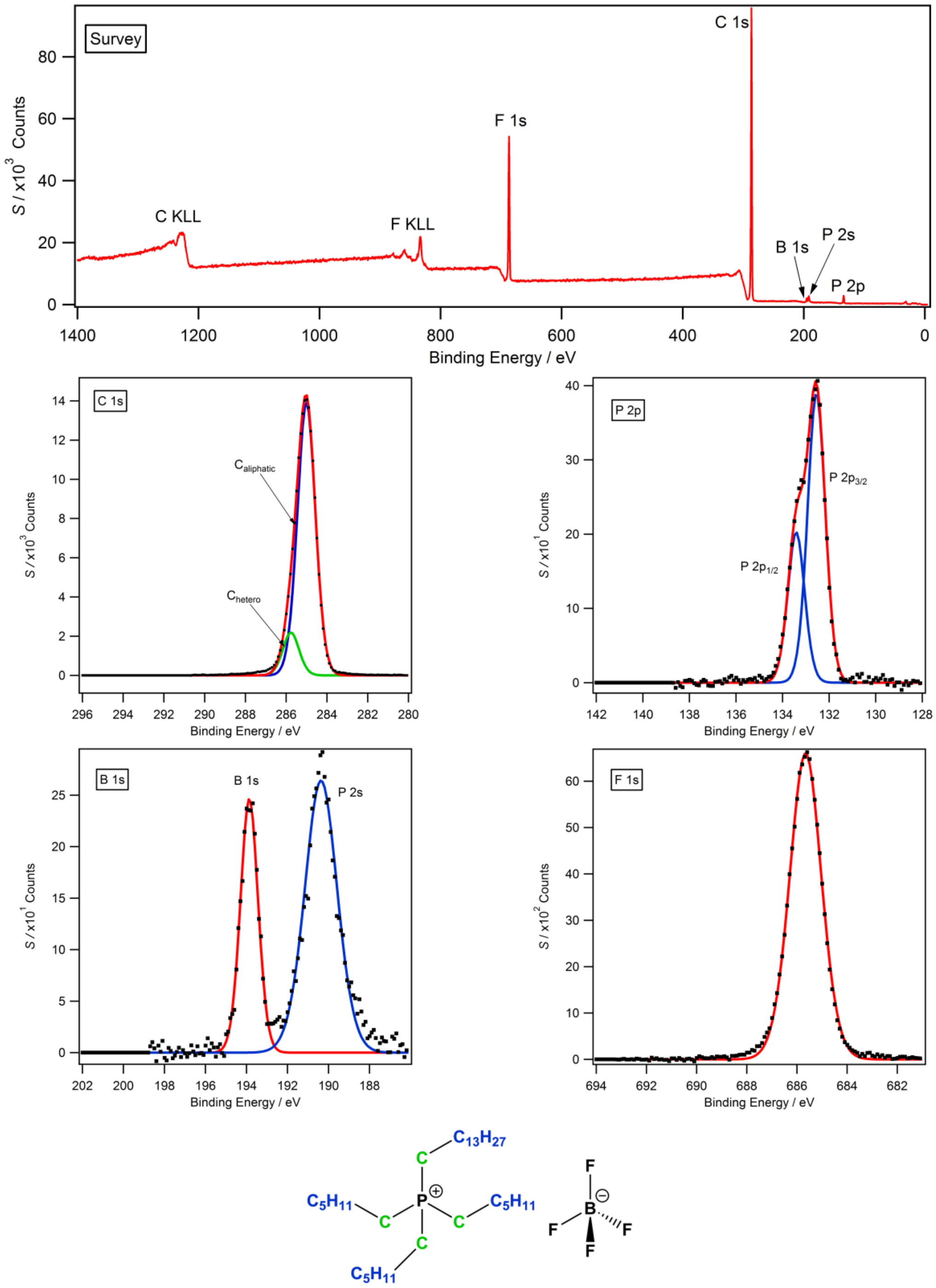

Figure A2.3. XP spectra with component fittings for $[P_{6,6,6,14}][PF_6]$.

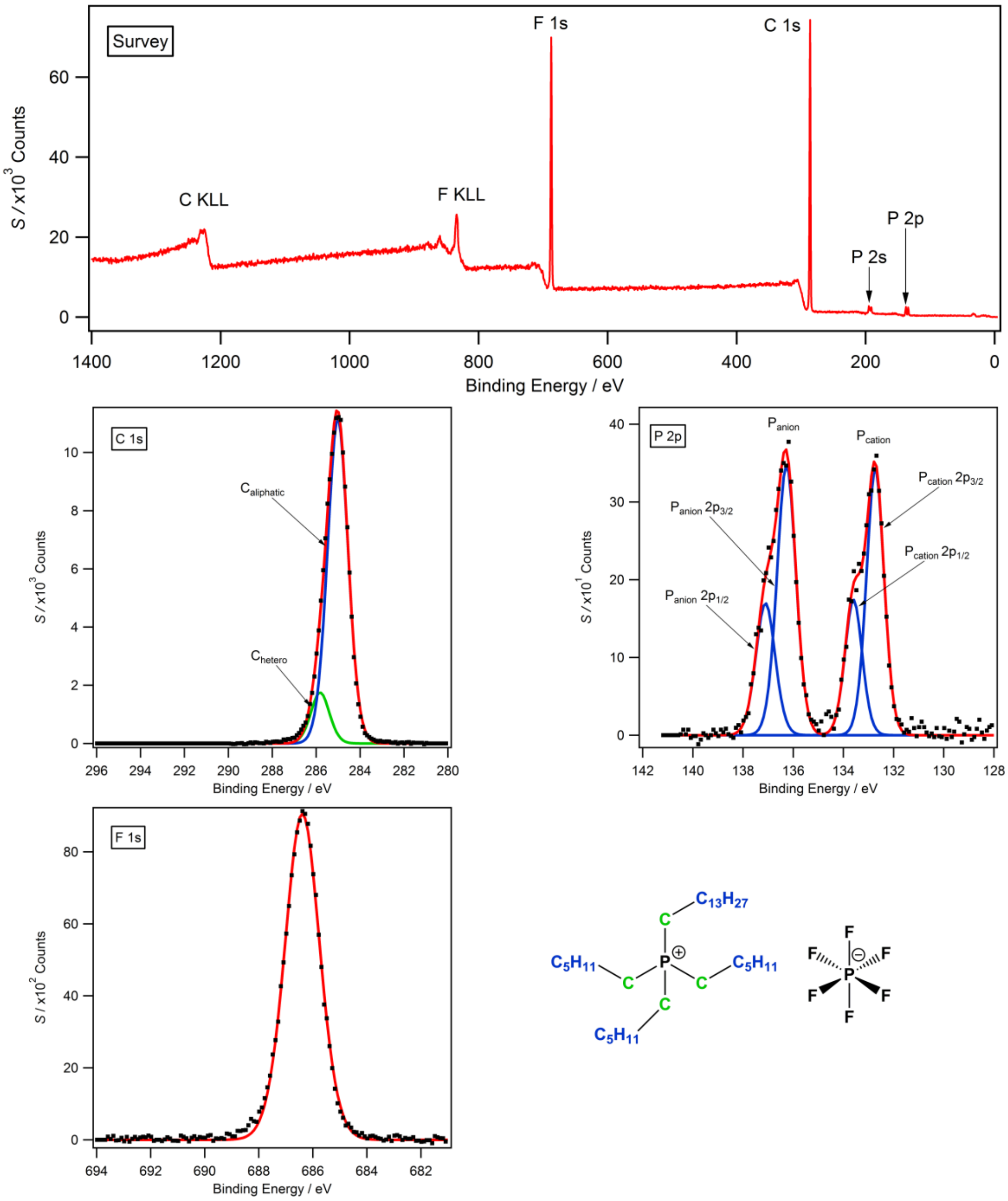

Figure A2.4. XP spectra with component fittings for [$P_{6,6,6,14}$][OTf].

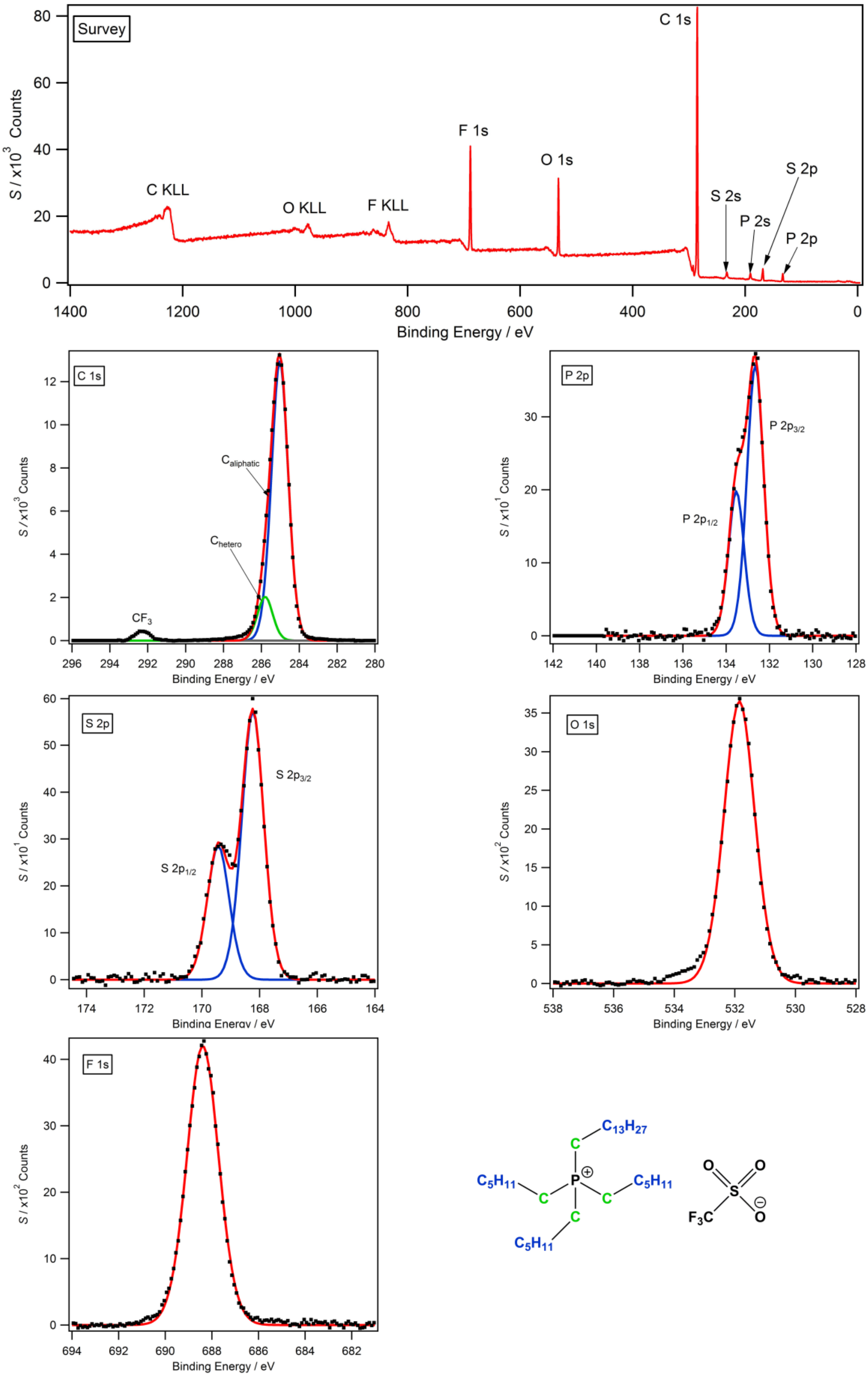

Figure A2.5. XP spectra with component fittings for [$P_{6,6,6,14}$][NTf_2].

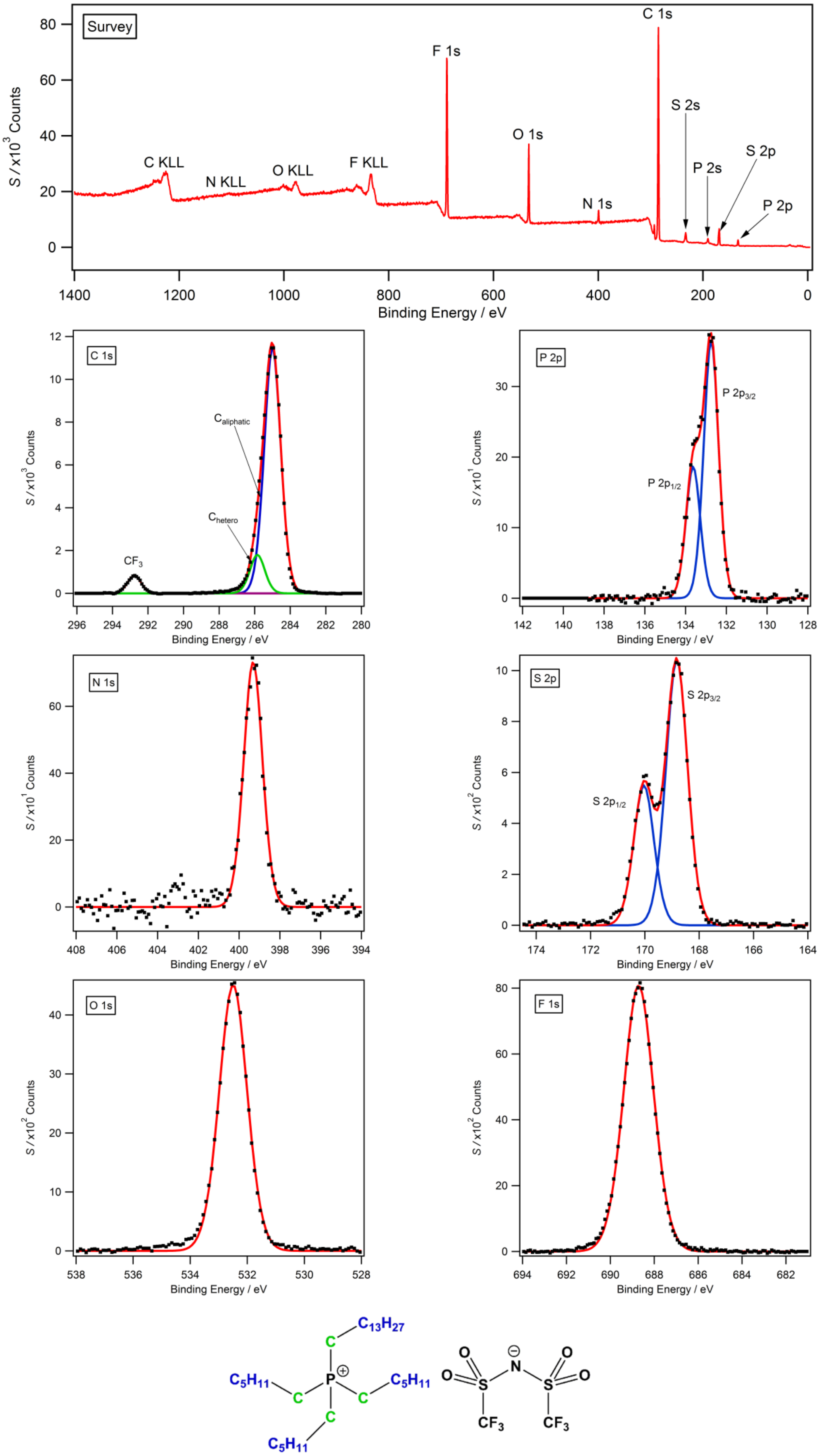

Figure A2.6. XP spectra with component fittings for $[P_{8,8,8,8}][NTf_2]$.

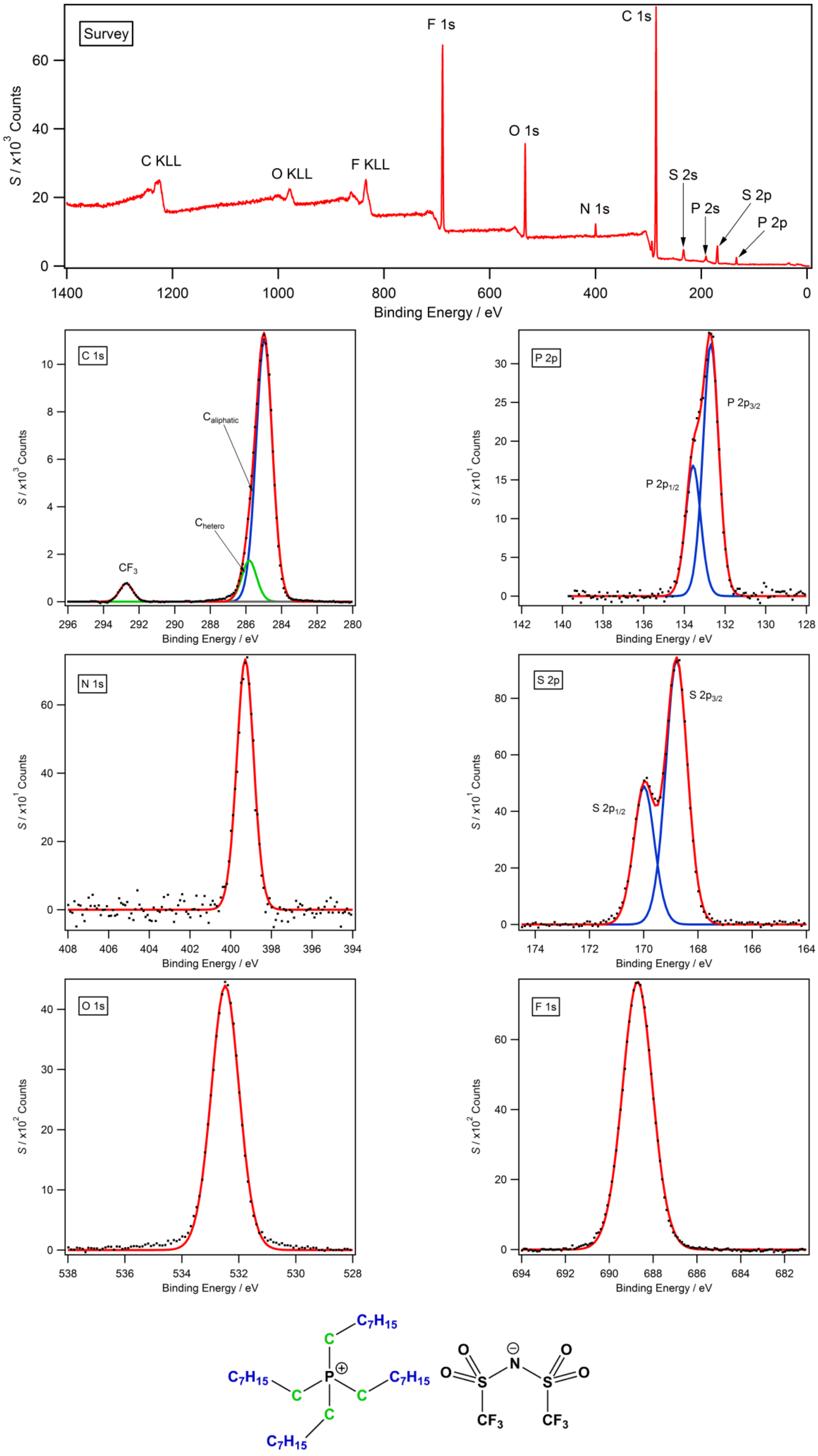

Figure A2.7. XP spectra with component fittings for [$P_{4,4,4,4}$][NTf_2].

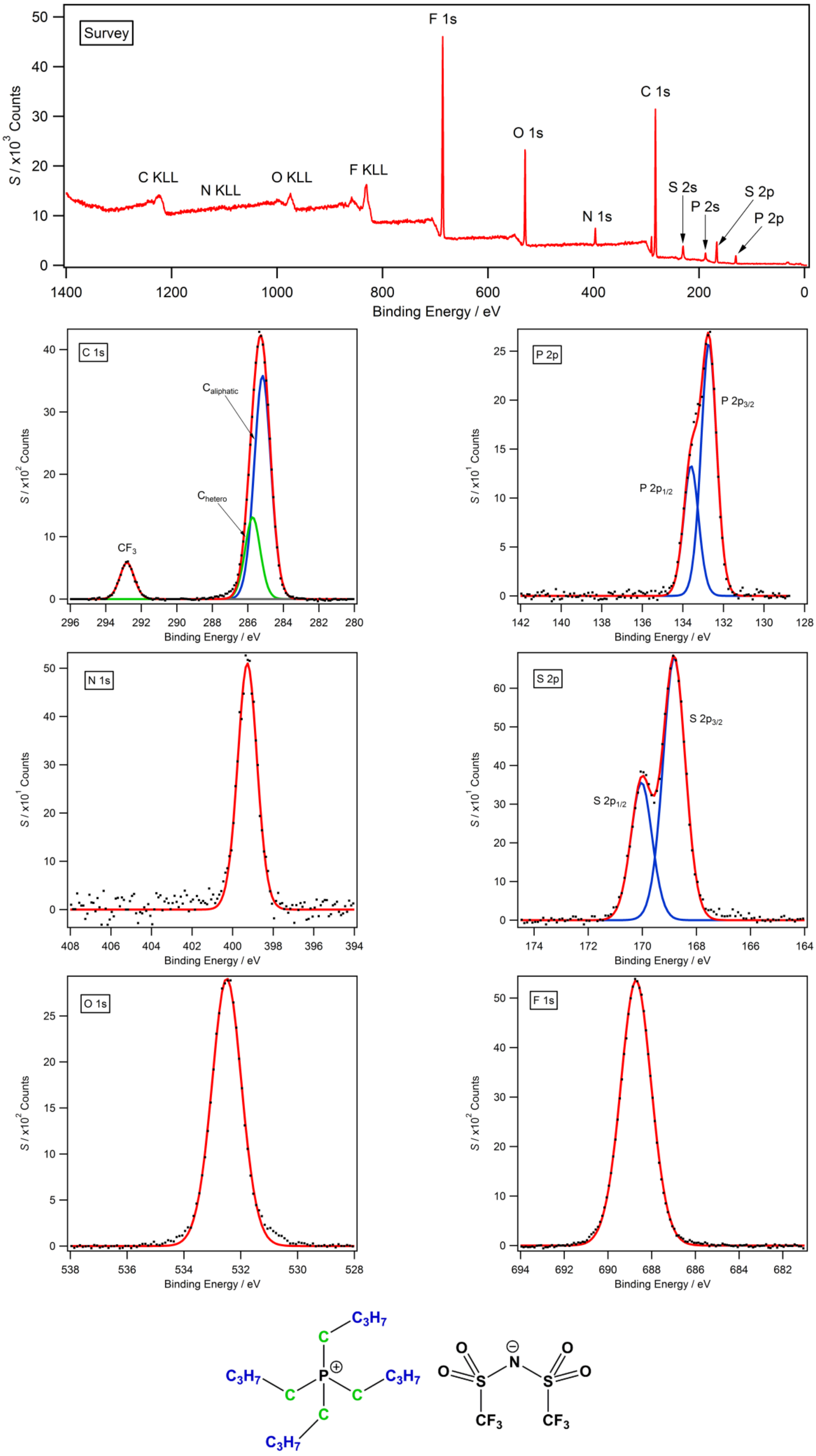

Figure A2.8. XP spectra with component fittings for $[P_{4,4,4,1}][NTf_2]$.

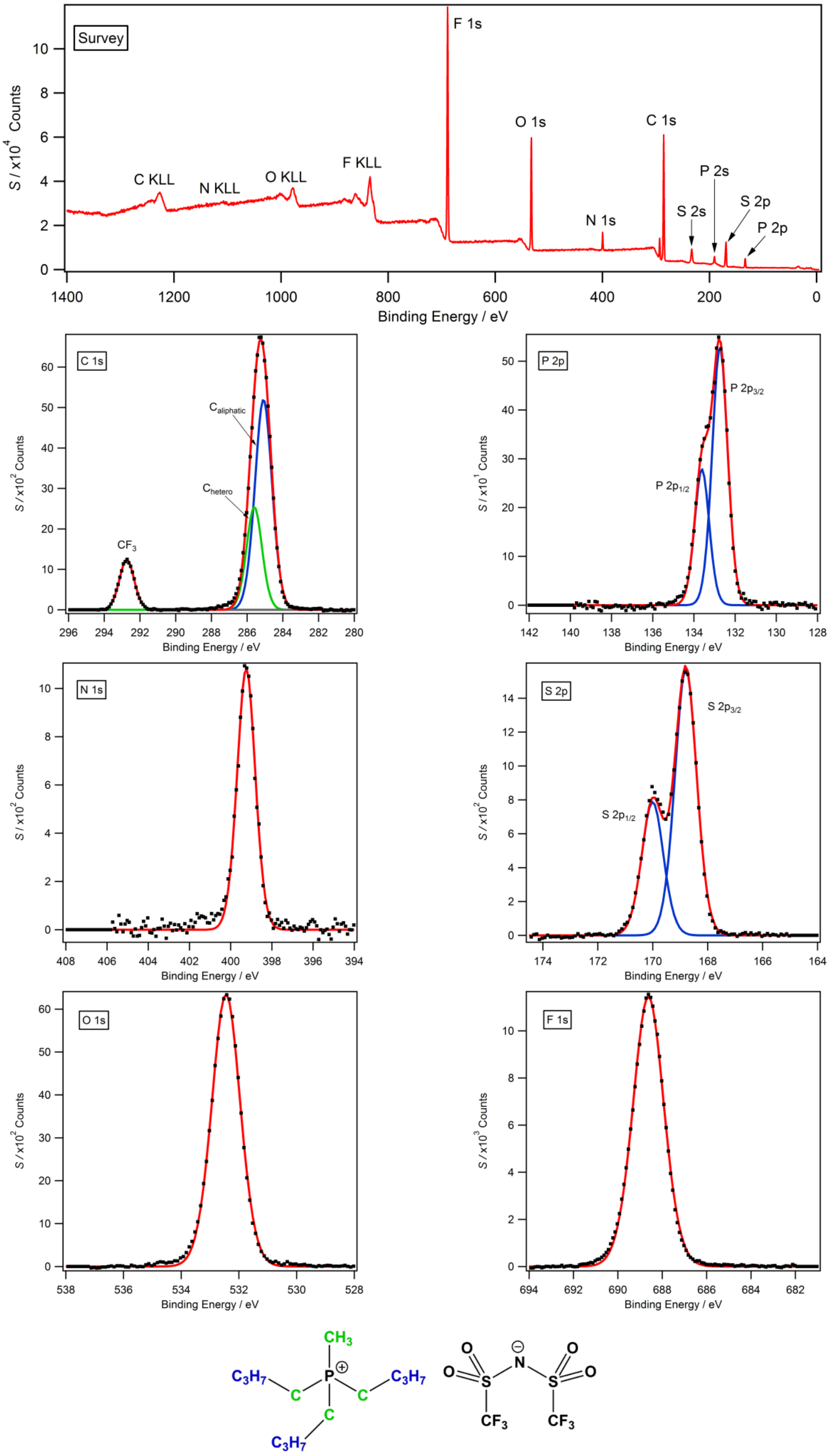

Figure A2.9. XP spectra with component fittings for $[P_{4,4,4,1}][BF_4]$.

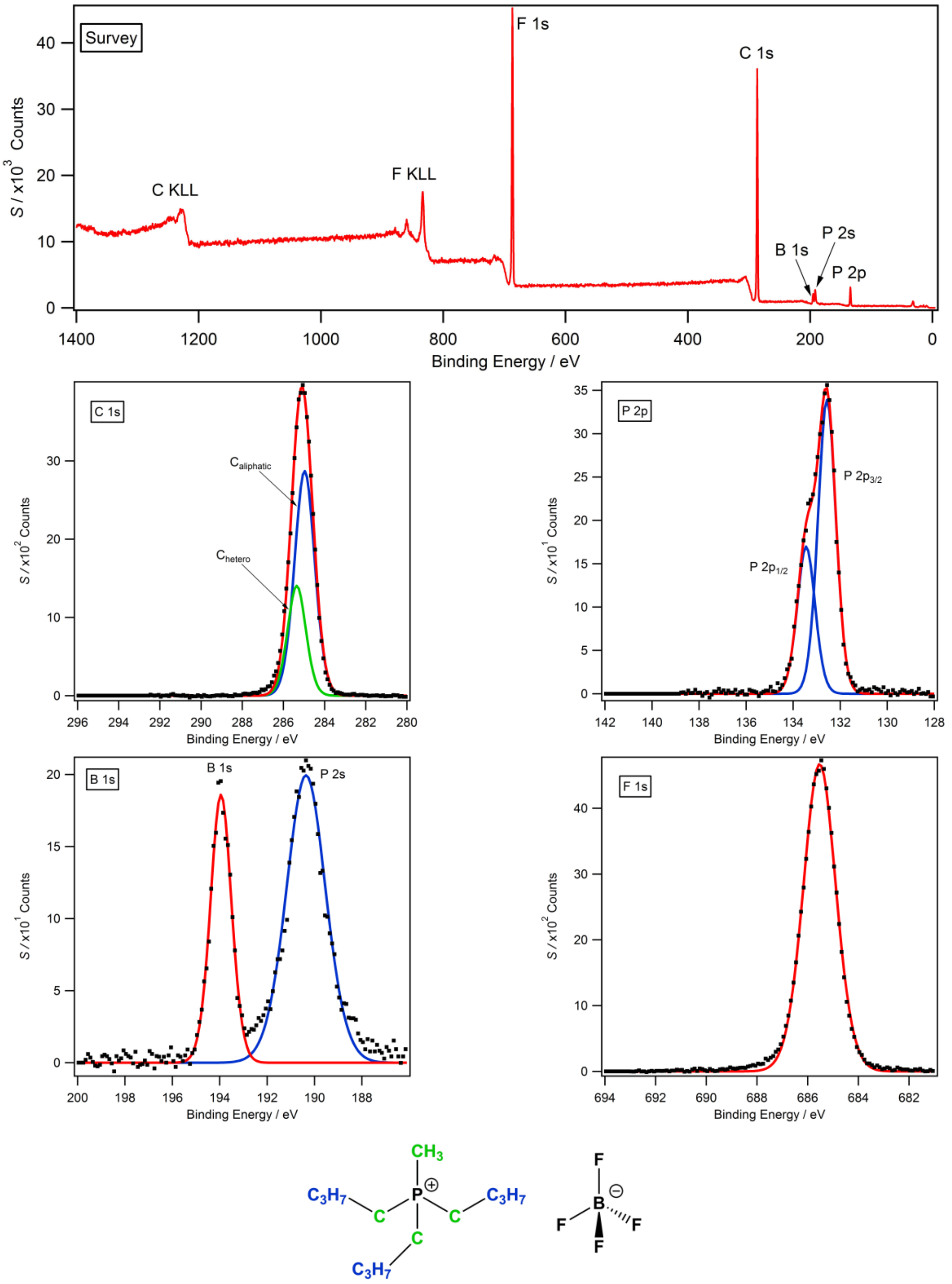

A3 XP Spectra – Pyrrolidinium-based ILs

Figure A3.1. XP spectra with component fittings for [C_8C_1Pyrr]Cl. *N.B.* O 1s signal detected in survey scan indicating trace amount of surface contaminant present – this is likely to be the result of laboratory grease/double-sided mounting tape – and is not expected to affect the recorded binding energies.

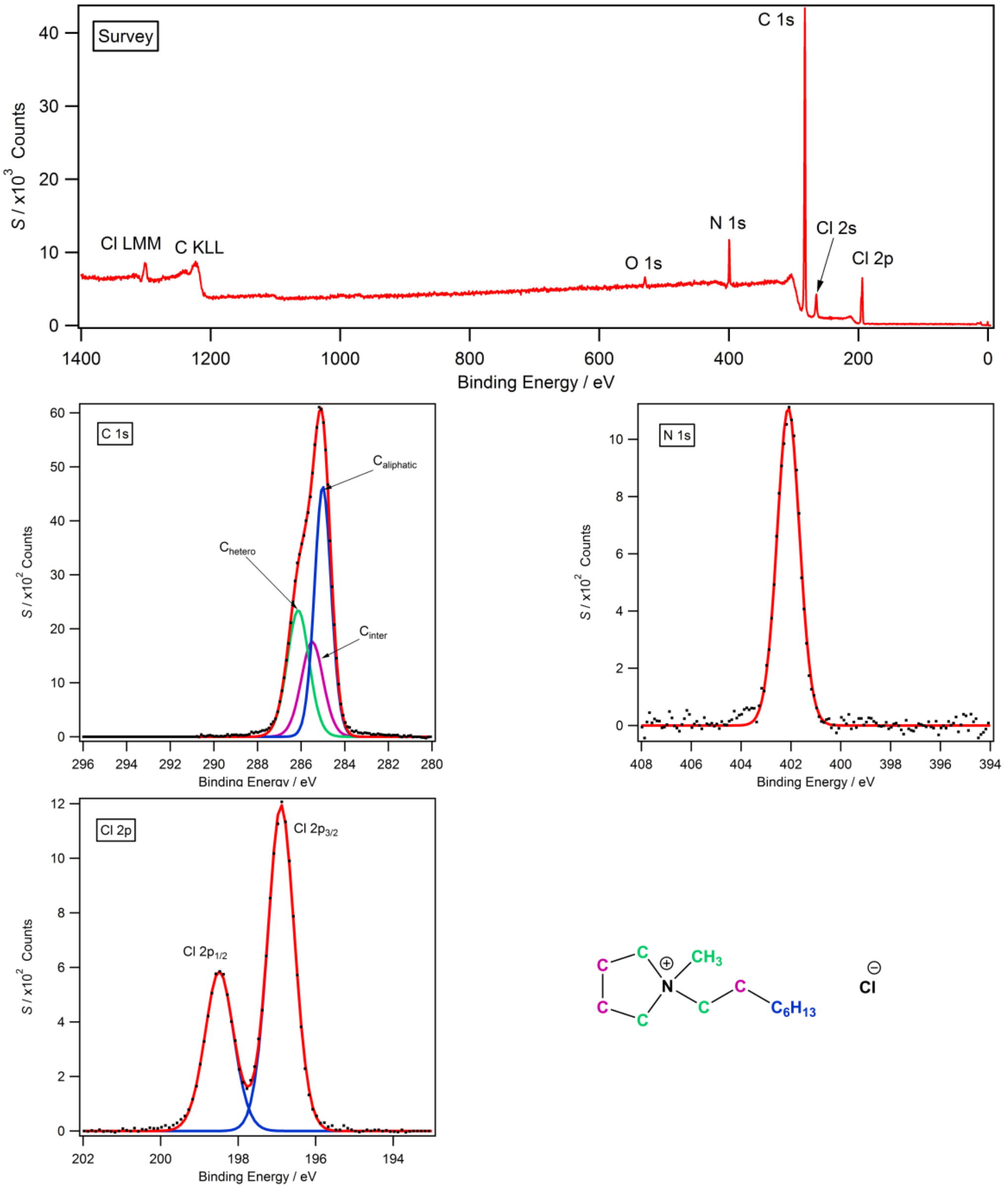

Figure A3.2. XP spectra with component fittings for [C_8C_1Pyrr][BF_4].

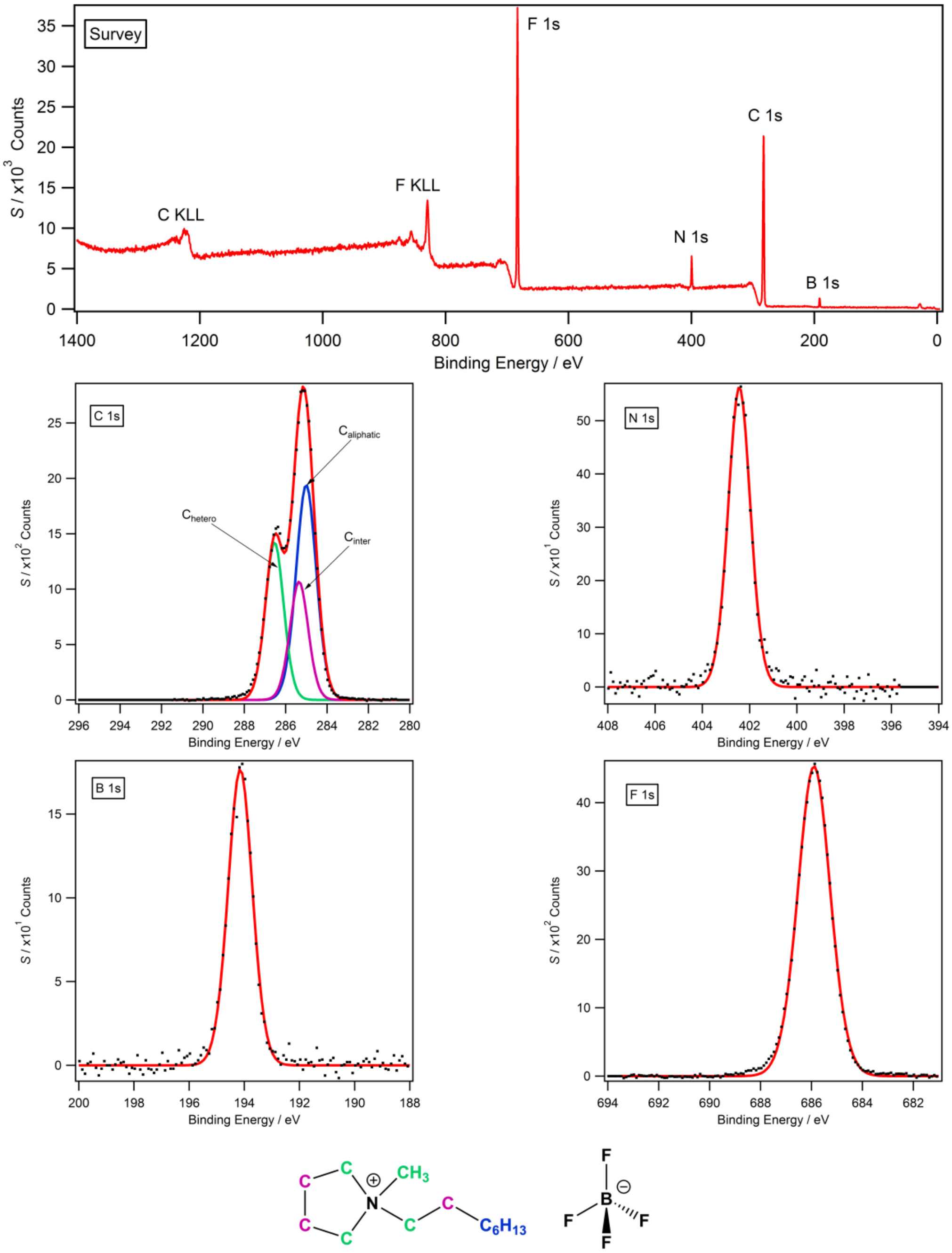

Figure A3.3. XP spectra with component fittings for [C_8C_1Pyrr][NTf_2].

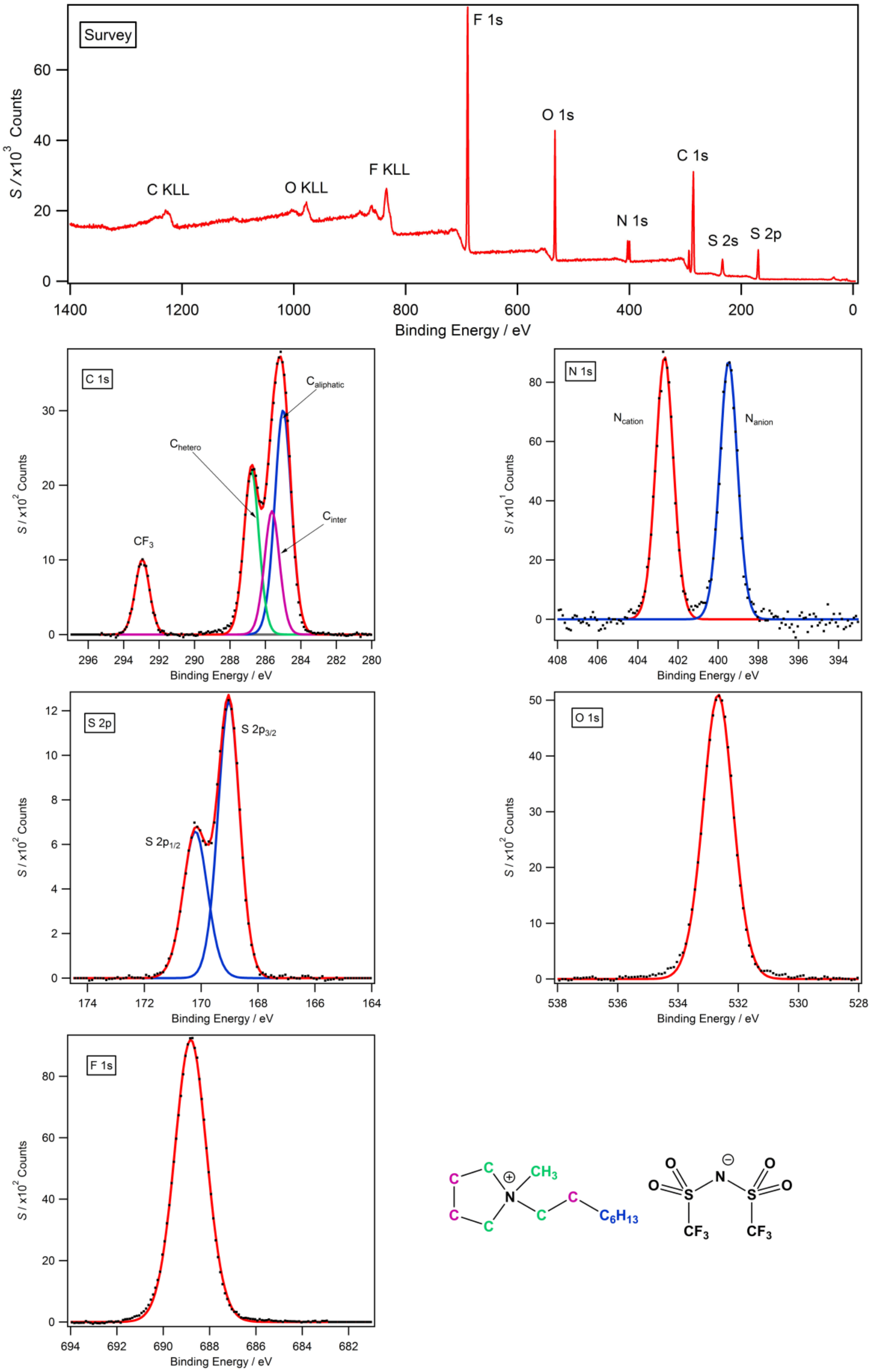

Appendix B: XP Spectra for Chapter 4

Survey and fitted high resolution spectra for neat ionic liquids studied in *Chapter 4* using the Ag Lα’ X-ray source and Al Kα X-ray source are presented in Figures B1.1 – B1.13 and Figures B2.1 – B2.3 respectively. Angle-Resolved XPS (ARXPS) spectra measured using the Al Kα X-ray source at emission angles $\theta = 0°$ and 80° (normalised to the area of the F 1s photoelectron emission peak recorded for the respective ionic liquid at $\theta = 0°$) are presented in Figures B3.1 – B3.5.

C 1s high resolution spectra were fitted according to the models described within *Chapters 3* and *4*. Cl 2p, P 2p and S 2p high resolution spectra were fitted taking into account spin-orbit coupling; whereby the area ratio of $2p_{1/2}$:$2p_{3/2}$ components are set to 1:2. The O 1s and S 2p high resolution spectra for ionic liquids containing the $[NTf_2]^-$ anion are affected by shake up/off phenomena and a 4 % intensity loss (per oxygen/sulfur atom involved in double bonding) was taken into account when calculating atomic percentages for these elements.

For ILs containing a long aliphatic chain ($n \geq 8$) spectra are charge corrected using an established internal reference method of setting the $C_{aliphatic}$ 1s component to 285.0 eV. For ILs comprising short aliphatic chains ($n < 8$) an indirect means of charge correction is applied; in which, spectra are charge corrected by referencing the binding energy of the cationic head group, N 1s/P $2p_{3/2}$, to the value obtained for its long-chain analogue. A full description of this procedure is provided within *Chapters 3* and *4*.

B1 XP Spectra – Ag Lα' X-ray source

Figure B1.1. XP spectra with component fittings for [C_8C_1Pyrr]Cl.

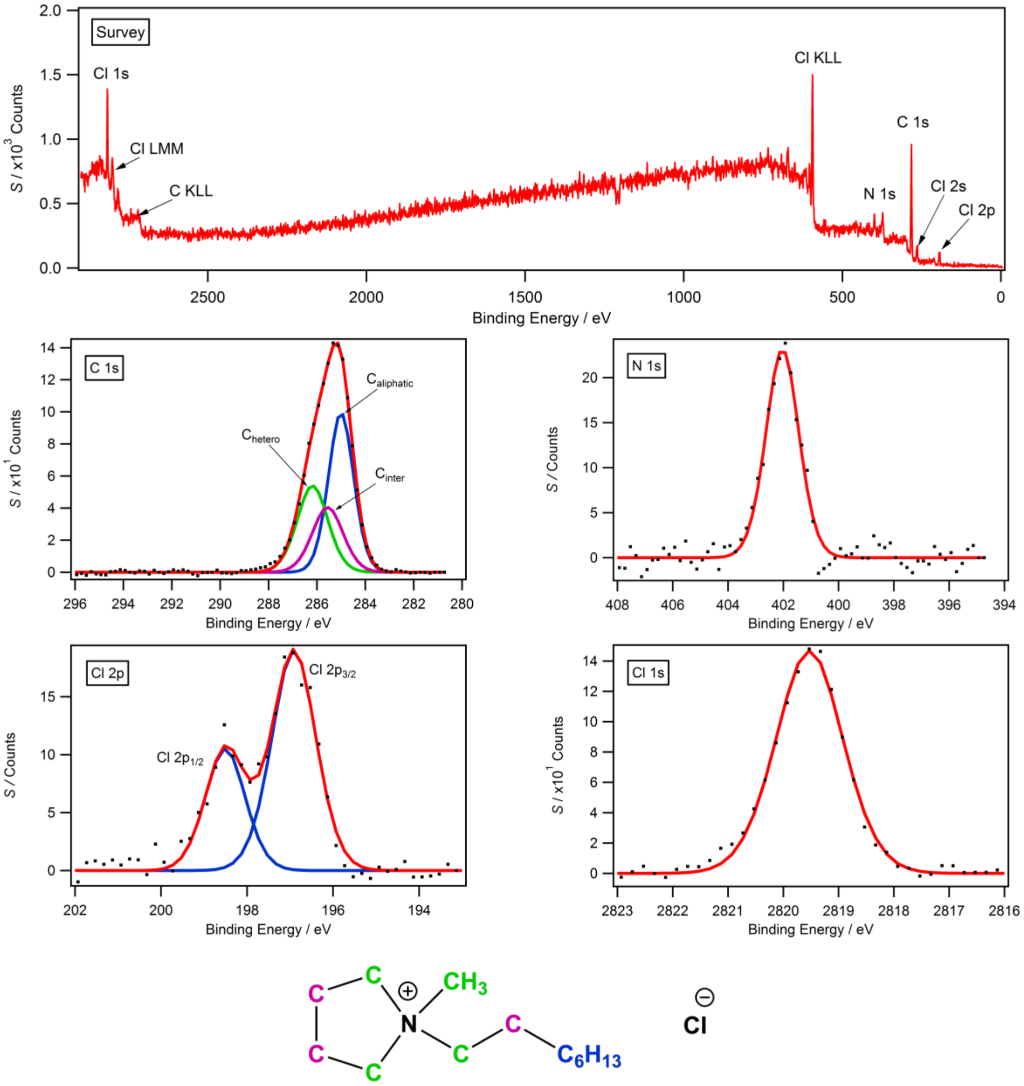

Figure B1.2. XP spectra with component fittings for [$P_{6,6,6,14}$]Cl.

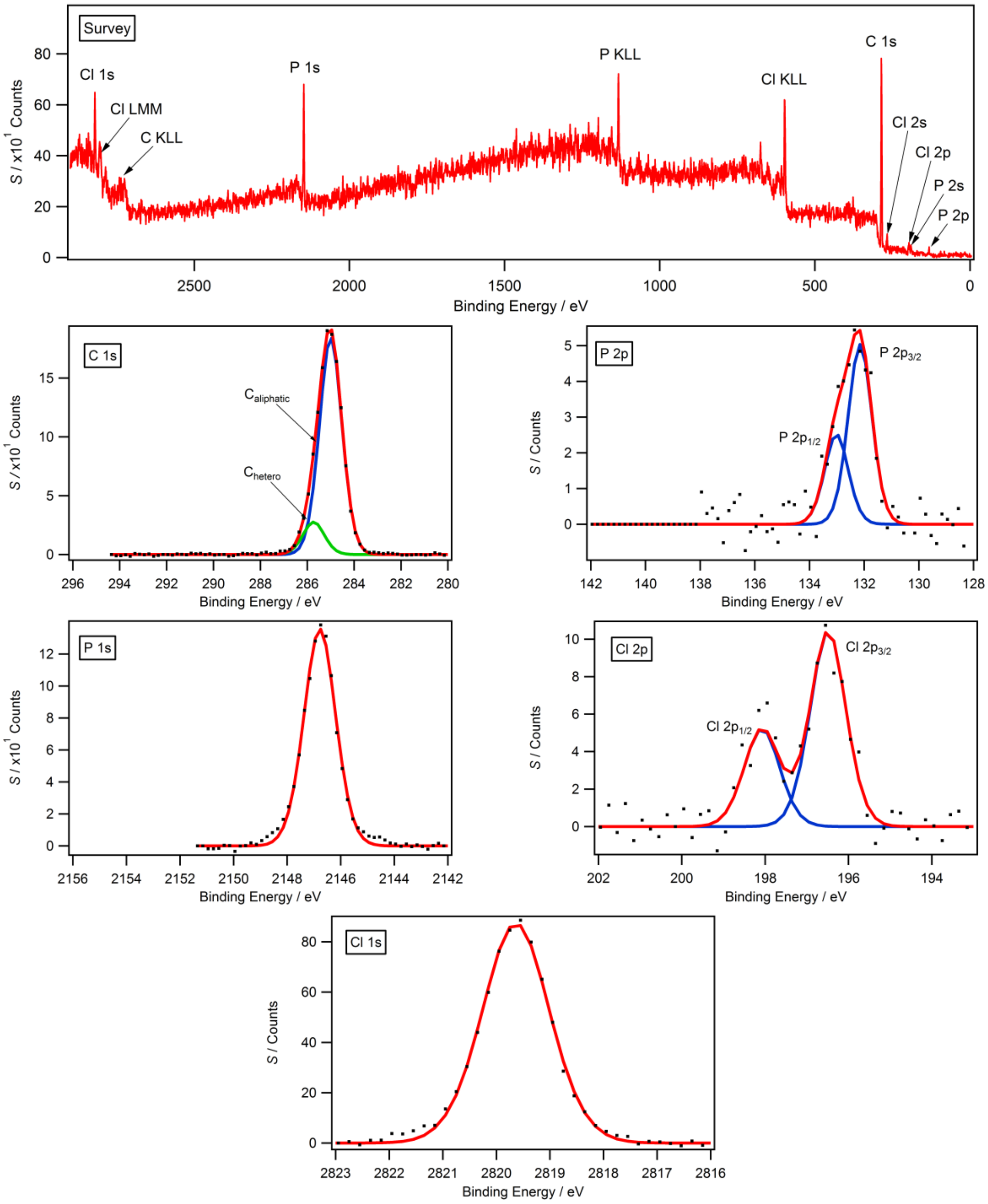

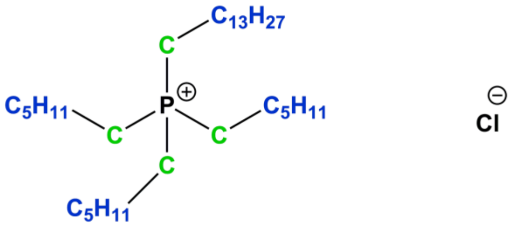

Figure B1.3. XP spectra with component fittings for [$P_{4,4,4,1}$]Cl. *N.B.* O 1s and Si 1s signals detected in survey scan indicating trace amount of surface contaminant present – this is likely to be the result of laboratory grease/double-sided mounting tape – and is not expected to affect the recorded binding energies.

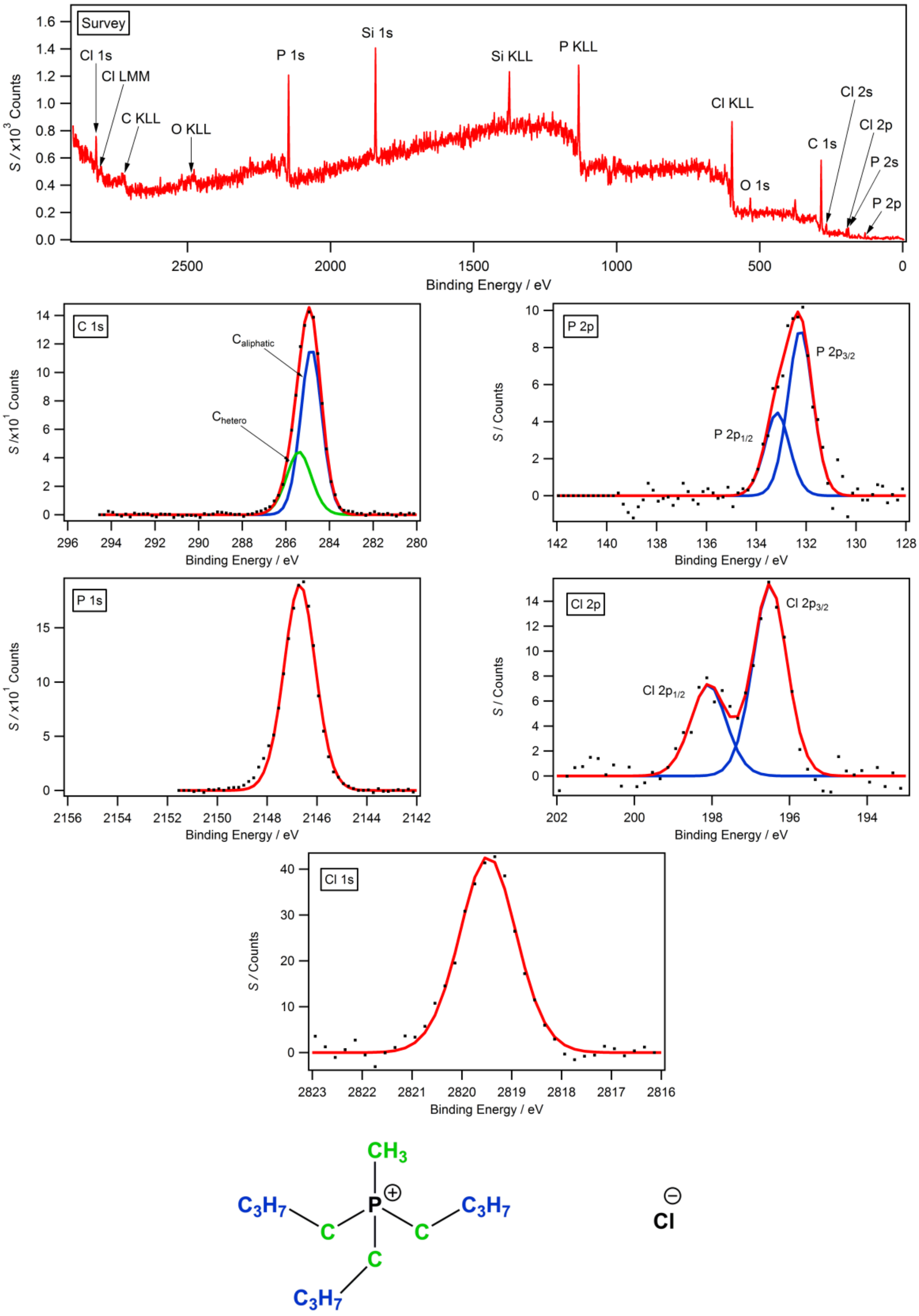

Figure B1.4. XP spectra with component fittings for [C_8C_1Pyrr][PF_6].

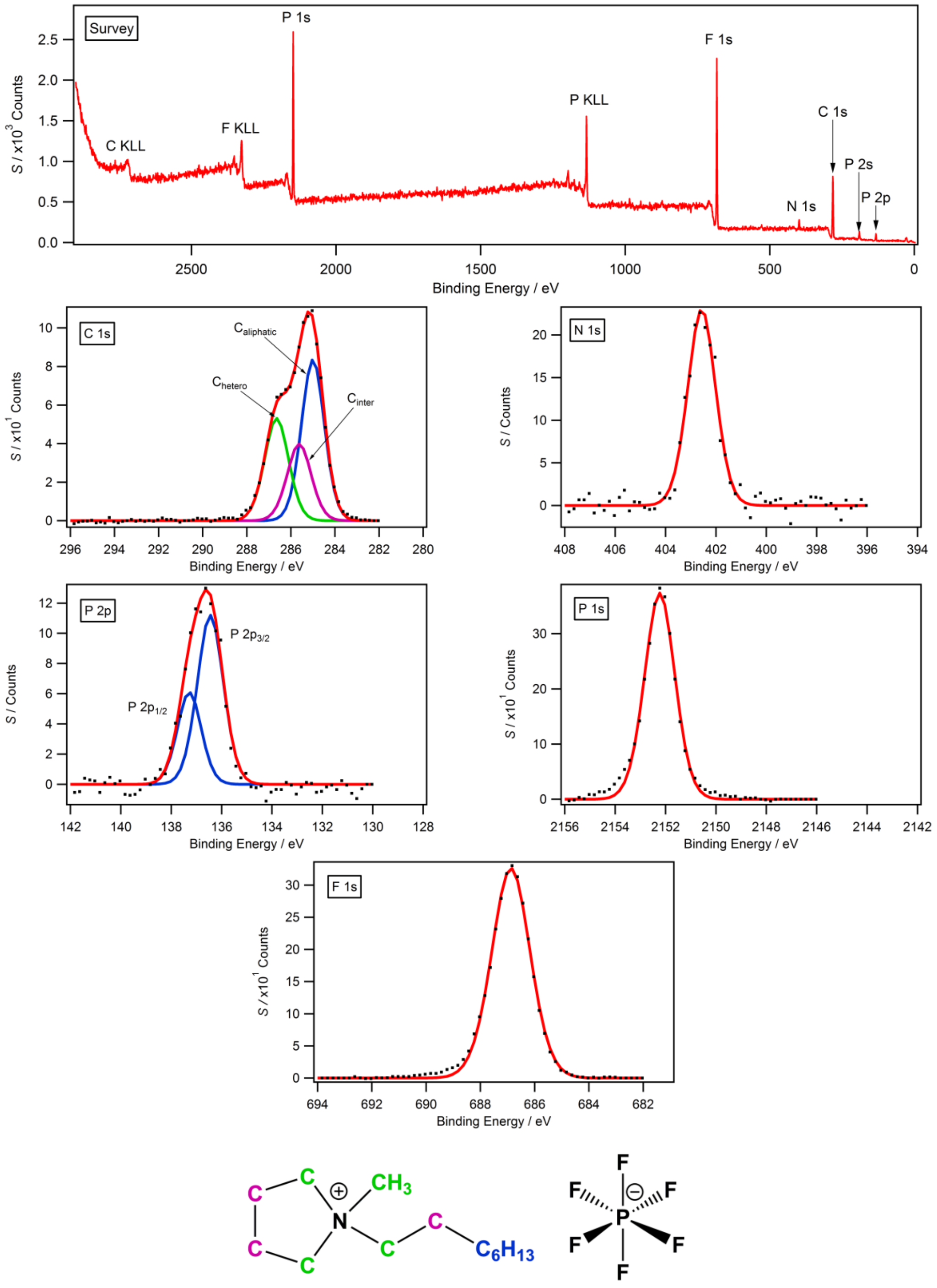

Figure B1.5. XP spectra with component fittings for $[N_{6,6,6,14}][PF_6]$. *N.B.* O 1s and Si 1s signals detected in survey scan indicating trace amount of surface contaminant present – this is likely to be the result of laboratory grease/double-sided mounting tape – and is not expected to affect the recorded binding energies.

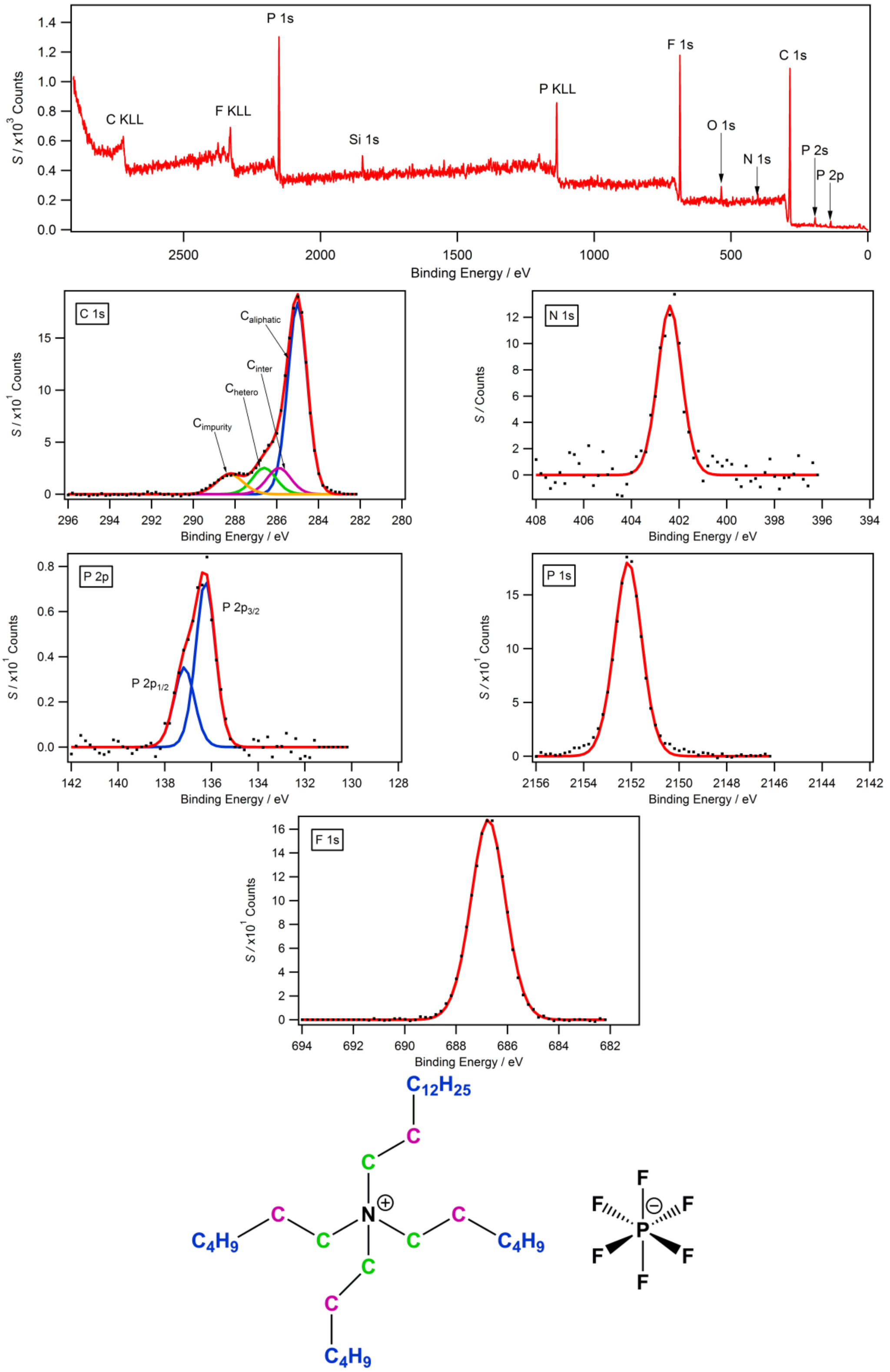

Figure B1.6. XP spectra with component fittings for $[N_{4,4,4,1}][PF_6]$.

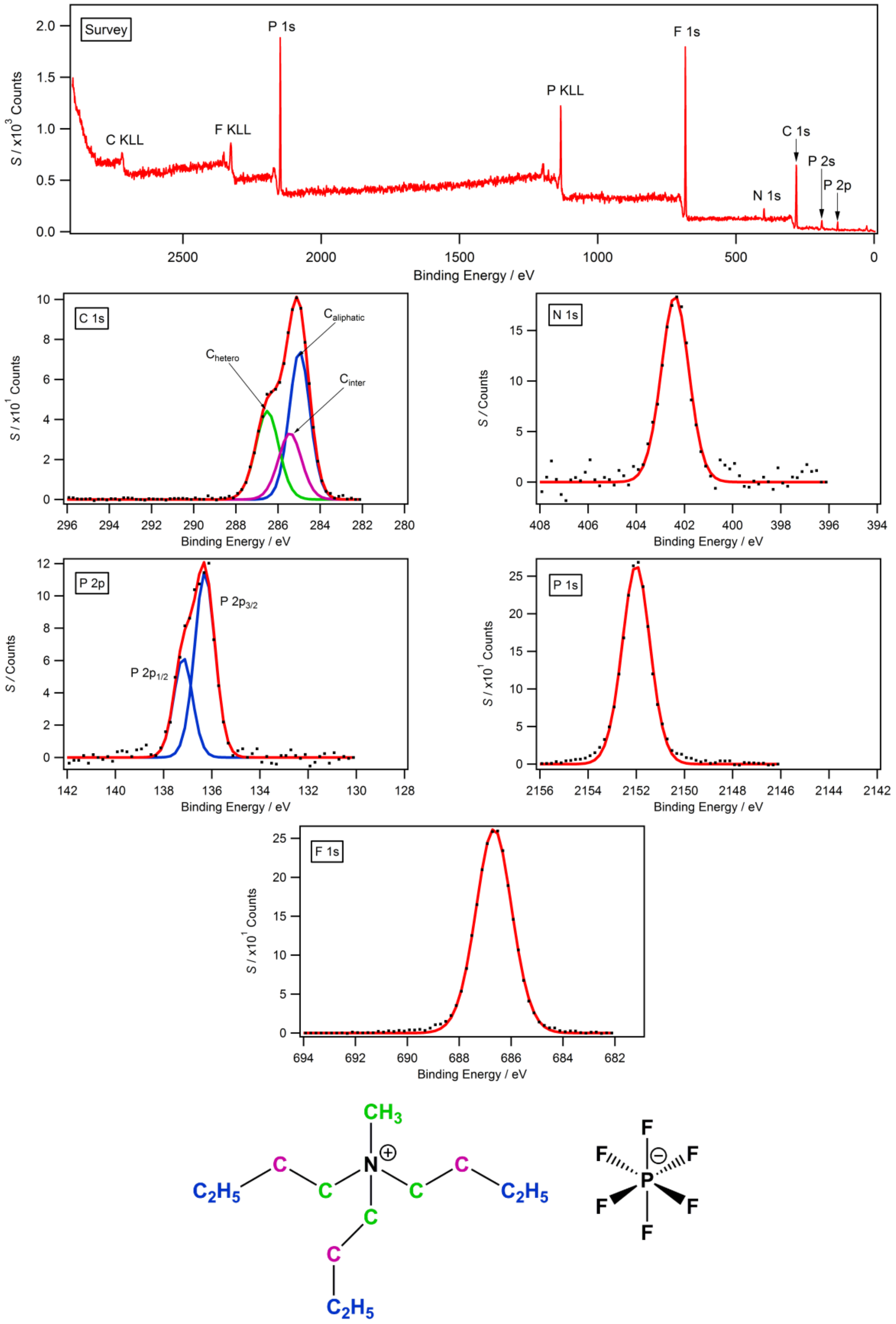

Figure B1.7. XP spectra with component fittings for [$P_{6,6,6,14}$][PF_6]. *N.B.* O 1s and Si 1s signals detected in survey scan indicating trace amount of surface contaminant present – this is likely to be the result of laboratory grease/double-sided mounting tape – and is not expected to affect the recorded binding energies. *N.B.* Reliable component fitting and binding energies could not be obtained for the P 2p region due to very poor resolution of the photoelectron peaks. This is due to the poor photoelectron flux exhibited by this compound which results in a low signal to noise ratio. Consequently, low intensity peaks (*i.e.* P 2p) are severely compromised as illustrated by the P 2p region shown below.

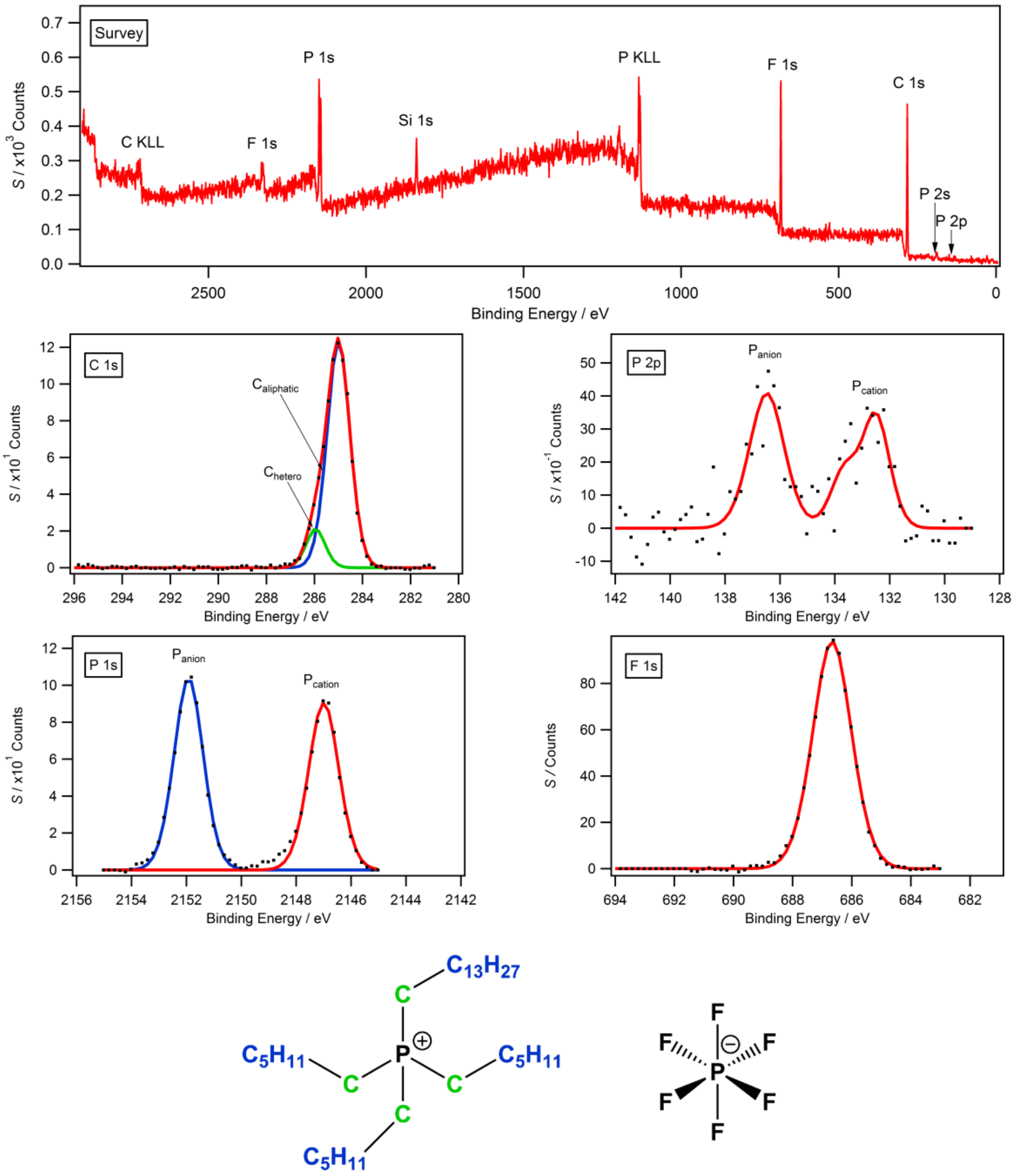

Figure B1.8. XP spectra with component fittings for [$P_{4,4,4,1}$][PF_6]. *N.B.* Reliable component fitting and binding energies could not be obtained for the P 2p region due to very poor resolution of the photoelectron peaks. This is due to the poor photoelectron flux exhibited by this compound which results in a low signal to noise ratio. Consequently, low intensity peaks (*i.e.* P 2p) are severely compromised as illustrated by the P 2p region shown below.

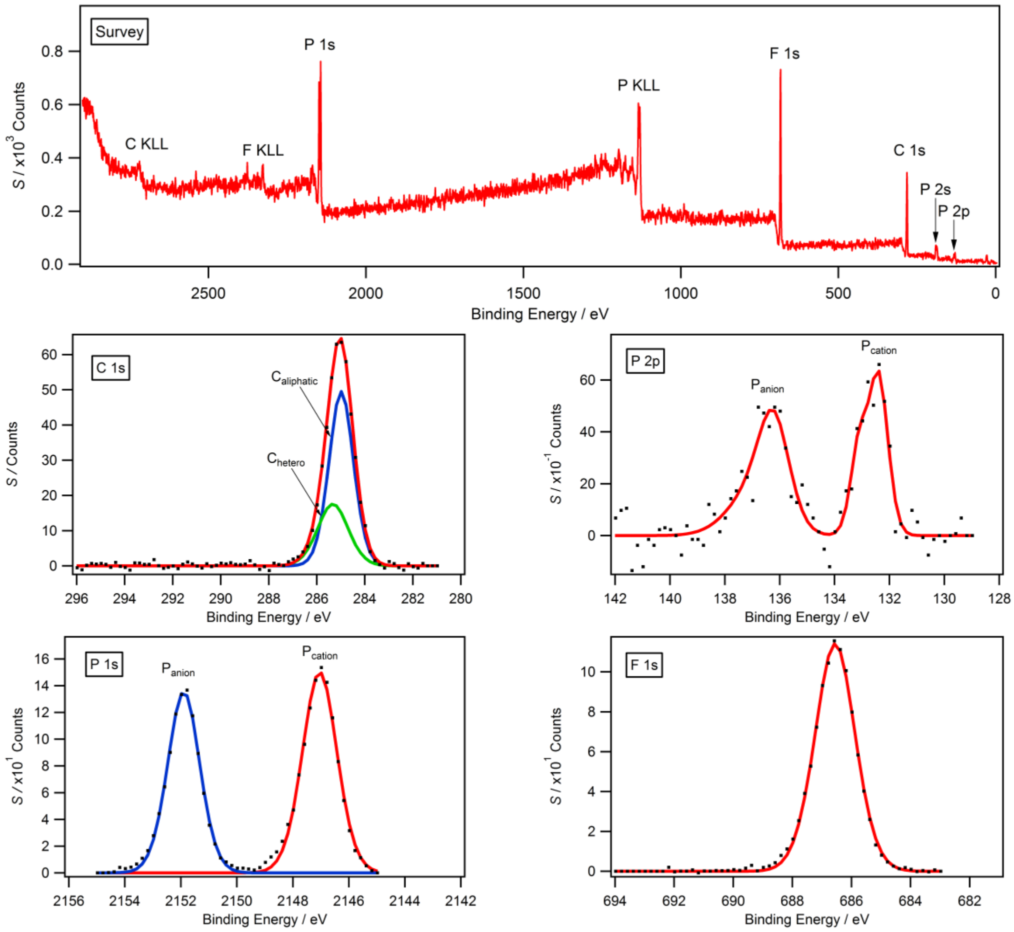

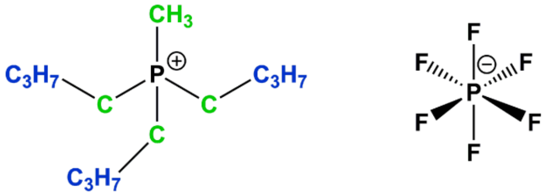

Figure B1.9. XP spectra with component fittings for [C_8C_1Pyrr][NTf_2].

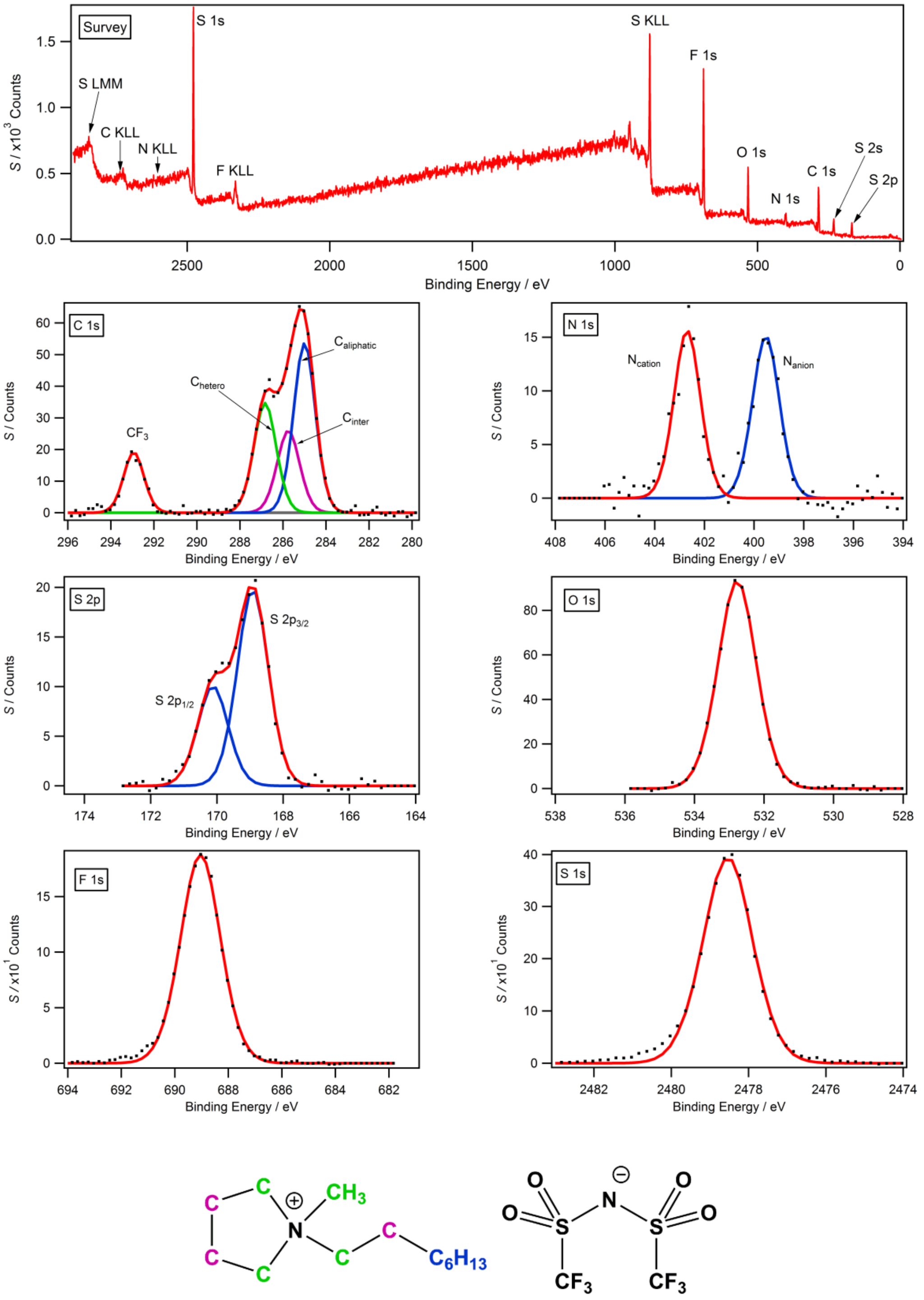

Figure B1.10. XP spectra with component fittings for $[N_{6,6,6,14}][NTf_2]$.

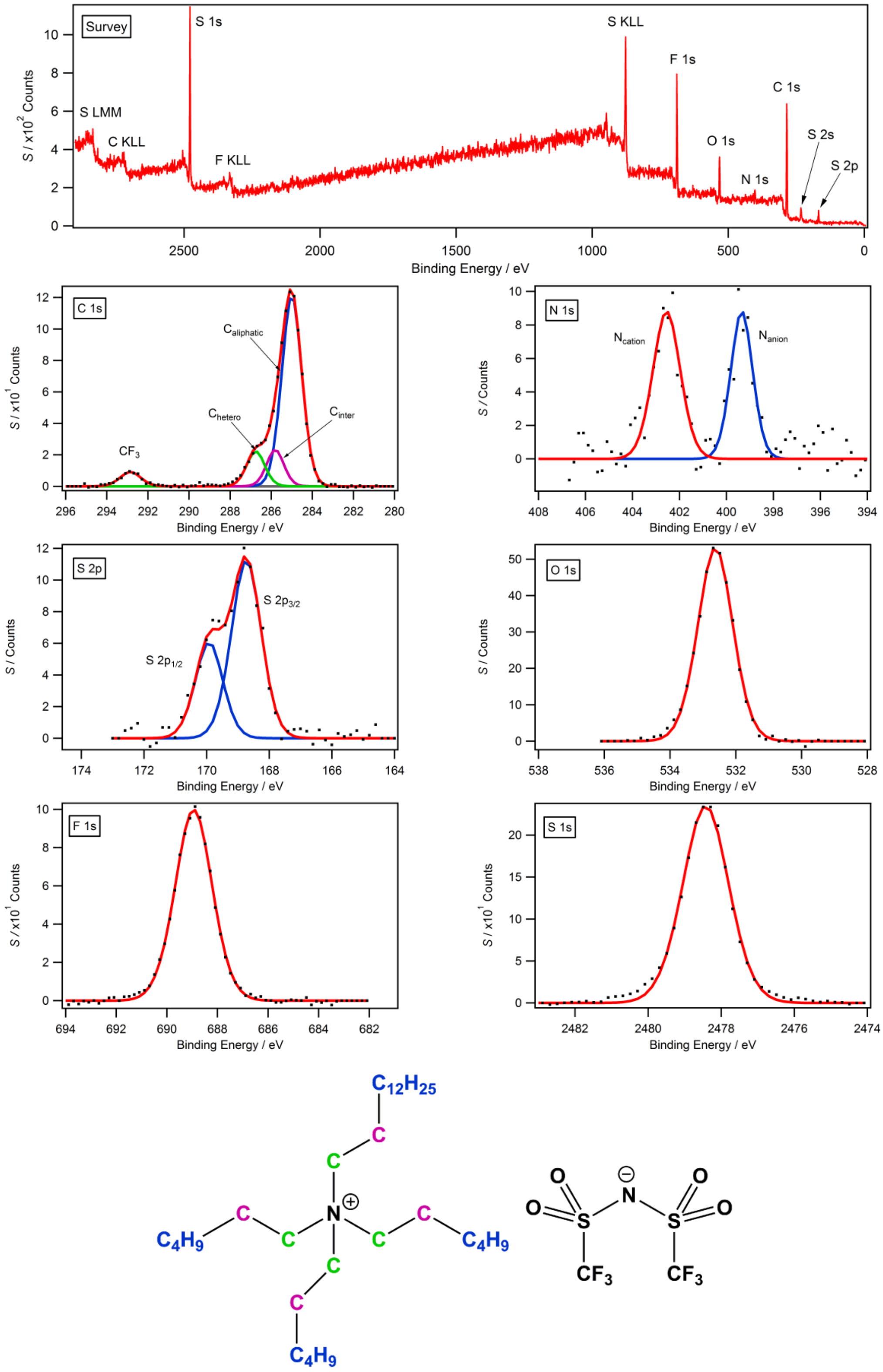

Figure B1.11. XP spectra with component fittings for [$N_{4,4,4,1}$][NTf_2].

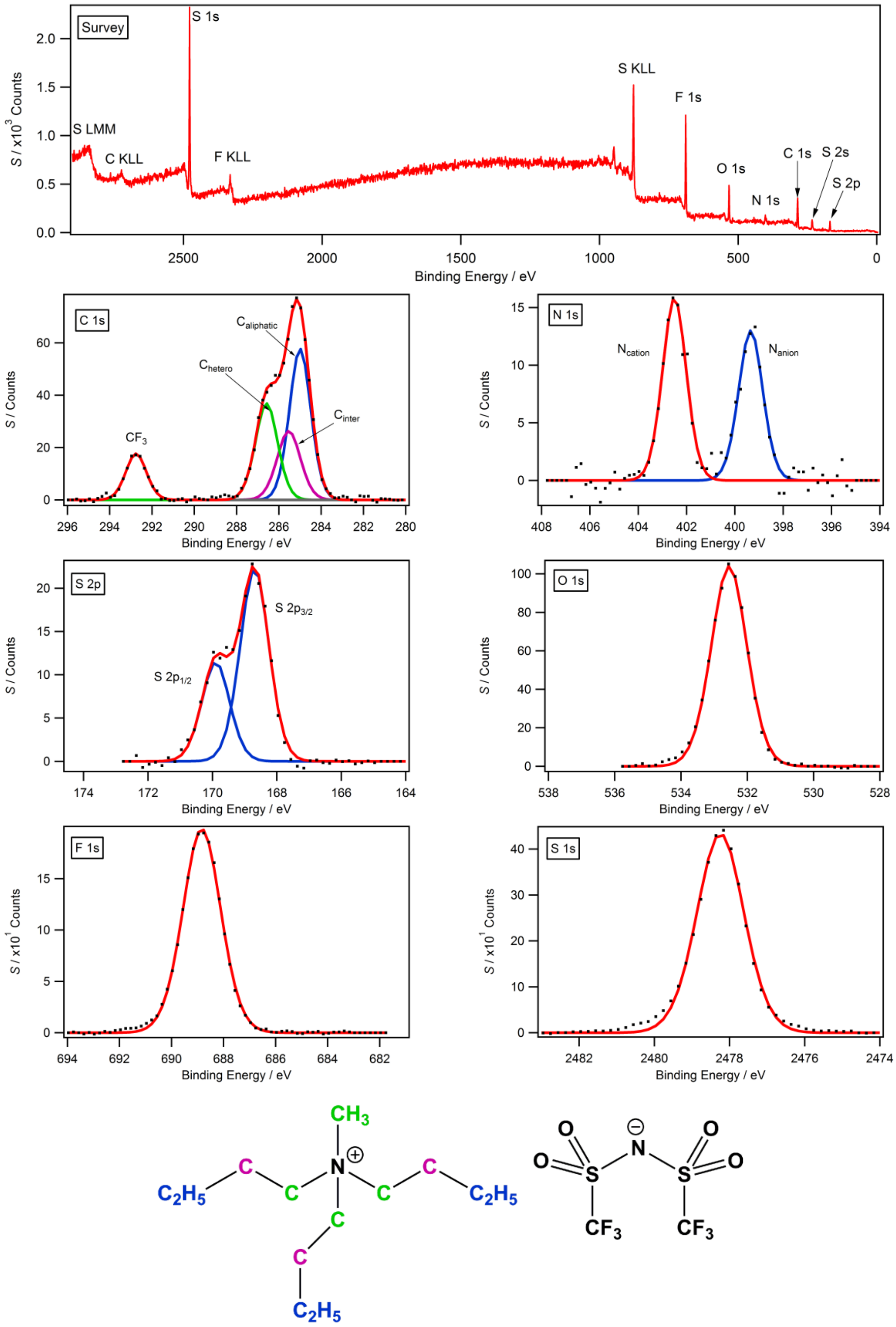

Figure B1.12. XP spectra with component fittings for [$P_{6,6,6,14}$][NTf_2].

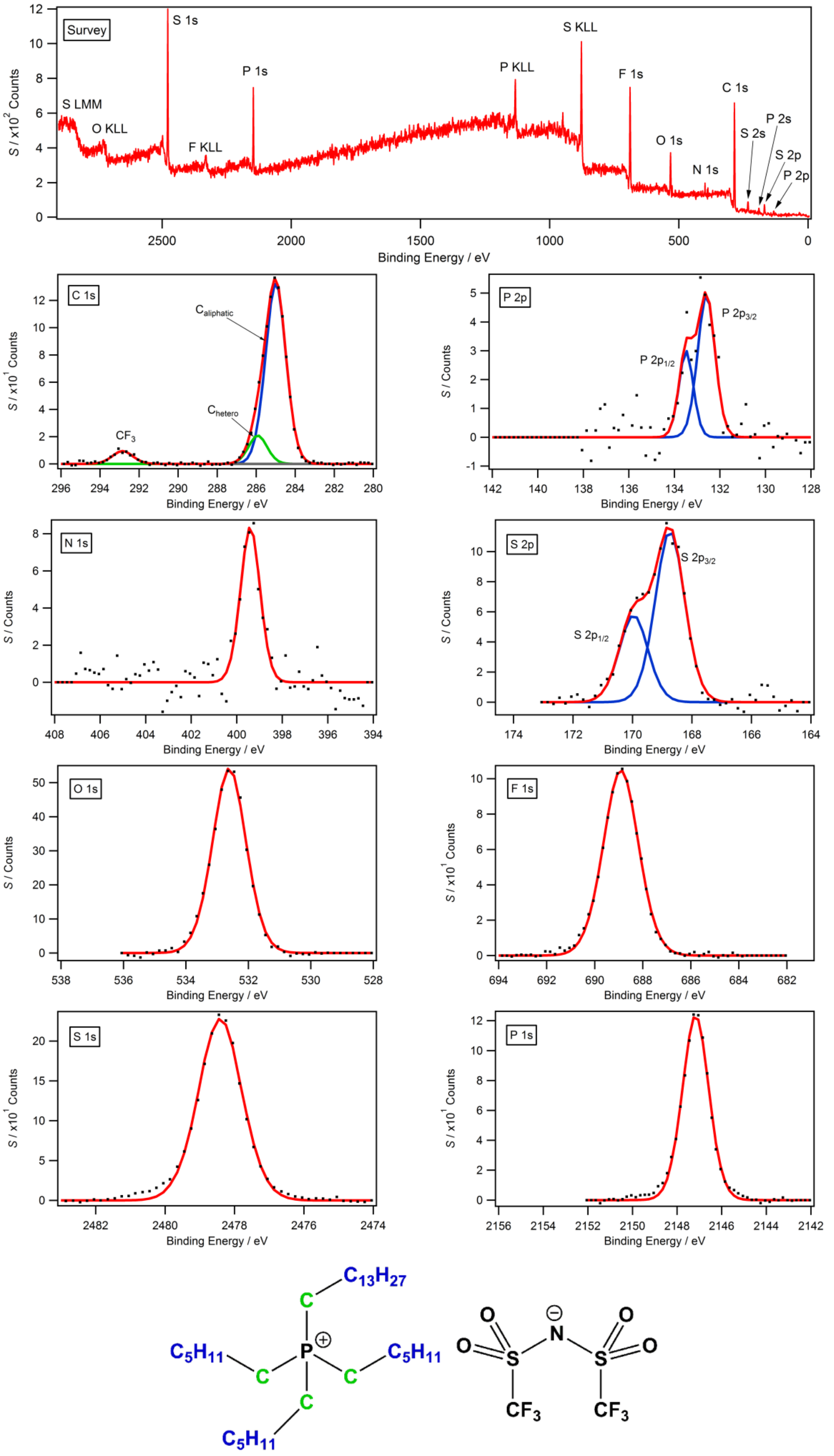

Figure B1.13. XP spectra with component fittings for [$P_{4,4,4,1}$][NTf_2].

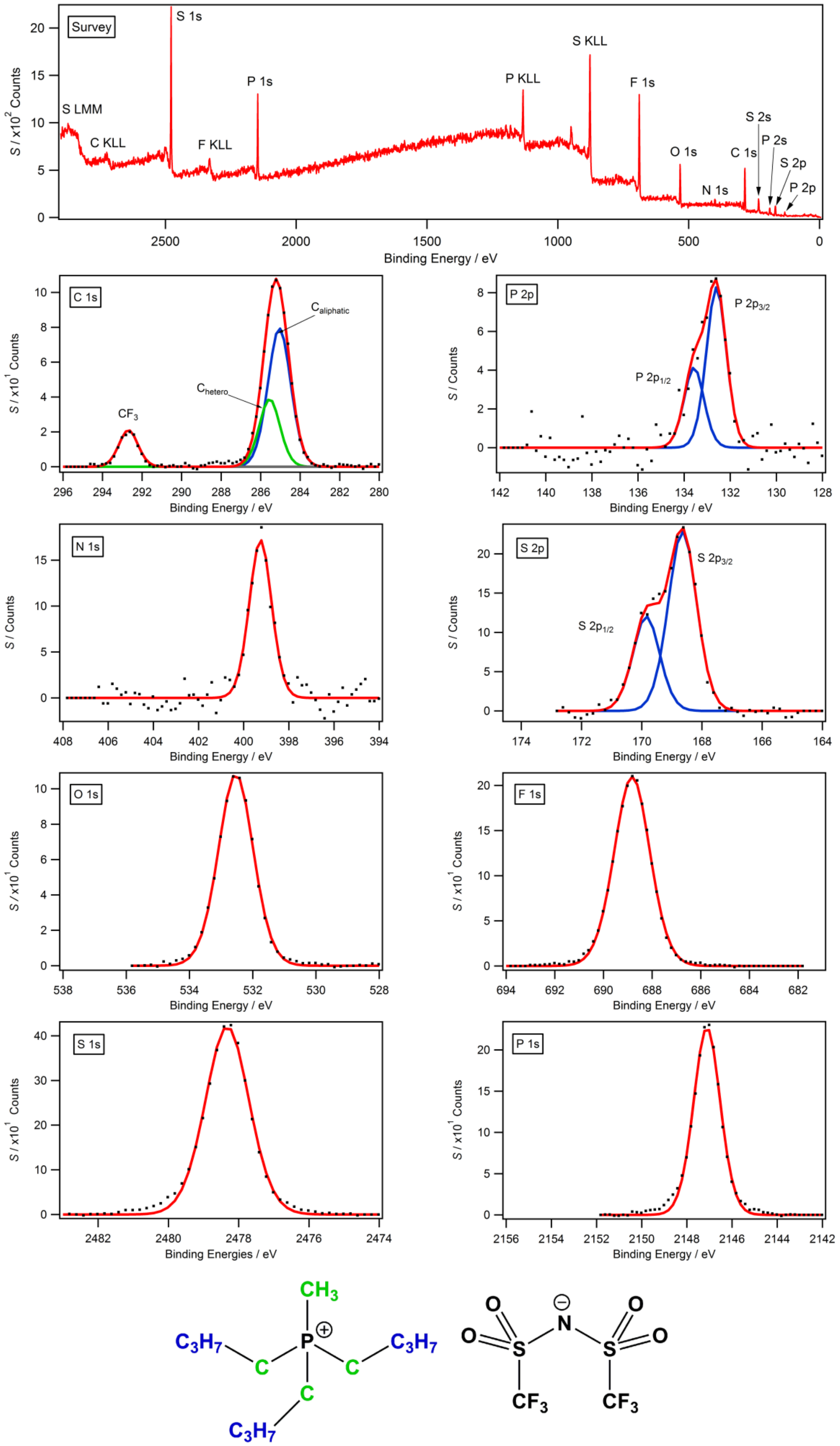

B2 XP Spectra – Al Kα X-ray source

Experimental stoichiometries, calculated from high resolution spectra, for tetraalkylammonium and tetraalkylphosphonium ILs not featured previously in *Chapter 3* are presented in Table B2.1. Experimental stoichiometries are within the typically quoted error of XPS quantification data of ± 20 %, and the majority are well within ± 10 %. As seen previously in *Chapter 3 Section 3.2.1* and *3.3.2* larger deviations are seen for the chlorine Cl 2p signal, which is associated with the small size of the chloride anion and its associated dampening from the large carbon content of the cations.

	Composition[a] (%)				
Compound	**C**	**N**	**F**	**P**	**Cl**
RSF	0.278	0.477	1.00	0.486	0.891
$[P_{4,4,4,1}]Cl$	89.2 (86.7)	-	-	5.4 (6.7)	5.3 (6.7)
$[N_{4,4,4,1}][PF_6]$	65.1 (61.9)	4.6 (4.8)	26.1 (28.6)	4.1 (4.8)	-
$[P_{4,4,4,1}][PF_6]$	67.9 (61.9)	-	23.4 (28.6)	8.7 (9.5)	-

Table B2.1. Measured experimental and nominal (in brackets) stoichiometries for ammonium and phosphonium ILs not featured previously in *Chapter 3*. [a]Relative sensitivity factors (RSFs) taken from the Kratos Library were used to derive atomic percentages from the most intense photoelectron peak for each element *i.e.* C = C 1s, N = N 1s, F = F 1s, P = P 2p and Cl = Cl 2p.

Figure B2.1. XP spectra with component fittings for [$P_{4,4,4,1}$]Cl. *N.B.* O 1s and Si 1s signals detected in survey scan indicating trace amount of surface contaminant present – this is likely to be the result of laboratory grease/double-sided mounting tape – and is not expected to affect the recorded binding energies.

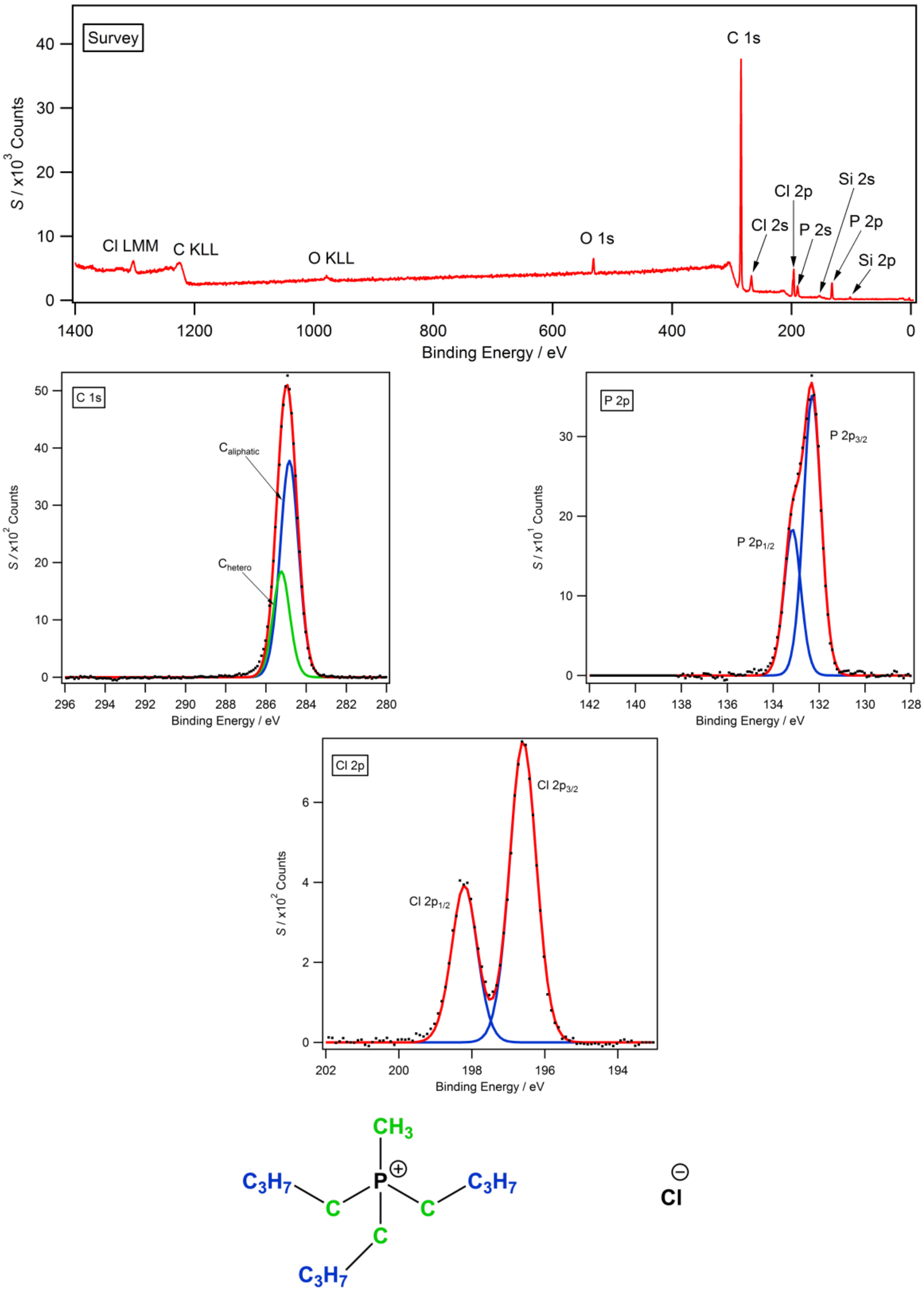

Figure B2.2. XP spectra with component fittings for $[N_{4,4,4,1}][PF_6]$. *N.B.* O 1s and Si 1s signals detected in survey scan indicating trace amount of surface contaminant present – this is likely to be the result of laboratory grease/double-sided mounting tape – and is not expected to affect the recorded binding energies.

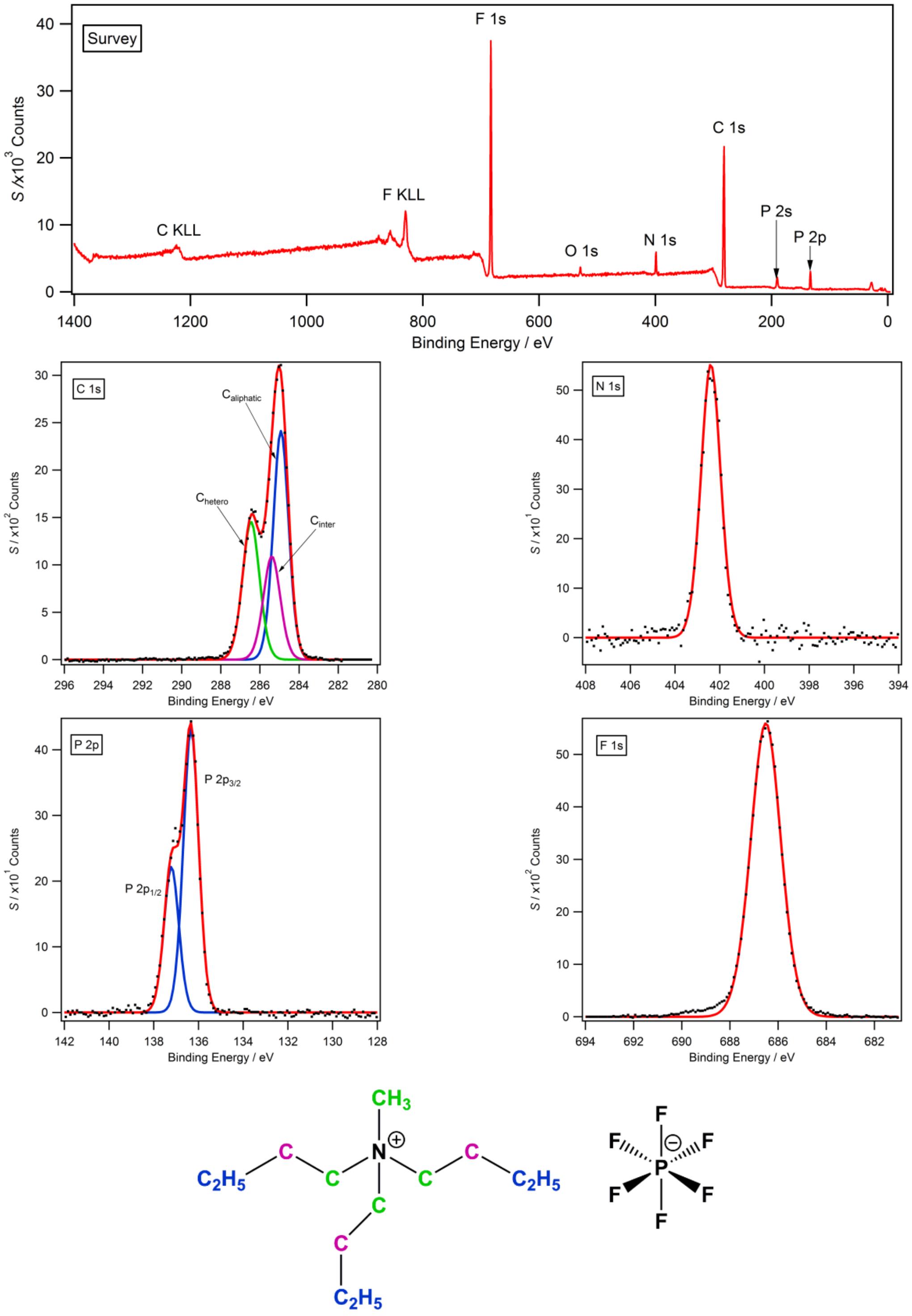

Figure B2.3. XP spectra with component fittings for $[P_{4,4,4,1}][PF_6]$. *N.B.* O 1s and Si 1s signals detected in survey scan indicating trace amount of surface contaminant present – this is likely to be the result of laboratory grease/double-sided mounting tape – and is not expected to affect the recorded binding energies

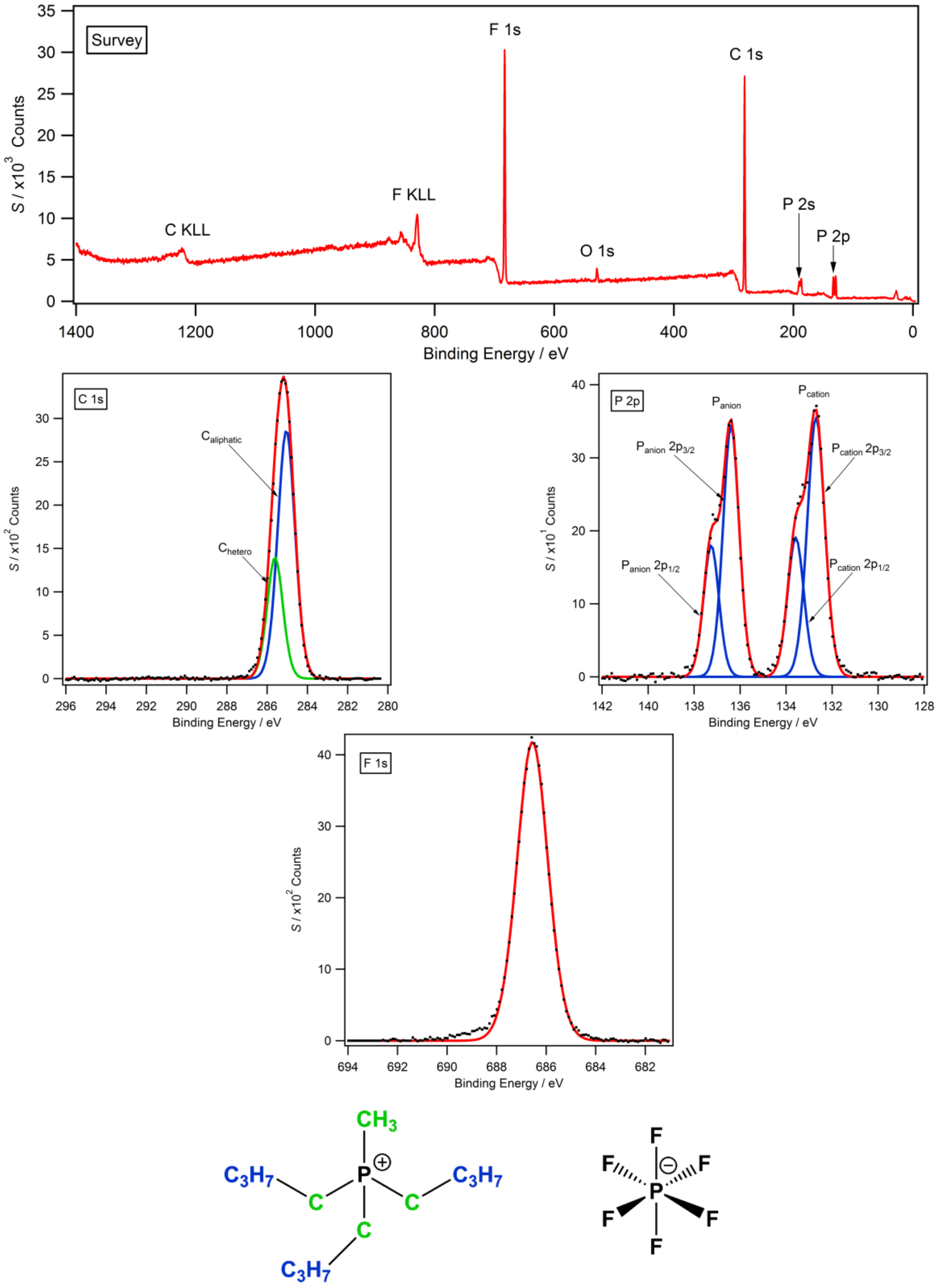

B3 Angle-resolved XP Spectra – Al Kα X-ray source

Figure B3.1. XP spectra recorded at θ = 0 and 80° for [C_8C_1Pyrr][NTf_2].

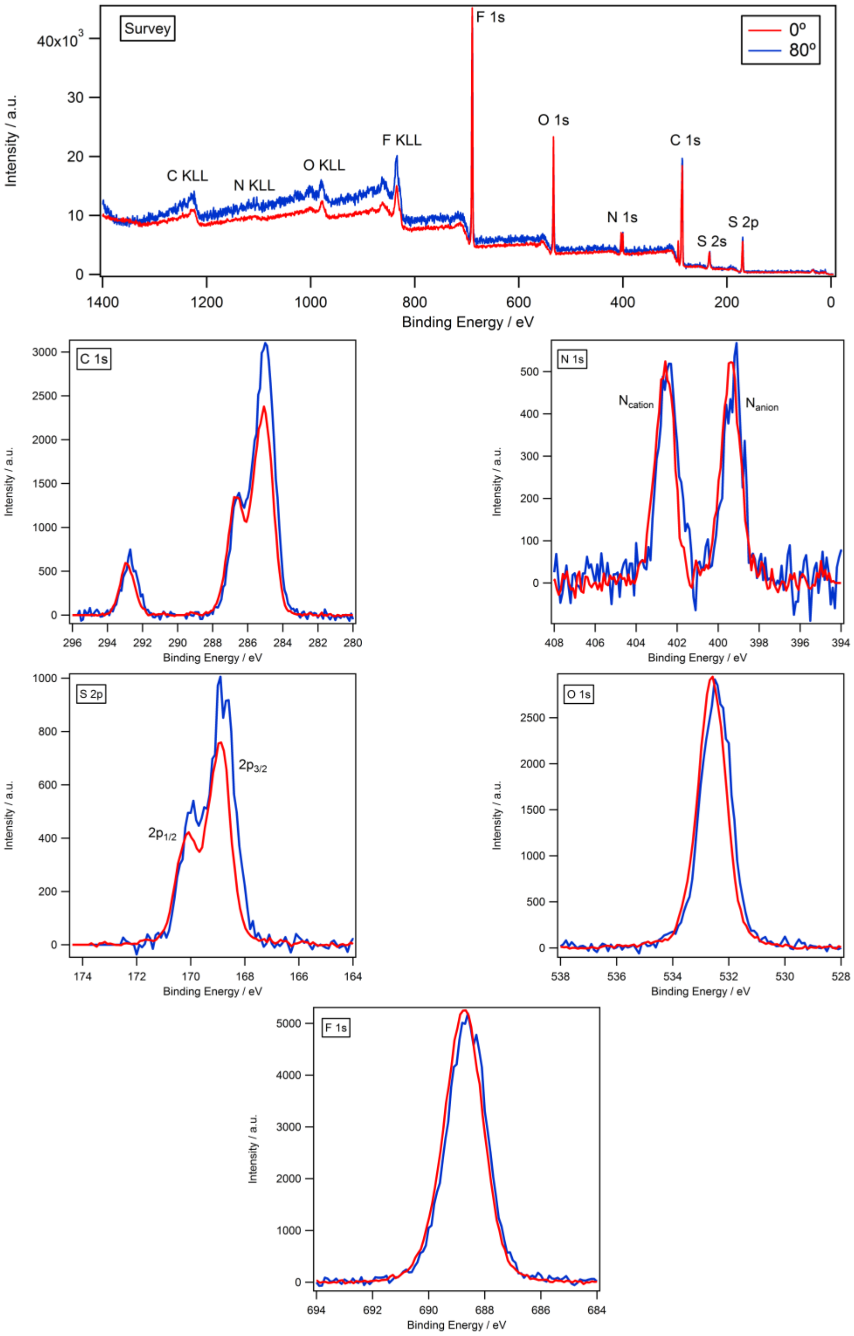

Figure B3.2. XP spectra recorded at θ = 0 and 80° for $[N_{6,6,6,14}][NTf_2]$.

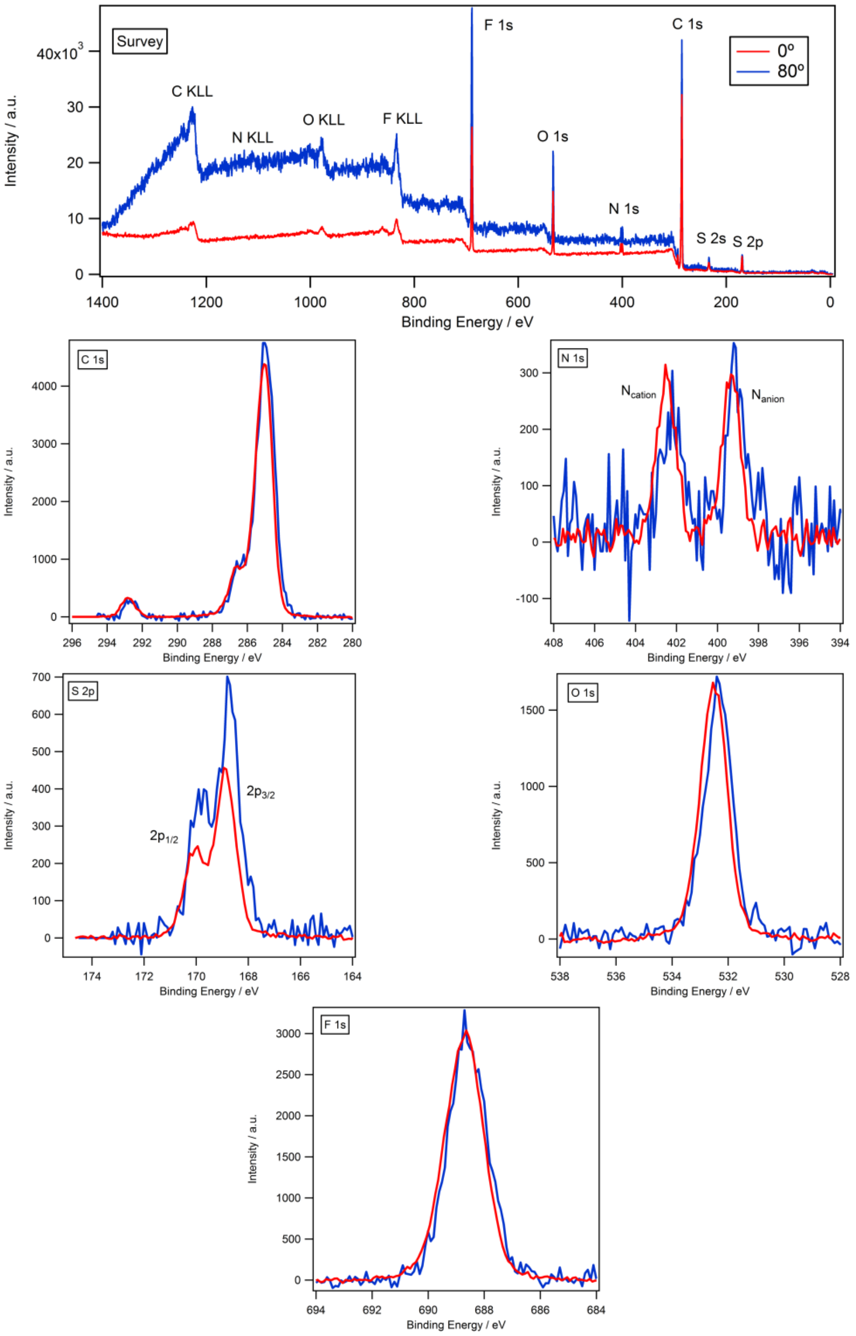

Figure B3.3. XP spectra recorded at θ = 0 and 80° for [$N_{4,4,4,1}$][NTf_2].

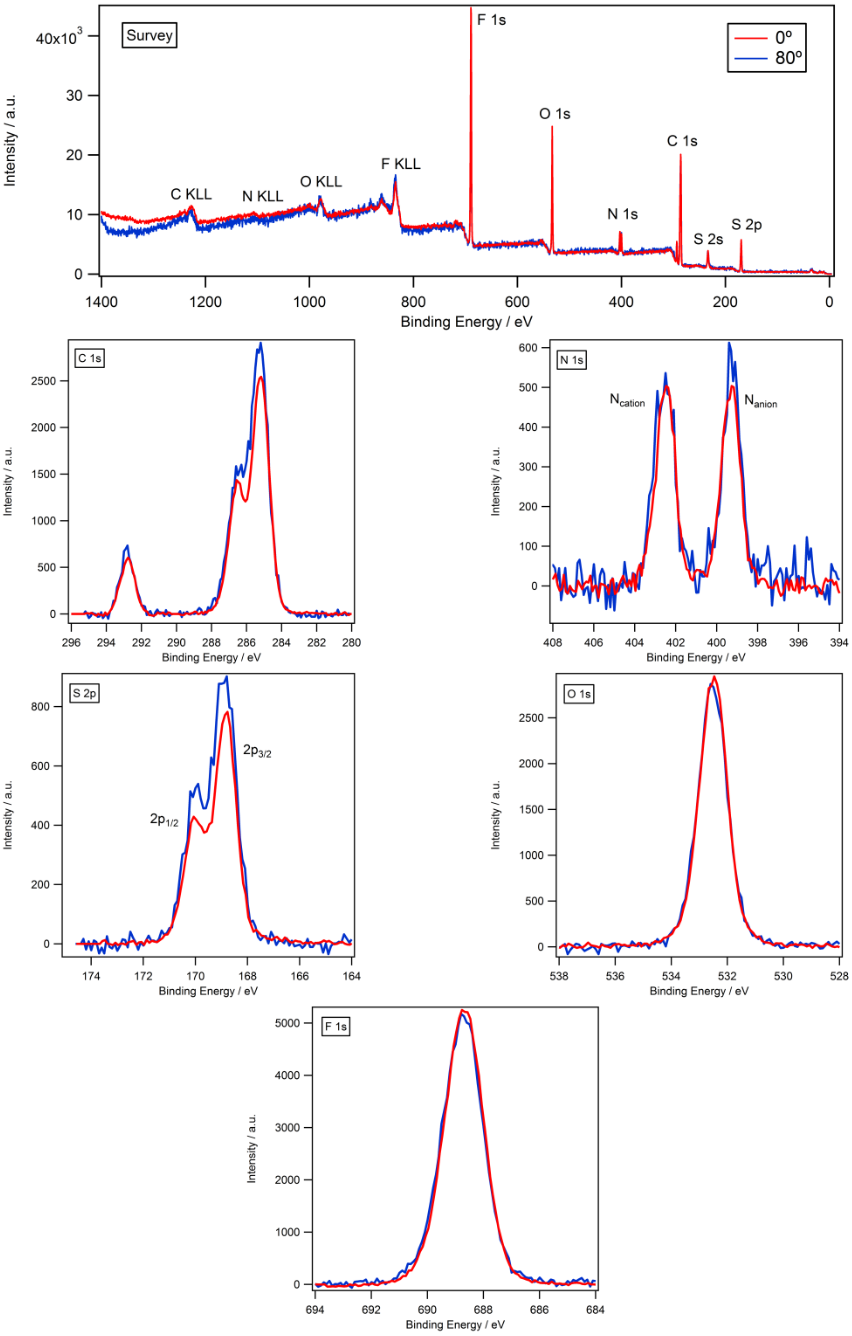

Figure B3.4. XP spectra recorded at $\theta = 0$ and 80° for $[P_{6,6,6,14}][NTf_2]$.

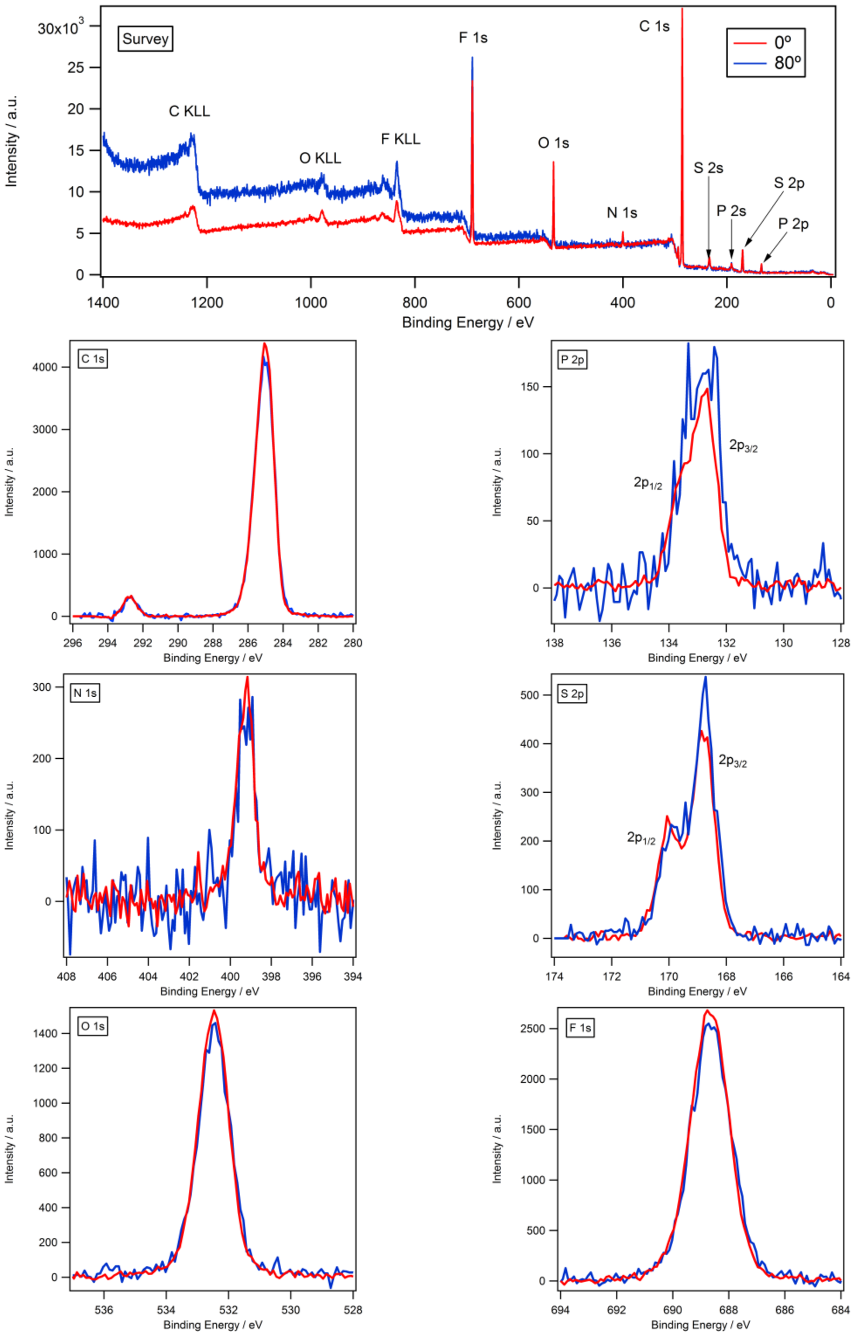

Figure B3.5. XP spectra recorded at θ = 0 and 80° for $[P_{4,4,4,1}][NTf_2]$.

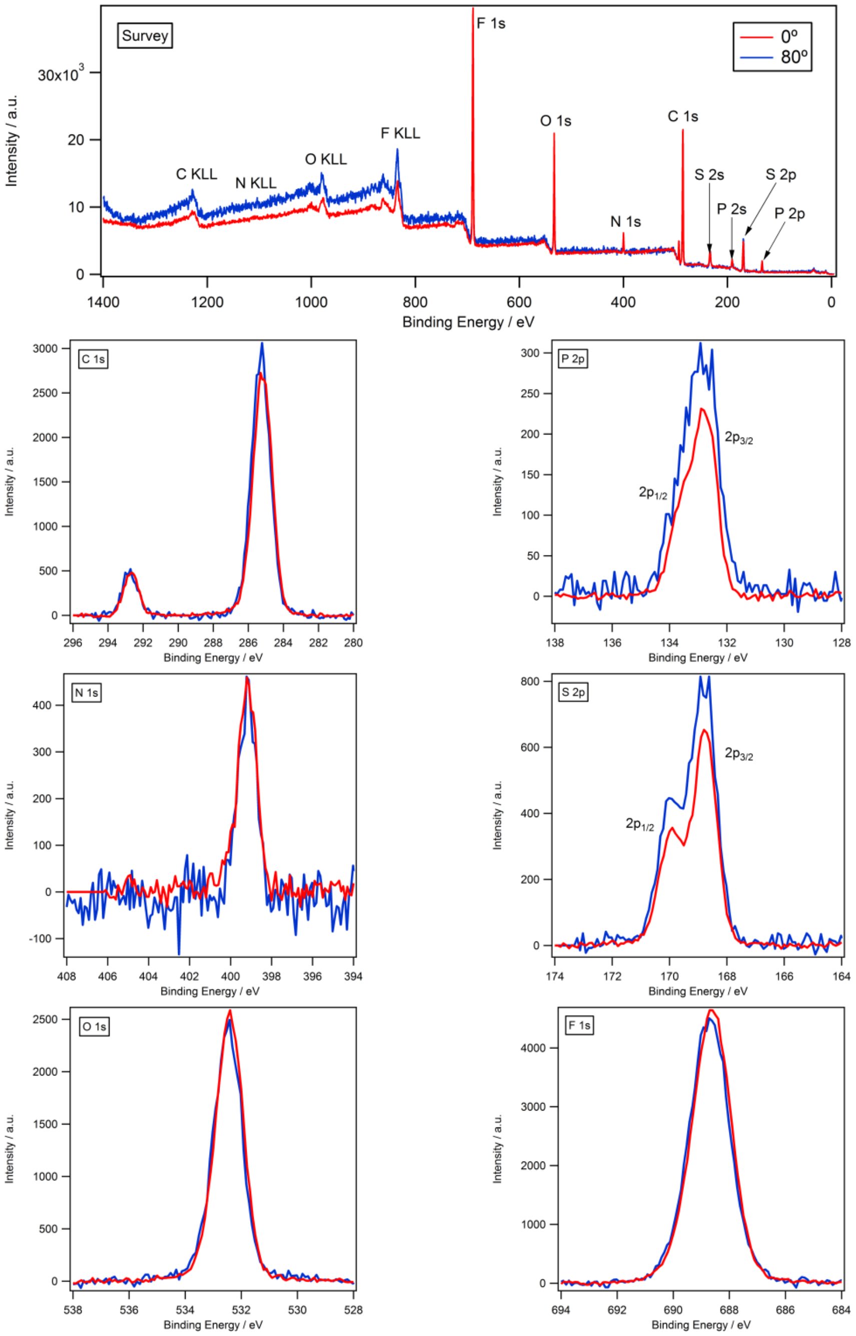

Appendix C: XP Spectra for Chapter 5

Survey and fitted high resolution spectra for neat ionic liquids studied in *Chapter 5* are presented in Figures C1.1 – C1.6. Spectra for the palladium-imidazolylidene complexes are presented in Figures C2.1 – C2.2.

C 1s high resolution spectra were fitted according to the models described within *Chapter 5*. S 2p and Pd 3d high resolution spectra were fitted taking into account spin-orbit coupling; whereby the area ratio of $2p_{1/2}$:$2p_{3/2}$ components are set to 1:2, and the area ratio of $3d_{3/2}$:$3d_{5/2}$ components are set to 2:3 respectively. The O 1s and S 2p high resolution spectra for ionic liquids containing the $[NTf_2]^-$ anion are affected by shake up/off phenomena and a 4 % intensity loss (per oxygen/sulfur atom involved in double bonding) was taken into account when calculating atomic percentages for these elements. For ionic liquids containing an imidazolium-based cation, any carbon or nitrogen atoms involved in conjugated bonding are affected by shake up/off phenomena and a respective 20 % and 12 % intensity loss is taken into account.

For non-functionalised ILs, *i.e.* $[C_8C_1Im][NTf_2]$, $[C_8C_1Pyrr][NTf_2]$ and $[N_{2,2,2,8}][NTf_2]$, spectra are charge corrected using an established internal reference method of setting the $C_{aliphatic}$ 1s component to 285.0 eV. For functionalised ILs an indirect means of charge correction is applied; in which, spectra are charge corrected by referencing the S $2p_{3/2}$ component to the value obtained for its non-functionalised analogue (for which, prior charge correction has been achieved by referencing $C_{aliphatic}$ 1s = 285.0 eV). A full description of this procedure is described within *Chapter 5*.

C1 – XP Spectra for neat ILs

Figure C1.1. XP spectra with component fittings for [C_8C_1Im][NTf_2].

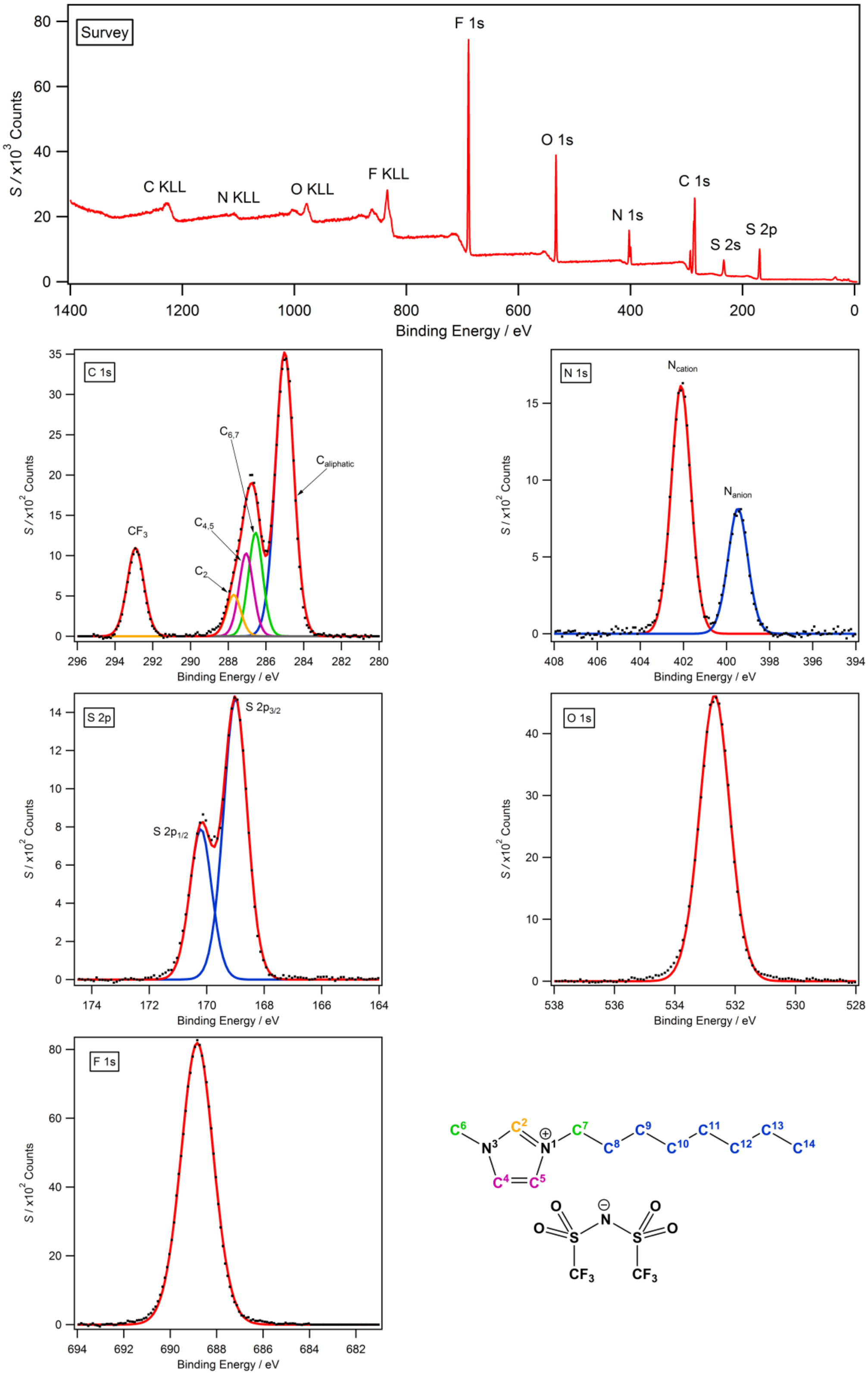

Figure C1.2. XP spectra with component fittings for [Et(PEG)$_2$MIm][NTf$_2$].

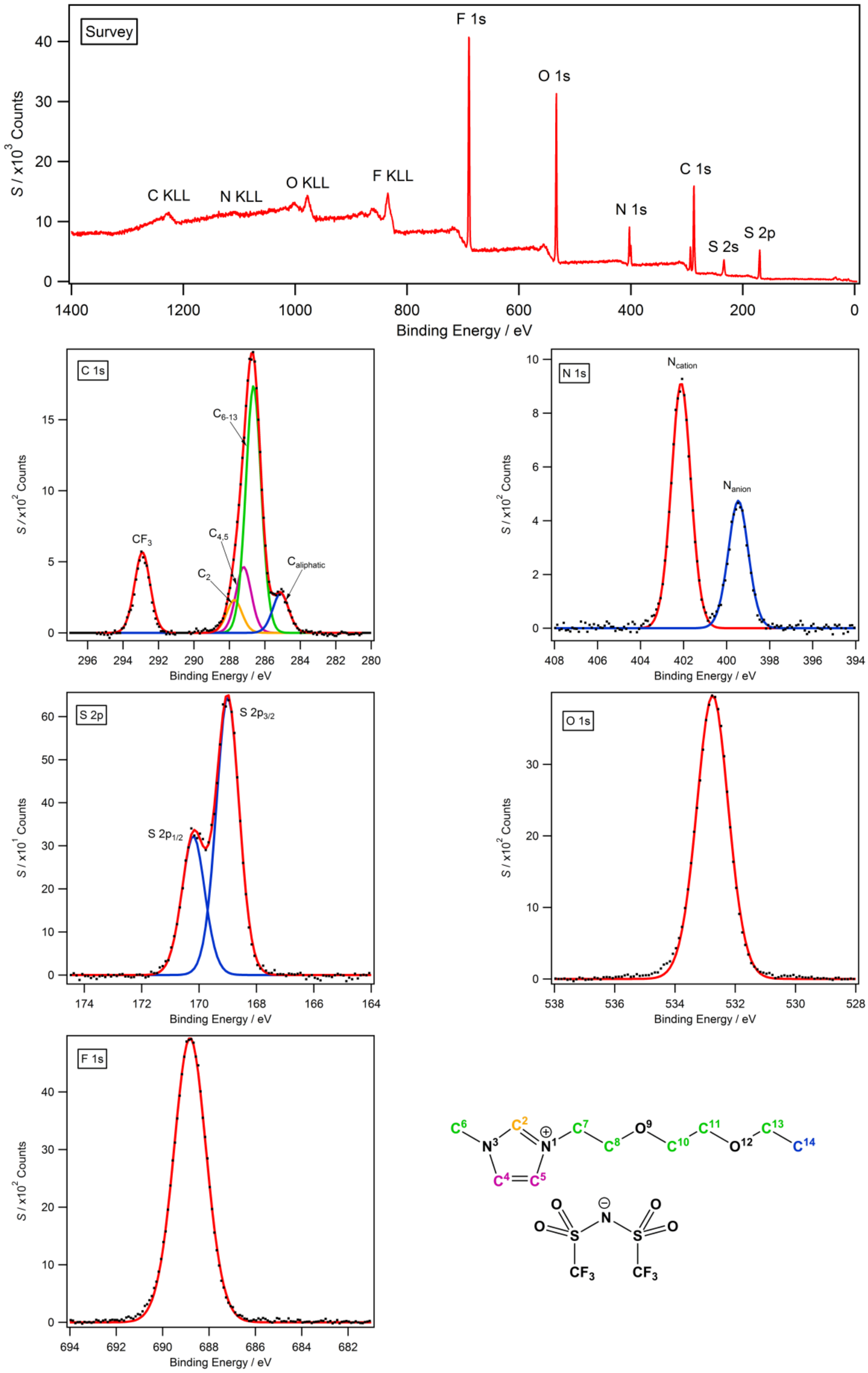

Figure C1.3. XP spectra with component fittings for [($F_{13}H_4C_8$)C_1Im][NTf_2].

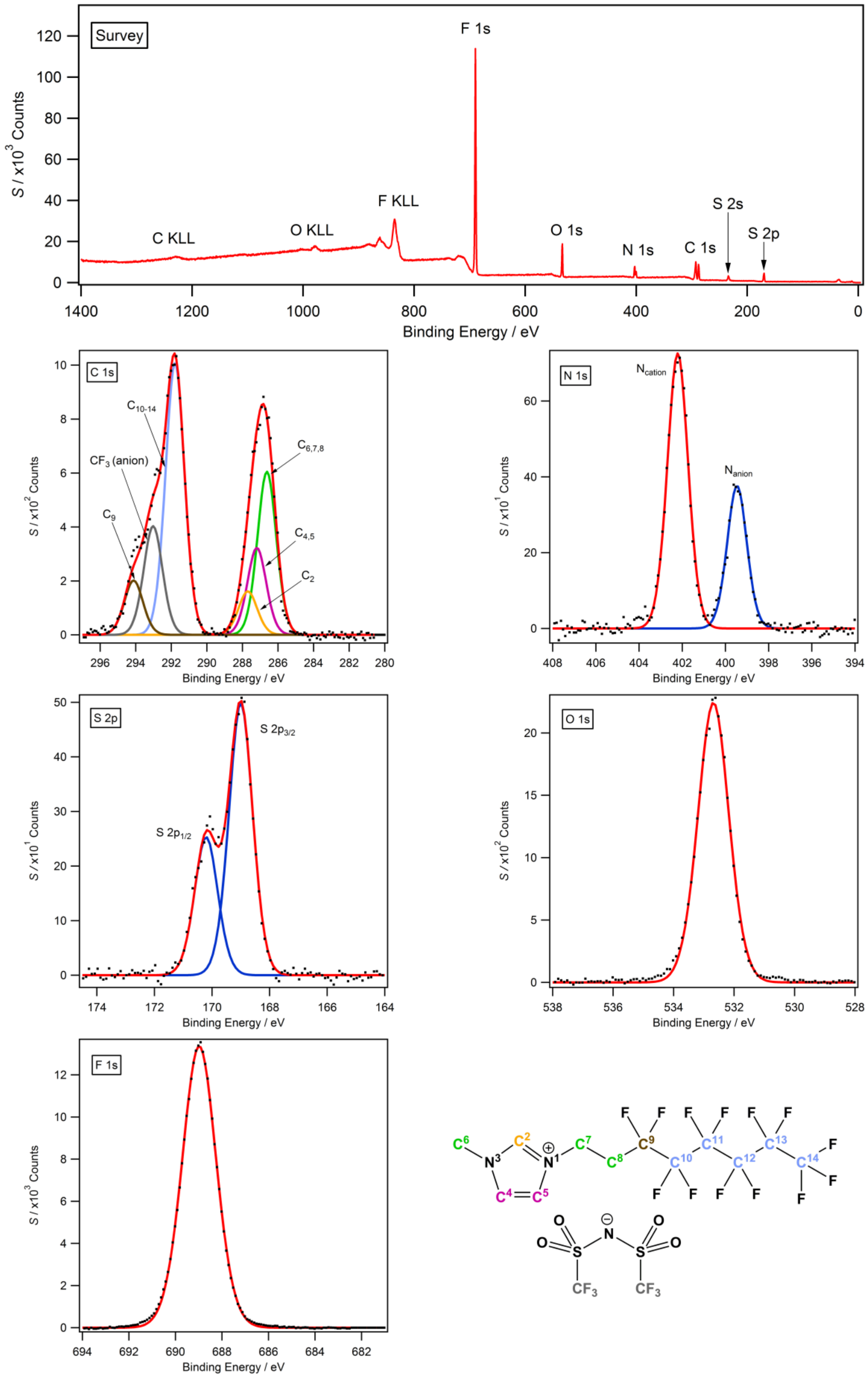

Figure C1.4. XP spectra with component fittings for [Et(PEG)$_2$MPyrr][NTf$_2$].

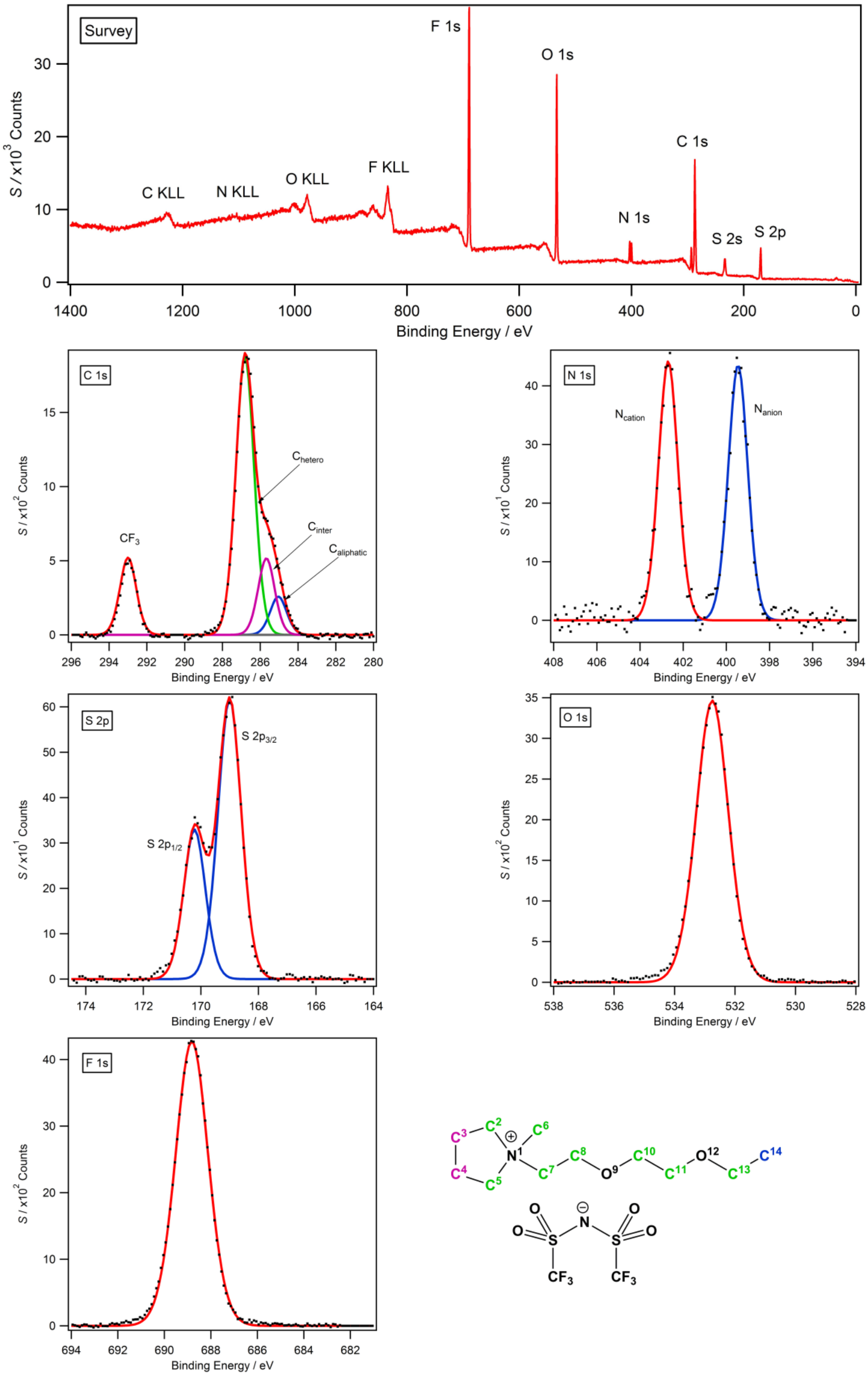

Figure C1.5. XP spectra with component fittings for $[N_{2,2,2,8}][NTf_2]$.

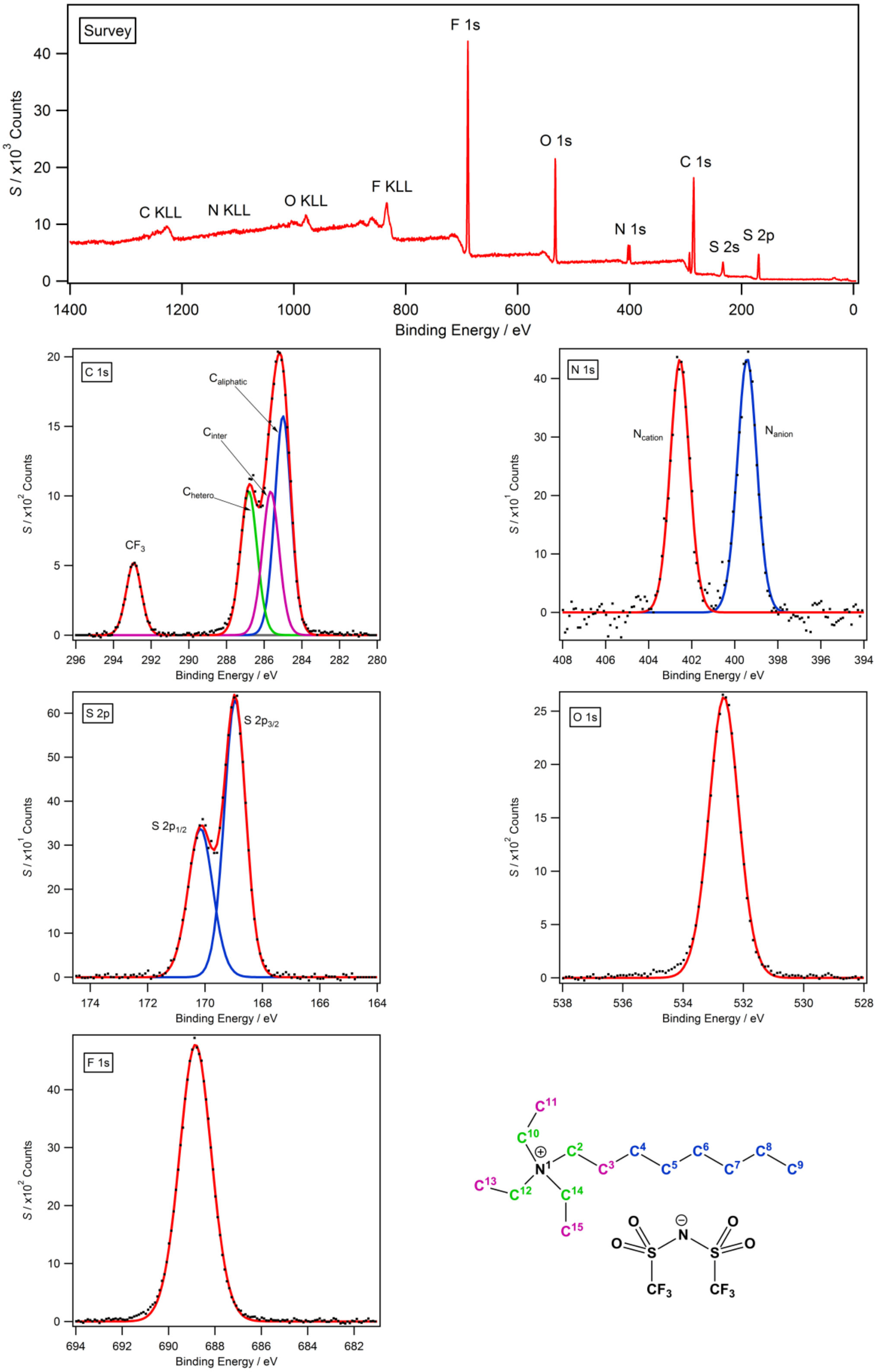

Figure C1.6. XP spectra with component fittings for [$N_{2,2,2,(Et(PEG)2)}$][NTf_2].

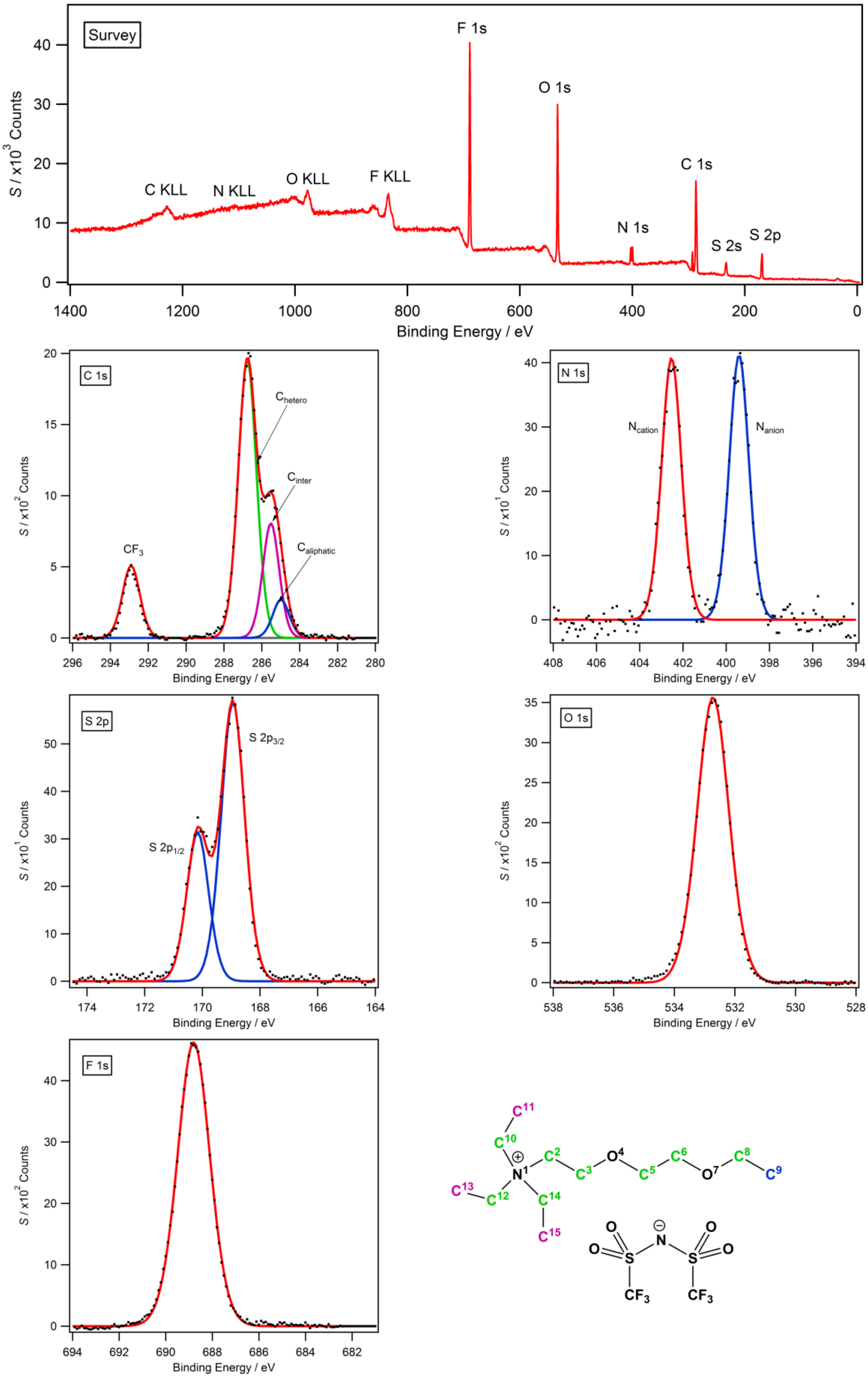

C2 – XP Spectra for palladium-imidazolylidene complexes

Figure C2.1. XP spectra for palladium-imidazolylidene complex formed in [C_8C_1Im][NTf_2]. Labelled C 1s components as for structure presented in Figure C1.1, C_{phenyl} corresponds to phenyl carbon environment present in the palladium-imidazolylidene complex.

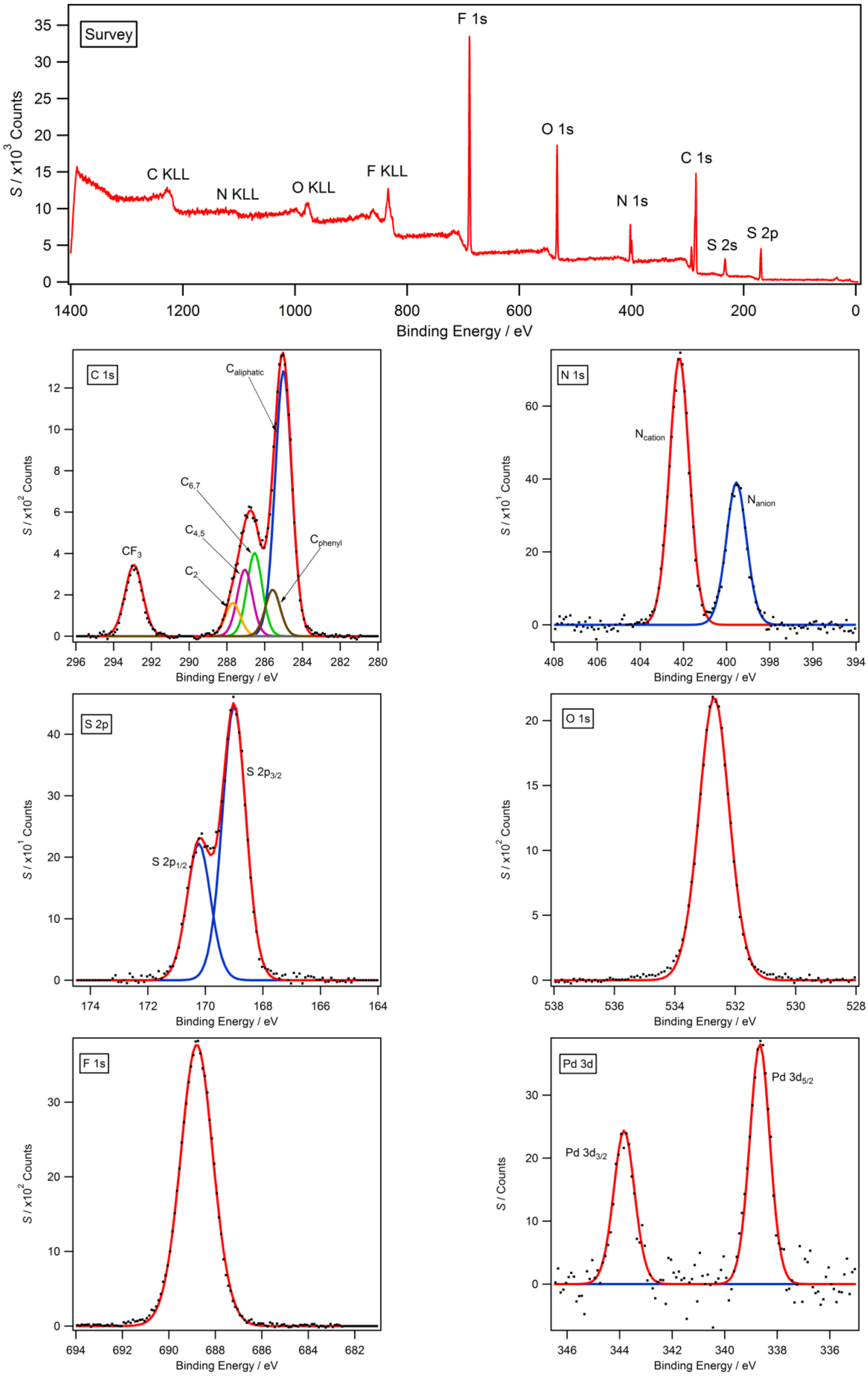

Figure C2.2. XP spectra for palladium-imidazolylidene complex formed in [Et(PEG)$_2$MIm][NTf$_2$]. Labelled C 1s components as for structure presented in Figure C1.2, C$_{phenyl}$ corresponds to phenyl carbon environment present in the palladium-imidazolylidene complex.

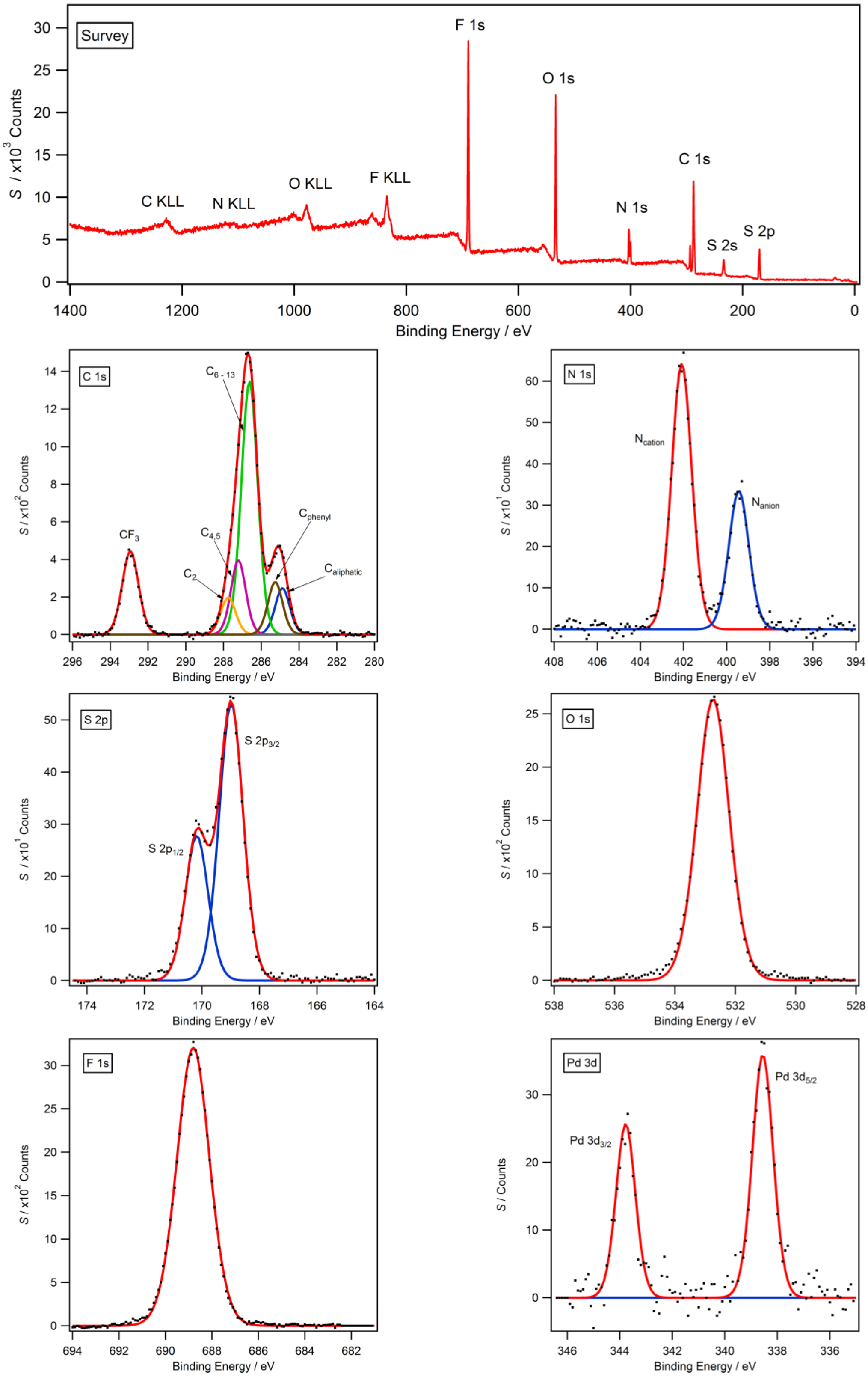

PUBLICATIONS

PCCP

PAPER

View Article Online
View Journal | View Issue

Quaternary ammonium and phosphonium based ionic liquids: a comparison of common anions†

Cite this: *Phys. Chem. Chem. Phys.*, 2014, **16**, 15278

Received 2nd May 2014,
Accepted 11th June 2014

DOI: 10.1039/c4cp01901f

www.rsc.org/pccp

Rebecca K. Blundell and Peter Licence*

A series of ammonium-based ionic liquids and their phosphonium analogues have been investigated using X-ray Photoelectron Spectroscopy (XPS). A robust C 1s peak fitting model has been developed and described for the tetraalkylphosphonium and tetraalkylammonium families of ionic liquid, with comparisons made between the two series. Cation–anion interactions have been investigated to determine the impact of changing the cationic core from nitrogen to phosphorus upon the electronic environment of the anion. Comparisons between long and short chain cationic systems are also described.

Introduction

Ionic liquids (ILs) – low temperature molten salts – have received significant interest in recent years due in part to their structural diversity.[1] By simply changing the ions, physico-chemical properties such as density, viscosity, melting point and polarity *etc.* can be tuned for specific functions. Tuning an ionic liquid to suit a specific application has attracted much interest, with this concept being taken even further by utilising mixtures of ionic liquids.[2,3] By considering binary and ternary mixtures of ionic liquids the scope for potential applications considerably broadens with some examples already shown in lithium ion batteries,[4] CO_2 absorption,[5] gas chromatography stationary phases,[6] and heavy metal extraction[7] to name but a few. The ability to predict and fine-tune the properties of an ionic liquid to meet a specific requirement is one of the greatest challenges in the field, and yet if fully achieved would provide an invaluable tool. To predict the behaviour for any given ionic liquid it must first be understood on a molecular level, where changes to the chemical architecture and its effect upon cation–anion interactions must be explored both theoretically and experimentally.

Over the past ten years X-ray photoelectron spectroscopy (XPS) has established itself as a robust technique to characterise ionic liquid-based systems.[8] To date the majority of investigations using this technique have focused upon nitrogen-based cations, particularly dialkylimidazolium systems.[8,9] XPS can be used to identify different electronic environments present for each element, as well as the determination of chemical composition and purity. So far, XPS of IL-systems has provided a wealth of information in areas such as bulk and surface composition,[10,11] *in situ* reaction monitoring,[12] and cation–anion interactions.[13] Cation–anion interactions, in particular, have only so far been investigated for imidazolium and pyrrolidinium cations, where the effect of the anion upon the electronic environment of the cation has been explored.[13,14] Correlations of these results to NMR spectroscopy, theoretical calculations and Kamlet–Taft parameters have also been achieved.[13] Furthermore, XPS has also been used to monitor the electronic environment of the constituent atoms for a binary IL mixture where the mole fraction of the anionic constituents are systematically varied, thus highlighting how changes in the anionic composition of IL mixtures can be used to tune the electronic environment of their constituents.[15]

A particularly interesting sub-set of ionic liquids are those based upon a tetraalkylphosphonium cation; research into these compounds has often been neglected in favour of their nitrogen-based counterparts with particular emphasis on the imidazolium and pyrrolidinium cations.[16] This is likely due to the high cost and air-sensitive nature of the trialkylphosphine starting materials; nevertheless, it has been observed that tetraalkylphosphonium-based ionic liquids can offer superior physico-chemical properties in comparison to their nitrogen-based relatives.[16–18] Furthermore, there are only a few systematic studies that directly investigate the effect of changing the central cationic heteroatom from nitrogen to phosphorus, *i.e.* tetraalkylammonium *versus* tetraalkylphosphonium.[19–23] It has been observed that changing the cationic centre from nitrogen to phosphorus has a marked effect upon the physico-chemical properties of ILs;[23] however, little is known about fundamental cation–anion interactions of such systems. The work described herein utilises XPS to probe these interactions for ILs in which the cation is varied (tetraalkylammonium *versus* tetraalkylphosphonium) for the

---

The GlaxoSmithKline Carbon Neutral Laboratory, School of Chemistry, The University of Nottingham, Nottingham NG7 2RD, UK.
E-mail: peter.licence@nottingham.ac.uk; Tel: +44 (0)115 8466176

† Electronic supplementary information (ESI) available. See DOI: 10.1039/c4cp01901f

same anion to examine the influence of the cationic heteroatom upon the electronic environment of the anion, with an aim to determine if a degree of tunability can be achieved *via* the cation.

The most important output from XPS analysis are binding energies; these provide both elemental and chemical information. Small changes in the electronic environment of an element by, for example, a change in chemical bonding or oxidation state will cause a shift in the measured binding energy much like the chemical shift in NMR spectroscopy. This allows both chemical structure and inter-ion interactions to be probed on a molecular level providing vital information on the impact of structural changes upon electronic environment and communication between ions. Accordingly, it is of great importance to obtain reliable and reproducible binding energies and a number of factors must be considered. Firstly, the possibility of surface charging must be taken into account. Ionic liquids in the solid state are poor conductors and charge neutralisation must be applied. Ionic liquids in their liquid state, however, are moderately conducting and can dissipate excess charge on the sample surface, thus charge neutralisation is not necessary. Despite this, it has been observed for imidazolium ionic liquids that surface charging can occur over time especially for viscous samples, causing subtle yet measurable shifts in binding energy.[24]

Secondly, charge correction must be applied using a suitable internal reference post data collection to ensure binding energies obtained are accurate and allow for reliable comparison between samples, a thorough description of charge correction methods for IL systems has recently been reported.[24]

Finally, development of fitting models to describe and deconstruct the electronic environment for each element is particularly important. This is especially relevant to carbon, which has been described as the most important core level for XPS of ILs.[8] Due to the variety and complexity in structure of ILs, C 1s fitting models must be developed on a case-by-case basis, with the aim of developing a fitting model that deconstructs these electronic environments into the minimum number of components possible.[8,14]

In this work we report an investigation into the XP spectra for seven tetraalkylphosphonium-based ionic liquids with comparison to their tetraalkylammonium analogues, see Table 1. The high purity of each sample is confirmed with a description of binding energies and multi-component fitting models. Furthermore, a robust C 1s peak fitting model has been developed and described for both the tetraalkylphosphonium and tetraalkylammonium families of ionic liquid. Cation–anion interactions have been probed by investigating: (1) the effect of varying the anion upon the cation for both families of ionic liquid; (2) the effect of varying the cationic core from phosphorus to nitrogen for a variety of different anions. Comparisons are also made between small and long alkyl chain systems.

Table 1 Structures and abbreviations of cations and anions investigated in this study, chloride anions were also studied

Abbreviation	Structure	Name
$[P_{6,6,6,14}]^+$	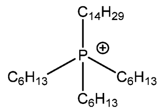	Trihexyl(tetradecyl)phosphonium
$[N_{6,6,6,14}]^+$	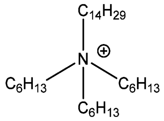	Trihexyl(tetradecyl)ammonium
$[P_{4,4,4,1}]^+$	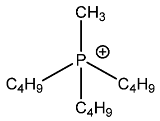	Tributyl(methyl)phosphonium
$[N_{4,4,4,1}]^+$	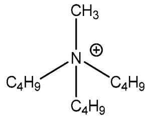	Tributyl(methyl)ammonium
$[BF_4]^-$	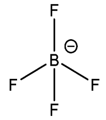	Tetrafluoroborate
$[PF_6]^-$	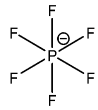	Hexafluorophosphate
$[OTf]^-$	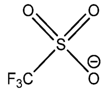	Trifluoromethanesulfonate
$[NTf_2]^-$	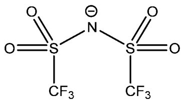	Bis(trifluoromethanesulfonyl)imide

Experimental

Materials

All compounds investigated herein were prepared in our laboratory using modified literature procedures.[25] A full description of each chemical synthesis is provided within the ESI.† Chemical precursors were obtained from commercial suppliers and used without further purification unless otherwise stated. Trihexyl(tetradecyl)phosphonium chloride (Cyphos IL 101) and tributyl(methyl)phosphonium methyl sulfate (Cyphos IL 108) were obtained from Cytec Industries Inc. The structures of the compounds investigated in this study are shown in Table 1. All compounds were dried *in vacuo* ($p \leq 10^{-2}$ mbar) at 50 °C and stored under argon before being fully characterised by ^1H, ^{13}C, ^{31}P and ^{19}F NMR (recorded at room temperature on a Bruker DPX-400 MHz spectrometer); IR (Perkin Elmer 1600 FT spectrometer); ESI-MS (Bruker MicroTOF 61 spectrometer) and XPS (Kratos Axis Ultra spectrometer). For syntheses which involved anion exchange chemistries, ion chromatography (Dionex ICS-3000, IonPack AS15, 4 × 250 mm analytical column) showed that residual halide was below the detection limits of the instrument (<10 ppm). Full data, including XPS spectra with peak deconstruction models, for all compounds investigated are provided within the ESI.†

XPS data collection

XP spectra were recorded using a Kratos Axis Ultra spectrometer employing a focused, monochromated Al Kα source ($h\nu$ = 1486.8 eV), hybrid (magnetic/electrostatic) optics, concentric hemispherical analyser, and a multi-channel plate and delay line detector (DLD) with an X-ray incident angle of 30° and a collection angle of 0° (both relative to the surface normal). X-ray source was operated at 10 mA emission current and 12 kV anode potential. All spectra were recorded using an entrance aperture of 300 × 700 mm with pass energy of 80 eV for survey scans and 20 eV for high resolution scans. The instrument sensitivity was 7.5 × 10^5 counts s^{-1} when measuring the Ag $3d_{5/2}$ photoemission peak for a clean Ag sample recorded at pass energy of 20 eV and 450 W emission power. Ag $3d_{5/2}$ full width at half maximum (FWHM) was 0.55 eV for the same instrument settings. Binding energy calibration was made using Au $4f_{7/2}$ (83.96 eV), Ag $3d_{5/2}$ (368.21 eV) and Cu $2p_{3/2}$ (932.62 eV). Charge neutralisation (used for solid samples only) was applied using a standard Kratos charge neutraliser consisting of a filament, coaxial with the electrostatic and magnetic transfer lenses, and a balance plate which creates a potential gradient between the neutraliser and sample. Charge neutralisation was applied at 1.9 A filament current and 3.3 V balance plate voltage. Sample stubs were earthed *via* the instrument stage using a standard BNC connector.

The preparation method for each sample was dependent upon the nature of the material to be analysed. Liquid samples were prepared by placing a small drop (≈10 mg) of ionic liquid onto a stainless steel multi-sample bar; solid samples were fixed to the bar using double-sided adhesive tape. All samples were pre-pumped in a preparative chamber to pressures lower than 1 × 10^{-6} mbar before transfer into the main analytical chamber.

Surface contaminants such as oxygen and silicon were removed *via* argon ion bombardment using a Kratos Minibeam III ion gun using a sputter energy of 4 kV for three minutes. Solid samples that required argon bombardment were prepared by placing a small amount of solid in a stainless steel powder stub, then heating the sample until melted, followed by argon bombardment. Surface cleaning by argon bombardment was effective for all of the compounds investigated, where necessary, excluding $[N_{6,6,6,14}][Cl]$ and $[N_{4,4,4,1}][BF_4]$ where irreparable damage to the sample occurred.

XPS data analysis

Data was analysed using the CASAXPS software. Relative sensitivity factors (RSF) were taken from the Kratos Library (RSF of F 1s = 1) and used to determine relative atomic percentages from high-resolution scans of the most intense photoelectron peak for each element. Peak areas were measured after performing a two-point linear or Shirley background subtraction. Peaks were fitted using GL(30) lineshapes (70% Gaussian, 30% Lorentzian). For compounds with a long alkyl chain ($n \geq 8$) charge-referencing was achieved by setting the experimentally determined binding energy of the aliphatic carbon component ($C_{aliphatic}$) equal to 285.0 eV.[14,24] For compounds with a short alkyl chain ($n < 8$) charge-referencing was achieved by setting the measured binding energy of the cationic heteroatom photoemission peak equal to that for its long chain analogue, *i.e.* N_{cation} 1s for $[N_{4,4,4,1}][BF_4]$ was set equal to 402.3 eV (where 402.3 eV is the measured binding energy for N_{cation} 1s for $[N_{6,6,6,14}][BF_4]$). A full description of charge-referencing for each family of ionic liquids investigated within this study is provided within the Results and discussion section.

Results and discussion

Sample purity

XP survey and high resolution scans were used to establish elemental composition and purity for each ionic liquid presented in this study. Fig. 1 shows a typical survey scan for $[P_{6,6,6,14}][PF_6]$ which displays all expected photoelectron and Auger lines. Previous XPS studies upon ionic liquids have highlighted the presence of hydrocarbon and silicone-based impurities in the near-surface region, which cannot be detected

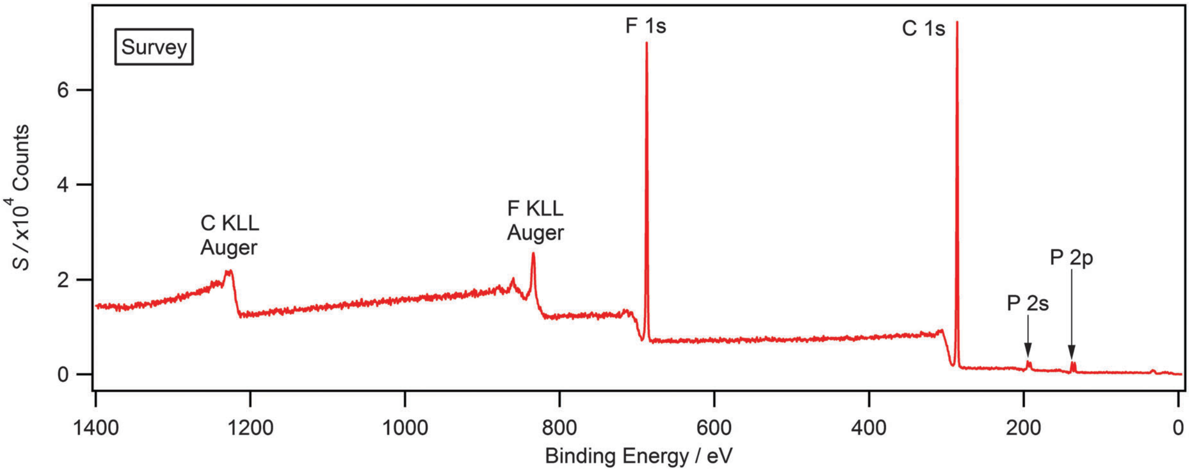

Fig. 1 Survey XP spectrum for $[P_{6,6,6,14}][PF_6]$. The absence of photoelectron lines corresponding to other elements, especially oxygen and silicon, highlights the high purity of the compounds used in this study.

by NMR or other bulk sensitive techniques.[26,28,29] A weak O 1s and Si 2p signal was observed in the case of $[N_{6,6,6,14}][Cl]$ and $[N_{4,4,4,1}][BF_4]$ (see ESI†); this is likely to be a result of laboratory grease during sample preparation and is not expected to impact upon the recorded binding energies.[24,26,30] Surface contaminants, such as grease, can be routinely removed through argon etching, a full description for this procedure in relation to the compounds studied herein is provided within the experimental section. There was no evidence of this contaminant in any of the other ionic liquids used in this study. Furthermore, there is no evidence of metal-based cations or halides that may be carried over from ionic liquid synthesis, particularly anion exchange chemistries. Experimental stoichiometries, calculated from high resolution spectra, are presented in Table 2. Experimental values are within the error of the nominal stoichiometry of ±10%.

Interestingly, deviations larger than ±10% are observed for the phosphorus P 2p signal, in which the calculated value is significantly and systematically less than the theoretical value. Previous angle resolved studies upon ionic liquids have shown that long alkyl chains ($n \geq 2$) point out towards the gas phase resulting in a surface enrichment of carbon.[10,31] The ionic liquids in this study have a large alkyl contribution which may significantly impact the stoichiometry of other elements as it has been seen that the cationic head group is pushed deeper into the bulk with increasing alkyl chain length.[32] It is feasible that differences in the conformations and mobility of the alkyl chains for tetraalkylammonium and phosphonium cations result in a nitrogen cationic core that is situated closer to the surface, but a phosphorus cationic core that is buried further within the bulk. This provides a possible explanation for the lower than expected intensity of the P 2p photoelectron peak. Earlier studies have shown a larger surface enrichment of carbon for ILs with small anions, such as chloride, whereby the anion is situated at the same level as the cation.[33] This could explain the smaller than expected Cl 2p signal.

Binding energies and multi-component fitting models for $[N_{R,R',R'',R'''}]X$, ($X = Cl^-$, $[BF_4]^-$, $[PF_6]^-$, $[OTf]^-$, $[NTf_2]^-$)

The measured binding energies for the ammonium series of ionic liquids investigated are presented in Table 3. To obtain accurate and reproducible binding energies an appropriate charge-referencing method must be used. It is well established that for ionic liquids with a long alkyl chain ($n \geq 8$), reliable charge-referencing can be achieved by setting the experimentally determined binding energy of the aliphatic carbon component ($C_{aliphatic}$) equal to a standard reference value, in the case of this work 285.0 eV.[14,24] For cations with shorter alkyl chains this procedure is not applicable. Previous studies indicate that length of the alkyl chain has negligible impact upon the binding energy of the cationic head group when the anion is kept the same.[14] Charge referencing for $[N_{4,4,4,1}][BF_4]$ was achieved by setting the measured binding energy of N_{cation} 1s to 402.3 eV; in this case 402.3 eV is the measured binding energy of N_{cation} 1s for $[N_{6,6,6,14}][BF_4]$, which has been charge referenced to $C_{aliphatic}$ as discussed previously. A similar procedure is used for $[N_{4,4,4,1}][NTf_2]$.

Due to the presence of several different carbon environments, peak identification and fitting of the C 1s region for ionic liquids is of particular importance. Fig. 2 shows some representative examples of the C 1s region for $[N_{6,6,6,14}]X$ ($X = Cl^-$, $[BF_4]^-$, $[NTf_2]^-$). In the case of $[N_{6,6,6,14}][NTf_2]$ there are three clear peaks, two of which are unresolved. The resolved peak at ≈293 eV is assigned to the CF_3 group of the $[NTf_2]$ anion as seen previously for imidazolium and pyrrolidinium ionic liquids.[14,24] The two unresolved peaks between 285–287 eV for $[N_{6,6,6,14}][Cl]$, $[N_{6,6,6,14}][BF_4]$ and $[N_{6,6,6,14}][NTf_2]$ arise from the different electronic environments of carbon present in the cation, thus it is necessary to develop a model to explain these different contributions. Previously we have developed a series of multi-component models to describe the C 1s spectra of a range of ionic liquid families including dialkyl-imidazolium, alkyl-pyridinium and pyrrolidinium based cations.[14] Here we extend this to include the tetraalkylphosphonium and tetraalkylammonium based cations.

Table 2 Measured experimental and nominal (in brackets) stoichiometries for ionic liquids studied in this work

	Composition[a] (%)							
Compound	C	N	O	F	B	S	P	Cl
RSF[26,27]	0.278	0.477	0.780	1.000	0.159	0.668	0.486	0.891
$[N_{6,6,6,14}][Cl]$	95.5 (94.0)	2.3 (2.9)	—	—	—	—	—	2.2 (2.9)
$[P_{6,6,6,14}][Cl]$	95.2 (94.1)	—	—	—	—	—	2.7 (2.9)	2.1 (2.9)
$[N_{6,6,6,14}][BF_4]$	84.0 (84.2)	2.5 (2.6)	—	10.7 (10.5)	2.8 (2.6)	—	—	—
$[P_{6,6,6,14}][BF_4]$	85.3 (84.2)	—	—	10.6 (10.5)	2.2 (2.6)	—	2.0 (2.6)	—
$[N_{6,6,6,14}][PF_6]$	80.5 (80.0)	2.5 (2.5)	—	15.0 (15.0)	—	—	2.0 (2.5)	—
$[P_{6,6,6,14}][PF_6]$	79.9 (80.0)	—	—	16.3 (15.0)	—	—	3.8 (5.0)	—
$[N_{6,6,6,14}][OTf]$	80.7 (80.5)	2.4 (2.4)	7.1 (7.3)	7.6 (7.3)	—	2.1 (2.4)	—	—
$[P_{6,6,6,14}][OTf]$	81.3 (80.5)	—	7.4 (7.3)	7.3 (7.3)	—	2.1 (2.4)	2.0 (2.4)	
$[N_{6,6,6,14}][NTf_2]$	70.5 (70.8)	3.9 (4.2)	8.9 (8.3)	12.9 (12.5)	—	3.8 (4.2)	—	—
$[P_{6,6,6,14}][NTf_2]$	70.8 (70.8)	2.2 (2.1)	8.9 (8.3)	12.6 (12.5)	—	3.9 (4.2)	1.7 (2.1)	—
$[N_{4,4,4,1}][BF_4]$	70.9 (68.4)	4.9 (5.3)	—	18.4 (21.1)	5.8 (5.3)	—	—	—
$[P_{4,4,4,1}][BF_4]$	68.6 (68.4)	—	—	21.3 (21.1)	5.0 (5.3)	—	5.0 (5.3)	—
$[N_{4,4,4,1}][NTf_2]$	52.3 (51.7)	6.6 (6.9)	14.2 (13.8)	20.6 (20.7)	—	6.4 (6.9)	—	—
$[P_{4,4,4,1}][NTf_2]$	52.6 (51.7)	3.5 (3.4)	13.8 (13.8)	20.8 (20.7)	—	6.5 (6.9)	2.8 (3.4)	—

[a] Relative sensitivity factors (RSF) taken from the Kratos Library were used to derive atomic percentages from the most intense photoemission peak for each element *i.e.* C═C 1s, N═N 1s, O═O 1s, F═F 1s, B═B 1s, S═S 2p, P═P 2p, Cl═Cl 2p.

Table 3 Experimental binding energies in eV for the ionic liquids studied in this work. The associated experimental error is ±0.1 eV. $[N_{6,6,6,14}]^+$/$[P_{6,6,6,14}]^+$ compounds charge corrected by setting $C_{aliphatic}$ 1s to 285.0 eV. $[N_{4,4,4,1}]^+$/$[P_{4,4,4,1}]^+$ compounds charge corrected by setting N_{cation} 1s/P_{cation} 2p to the value obtained for the $[N_{6,6,6,14}]^+$/$[P_{6,6,6,14}]^+$ analogue

		Binding energy/eV												
Compound		Cation					Anion							
Cation	Anion	$C_{aliphatic}$ 1s	C_{inter} 1s	C_{hetero} 1s	N_{cation} 1s	P_{cation} $2p_{3/2}$	C_{anion} 1s	N_{anion} 1s	O 1s	F 1s	B 1s	Cl $2p_{3/2}$	S $2p_{3/2}$	P_{anion} $2p_{3/2}$
$[N_{6,6,6,14}]^+$	$[Cl]^-$	285.0	285.6	286.3	402.1	—	—	—	—	—	—	196.6	—	—
$[P_{6,6,6,14}]^+$	$[Cl]^-$	285.0	—	285.7	—	132.3	—	—	—	—	—	196.6	—	—
$[N_{6,6,6,14}]^+$	$[BF_4]^-$	285.0	285.6	286.5	402.3	—	—	—	—	685.7	194.0	—	—	—
$[P_{6,6,6,14}]^+$	$[BF_4]^-$	285.0	—	285.8	—	132.6	—	—	—	685.7	193.9	—	—	—
$[N_{6,6,6,14}]^+$	$[PF_6]^-$	285.0	285.7	286.6	402.4	—	—	—	—	686.6	—	—	—	136.4
$[P_{6,6,6,14}]^+$	$[PF_6]^-$	285.0	—	285.8	—	132.7	—	—	—	686.5	—	—	—	136.3
$[N_{6,6,6,14}]^+$	$[OTf]^-$	285.0	285.7	286.6	402.4	—	292.3	—	531.8	688.3	—	—	168.2	—
$[P_{6,6,6,14}]^+$	$[OTf]^-$	285.0	—	285.8	—	132.7	292.3	—	531.9	688.4	—	—	168.2	—
$[N_{6,6,6,14}]^+$	$[NTf_2]^-$	285.0	285.7	286.7	402.5	—	292.8	399.3	532.5	688.7	—	—	168.9	—
$[P_{6,6,6,14}]^+$	$[NTf_2]^-$	285.0	—	285.9	—	132.7	292.8	399.3	532.5	688.7	—	—	168.8	—
$[N_{4,4,4,1}]^+$	$[BF_4]^-$	285.0	285.2	286.4	402.3	—	—	—	—	685.7	194.1	—	—	—
$[P_{4,4,4,1}]^+$	$[BF_4]^-$	285.0	—	285.4	—	132.6	—	—	—	685.5	193.9	—	—	—
$[N_{4,4,4,1}]^+$	$[NTf_2]^-$	285.1	285.4	286.6	402.5	—	292.8	399.3	532.5	688.7	—	—	168.8	—
$[P_{4,4,4,1}]^+$	$[NTf_2]^-$	285.1	—	285.6	—	132.7	297.7	399.2	532.4	688.6	—	—	168.8	—

As the structure of the ammonium cation is not dissimilar to that of the pyrrolidinium, a three-component model was adopted for the ammonium-based ionic liquids in this study. An analysis of the structure of $[N_{6,6,6,14}]^+$ (see structure shown in Fig. 2) highlights the three chemical environments of carbon. The carbon directly bound to the nitrogen (C_{hetero}) is expected to have the highest binding energy as it is in closest proximity to the electropositive nitrogen, and thus feels a larger effect of the electron-withdrawing influence of the cationic nitrogen. The next carbon atom along the chain (C_{inter}) is designated as an "intermediate" carbon environment; here the electron-withdrawing impact of the nitrogen centre is less pronounced, resulting in a slightly lower binding energy. The remaining carbons are essentially aliphatic and give rise to the third contribution, $C_{aliphatic}$, which exhibits the lowest binding energy.

To obtain a satisfactory fit that accurately describes the chemical environment it is necessary to constrain certain parameters. Component areas are constrained to their nominal stoichiometries, *i.e.* for $[N_{6,6,6,14}][BF_4]$ $C_{aliphatic} : C_{hetero} : C_{inter}$ equates to $6:1:1$. The full width at half maximum (FWHM) for C_{hetero} and C_{inter} are set to be equal (and constrained to be between 0.8 and 1.5 eV). The FWHM for $C_{aliphatic}$ is set to be 1.1 times larger than for C_{hetero} as studies upon other similar ionic liquid systems have characteristically shown the FWHM ratio of $C_{aliphatic} : C_{hetero}$ to be $1.1:1$.[14,24] Binding energy constraints were not applied as the binding energy shift between C_{hetero} and C_{inter} is expected to be dependent upon the nature of the anion.[13,14] The fitting envelopes (red curve), shown in Fig. 2a–c, demonstrate excellent agreement to the experimental spectra (black dots). C 1s fittings for $[N_{6,6,6,14}]$X (X = $[PF_6]^-$, $[OTf]^-$) and $[N_{4,4,4,1}]$X (X = $[BF_4]^-$, $[NTf_2]^-$) are included in the ESI† and are also in agreement with the experimental spectra.

Binding energies and multi-component fitting models for $[P_{R,R',R'',R'''}]$X, (X = Cl^-, $[BF_4]^-$, $[PF_6]^-$, $[OTf]^-$, $[NTf_2]^-$)

The C 1s region for phosphonium ionic liquids differs quite considerably from that of ammonium ionic liquids. Fig. 3 shows some representative examples of the C 1s region for $[P_{6,6,6,14}]$X (X = Cl^-, $[BF_4]^-$, $[NTf_2]^-$). In the case of $[P_{6,6,6,14}][NTf_2]$ there are two clearly resolved peaks with the peak at higher binding energy corresponding to the CF_3 group of the anion. A broad peak with slight asymmetry occurs between 284–286 eV for $[P_{6,6,6,14}]$X (X = Cl^-, $[BF_4]^-$, $[NTf_2]^-$); which is distinctly lacking the obvious shoulder at higher binding energy seen in the case of the ammonium analogues (Fig. 2 and 3). Consequently, this peak was fitted using a two-component model; the first contribution arising from carbons directly bound to the phosphorus atom, C_{hetero}, and the remaining carbons considered as aliphatic, $C_{aliphatic}$.

A comparison of binding energies (Table 3) for the C_{hetero} component of the $[N_{6,6,6,14}]^+$ and $[P_{6,6,6,14}]^+$ cations show that C_{hetero} for $[N_{6,6,6,14}]^+$ is ~0.6–0.8 eV larger than for the $[P_{6,6,6,14}]^+$ analogue. This can be attributed to the difference in charge density of the nitrogen and phosphorus cationic centres. The smaller atomic radius of the nitrogen atom, in comparison to phosphorus, results in a higher charge density. Consequently, the C_{hetero} carbons for ammonium-based ionic liquids experience a stronger electron-withdrawing effect from the positively charged nitrogen centre, which is reflected by a shift to higher binding energy.

Furthermore, from Table 3 it can be seen that C_{hetero} binding energies for phosphonium-based ionic liquids are more similar in value to the C_{inter} component for the ammonium analogues. This highlights the weaker electron-withdrawing effect of the phosphorus centre, as a result of its lower charge density, and validates the use of a two-component fitting model to describe the C 1s region for phosphonium-based ionic liquids.

Cations with short alkyl chain length *i.e.* $[P_{4,4,4,1}]^+$ were fitted using the same method and charge referenced in a similar way to the short chain ammonium cations as discussed previously.

Effect of anion: cation–anion interactions

It has been previously established that XPS can be used to probe cation–anion interactions.[13,14,34] Earlier work has demonstrated

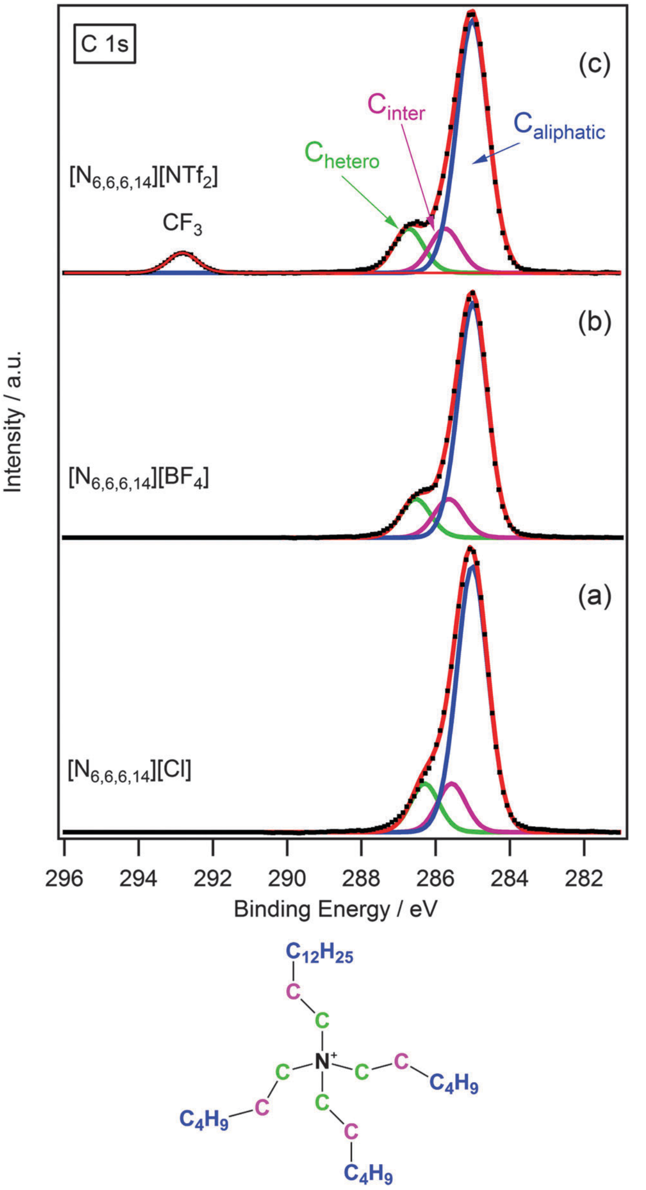

Fig. 2 High resolution XP spectra of the C 1s region with component fittings for (a) $[N_{6,6,6,14}][Cl]$, (b) $[N_{6,6,6,14}][BF_4]$ and (c) $[N_{6,6,6,14}][NTf_2]$. Areas are normalised to the N_{cation} 1s photoemission peak for $[N_{6,6,6,14}][BF_4]$. All XP spectra charge corrected to $C_{aliphatic}$ = 285.0 eV.

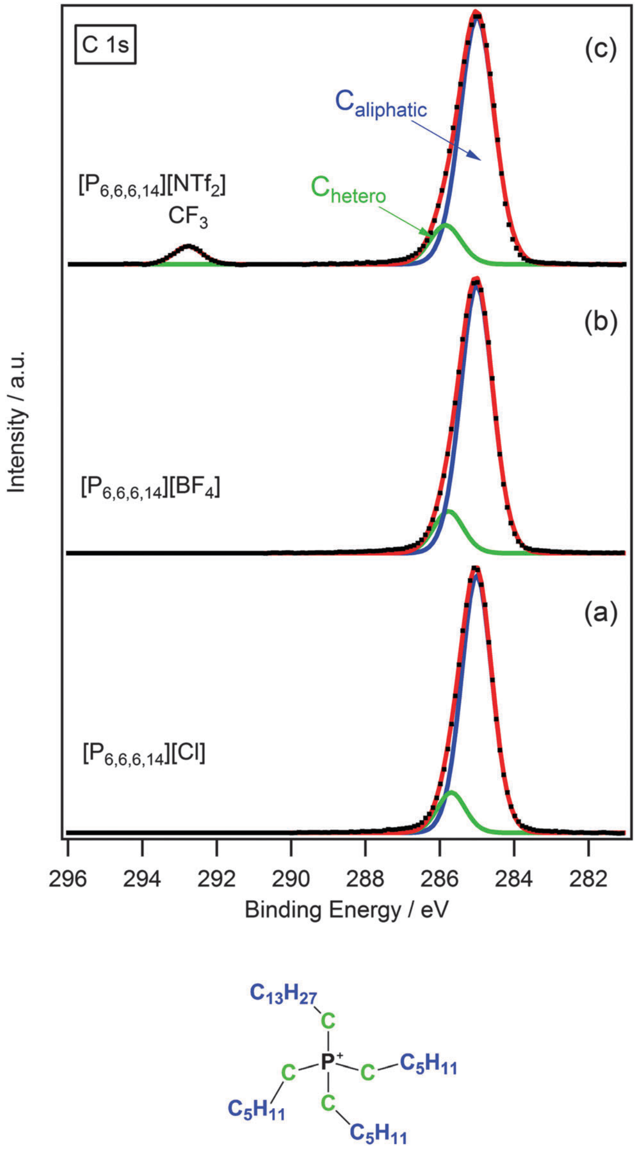

Fig. 3 High resolution XP spectra of the C 1s region with component fittings for (a) $[P_{6,6,6,14}][Cl]$, (b) $[P_{6,6,6,14}][BF_4]$ and (c) $[P_{6,6,6,14}][NTf_2]$. Areas are normalised to the area of P_{cation} 2p photoemission peak for $[P_{6,6,6,14}][BF_4]$. All XP spectra are charge corrected by setting the measured binding energy of $C_{aliphatic}$ = 285.0 eV.

that binding energies of C_{hetero} 1s and N_{cation} 1s for imidazolium and pyrrolidinium-based ionic liquids are dependent upon the basicity of the anion.[13,14] High basicity anions such as halides result in lower binding energies, which indicate that the cation is in a more electron-rich environment. This is indicative of a significant amount of charge-transfer from anion to cation. Low basicity anions such as $[NTf_2]^-$ give rise to higher binding energies signifying that the cation is more electron-poor due to the reduction in charge-transfer.

The influence of the anion on the electronic environment of the cation has been investigated for three $[N_{6,6,6,14}][X]$ ionic liquids, where X = $[NTf_2]^-$, $[BF_4]^-$ and Cl^- (Fig. 4). It is seen that the binding energy of N_{cation} 1s follows the trend: $[NTf_2]^- > [BF_4]^- > Cl^-$, this can be interpreted as an increase in charge transfer with increasing anion basicity, and is in accordance with earlier studies upon imidazolium[13] and pyrrolidinium[14] ionic liquids. Binding energies for C_{hetero} 1s (Table 3 and Fig. 2) also exhibit an identical trend.

The effect of varying the anion has also been investigated for the analogous phosphonium series, $[P_{6,6,6,14}][X]$ where X = $[NTf_2]^-$, $[BF_4]^-$ and Cl^- (Fig. 5). The P 2p region shows two unresolved peaks, P $2p_{1/2}$ and P $2p_{3/2}$, observed in an intensity ratio of 1 : 2. This is a result of spin–orbit coupling and is an inherent property of p-orbitals and does not indicate two different electronic environments of phosphorus. The same trend as for ammonium-based ionic liquids is observed in that binding energies for the P_{cation} $2p_{3/2}$ component are in

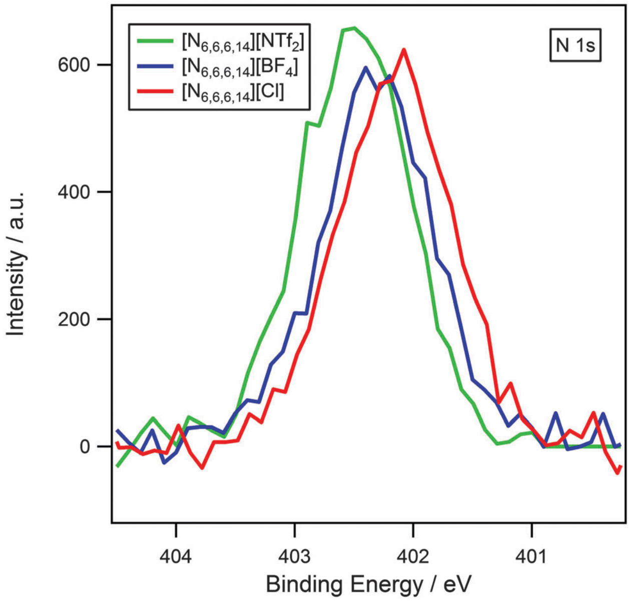

Fig. 4 N 1s XP spectra of $[N_{6,6,6,14}][NTf_2]$, $[N_{6,6,6,14}][BF_4]$ and $[N_{6,6,6,14}][Cl]$. Areas are normalised to the N_{cation} 1s peak for $[N_{6,6,6,14}][BF_4]$. XP spectra were charge corrected by referencing the aliphatic C 1s photoemission peak to 285.0 eV. *N.B.* spectra truncated to only show the cation region.

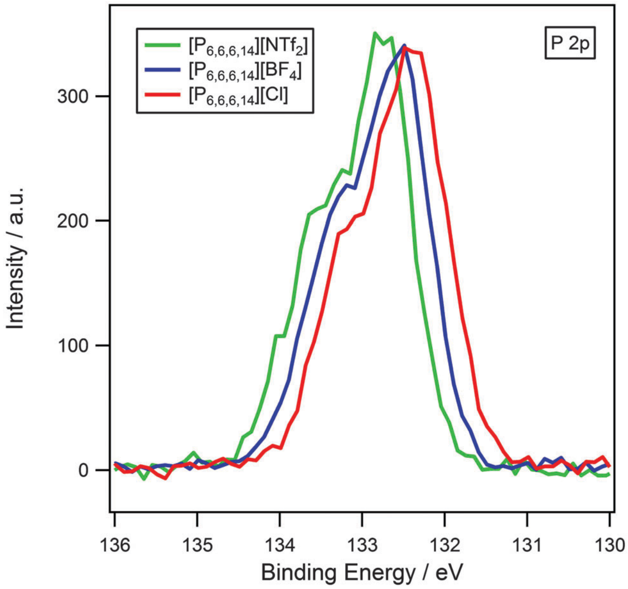

Fig. 5 P 2p XP spectra of $[P_{6,6,6,14}][NTf_2]$, $[P_{6,6,6,14}][BF_4]$ and $[P_{6,6,6,14}][Cl]$. Areas are normalised to the P 2p peak for $[P_{6,6,6,14}][BF_4]$. XP spectra were charge corrected by referencing the aliphatic C 1s photoemission peak to 285.0 eV.

the order: $[NTf_2]^- > [BF_4]^- > Cl^-$, with C_{hetero} 1s following a similar pattern.

A linear correlation of N_{cation} 1s and C_{hetero} 1s binding energies with the Kamlet–Taft β parameter (a measure of hydrogen bond acceptor ability of the anion) has been established for imidazolium-based ionic liquids.[13] However, to date, β has been less extensively studied for ammonium and phosphonium ionic liquids with only a select few examples in the literature.[35–39] Consequently, a comparison of β with binding energy cannot be made for the compounds investigated in this study, however it is expected that a similar trend to imidazolium-based ionic liquids would be observed.

Effect of cation: cation–anion interactions, $[N_{6,6,6,14}]^+$ *versus* $[P_{6,6,6,14}]^+$

As discussed previously, it is expected that the difference in charge density of the ammonium and phosphonium cationic centres will affect the degree of charge-transfer, which would be reflected in the binding energy of the anionic components. We postulated that a greater degree of charge-transfer would occur for the ammonium cation, as the larger charge density would be more effective in removing excess negative charge from the anion; hence, the binding energies of the anion were expected to indicate a more electron-poor environment in contrast to the phosphonium analogue.

A comparison of binding energies, however, did not support this assumption. Fig. 6 illustrates a comparison between $[N_{6,6,6,14}][BF_4]$ and $[P_{6,6,6,14}][BF_4]$ for all regions. All XP spectra are charge corrected by referencing $C_{aliphatic}$ 1s to 285.0 eV; and are normalised to the area of the F 1s photoemission peak for $[N_{6,6,6,14}][BF_4]$ as the number of fluorine atoms are equivalent for both samples. It can be seen that the binding energies of the anionic components are identical, within the error of experiment (±0.1 eV), for example the F 1s component for $[N_{6,6,6,14}][BF_4]$ and $[P_{6,6,6,14}][BF_4]$ is 685.7 eV in each instance, (Fig. 6 and Table 3). This is also true for the B 1s component where binding energies are 194.0 eV and 193.9 eV for $[N_{6,6,6,14}][BF_4]$ and $[P_{6,6,6,14}][BF_4]$ respectively. The P 2s photoemission peak is also observed in the B 1s XP spectrum for $[P_{6,6,6,14}][BF_4]$ at a lower binding energy of 190.4 eV.

The binding energies for a range of anions of varying size and basicity, including Cl^-, $[PF_6]^-$, $[OTf]^-$ and $[NTf_2]^-$, also match within experimental error for the $[N_{6,6,6,14}]^+$ and $[P_{6,6,6,14}]^+$ cations. This suggests that the anion cannot "see" the difference in charge density of the cation, and it is proposed that the long alkyl chains are wrapped around the cationic centre effectively shielding it from the anion. This is in agreement with measurements on the enthalpy of vaporisation at 298 K, $\Delta_{vap}H_{298}$, for $[P_{6,6,6,14}][BF_4]$, which describe how the experimentally determined van der Waals contribution is significantly smaller than the theoretical value, it is suggested that parts of the alkyl chain close to the phosphorus are unavailable for van der Waals bonding with adjacent species due to shielding from the outer parts of the chain.[40] In contrast, molecular dynamics simulations indicate that the alkyl chains are in a fully stretched conformation, with a small degree of bending for longer chains ($n > 6$) and no evidence of coiling or wrapping.[41,42]

It should be noted that although the anion is shielded from the difference in charge density of the two different cations, it is not shielded from "seeing" a positive charge completely. In this way, the "wrapping" of the aliphatic chains has no impact on the actual ability of the anion to transfer charge, and hence we see a shift in B.E. of the cationic core for anions of different

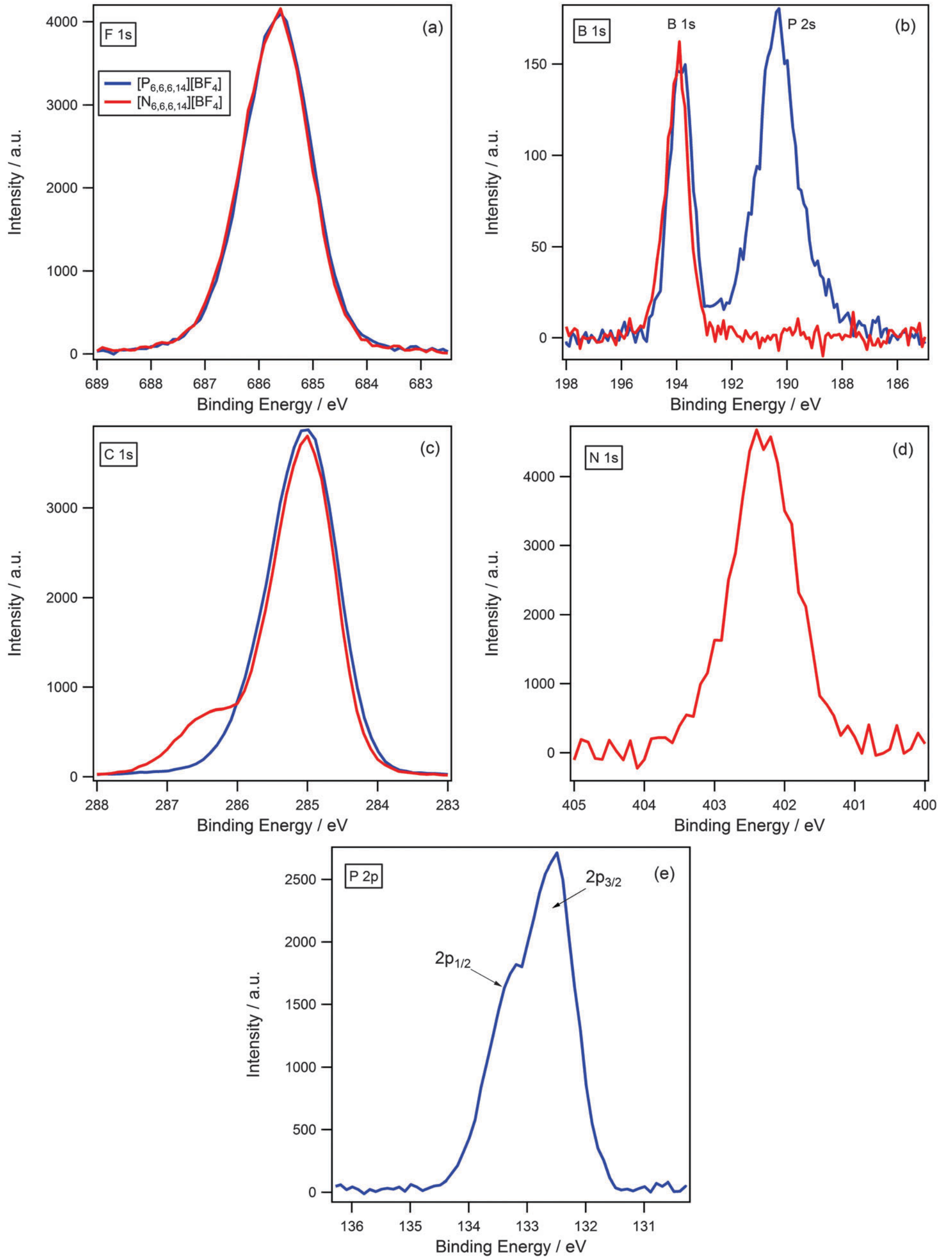

Fig. 6 XP spectra of $[N_{6,6,6,14}][BF_4]$ and $[P_{6,6,6,14}][BF_4]$ for: (a) F 1s, (b) B 1s, (c) C 1s, (d) N 1s and (e) P 2p. Areas normalised to area of F 1s peak for $[N_{6,6,6,14}][BF_4]$. All XP spectra were charge corrected by setting $C_{aliphatic}$ 1s = 285.0 eV.

basicity as mentioned previously in the section ''Effect of the Anion: Cation–Anion Interactions''.

Effect of cation: cation–anion interactions, $[N_{4,4,4,1}]^+$ *versus* $[P_{4,4,4,1}]^+$

In the previous section we determined that for ammonium and phosphonium cations with long alkyl chains, there is no difference in binding energy of the anionic components for a variety of different anions. To test whether the length of the alkyl chain impacts upon cation–anion interactions and the ability of the anion to ''see'' the difference in charge density of the cationic centres, a series of short chain analogues were investigated where the cation size has been reduced to $[N_{4,4,4,1}]^+$ and $[P_{4,4,4,1}]^+$.

A visual comparison between $[N_{4,4,4,1}][BF_4]$ and $[P_{4,4,4,1}][BF_4]$ for all regions is shown in Fig. 7. The F 1s binding energy for $[N_{4,4,4,1}][BF_4]$ is 0.2 eV higher than for $[P_{4,4,4,1}][BF_4]$ (Fig. 7 and Table 3), this is slightly larger than the accepted experimental error and suggests that the shift is real. As the F 1s binding energy is higher for $[N_{4,4,4,1}]^+$ relative to $[P_{4,4,4,1}]^+$ this is indicative that the fluorine atoms are more electron-poor for $[N_{4,4,4,1}]^+$, which suggests a greater degree of charge-transfer is occurring for the ammonium-based ionic liquid. This supports our initial hypothesis that charge-transfer should be more significant for ammonium-based ionic liquids due to the larger charge density of the cationic centre relative to their phosphonium analogues. Additionally, it indicates that reducing the length of

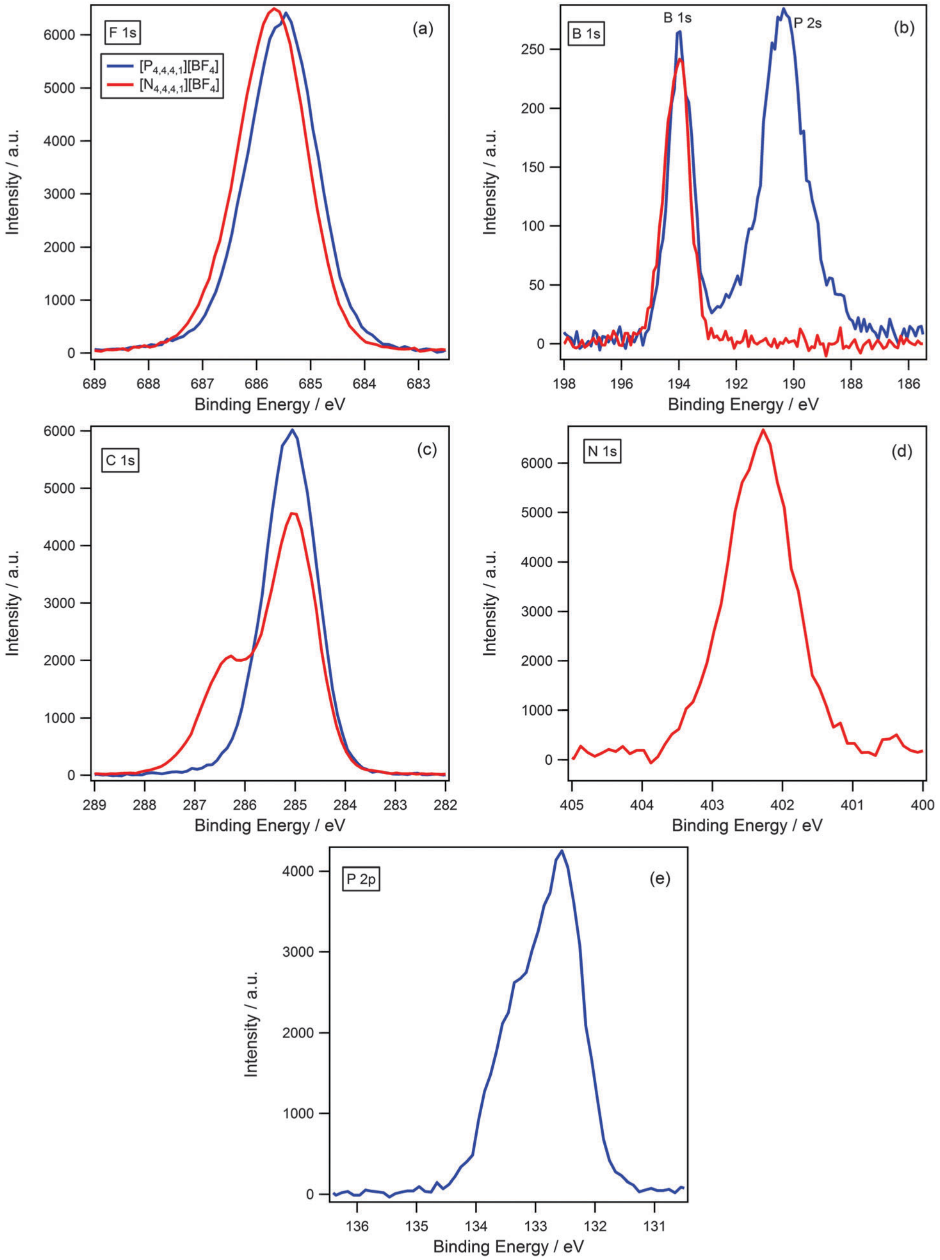

Fig. 7 XP spectra of $[N_{4,4,4,1}][BF_4]$ and $[P_{4,4,4,1}][BF_4]$ for: (a) F 1s, (b) B 1s, (c) C 1s, (d) N 1s and (e) P 2p. Areas normalised to area of F 1s peak for $[N_{4,4,4,1}][BF_4]$. $[N_{4,4,4,1}][BF_4]$ XP spectra are charge corrected by setting N_{cation} 1s to 402.3 eV. $[P_{4,4,4,1}][BF_4]$ XP spectra are charge corrected by setting P_{cation} $2p_{3/2}$ to 132.6 eV.

the alkyl chain allows for a more open structure of the cation which permits the anion to "see" the difference in charge density of the cationic centre.

Fabris *et al.* found that a trioctylmethylphosphonium ($[TOMP]^+$) cation coupled with a methylcarbonate ($[MeOCOO]^-$) or hydrogen carbonate ($[HOCOO]^-$) anion exhibited stronger basicity than its ammonium counterparts and other conventional basic catalysts, and as a result was a more efficient catalyst for Michael reactions.[43] This could support the assertions made from the work described here, as the high basicity of [TOMP] [MeOCOO] and [TOMP] [HOCOO] may arise from a smaller degree of charge-transfer occurring from anion to cation; consequently the anion is more electron-rich thus the electrons are more available for donation. In contrast, a higher degree of charge-transfer occurs for the ammonium analogues and inorganic bases as a result of the larger charge density of the cationic centre, hence basicity is reduced as electron density is less available for donation.

It is still unclear to us at this time how the charge-transfer phenomenon is mediated. Previous studies upon 1-methyl-3-alkylimidazolium systems have shown a correlation between anion basicity and hydrogen-bonding at the C-2 position, and also with N_{cation} 1s and C 1s binding energy.[13] However, upon methylation of the C-2 position (hence decreasing the hydrogen-bonding contribution) an anion-dependent shift of the

N_{cation} 1s and C 1s binding energies is still observed at a similar magnitude as the non-methylated analogues.[13] This indicates that charge-transfer cannot solely be mediated through hydrogen-bonding, which is especially relevant in the case of tetraalkyl-ammonium and phosphonium ILs where the proton alpha to the heteroatom is even less available due to steric hindrance of the long alkyl chains. This suggests charge-transfer is also dependent upon the strength of the coulombic interaction of the cation and anion.

It should be noted that for $[N_{4,4,4,1}][NTf_2]$ and $[P_{4,4,4,1}][NTf_2]$ only a small shift (~0.1 eV) to a higher binding energy is observed for the anionic components of $[N_{4,4,4,1}]^+$ relative to $[P_{4,4,4,1}]^+$ (Table 3), this is within the experimental error so no real conclusion can be made; however, as $[NTf_2]^-$ is weakly basic it is likely that it participates in charge-transfer to a very small degree, hence little or no difference is observed when comparing the different cationic centres.

Conclusion

The impact of changing the cation core from nitrogen to phosphorus on cation–anion interactions has been investigated using XPS. For long chain systems, *i.e.* $[N_{6,6,6,14}]^+$ *versus* $[P_{6,6,6,14}]^+$, it appears that changing the cation core has minimal impact on the electronic environment of the anion due to a perceived shielding effect of the long alkyl chains. In an effort to reduce the effect of hydrocarbon based shielding of the heteroatom, a second series of experiments were conducted where the alkyl components are pruned back, hence allowing a more clear investigation of the role of the heteroatom based charge carrier. A decrease in alkyl chain length to $[N_{4,4,4,1}]^+$ and $[P_{4,4,4,1}]^+$ indicates that changing the cation core from nitrogen to phosphorus does indeed influence the electronic environment of the anion; with an increase in charge-transfer shown for ammonium ILs. Further investigation into binary cationic mixtures by XPS was not attempted as any shift in the measured binding energies, with adjusted mol. fraction, would lie within the experimental error of the XPS instrument. This indicates that tunability of the electronic environment for IL systems is more strongly influenced by the anion than the cation.

Interestingly, Carvalho *et al.*[23] investigated the influence of the cationic heteroatom for ammonium- and phosphonium-based ILs on physical properties such as densities, viscosities, melting temperatures and refractive indices. A shielding effect was expected but not observed, and it was seen that the properties investigated were markedly affected by the cationic core. Taking this into consideration with the work described herein a dual tunability of IL systems could be proposed, where electronic environments, *i.e.* chemical properties, are tuned *via* the anion and physical properties are tuned *via* the cation. This work provides a step toward being fully able to fine-tune both the chemical and physical properties of an IL system by altering their constituent ions to suit a specific function.

Acknowledgements

We thank the EPSRC (EP/K005138/1) for financial support and provision of the Ionic Liquids XPS Facility. RKB acknowledges the University of Nottingham for support. The authors are grateful to Ms Emily F. Smith for helpful discussions and critical advice. Cytec Industries Inc. are thanked for kindly donating the samples of Cyphos 101 and Cyphos 108 used in this study.

References

1 *Ionic Liquids in Synthesis*, ed. P. Wasserscheid, T. Welton, 2nd edn, Wiley-VCH, Weinheim, 2007, ISBN 978-3-527-31239-9.

2 H. Niedermeyer, J. P. Hallett, I. J. Villar-Garcia, P. A. Hunt and T. Welton, *Chem. Soc. Rev.*, 2012, **41**, 7780–7802.

3 G. Chatel, J. F. B. Pereira, V. Debbeti, H. Wang and R. D. Rogers, *Green Chem.*, 2014, **16**, 2051–2083.

4 M. A. Taige, D. Hilbert and T. J. S. Schubert, *Z. Phys. Chem.*, 2012, **226**, 129–139.

5 A. M. Pinto, H. Rodriguez, Y. J. Colon, A. Arce and A. Soto, *Ind. Eng. Chem. Res.*, 2013, **52**, 5975–5984.

6 Q. Q. Baltazar, S. K. Leininger and J. L. Anderson, *J. Chromatogr. A*, 2008, **1182**, 119–127.

7 S. Katsuta, Y. Yoshimoto, M. Okai, Y. Takeda and K. Bessho, *Ind. Eng. Chem. Res.*, 2011, **50**, 12735–12740.

8 K. R. J. Lovelock, I. J. Villar-Garcia, F. Maier, H. P. Steinruck and P. Licence, *Chem. Rev.*, 2010, **110**, 5158–5190.

9 H. P. Steinruck, *Phys. Chem. Chem. Phys.*, 2012, **14**, 5010–5029.

10 K. R. J. Lovelock, C. Kolbeck, T. Cremer, N. Paape, P. S. Schulz, P. Wasserscheid, F. Maier and H. P. Steinruck, *J. Phys. Chem. B*, 2009, **113**, 2854–2864.

11 F. Maier, T. Cremer, C. Kolbeck, K. R. J. Lovelock, N. Paape, P. S. Schulz, P. Wasserscheidc and H. P. Steinruck, *Phys. Chem. Chem. Phys.*, 2010, **12**, 1905–1915.

12 I. Niedermaier, C. Kolbeck, N. Taccardi, P. S. Schulz, J. Li, T. Drewello, P. Wasserscheid, H. P. Steinruck and F. Maier, *ChemPhysChem*, 2012, **13**, 1725–1735.

13 T. Cremer, C. Kolbeck, K. R. J. Lovelock, N. Paape, R. Wolfel, P. S. Schulz, P. Wasserscheid, H. Weber, J. Thar, B. Kirchner, F. Maier and H. P. Steinruck, *Chem. – Eur. J.*, 2010, **16**, 9018–9033.

14 S. Men, K. R. J. Lovelock and P. Licence, *Phys. Chem. Chem. Phys.*, 2011, **13**, 15244–15255.

15 I. J. Villar-Garcia, K. R. J. Lovelock, S. Men and P. Licence, *Chem. Sci.*, 2014, **5**, 2573–2579.

16 K. J. Fraser and D. R. MacFarlane, *Aust. J. Chem.*, 2009, **62**, 309–321.

17 R. E. Del Sesto, C. Corley, A. Robertson and J. S. Wilkes, *J. Organomet. Chem.*, 2005, **690**, 2536–2542.

18 G. Adamova, R. L. Gardas, M. Nieuwenhuyzen, A. V. Puga, L. P. N. Rebelo, A. J. Robertson and K. R. Seddon, *Dalton Trans.*, 2012, **41**, 8316–8332.

19 K. Tsunashima and M. Sugiya, *Electrochem. Commun.*, 2007, **9**, 2353–2358.

20 K. Tsunashima, E. Niwa, S. Kodama, M. Sugiya and Y. Ono, *J. Phys. Chem. B*, 2009, **113**, 15870–15874.

21 H. Shirota, H. Fukazawa, T. Fujisawa and J. F. Wishart, *J. Phys. Chem. B*, 2010, **114**, 9400–9412.

22 H. Y. Lee, H. Shirota and E. W. Castner, *J. Phys. Chem. Lett.*, 2013, **4**, 1477–1483.

23 P. J. Carvalho, S. P. M. Ventura, M. L. S. Batista, B. Schroder, F. Goncalves, J. Esperanca, F. Mutelet and J. A. P. Coutinho, *J. Chem. Phys.*, 2014, **140**, 64505.

24 I. J. Villar-Garcia, E. F. Smith, A. W. Taylor, F. L. Qiu, K. R. J. Lovelock, R. G. Jones and P. Licence, *Phys. Chem. Chem. Phys.*, 2011, **13**, 2797–2808.

25 A. Cieniecka-Roslonkiewicz, J. Pernak, J. Kubis-Feder, A. Ramani, A. J. Robertson and K. R. Seddon, *Green Chem.*, 2005, **7**, 855–862.

26 E. F. Smith, F. J. M. Rutten, I. J. Villar-Garcia, D. Briggs and P. Licence, *Langmuir*, 2006, **22**, 9386–9392.

27 C. D. Wagner, L. E. Davis, M. V. Zeller, J. A. Taylor, R. H. Raymond and L. H. Gale, *Surf. Interface Anal.*, 1981, **3**, 211–225.

28 E. F. Smith, I. J. Villar Garcia, D. Briggs and P. Licence, *Chem. Commun.*, 2005, 5633–5635.

29 K. R. J. Lovelock, E. F. Smith, A. Deyko, I. J. Villar-Garcia, P. Licence and R. G. Jones, *Chem. Commun.*, 2007, 4866–4868.

30 A. W. Taylor, S. Men, C. J. Clarke and P. Licence, *RSC Adv.*, 2013, **3**, 9436–9445.

31 V. Lockett, R. Sedev, C. Bassell and J. Ralston, *Phys. Chem. Chem. Phys.*, 2008, **10**, 1330–1335.

32 C. Ridings, V. Lockett and G. Andersson, *Phys. Chem. Chem. Phys.*, 2011, **13**, 17177–17184.

33 C. Kolbeck, T. Cremer, K. R. J. Lovelock, N. Paape, P. S. Schulz, P. Wasserscheid, F. Maier and H. P. Steinruck, *J. Phys. Chem. B*, 2009, **113**, 8682–8688.

34 B. B. Hurisso, K. R. J. Lovelock and P. Licence, *Phys. Chem. Chem. Phys.*, 2011, **13**, 17737–17748.

35 A. Jelicic, N. Garcia, H. G. Lohmannsroben and S. Beuermann, *Macromolecules*, 2009, **42**, 8801–8808.

36 S. K. Poole, P. H. Shetty and C. F. Poole, *Anal. Chim. Acta*, 1989, **218**, 241–264.

37 N. D. Khupse and A. Kumar, *J. Phys. Chem. B*, 2010, **114**, 376–381.

38 S. Coleman, R. Byrne, S. Minkovska and D. Diamond, *Phys. Chem. Chem. Phys.*, 2009, **11**, 5608–5614.

39 P. G. Jessop, D. A. Jessop, D. B. Fu and L. Phan, *Green Chem.*, 2012, **14**, 1245–1259.

40 A. Deyko, S. G. Hessey, P. Licence, E. A. Chernikova, V. G. Krasovskiy, L. M. Kustov and R. G. Jones, *Phys. Chem. Chem. Phys.*, 2012, **14**, 3181–3193.

41 L. Gontrani, O. Russina, F. Lo Celso, R. Caminiti, G. Annat and A. Triolo, *J. Phys. Chem. B*, 2009, **113**, 9235–9240.

42 X. M. Liu, Y. L. Zhao, X. C. Zhang, G. H. Zhou and S. J. Zhang, *J. Phys. Chem. B*, 2012, **116**, 4934–4942.

43 M. Fabris, V. Lucchini, M. Noe, A. Perosa and M. Selva, *Chem. – Eur. J.*, 2009, **15**, 12273–12282.

ChemComm

COMMUNICATION

View Article Online
View Journal | View Issue

Cite this: *Chem. Commun.*, 2014, **50**, 12080

Received 16th July 2014,
Accepted 19th August 2014

DOI: 10.1039/c4cc05505e

www.rsc.org/chemcomm

Tuning cation–anion interactions in ionic liquids by changing the conformational flexibility of the cation†

R. K. Blundell and P. Licence*

Cation–anion interactions can be tuned *via* the degree of cation constraint. X-ray Photoelectron Spectroscopy (XPS) experiments reveal that anion–cation based interactions may be enhanced by introducing conformational restriction into the substituent chains of quaternary ammonium cations. A larger degree of charge-transfer was observed for the constrained $[C_8C_1Pyrr]^+$ cation relative to the $[N_{6,6,6,14}]^+$ cation.

Ionic liquids (ILs) are often referred to as ‘‘designer solvents’’, due to the fact that by simply changing the component ions chemical and physical properties can be altered to suit a specific function.[1] Therefore, one of the key goals in the field is to be able to predict how changes to the component ions will influence the properties of an ionic liquid system. To achieve this, ionic liquids must first be understood at a molecular level, and hence changes to the chemical structure and its effect upon inter-ion interactions must be explored. Thus far most ionic liquid research has focused upon cyclic nitrogen-based cations such as 1-alkyl-3-methylimidazolium, 1-alkyl-1-methylpyrrolidinium and 1-alkylpyridinium, and there are relatively few studies that address the distinction between cyclic cations and their acyclic counterparts, for example 1-alkyl-1-methylpyrrolidinium *versus* tetraalkylammonium.[2–6] Herein, we describe a series of experiments designed to probe the influence of constrained and unconstrained cations upon cation–anion interactions utilising X-ray Photoelectron Spectroscopy (XPS).

XPS is now an established technique that can be used to monitor how changes to the chemical architecture of an IL may influence the electronic environment of the elements contained in the constituent ions, as well as providing quantitative information on the elemental composition of a sample.[7] It has been suggested that ‘‘many (ionic liquid) applications could potentially profit from XPS analysis capabilities’’.[7] Most noticeably XPS of ionic liquids has entered a new domain with the advent of *in situ* reaction monitoring, the main advantage compared to other spectroscopic techniques being the simultaneous monitoring of all elements,[8–10] thus exemplifying the power and value of this technique.

XPS investigations into cation–anion interactions have indicated a degree of charge-transfer from anion to cation which is correlated to anion basicity;[11,12] however, little is known about the influence of the cation upon charge-transfer. In a recent XPS study upon tetraalkylammonium-based ILs and their phosphonium analogues we found that changing the cationic core from nitrogen to phosphorus had minimal impact upon charge-transfer due to a perceived hydrocarbon-based shielding of the cationic core.[13] In this work we explore the concept of hydrocarbon-based shielding of the cationic core and its impact upon cation–anion interactions by comparison of a relatively unconstrained $[N_{6,6,6,14}]^+$ cation with a conformationally constrained $[C_8C_1Pyrr]^+$ cation.

XP spectra were recorded using a Kratos Axis Ultra Spectrometer employing a monochromated Al Kα source (1486.6 eV), hybrid (magnetic/electrostatic) optics, hemispherical analyser and a multi-channel plate and delay line detector (DLD). Liquid samples were prepared by placing a small drop ($\approx$10 mg) of ionic liquid onto a stainless steel multi-sample bar; solid samples were fixed to the bar using double-sided adhesive tape. All samples were pre-pumped in a preparative chamber to pressures lower than 10^{-6} mbar before transfer into the main analytical chamber to ensure removal of any volatile material. Charge referencing was achieved post-data collection by setting the $C_{\text{aliphatic}}$ 1s component to 285.0 eV, a full description of this procedure has been described elsewhere.[14]

The 1-octyl-1-methylpyrrolidinium and trihexyl(tetradecyl)-ammonium cations are structurally very similar; however, a large proportion of the alkyl chain for $[C_8C_1Pyrr]^+$ is effectively ‘‘pinned back’’ in a 5-membered heterocyclic ring. Subsequently, we expect the nitrogen core to be more exposed than in the case of $[N_{6,6,6,14}]^+$ in which the central nitrogen is shielded by a layer of conformationally flexible long-chain hydrocarbon. Crystallographic data reported by Adamova *et al.*[15] supports this assertion

---

School of Chemistry, The University of Nottingham, Nottingham, NG7 2RD, UK.
E-mail: peter.licence@nottingham.ac.uk

† Electronic supplementary information (ESI) available: Experimental procedures, characterisation data and XP spectra. See DOI: 10.1039/c4cc05505e

since they describe the N···Cl distance for $[N_{2,2,2,2}]Cl$ as significantly longer than for $[C_3C_1Pyrr]Cl$; owing to the fact that the presence of strained rings around the central nitrogen atom for $[C_3C_1Pyrr]Cl$ allows a closer approach of the halide anion.[15]

By consideration of the Coulomb potential, the interaction energy of two point charges is inversely proportional to separation distance. Consequently, the closer two point charges are to each other the stronger the interaction between them. Therefore, it is anticipated that a greater degree of charge transfer will occur in the case of the constrained $[C_8C_1Pyrr]^+$ cation due to a stronger interaction with the anion, which would be reflected in the measured binding energy (BE) values for the anionic components.

The Cl 2p high resolution scan for each cation is presented in Fig. 1. It should be noted that due to spin–orbit coupling the photoelectron line is split into a doublet by a ratio of 1 : 2 ($2p_{1/2} : 2p_{3/2}$). This is an inherent property of p-orbital photoelectron lines and does not indicate two different electronic environments of chlorine.

A 0.3 eV shift to higher binding energy is observed for the Cl $2p_{3/2}$ component of $[C_8C_1Pyrr]Cl$ (Table 1, Fig. 1), this is greater than the experimental error (±0.1 eV) and indicates a noticeable change in the electronic environment of the anion, which we attribute to the availability of the cationic core. It should be noted that ΔBE(Cl $2p_{1/2}$–$2p_{3/2}$) is 1.6 eV for each cation, this consistency reinforces that a true shift is observed and is not the result of other processes such as beam damage. A small broadening of the Cl 2p peaks is observed for the $[N_{6,6,6,14}]^+$ cation, which is likely to be a result of differences in surface charging of the samples. The increase in binding energy of the Cl $2p_{3/2}$ component for $[C_8C_1Pyrr]Cl$, relative to $[N_{6,6,6,14}]Cl$, suggests that the chloride anion is more electron deficient when partnered with the 1-octyl-1-methylpyrrolidinium cation and indicates a greater degree of charge-transfer from anion to cation for this ionic liquid. This supports our proposal of a hydrocarbon-based shielding of the cationic core from the anion for cations containing long alkyl chains such as $[N_{6,6,6,14}]Cl$.

A similar trend is also observed when comparing the F 1s high resolution scans for $[C_8C_1Pyrr][BF_4]$ and $[N_{6,6,6,14}][BF_4]$ (Table 1, Fig. 2), in which a 0.2 eV shift is observed. The B 1s component also shifts slightly to higher binding energy by 0.1 eV for the $[C_8C_1Pyrr]^+$ cation, however this is within the

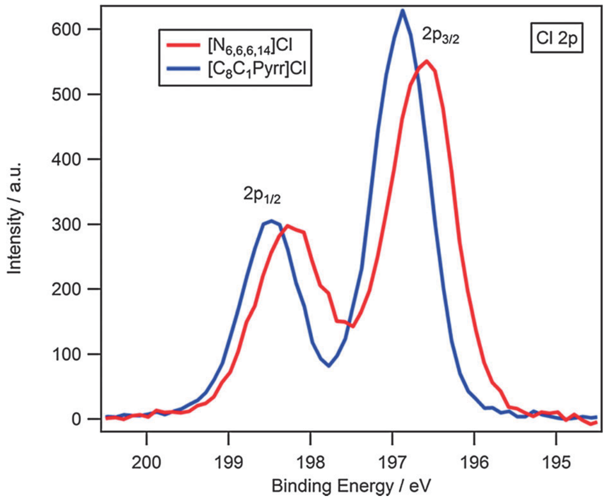

Fig. 1 High resolution XP spectra of the Cl 2p region for $[N_{6,6,6,14}]Cl$ and $[C_8C_1Pyrr]Cl$. Areas normalised to the area of Cl 2p photoemission peak for $[N_{6,6,6,14}]Cl$.

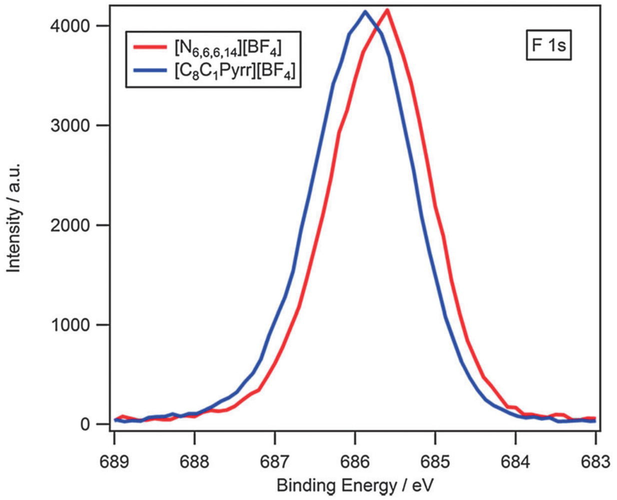

Fig. 2 High resolution XP spectra of the F 1s region for $[N_{6,6,6,14}][BF_4]$ and $[C_8C_1Pyrr][BF_4]$. Areas normalised to the area of F 1s photoemission peak for $[N_{6,6,6,14}][BF_4]$.

Table 1 Experimental binding energies in eV for the ionic liquids used in this study. The associated experimental error is ±0.1 eV. Charge referencing achieved by setting the $C_{aliphatic}$ component to 285.0 eV

	Binding energy/eV										
	Cation				Anion						
Compound	N_{cation} 1s	$C_{aliphatic}$ 1s	C_{inter} 1s	C_{hetero} 1s	Cl $2p_{3/2}$	B 1s	F 1s	C_{anion} 1s	N_{anion} 1s	O 1s	S $2p_{3/2}$
$[N_{6,6,6,14}]Cl$	402.1	285.0	285.6	286.3	196.6	—	—	—	—	—	—
$[C_8C_1Pyrr]Cl$	402.1	285.0	285.5	286.1	196.9	—	—	—	—	—	—
$[N_{6,6,6,14}][BF_4]$	402.3	285.0	285.6	286.5	—	194.0	685.7	—	—	—	—
$[C_8C_1Pyrr][BF_4]$	402.4	285.0	285.4	286.5	—	194.1	685.9	—	—	—	—
$[N_{6,6,6,14}][NTf_2]$	402.5	285.0	285.7	286.7	—	—	688.7	292.8	399.3	532.5	168.9
$[C_8C_1Pyrr][NTf_2]$	402.7	285.0	285.6	286.8	—	—	688.8	292.9	399.5	532.7	169.0

experimental error and so we can deduce that the cationic structure has minimal impact upon the electronic environment of the central boron atom. This may simply be the result of the inversely proportional relationship between interaction energy and separation distance, *i.e.* the fluorine atoms are closer to the cationic core and experience a stronger interaction, whereas the increased distance to the boron atom results in a weaker interaction.

Furthermore, point charges calculated by de Andrade *et al.*[16] and Tsuzuki *et al.*[17] indicate that the negative charge of the $[BF_4]^-$ anion is distributed across the four fluorine atoms, which could provide justification for the fact that changes in charge-transfer are more noticeable in the F 1s binding energies.

It has been previously shown that there is a strong correlation between the degree of charge-transfer and the solvatochromically determined hydrogen-bond basicity (β) of the anion; whereby high basicity anions such as halides transfer a significant amount of charge, with the opposite true for low basicity anions such as $[NTf_2]^-$.[11,12] This could also provide an explanation for the smaller difference in F 1s binding energy (0.2 eV) than the observed Cl $2p_{3/2}$ shift of the chloride ionic liquids, as the $[BF_4]^-$ anion naturally transfers less charge than the Cl^- anion. To date, solvatochromic parameters have been extensively reported for 1-alkyl-3-methylimidazolium-based ionic liquids, whereas significantly fewer have been reported for 1-alkyl-1-methylpyrrolidinium and tetraalkylammonium-based ILs.[18] Subsequently, a comparison of the Kamlet–Taft (β) parameter with N_{cation} 1s binding energy cannot be made in this study, although an analogous trend to the imidazolium based systems would be expected.

A comparison of binding energies for $[C_8C_1Pyrr][NTf_2]$ and $[N_{6,6,6,14}][NTf_2]$ indicate that the anionic components all match within the experimental error excluding O 1s and N 1s (Table 1). The O 1s and N 1s binding energies are shifted to higher binding energy by 0.2 eV for $[C_8C_1Pyrr][NTf_2]$ in comparison to $[N_{6,6,6,14}][NTf_2]$. Examination of point charges determined by Hunt *et al.*,[19] Canongia Lopes *et al.*[20] and Tsuzuki *et al.*[17] demonstrate that the negative charge is mainly distributed across the oxygen and nitrogen atoms of the $[NTf_2]^-$ anion. Therefore, it is likely that the electronic environment and hence binding energies of these atoms will be most affected by changes to electron density, which can be seen in this study (Table 1).

The N 1s high resolution scan for $[C_8C_1Pyrr][NTf_2]$ and $[N_{6,6,6,14}][NTf_2]$ is presented in Fig. 3. It can be seen that there are two distinguished nitrogen environments for each compound corresponding to cationic and anionic nitrogen. A shift to higher binding energy of anionic nitrogen for $[C_8C_1Pyrr][NTf_2]$ can clearly be seen.

Interestingly, the cationic nitrogen peak is also shifted 0.2 eV higher for $[C_8C_1Pyrr][NTf_2]$ relative to $[N_{6,6,6,14}][NTf_2]$, which indicates that the electronic environment of N_{cation} for $[N_{6,6,6,14}][NTf_2]$ is significantly more electron-rich than $[C_8C_1Pyrr][NTf_2]$.

To explain this observation the charge-transfer ability of the anion must be considered. It has been established that the N_{cation} 1s binding energy follows the trend $[NTf_2]^- > [BF_4]^- > Cl^-$, which corresponds to an increase in charge transfer with increasing anion basicity;[11] thus, the electronic environment of N_{cation} is more electron-poor when coupled with the $[NTf_2]^-$ anion. Consequently, a stronger electron-releasing effect of the aliphatic chains will be induced for ionic liquids containing an $[NTf_2]^-$ anion.

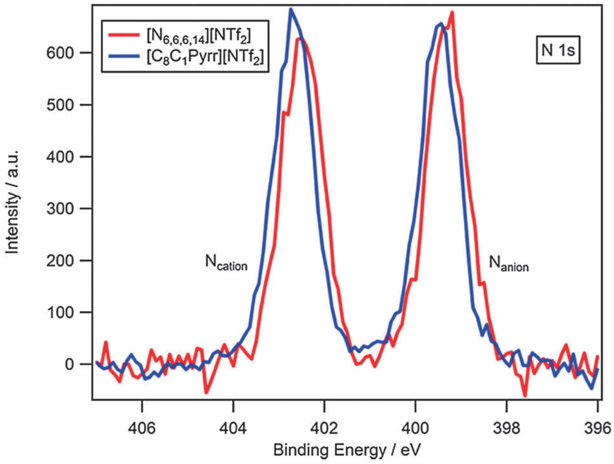

Fig. 3 High resolution XP spectra of the N 1s region for $[N_{6,6,6,14}][NTf_2]$ and $[C_8C_1Pyrr][NTf_2]$. Areas normalised to the area of F 1s photoemission peak for $[N_{6,6,6,14}][NTf_2]$.

Considering that the $[N_{6,6,6,14}]^+$ cation has a substantially larger aliphatic contribution than $[C_8C_1Pyrr]^+$, it seems reasonable that the N_{cation} environment for $[N_{6,6,6,14}][NTf_2]$ experiences a stronger inductive effect from the surrounding alkyl chains causing a subsequent shift to lower binding energy.

In conclusion, the electronic environment of the anion is dependent upon cationic structure, with an increase in charge-transfer from anion to cation achieved for the more constrained structure of a 1-octyl-1-methylpyrrolidinium cation. This provides evidence for a hydrocarbon-based shielding of the cationic core for cations containing long-alkyl chains, which subsequently impacts upon cation–anion interactions. This research not only furthers our understanding of inter-ion interactions of ILs, but also provides a step towards being able to predict how changing the different components of an ionic liquid will impact upon their respective electronic environments, a step that is key to developing the ability to tune an ionic liquid system to meet a specific function.

We gratefully acknowledge the University of Nottingham and EPSRC (EP/K005138/1) for financial support and Ms Emily F. Smith for helpful discussions and critical advice.

Notes and references

1 M. J. Earle and K. R. Seddon, *Pure Appl. Chem.*, 2000, **72**, 1391.
2 H. Tokuda, K. Ishii, M. Susan, S. Tsuzuki, K. Hayamizu and M. Watanabe, *J. Phys. Chem. B*, 2006, **110**, 2833.
3 S. Tsuzuki, H. Matsumoto, W. Shinoda and M. Mikami, *Phys. Chem. Chem. Phys.*, 2011, **13**, 5987.
4 T. M. Alam, D. R. Dreyer, C. W. Bielwaski and R. S. Ruoff, *J. Phys. Chem. A*, 2011, **115**, 4307.
5 T. M. Alam, D. R. Dreyer, C. W. Bielawski and R. S. Ruoff, *J. Phys. Chem. B*, 2013, **117**, 1967.
6 C. H. Xu, A. Durumeric, H. K. Kashyap, J. Kohanoff and C. J. Margulis, *J. Am. Chem. Soc.*, 2013, **135**, 17528.

7 K. R. J. Lovelock, I. J. Villar-Garcia, F. Maier, H.-P. Steinrück and P. Licence, *Chem. Rev.*, 2010, **110**, 5158.

8 C. Kolbeck, I. Niedermaier, N. Taccardi, P. S. Schulz, F. Maier, P. Wasserscheid and H.-P. Steinrück, *Angew. Chem., Int. Ed.*, 2012, **51**, 2610.

9 I. Niedermaier, C. Kolbeck, N. Taccardi, P. S. Schulz, J. Li, T. Drewello, P. Wasserscheid, H.-P. Steinrück and F. Maier, *ChemPhysChem*, 2012, **13**, 1725.

10 H. P. Steinruck, *Phys. Chem. Chem. Phys.*, 2012, **14**, 5010.

11 T. Cremer, C. Kolbeck, K. R. J. Lovelock, N. Paape, R. Wölfel, P. S. Schulz, P. Wasserscheid, H. Weber, J. Thar, B. Kirchner, F. Maier and H.-P. Steinrück, *Chem. – Eur. J.*, 2010, **16**, 9018.

12 S. Men, K. R. J. Lovelock and P. Licence, *Phys. Chem. Chem. Phys.*, 2011, **13**, 15244.

13 R. K. Blundell and P. Licence, *Phys. Chem. Chem. Phys.*, 2014, **16**, 15278.

14 I. J. Villar-Garcia, E. F. Smith, A. W. Taylor, F. L. Qiu, K. R. J. Lovelock, R. G. Jones and P. Licence, *Phys. Chem. Chem. Phys.*, 2011, **13**, 2797.

15 G. Adamova, R. L. Gardas, M. Nieuwenhuyzen, A. V. Puga, L. P. N. Rebelo, A. J. Robertson and K. R. Seddon, *Dalton Trans.*, 2012, **41**, 8316.

16 J. de Andrade, E. S. Boes and H. Stassen, *J. Phys. Chem. B*, 2002, **106**, 13344.

17 S. Tsuzuki, H. Tokuda, K. Hayamizu and M. Watanabe, *J. Phys. Chem. B*, 2005, **109**, 16474.

18 P. G. Jessop, D. A. Jessop, D. B. Fu and L. Phan, *Green Chem.*, 2012, **14**, 1245.

19 P. A. Hunt, I. R. Gould and B. Kirchner, *Aust. J. Chem.*, 2007, **60**, 9.

20 J. N. Canongia Lopes, J. Deschamps and A. A. H. Padua, *J. Phys. Chem. B*, 2004, **108**, 2038.